UV-triggered Encapsulation and Release by Multilayer Microcapsules

A Thesis Submitted to the University of London for the Degree of Doctor of Philosophy

By

Qiangying Yi

Supervisor: Professor Gleb B. Sukhorukov

School of Engineering and Materials Science

Queen Mary University of London

June 2013

Declaration

I certify that the present work is prepared solely by me during the course of my studies at Queen Mary, University of London. It has not been submitted for a degree at this or any other University. Any words and/or figures from the work of other people are fully acknowledged according to standard referencing.

This thesis fully complies with the regulations set by the University of London and the Queen Mary, University of London.

Qiangying Yi

June 2013

Abstract

Nowadays, the development of externally stimuli responsive vesicles possessing novel functionalities is full of challenging for various potential applications. As a practical matter, ultraviolet (UV) light responsive vesicles are finding intensive interest, as their micro/nano-structures can be tuned remotely by UV lights without involving direct contact or interaction. The development of such highly UV responsive vesicle is of great importance, where sometimes light would be the only available stimulus to drive the systems.

The mainly aim of this work was to design polyelectrolyte capsules with unique externally UV responsive properties by using layer-by-layer assembly technique, to develop their applications for cargo encapsulation and release, and to get a better understanding of underlying mechanism based on UV light triggered phenomena. Strategically, three kinds of UV sensitive chemical compounds, benzophenone, azobenzene and diazonium, were introduced into building blocks for capsule preparation. Different functionalities of these capsules were studied, and their potential applications were investigated.

To get a better understanding on the topic and contents discussed, an introduction and a literature review were first presented. Then experimental section containing materials, methods and instruments was followed in Chapter 3. In Chapter 4, weak polyelectrolyte microcapsules containing benzophenone groups were prepared. Bezophenone related crosslinking showed a reliable and swift approach to tighten and stabilize the shells without losing their pH-responsive properties. Chapter 5 investigated the microcapsules containing azobenzene groups, which could be activated to form J aggregates and further to destroy the integrity of shells upon exposure to UV light. In Chapter 6, microcapsules were fabricated with diazo-resin containing diazonium groups, which showed the ability to seal the porous shells *via* photolysis between diazonium and paired nucleophilic groups. Finally, in Chapter 7, Dual-function complex microcapsules containing both azobenzene and diazonium groups were fabricated to achieve both encapsulation and release trigged by same externally UV stimulus.

Table of Contents

Acknowledgements

First and foremost, I would like to express my heartfelt thanks to my PhD supervisor, Professor Gleb B. Sukhorukov, who offered me an opportunity to study at QMUL, and always provided his constant encouragement and guidance. I would also like to thank Dr. Dongsheng Wen, for his guidance, help and concern all the while.

I am indebted to the colleagues and friends, who helped me a lot with the experimental things. Specially, I would like to thank Dr. Zofia Luklinska, Dr. Nima Roohpour, Dr. Anton Pavlov, Dr. Steffi Krause, Dr. Charles Ryan, Dr. Jerome Irianto and Dr. Kyrstelle Mafina. And I also appreciate the help of Mr. Chris Straw and Mr. Chris Mole, for their help with general lab equipment use and lab management.

It was a great honour for me to work with our collaborators, personally, Professor Yurii Gun'ko (Trinity College Dublin, Ireland), Dr. Andrew Greaves (L'Oreal Paris, France) and Professor Hua Ai (Sichuan University, China).

I am grateful to all the members of Gleb's group for a nice working atmosphere, free communication, sharing skill and knowledge about experiments. And I am also grateful to my friends who gave me their help and time in listening to me.

I dedicate this thesis to my beloved parents, for their kindness, endless love and encouragement all through these years. I would not be where I am today without their help and support.

List of Schemes

List of Figures

List of Symbols and Abbreviations

AF488-Dextran – Alexa fluor® 488-labeled dextran (10 kda)

AFM – Scanning force microscopy

AZO – Azobenzene

BP – Benzophenone

BSA – Bovine serum albumin

CLSM – Confocal laser scanning microscopy

DAR – Dazio-resin

DCC – N,N′-dicyclohexylcarbodiimide

DMAP– 4-(dimethylamino) pyridine

EDTA – Ethylenediaminetetraacetic acid disodium salt

FITC – Fluorescein isothiocyanate

GNP – Gold nanoparticles

LbL – Layer-by-layer

NP – Nanoparticle

PAH – Poly(allylamine hydrochloride) (70 kDa)

PAZO – Poly[1-[4-(3-carboxy-4-hydroxyphenylazo)benzenesulfonamido]-1,2-ethanediyl, sodium salt]

PDADMAC – Poly(diallyldimethylammonium chloride) (100~200 kDa)

PMA – Poly(methacrylic acid) (100 kDa)

PMA-BP – Benzophenone-substituted poly(methacrylic acid)

pKa – Acid dissociation constant

PSS – Poly(styrene sulfonate sodium salt) (70 kDa)

QCM – Quartz crystal microbalance

RBITC – Rhodamine B isothiocyanate

RBITC-PAH – Rhodamine B isothiocyanate labeled PAH

RhB – Rhodamine B

SEM – Scanning electron microscopy

SDS – Sodium dodecyl sulfate

SiO_2 particles – Monodisperse silica particles

TEM – Transmission electron microscopy

TRITC – Tetramethylrhodamine isothiocyanate

TRITC-Dextan – Tetramethylrhodamine isothiocyanate-dextran (500 kDa)

UV-Vis – Ultraviolet-Visible (Spectroscopy)

1. Introduction

1.1 Polyelectrolyte Capsules for Encapsulation and Release

In recent years, a great deal of interest has been focused on the studies in the field of nanostructured material formations, benefitting from the fast developed impact and promising prospects of nanoscience and nanotechnology. A wide variety of methods have been developed to prepare potential delivery systems with novel micro-/nano-structures. The main objectives in designing and fabrication intelligent delivery systems are to protect their cargos from external influences and release them at specific sites in desired manners. To achieve the goals, various carrier systems based on different fabrication approaches have been developed. Typical examples are nanoparticles[1], micelles[2], liposomes[3], dendrimers[4], etc. Depending on the desired characteristics, each carrier system has its own advantages for specific applications, such as tunable size, chemical components, and physical properties, etc. Nevertheless, a multifunctional delivery system that can integrate all these properties is preferred, in order to meet the demands in complicated practical application. And most importantly, such multifunctional system should include increased stability and longevity in the circulation, great potential to be functionalized, and abilities to respond to numerous external stimuli[5]. Remarkably, Lay-by-Layer (LbL) assembled multilayer capsules have been intensively studied and developed as optional candidates.

Generally, the LbL technique requires basic electrostatic interactions of the paired building blocks, as first proposed by Decher and co-workers[6]. Regarding to the versatile multilayer fabrication process, the employments of the complementary building block materials, and furthermore the various combinations with other assembly procedures facilitate the engineering of a series of unique multilayer systems with high application potential in different areas. Typically, multilayer systems composing of natural and/or synthetic polyelectrolytes, inorganic components and other charged substances have been fabricated by using such electrostatic self assembly method, and their specific architectures and properties have been well studied[5, 7, 8]. In particular, when the LbL assemble is carried out on spherical surfaces, steady hollow shell formations, termed as *"capsules"*, can be obtained after removal of sacrificial

templates, as developed by Sukhorukov et al. firstly[9]. This method based on electrostatic interaction of the oppositely charged polyelectrolytes/components has recently attracted increasing interests and found many potential applications in numerous areas[10, 11]. Many nano- and micro- capsules with tunable size, composition, stability and surface functionality, have been fabricated and their various potential applications have been widely developed[5, 12, 13].

Besides the LbL assembly environmental parameters (e.g., salt concentration, pH), the multilayer components predominately take responsibility for the physical and chemical properties of multilayer capsules. Since the properties of the charged polyelectrolytes are mainly controlled by the functional groups/structures along the polymer chains, the stimuli-responsive abilities of the polyelectrolyte multilayer preferentially afford the control over the properties of the built-up capsule systems. In return, LbL capsules composed of polyelectrolytes demonstrate various unique stimuli responsive properties. Basic principles and recent developments of such stimuli responsive capsules have been studied and reviewed systematically[14]. With these external stimuli, these stimuli-responsive capsules exhibit numerous functionalities and potential applications, have been widely used as promising delivery systems in various areas ranging from medicine and pharmaceutics to chemical synthesis and catalysis[14, 15].

As one of the most interesting part of the stimuli-responsive capsules, light responsive capsules are capable to affect their micro-/nano- structures come in the form of remote control triggered by light (e.g., laser, sun light) without requirement of direct contact or interactions. The development of such highly light sensitive vesicles is of great importance, especially in the fields of surface sciences and environmental applications, where sometimes lights would be the only available stimuli to activate the systems. Various strategies were applied to develop light addressable vesicles with different functionalities. For applications in agriculture and cosmetics, UV-Visible sensitive vesicles are the optimized options due to the abundant existence of sun light[16, 17]. Meanwhile, Near-IR-absorbing vesicles are of greater interest in turbid medium (e.g., biological tissues or pharmaceutical solids) because of their deep penetration and low light scattering effect at specific wavelengths[18, 19]. As a practical matter, the stepwise LbL assembly would be a promising technique to develop light responsive capsules due to its simplicity and versatility. The step by step polymer deposition of the multilayers

facilitates the modification and functionalization of these capsules, providing availabilities of engineer a novel class of capsules with desired structures, chemical groups, and reactive functional groups/sites. Thus, a series of light responsive capsules could be obtained *via* modified LbL assembly procedure, to which the light sensitive moieties and components can be introduced easily.

One of the most essential attributes and functionalities of the capsules is encapsulation, which stems from entrapment of cargo substances in capsules' large cavities. Basically, encapsulation of the substances, e.g. proteins and polymers, can be conducted during template preparation step (e.g., by co-precipitating with $CaCO_3$)[20] or after template removal procedure (e.g., by diffusing through porous shells[21]). The principle advantage of such capsules as delivery vehicles is that the multilayer structures provide storage and essential protection for the substances against degradation or potential harmful effect from outer environmental parameters on their way to desired sites, where they can be released and activated. The substances such as proteins[20], DNA[22], small inorganic materials[23], enzymes[24], etc., were successful entrapped and studied. Theoretically, fabricated capsules are porous network-like structures, which are high permeable to molecules with a molecular weight below 5 kDa[25]. Therefore, strategies such as heat treatment[26], crosslinking within shell[27] and shell shrinking based on chemical transitions[16] were developed to decrease shell permeability, and to help cargo substance retention. On the other hand, the ultimate purpose of effective encapsulation should be accomplished by controlled or modulated substance entrapment in the capsules which could benefit a long enough storage duration with desired release properties. Practically, responsiveness to external stimuli endows the stimuli-responsive capsule a novel way to release encapsulated substances. As a consequence, a lot of methods have been developed, based on the stimuli-responsive properties of capsules, to achieve the goals. Classically, physical (laser, magnetic field, ultrasound), chemical (pH, salt) and biological (enzymatic/bio- degradation) approaches have been well investigated and summarized [28-30].

1.2 Motivation and Aims

Since the development of LbL assembly technique, the fast developed multilayer capsule formations with great versatility and architectures have emerged as a kind of

novel vesicle/container system, demonstrating a lot of advantages and applications in various areas. LbL assembled multilayer capsules with stimuli-responsive abilities have attracted great interests in multidisciplinary fields. Recently, there has been a growing interest in light responsive capsules which are able to be activated upon light exposure. The use of light, especially the abundantly existed UV light, as an external trigger is highly desirable since it requires no direct contact or interaction to accomplish functionality of fabricated capsule systems.

Despite the broad range of possible applications for such UV light responsive micro-/ nano- vesicles have been proposed, obviously only several studies dealt with the fabrication and functionalization of the LbL capsules have been reported. This motivates the author to focus work on development capsule systems which could respond to external UV light. To obtain such capsules with desired functionalities, studies on the potential UV-sensitive chromospheres/groups and their UV induced possible chemical transitions are needed. There are many kinds of such chromospheres/groups available, but to the best of our knowledge, only few are introduced to build up multilayer capsules, and moreover their underlying mechanism to push forward chemical changes are still lacking.

Cargo substances of interest, either with small- or macro- molecular weight, can be encapsulated into the capsule interior for delivery applications. Once the capsules are loaded with cargo substances, defined shell permeability is required in order to improve such loading and benefit a long enough storage time with desired release properties. Crosslinking within multilayers would be one of the optimal methods to decrease cargo diffusion. A most convenient way is to crosslink related ionic groups in multilayers. However, if the capsules are composed of weak polyelectrolytes, the resulting multilayers are favorable in many cases, because of their ability to answer to outer pH stimulus. For practical applications, such pH-responsive property allows modulated cargo release through the shrunk or swollen capsule shells, by adjusting the dissociation equilibrium of related weak polyelectrolytes. Therefore, development of an intelligent delivery vesicle system is complicated in practice, where more than one stimuli-responsive property also needs to be reserved. Typically, to enhance the encapsulation effect of weak polyelectrolyte capsules, a strategy for encapsulation needed here aims to decrease shell permeation and also retain related pH-responsive ability. **Chapter 4**

introduces the benzophenone group for capsule preparation consequently, to provide high efficient crosslinking within multilayers triggered by UV light. Avoiding consumption of the functional groups of individual polyelectrolytes (mainly paired ionic charges), pH responsive property of the built capsule would be greatly reserved, which would benefit capsules' further applications, for instance pH controlled shell stability adjustment.

Release, as one of the major aims in the field of delivery is to liberate the entrapped substances at intended location with desired speed. The most straightforward method to achieve release is to destroy the integrity of vesicles/containers. Two distinct ways of releasing have been demonstrated, either instantly or sustained. Generally, capsules rupture upon exposure to near-infrared laser (incorporating with heating effect of gold naonparticles) or degradation can realize the burst release of encapsulated substances; whereas the slowly release over an extended period can be achieved by the slow diffusion through porous structures or increasing permeability of the shells. Regarding to the UV responsive capsules discussed in this thesis, strategies are expected to affect capsules' nano- and/or micro- structures come in the form of remote control triggered by UV light. **Chapter 5** therefore employs the polyelectrolytes containing UV responsive azobenzene groups as building blocks to achieve the goal. Hopefully, incorporating of the robust azobenzene molecules into multilayer capsule system would be able to influence related photoresponse, and generate crystallization or phase separation in micro-domains, which would provide damage to the spherical capsule structures and then achieve potential release.

Micro- and nano- polymeric capsules made of LbL assembly technique have been intensively explored to achieve substance encapsulation. Many efforts have been devoted to develop strategies for macromolecule encapsulation. Particularly, several research works concerning about UV responsive microcapsules have reported to encapsulate the substances with an average molecular weight above 10 kDa through multilayer crosslinking or shell strengthen triggered by UV light. However, small molecules encapsulation remains a bottleneck. Because these small molecules, such as drugs, dyes, and other bioactive substances that have a molecular weight below 1 kD are small in size and relatively difficult to be encapsulated by the porous polyelectrolyte structures. Therefore, the encapsulation for such small molecules remains of great

challenging due to possible requirements in drug delivery and microreactors applications. An intrinsically hydrophobic multilayer capsule system with less and small pores as well as low water permeability is thus preferred. A robust and reliable approach to seal capsule shells *via* mild, preferentially externally induced, chemical modification is required to achieve the goal. **Chapter 6** proposes a controllable method to modify the assembled polyelectrolytes *via* chemical reactions to change functional groups, which would lead to avoiding charges and hence expel water voids in between layers after capsule fabrication. A study is performed to investigate macro- and small-molecules encapsulation in capsule systems containing diazonium groups, which could help seal the prepared capsules *via* UV induced photolysis.

Prepared LbL capsules with different stimuli-responsive ability endow themselves different functionalities. In order to achieve different functions in one capsule system, different stimuli are normally required. For example, UV light was used to encapsulate cargo substance, whereas pH adjustment was applied to modulate the release. Concerning about the UV responsive capsules discussed here, sometimes the continuous UV light (e.g., sunlight) would be the only one stimulus to functionalize such system. Ideally, by introducing UV sensitive chemical groups causing different potential response as building blocks, fabricated LbL capsules can be endowed with dual UV responsive properties in specific layers. One block is responsible for fast capsule sealing and the other for longer term capsule swelling and rupture. Therefore, the multi-function of these capsules could be activated selectively when exposed to external UV light with suitable wavelengths. Considering the stepwise capsule fabrication procedure, **Chapter 7** offers the strategy to functionalize dual properties of microcapsules by introducing UV sensitive groups with opposite potential functions. Consequently, a complex capsule system containing azobenzene and diazonium groups is prepared, to realize both encapsulation and release through selective chemical transitions triggered by UV light.

The aim of this thesis is to investigate the UV-responsive multilayer capsules with regards to the potential functionalities mentioned above by using LbL assembly technique. The most challenging task and ultimate purpose of this thesis is to design and explore the strategies for such UV responsive capsule fabrication as well as to accomplish their corresponding functionalities by using the externally UV stimuli.

Generally, different UV sensitive chemical groups/components are introduced in/as building blocks to prepare microcapsules. Cargo substances, for instance fluorescent polymers (AF488-Dextran and TRITC-Dextran) and small molecules (rhodamine B and fluorescein) are used as typical examples for further UV triggered encapsulation and release studies. Moreover, basic mechanism which represents the corresponding changes of microcapsule mechanical properties as well as morphologies is also investigated. The most essential attribution of this work is the development of UV induced encapsulation and release for the applications in the fields such as surface science and photochemical areas.

2. Literature Review

This review mainly focuses on the preparation and application of polyelectrolyte microcapsules, with particular emphasis on developments of light-responsive microcapsules in recent years. Mainly, three areas will be addressed: (1) general capsule preparation process, (2) encapsulation and release based on multilayer capsules and (3) light responsive capsule. The different strategies using UV light to remote active capsules are highlighted, and the potential applications are discussed.

2.1 Polyelectrolytes

The term *'polyelectrolyte'* refers to a kind of polymer who's repeating units bear electrolyte groups, which will dissociate in aqueous solutions and generate free ions, producing an electrically conductive solution. If the resulting solution is positively charged, this polyelectrolyte is referred to as a polycation. On the contrary, if the solution is negatively charged, this polyelectrolyte is referred to as a polyanion.

According to their dissociation degree in water, polyelectrolytes can be classified into *'strong'* or *'weak'* types. A strong polyelectrolyte is the one which dissociates completely in solution within a normal pH range (~2 to ~10). By contrast, a weak polyelectrolyte only partially dissociates in water. Thus, the weak polyelectrolytes are not fully charged over a normal pH range, and their ionization degree depends on the solution pH value.

Many polyelectrolytes, including natural, synthetic and composite, have been widely studied and used to fabricate LbL capsules.

2.2 Dissociation Behavior of Weak Polyelectrolyte

The dissociation behavior of weak polyelectrolyte in solution is described by the term apparent dissociation constant (K_a)[31]. For example, if a weak polyelectrolyte is dissolved in water, the acid dissociation reaction of the polyelectrolyte ion pair should be:

$$HA \rightleftharpoons H^+ + A^- \tag{1.1}$$

Where the weak polyelectrolyte HA reversibly dissociates by splitting into cationic H^+ and anionic A^-. Considering the weak polyelectrolyte is only partially dissociated in water, so the dynamic equilibrium can be described by the dissociation constant (K_a) as a quotient of the equilibrium concentrations:

$$K_a = \frac{[H^+]\,[A^-]}{[HA]} \tag{1.2}$$

The acid dissociation equilibrium can be described as a modified HENDERSON-HASSELBALCH equation as below:

$$pK_a = pH - n\log\frac{[a]}{[1-a]} \tag{1.3}$$

Where the parameter pK_a is the acid dissociation constant, n is related to the extension of the polymer chains, which depends on their charge, α is degree of protonation or occupancy.

From Equation 1.3, the pK_a of a titrating site can be defined as the pH for which the site is 50% occupied (α=0.5). For a polyanion, when pH > pK_a, the dissociation is improved because the neighboring negatively charged ions create an attractive potential for the proton, which pushes the departing proton of the acid group out more easily. Likewise, one can understand the repressed dissociation when pH < pK_a with the increase of positively charged neighboring ions in the solution. For a polycation, the pH-dependent dissociation behavior is exactly the opposite.

For the capsules made of weak polyelctrolytes, pH denpendent charge density along the molecule chains would be one of the most important properties of multilayer system. Thus, the acid-base equilibrium would influence the electrostatic interactions between the weak polyelectrolytes as well as the formation of the polyelectrolyte multilayers. Clear examples were demonstrated by Tatjana Mauser and co-workers[32, 33], as shown in Scheme 2.1. The microcapsules composed of the weak polyelectrolytes poly(allylamine hydrochloride) (PAH) and poly(methacrylic acid) (PMA) were stable in the pH range from 2.5 to 11.5. Decreasing pH caused these capsules swelling, due to a 90 % of protonation effect on PMA.

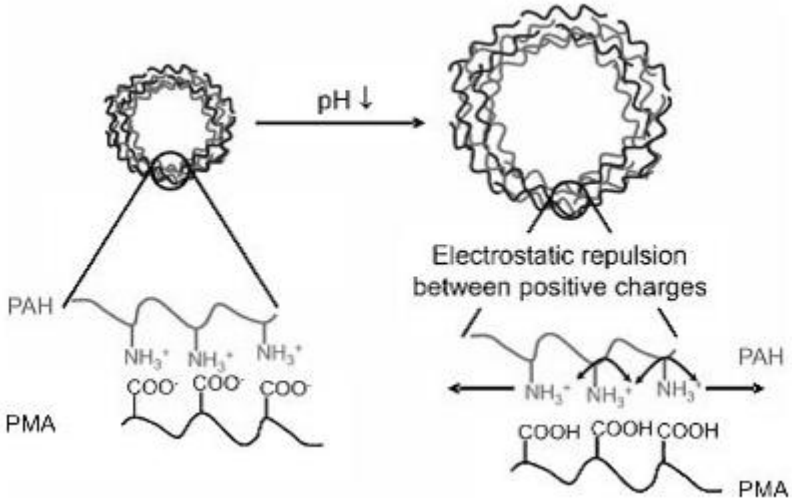

Scheme 2.1 Model of swelling of $(PAH/PMA)_2$ capsules in acidic conditions[32].

The pH-dependent dissociation behavior of the weak polyelectrolytes helps researchers facilitate the capsule preparation and their potential applications. For example, in order to ensure a fully charged polyelectrolyte solution one can adjust the pH of polyelectrolyte solution; to obtain stable hollow capsules one can choose a mild core dissolution solvent; to adjust the permeability and stability of fabricated capsules one can adjust the environment pH values.

2.2 Polyelectrolyte Complexes

When mixing the oppositely charged polyelectrolyte solutions together, the polycation and polyanion usually attract and bind, resulting in the formation of bulk polyelectrolyte complex (PEC). The main attractive force involved are Coulombic and hydrophobic interactions, and the main driving force for the PECs formation is suggested to be the entropy gain when the counterions are released into solution[34]. Since the ability to be attracted to an opposite charged polyelectrolyte is the predominate force for the complex formation, it is obvious that the addition of salt or conductive polyelectrolyte will affect the interactions among the polyelectrolytes.

Generally, the concentration of salt (e.g., NaCl) in the polyelectrolyte complex system has a profound influence on its formation and stability[35]. For the soluble complexes consist of weak polyelectrolytes with significant different molecular weights in non-stoichiometric systems, the influence of addition of salt is quite complicated. Comprehensive studies have been reported by the groups of Tsuchida and Kabanov[36-

[38]: First addition of small amount of salt helps the PECs rearrangement and shifts the reaction to a thermodynamic equilibrium, facilitating the uniform distribution of short chain components. Subsequent addition of salt leads to a shrinking of the PECs due to the shielding of the charges by salt (Scheme 2.2); when at a critical ionic strength, a disproportionation occurs, resulting in the appearance of the insoluble PECs; further addition of salt causes the complete dissociation of the PEC, leading to the free polyelectrolyte chains in solution. In the case of strong polyelectrolyte system, the mechanism becomes a little different. According to Dautzenberg's research work[39, 40], the addition of small amount of salt leads to a drastic lower amount of aggregation; whereas at higher ionic strength, a secondary aggregation happens, resulting in macroscopic flocculation, leading to a precipitate out of solution.

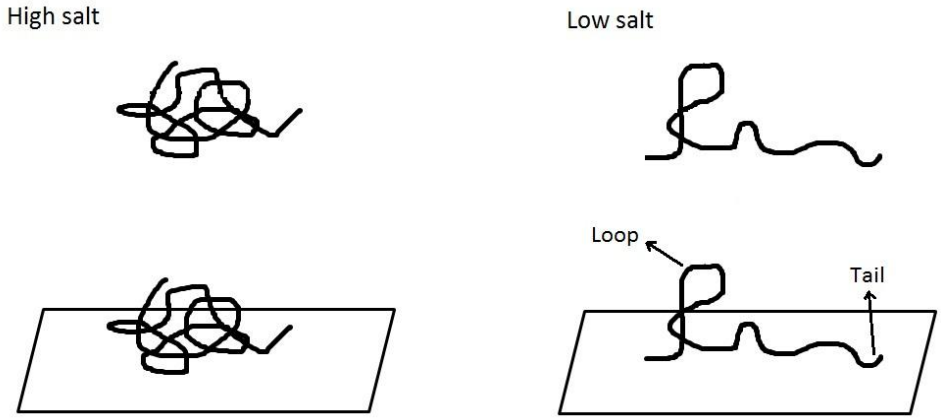

Scheme 2.2 Effect of salt on a polyelectrolyte in solution.

2.4 Polyelectrolyte Multilayer

When a charged surface is placed in an oppositely charged polyelectrolyte solution, the free polymers in the solution will adsorb onto the surface. If the adsorbed polyeletrolytes are enough to cover the solid surface, the polymer-coated system will carry the charge of the 1st polyelectrolyte, providing an electro-absorbable polyelectrolyte layer for the 2nd polyelectrolyte. Thus, alternating deposition of the oppositely charged polyelectrolyte on the solid surface will build up a polyelectrolyte multilayer (PEM) (as shown in Scheme 2.3). The general process for building up multilayers is the so called Layer-by-Layer assembly. Different from the polyelectrolyte complex, this LbL polyelectrolyte multilayer assembly process can be

repeated as many times as desired theoretically. Typically, a porous PAH/PAA film containing more than 100 assembled bilayers has been reported[41].

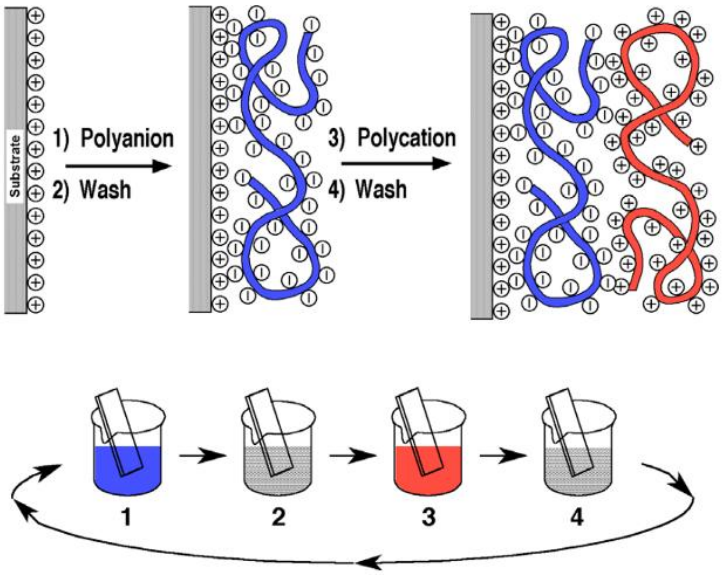

Scheme 2.3 Polyelectrolyte multilayer preparation[42].

After the first reported research work in 1990s, the field of polyelectrolyte multilayers has obtained a tremendous increased development. During the past decades, novel characterization techniques were used to investigate polyelectrolyte multilayer properties and their potential applications. These investigations revealed and summarized the multilayer components (polyelectrolytes, biopolymers, and inorganic particles), structure (thickness, pore size distribution), hydration properties (water content, water mobility, and swelling behavior), permeability, elasticity, dielectric properties and mechanical properties[34].

2.4.1 Driving Forces and Influence Factors for LbL Assembly

Similarly as the main driving force for the PECs formation, the adsorption of the polyelectrolyte to a solid surface is driven by the decreased overall free energy of the whole multilayer-free polymer solution system. The step-by-step assembly process is controlled by several intermolecular interactions. The multilayer formation and the final internal structure are complex balances between different types of interactions. Mainly, these interactions could be classified as electrostatic interactions and non-electrostatic interactions (including hydrophobic interactions, hydrogen bonding, entropy and van

der Waal forces). Further, the importance of these interactions is controlled over the polymer configuration, charge and the solvent affinity. The types of these interactions and their contributions to enthalpic and/or entropic parts have been studied in detail and reviewed by Klitzing[34]. Briefly, For LbL assembly, a basic electrostatic (coulombic) interaction is required, which would be influenced by the following two factors: charge density and ionic strength of the solution.

1) The effect of the charge density can be illustrated in two parts, the surface charge density and polymer density. On one hand, the charge density of template surface or polymer-coated template surface will affect the arrangement of the absorbed polymer layers. Briefly, when the surface charge density is 1:1 stoichiometric ratio to that of the polyelectrolyte, a flat conformation will be deposited (Scheme 2.4 b); when the surface charge is not 1:1 stoichiometric ratio to that the adsorbed polyelectrolyte, a tail-/loop-like formation will be deposited on the surface due to the standard of charge neutrality of the complete system (Scheme 2.4 a)[43]. On the other hand, the charge density along the polyelectrolyte chains will affect the interaction of the counter ions. For the strong polyelectrolytes, the charge density only depends on the chemical structure of themselves. However, for the weak polyelectrolytes, an intermediate charge density is favorable for the multilayer formation, because the charge density of the weak polyelectrolyte depends on the solution pH. Based on the theory of dissociation equilibrium, at a certain pH value, if the charge density of one polyelectrolyte is maximal, the other oppositely charged one must be very low, which will definitely result in a very small amount of polymer deposition (Scheme 2.4 c)[32].

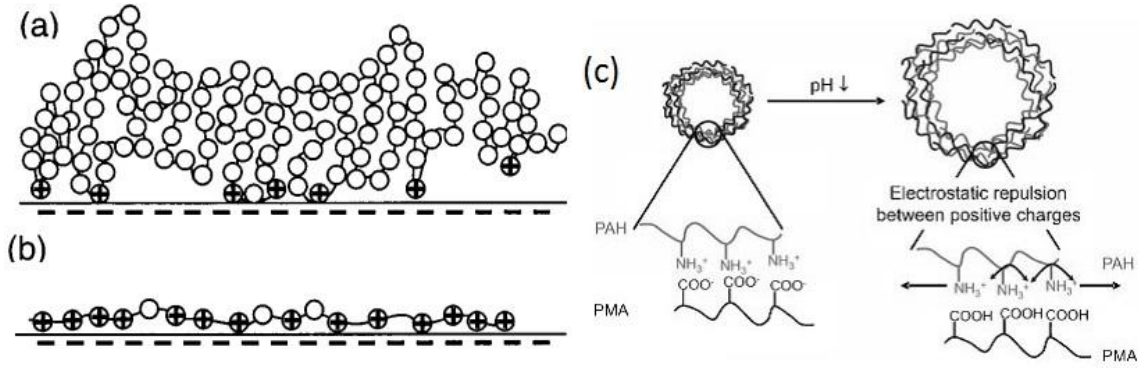

Scheme 2.4 Effect of charge density on adsorbed polyelectrolytes.

* Configuration at the interface of adsorbed polyelectrolytes influenced by low (a) and high charge density (b)[43]. Electrostatic interaction of weak polyelectrolyte influenced by their charge densities (c) [32].

2) The ionic strength (related to the addition of salt or electrolyte) in the polyion solution, influences the attraction of the polyelectrolyte and the oppositely charged interface. At low ionic strength, the polymer adsorption conformation and mass mainly depend on the dissociation degree of the polyelectrolytes. Thus the adsorption is similar as that of the charge density-dependent situation (as we discussed in the above paragraph). Mainly, at high dissociation degree, polyelectrolyte deposition layer will be flat; at low dissociation degree, more polyelectrolytes will be adsorbed with tail/loop-like conformation on the surface. While at high ionic strength concentration, the electrostatic interactions between polyelectrolytes and the oppositely charged surface should be screened, resulting in a decrease of adsorbed polyelectrolyte amount[44].

Beside the electrostatic interactions, the non-electrostatic interactions between the charged polyelectrolytes and the solid surface are also the basic factors for multilayer fabrication. With these factors, the multilayer deposition on the surface becomes dominant part instead of complex formation.

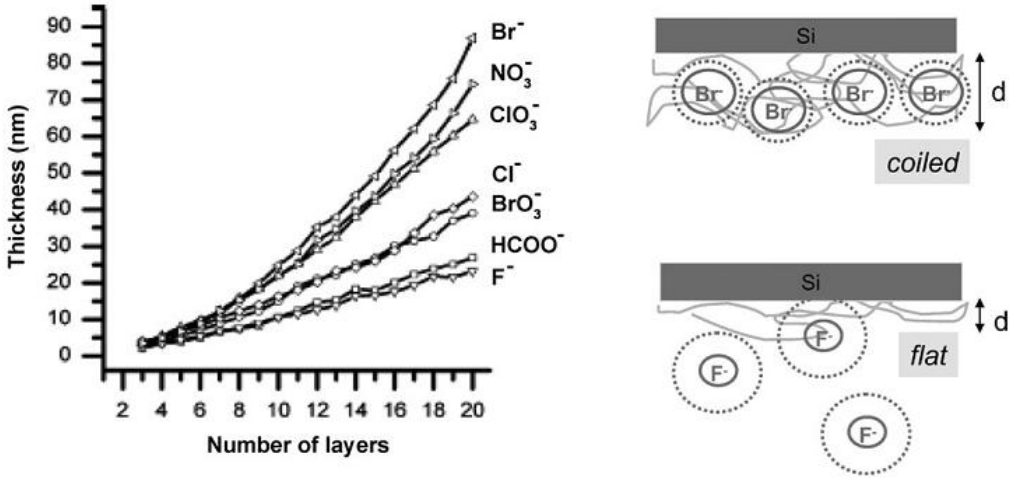

Figure 2.1 Multilayer thickness determined with ellipsometry.

* PSS/PDADMAC multilayer deposited in 0.1 M sodium salt of the corresponding anions. The scheme on the right hand side illustrates the effect of different counterions[34].

1) The type of counter ions in polyelectrolyte solutions plays important roles in multilayer formation. As the rule of "Hofmeister series", the cations and anions in the solutions have effects on the solubility of the polyions and on the stability of their secondary and tertiary structure. Usually, small ions appear to have a larger effect than the big ones, due to their relatively small polarizibilty and tendency to keep their water of hydration. The reduction in intrachain repulsion will lead to a stronger chain coiling,

which will cause an increase in the multilayer thickness and roughness. For example, the thickness of the multilayer will be effected in the presence of different salts in the order: $Li^+ < Na^+ < K^+$ and $F^- < Cl^- < Br^-$ [45], as shown in Figure 2.1.

2) Solvent affinity affects the polyelectrolytes and the counterions in the solutions. For example, water has a stronger solvating effect on the ions than methanol and ethanol. Dissolution of polyelectrolytes in methanol or ethanol will result in a stronger ion-polyelectrolyte association. Thus due to the stronger coiling effect of the polyelectrolyte chains, the increase of the multilayer thickness will happen when increase the ethanol concentration[46].

2.4.2 Multilayer Growth

With the repeating of the LbL assembly procedure, the multilayer thickness increases as a function of the deposited layer numbers. Mainly, the thickness increase model, linear or exponential, depends on the polyelectrolytes used.

Generally, the thickness of multilayer composing of strong polyelectrolytes increases linearly with the number of deposition cycles[47]. The linear growth mode shows a constant change of the layer thickness and surface roughness. Unlike the linear growth, lots of the weak polyelectrolytes, especially the biologically relevant polyelectrolyte (e.g., polysaccharides and polypeptides), whose thickness growth increase exponentially[48, 49]. Compared with the linear growth mode, exponential molded film multilayer thickness increases more rapidly. It is reported that the exponential growth is caused as a consequence of constituent polymer diffusion, where one or both of the polyelectrolytes diffuses within the multilayers. Studies on polypeptides (e.g., poly(l-lysine) and poly(L-glutamic acid)) revealed the diffusion theory[49, 50]: on one hand, a regular adsorption occurs when the oppositely charged polyelectrolytes meet. On the other hand, the excess amount of free polyelectrolytes can diffuse within the multilayer and form complexation with the counterpart polyions.

However, it should be pointed out that for the exponentially growing films, the exponential increase of the film thickness occurs only during the initially deposited pairs of layers, and then a linear thickness increase is followed, as reported by Schaaf and co-workers[51, 52]. As shown in Scheme 2.5, the preparation process of hyaluronic

acid/poly (L-lysine) (HA/PLL) multilayers, which is one of the best known exponentially growing systems, was studied as typical example. Zone I showed the first layers deposition, where the substrate surface played the main role. Increase the number of deposited polymers, the diffusion occurred in Zone III, leading to the film thickness growth as an exponential manner. Later, further increase deposited layer numbers, a new Zone II as an internal part was then restructured, due to the restructuration of the bottom layers of Zone III. Because of the formation of Zone II, a continuous growth of Zone III was thus hindered, resulting in a constant layer thickness when the deposition process went on.

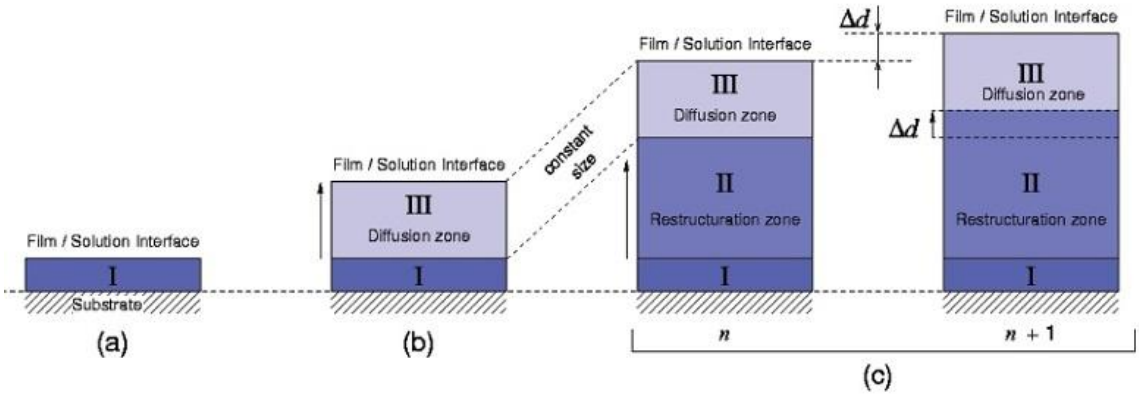

Scheme 2.5 Schematic representation for the three-zone build-up mechanism model of an exponentially growing PEM film.

* (a) At the beginning, the deposition of the first layers mainly depends on the properties of the substrate surface. Only the first pairs of layers in the vicinity of the substrate surface belong to this case, and they represent zone I. (b) As the number of deposition steps increases, the diffusion process takes place in zone III, leading to an exponential growth of the film thickness. (c) The construction goes on, and the film undergoes a restructuration of the bottom layers of zone III, leading to the formation of a restructured zone denoted as zone II. This new zone is supposed to hinder the diffusion process, so zone III reaches a constant thickness. From this point on, the film grows linearly with the number of deposition steps, the thickness increment per polyanion/polycation deposition step being equal to Δd as indicated when the number of deposition steps increases from *n* to *n*+1. The further thickness increment of the film concerns exclusively zone II [51].

The authors found that this exponential-to-linear transition always took place after about 12 deposition steps, showing exclusive relationship with the values of parameters in deposition cycles. Combining with hypothesis model, the found results were attributed to the film restructuring which progressively forbade the diffusion of the film components (polyelectrolytes) over part of the film.

2.4.3 Polyelectrolyte Multilayer Surface Charge Reversal

There are mainly three kinds of methods established to prepare thin multilayers, they are Langmuir-Blodgett technique, stepwise chemisorption and alternating deposition of oppositely charged polyions[53]. The first two are based on hydrophobic effect and covalent bonding, respectively. The last method requires electrostatic interactions of the paired polyelectrolytes. As the multilayers fabricated through physisorption need alternating deposition of two complementary polyions, the prepared multilayer film is centrosymmetric, having a centre of symmetry. The sublayer structure is chemically ill-defined due to randomly distributed polyelectrolyte molecular fragments.

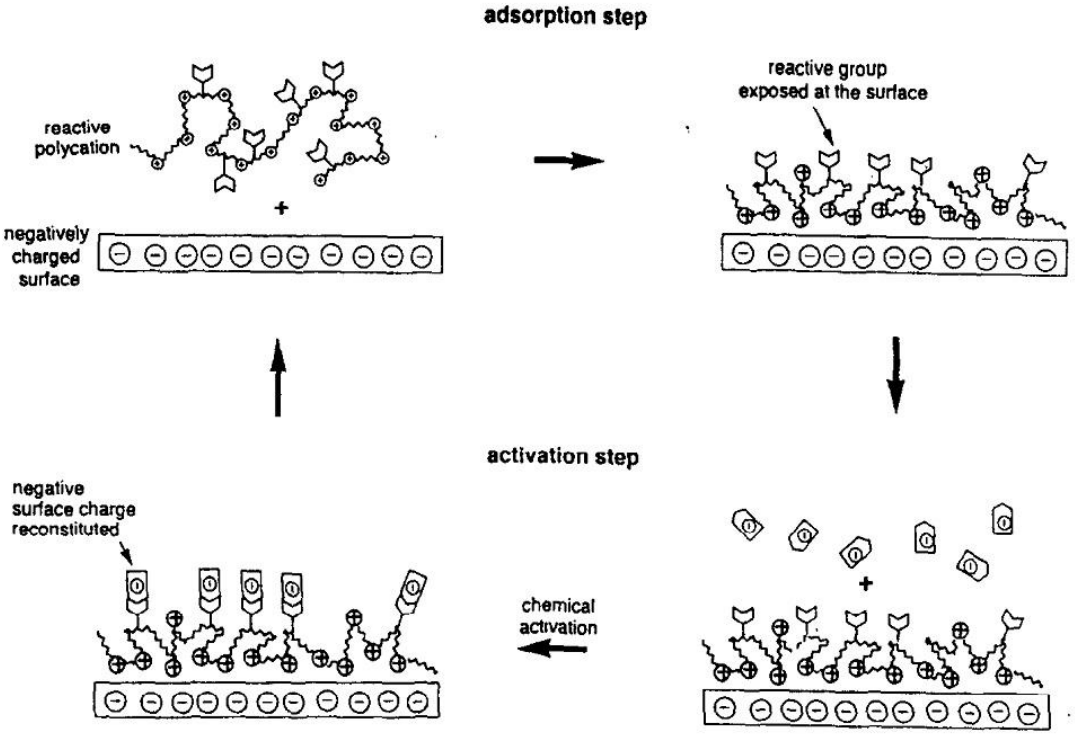

Scheme 2.6 Schematic illustration of coating by multiple polyelectrolyte adsorption-surface activation (CoMPAS) procedure[53].

Unlike the centrosymmetric multilayer, non-centrosymmetric multilayer has a preferential chemical group alignment direction, either parallel or vertical to the template[53]. A drawback for such non-centrosymmetric multilayer fabrication is the low mechanical stability and cohesion, due to the weak adjacent layer adhesion (e.g., hydrophobic effect). In order to solve this problem which existed in the traditional non-centrosymmetric multilayer preparation progress, a new technique based on physisorption and surface activation was developed to fabricate thin multilayers with

defined chemical components, known as *coating by multiple polyelectrolyte adsorption-surface activation* (CoMPAS), as proposed by Laschewsky et al[53]. This technique is easily providing strong bonding for non-centrosymmetric multilayers (not having a centre of symmetry) through electrostatic interactions and following site-specific charge reversal.

As shown in Scheme 2.6, polyelectrolytes carrying reactive groups are necessary for further chemical activation steps. Once the charged polyelectrolyte is adsorbed on an oppositely charged surface, the reactive groups are exposed at the surface and can accept activation reagents which would create reversed charges for next polyelectrolyte deposition step.

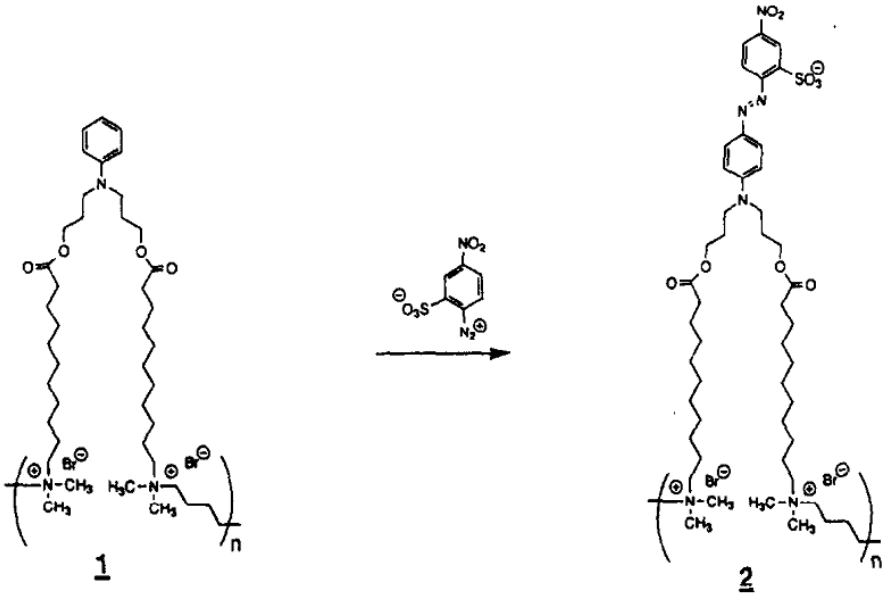

Scheme 2.7 Schematic illustration of polyelectrolyte charge reversal reaction[53].

A typical example for preparation of non-centrosymmetic thin multilayer was also given by Laschewsky and co-workers[53], as shown in Scheme 2.7. Briefly, a positively charged polymer **1** containing reactive moiety (tertiary aniline residue) was deposited on glass slides, and then the surface charges of polymer-coated glass slide were converted by a diazonium salt solution (sodium 2-amino-5-nitrobenzenesulfonate), producing negatively charged polymer **2**. Repeating polyelectrolyte deposition and surface charge reversal cycles yielded stable homogeneous multilayers with a single layer thickness of 1.3 nm. It is worth noting that a preferred ordering of polymer at the surface was established due to the hydrophobic effect, demonstrating as exposure of the reactive groups at the surface of coating.

Several attempts based on CoMPAS method have been made to fabricate such thin films[54, 55]. Technically, when activation reagents are small enough (e.g., HSO_3^-), the fabricated multilayer film could be counted as single component. A clear example of single component multilayer composing of daizo-resin was reported by Cao and co-worker[56]. This idea inspired a brilliant strategy to engineer a kind of polyelctrolyte capsules with single components, which will be discussed in Chapter 6.

2.5 Polyelectrolyte Multilayer Capsules

When the layer-by-layer assembly is applied onto colloidal particles, this technique permits the fabrication of composite core-shell particle formations. After core removal, hollow capsules with engineered features (unique size, shape, composition and functionality) could be obtained.

2.5.1 General Preparation Process

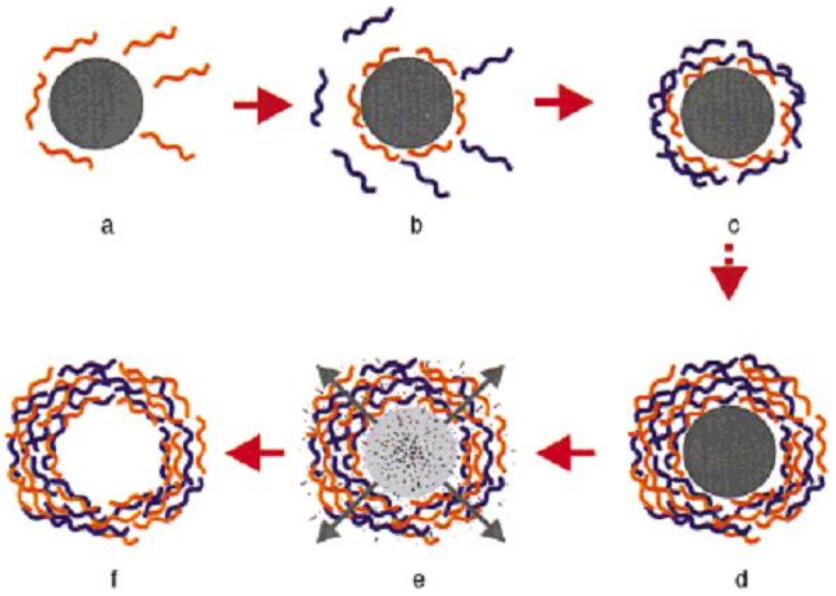

Scheme 2.8 Schematic representation of the LbL capsule preparation process[57].

Generally, the capsule preparation process includes three steps: colloidal template employment, stepwise polymer deposition and template removal procedures (as shown in Scheme 2.8)[57]. First, colloidal templates various from spherical inorganic particles to non-spherical bio-colloids with diameters in nano- to micro-scale can be used. Then the deposition of a charged polymer (oppositely from the charge of template surface) layer onto the templates is applied. The electrostatic interactions between the two

oppositely charged polymer-colloidal surfaces allow the combination of the polymer and templates, resulting in the polymer-coated colloids. Subsequent treating the polymer-coated colloids with oppositely charged polymers results in a deposition of multilayer shell formation on the template. After each polymer deposition procedure, the excess un-adsorbed/free polyelectrolytes are removed by following wash steps using either centrifugation or micro-filtration setups. Finally, after polymer deposition, the colloidal templates are removed by treatment with corresponding solvents (either chemically or thermally), thereby hollow capsules are produced.

2.5.2 Templates

Generally, templates provide supports (stable/metastable) for the LbL multilayer deposition [10, 58, 59]. It is very important to choose the initial templates for capsule preparation, because the properties of fabricated capsules and the further use strategies (loading, release, targeting) will be significantly influenced by the templates. For instance, it has been found that the capsules built up on commercial organic cores have better mono-dispersity than those on the laboratory-made inorganic ones[60]. Briefly, multilayer capsules have been built on the organic, inorganic and biological templates.

2.5.2.1 Organic Templates

For the capsules deposited on organic colloidal templates, the majority templates used are melamine formaldehyde (MF) particles (Scheme 2.9). These commercial available MF particles are weakly crosslinked monodisperse ones with a size range from nano- to micro-meter (Micro-particle GmbH, Germany). Due to their good stability at pH values above 5, LbL assembly can be carried out at neutral pH, and cores can be dissolved by treatment with 0.1M HCl[61]. One of the disadvantages of using MF is that the dissolved MF oligomers are too large to diffuse easily out of the capsule shells during the core dissolution procedure. Bulk deposition of the oligomers inside the shells will lead to a high osmotic pressure inside, which resulting in swelling behaviours of capsules and mechanical stress on the shells[10]. With increase of multilayer numbers, this effect increases remarkably, which will lead to breakage and high permeability of multilayer capsules[62]. Another drawback is that the positively charged MF oligomers by-product will stick to the capsule negatively charged shell layers, resulting in difficulty of getting rid of the core material completely even after several dissolving steps[63].

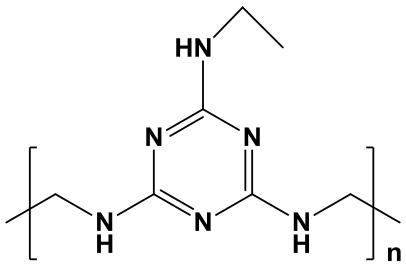

Scheme 2.9 Chemical structure of melamine formaldehyde.

Similarly, other organic templates such as Polystyrene (PS) latices[64], and bio-friendly Poly(DL-lactic acid)/poly(DL-lactic-co-glycolic acid) (PLA/PLGA) particles[65] have been used in a few research works. These particles provide well-stable templates for LbL assembly, but unfortunately, they all have disadvantages of large oligomers and difficult to be totally removed.

2.5.2.2 Inorganic Templates

Considering the difficulty of organic templates removal, inorganic particles may be promising templates due to their small products after core dissolution. These particles could be either inorganic salt or molecular crystals that can be dissolved in acidic or organic solvent.

Highly monodispersite silicon dioxide (SiO_2) particles with a broad size range have been used as promising templates recently and subsequently removed by suspending in hydrofluoric acid (HF). The advantage of using the SiO_2 as templates is because of its fast decomposition and integration of the capsule formations when treated with 1M HF solution. Comparing with the MF capsules, the capsules templated on SiO_2 are quite intact, and possess low permeability that can prevent from fluorescent macromolecule permeation (rhodamine-labeled PAH, 2×10^{-2} M; 70 kDa)[10]. However, it should be noted that attention must be paid on the core dissolution procedure when handling dangerous HF solution.

Due to the fast development of inorganic crystals currently, carbonate particles such as calcium carbonate ($CaCO_3$)[66], cadmium carbonate ($CdCO_3$)[67], and manganese carbonate ($MnCO_3$)[68] are used as promising templates for capsule preparation. These particles can be prepared in several micro-scales. For example, if the Na_2CO_3 and $CaCl_2$ solutions were mixed together, a white precipitate will be formed. Leaving the

mixture still for several minutes, nano-scale particles will aggregate to generate micro-scale particles ($CaCO_3$). After a desired multilayer deposition, core dissolution can be performed mildly by treatment with ethylene diamine tetraacetic acid (EDTA), and the small molecule products can leave the capsule interior without problem. However, one disadvantage of the carbonate cores would be their high polydispersity and non-spherical products (e.g., $CaCO_3$ crystal)[20].

Most interesting, the porous structure of these inorganic particles provides useful cavities for the active loading of cargo materials, such as protein[69], DNA[70] and other materials. After core dissolution, the cargo materials will be encapsulated inside the capsules automatically.

2.5.2.3 Other Templates

Besides the organic and inorganic (non-metallic) particles, a large variety of materials can be used for the capsule preparation. Gold nano-particles[71], living cells[72-74], oil emulsion[75], as well as the metastable air bubbles[76] have been used as templates to fabricate capsules, as shown in Figure 2.2. Considering the practical applicability, if the cargo materials were used as the templates directly, they were already encapsulated without the core dissolution steps after LbL assembly. Specially, this strategy will facilitate the encapsulation of biological materials, like cell, gene, virus, etc. This diversity of template options makes the LbL capsules attractive for numerous applications in different areas.

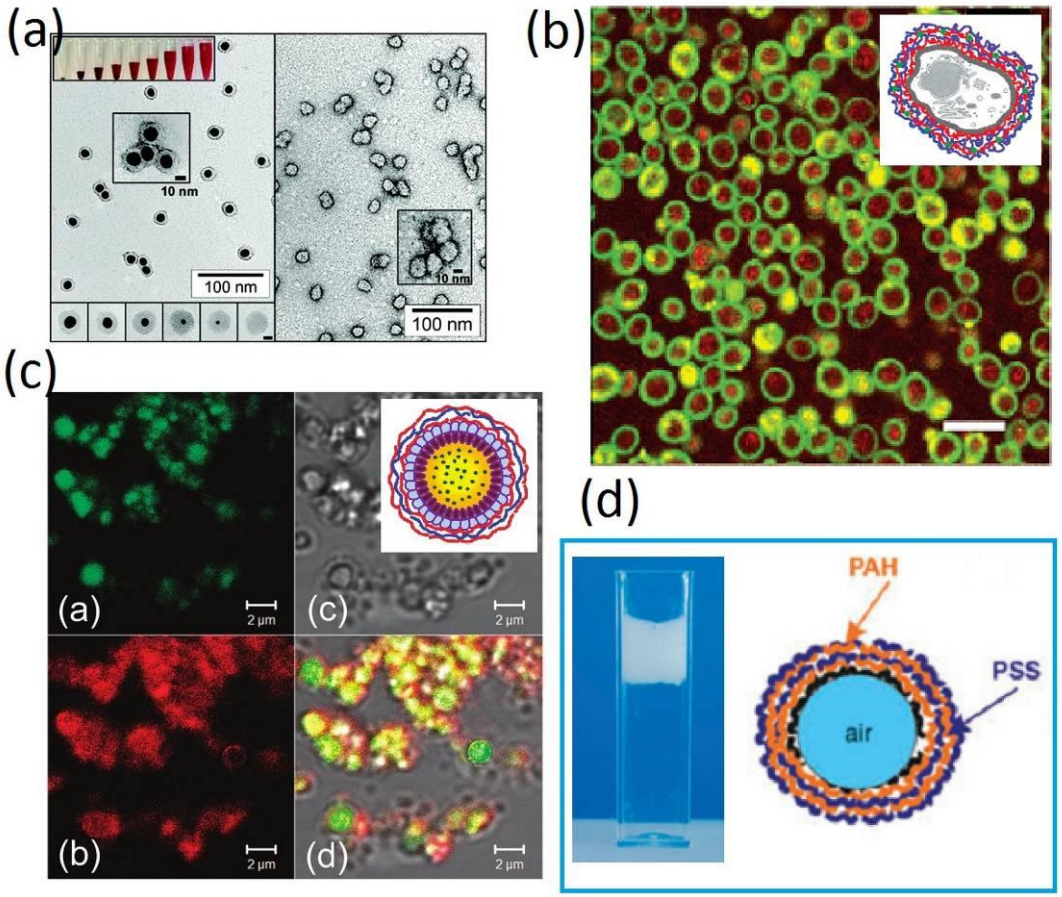

Figure 2.2 LbL capsules deposited on various templates.

* (a) TEM images of capsules deposited on gold nanopaticules before (left) and after (right) core removal[71]. (b) Fluorescent image of capsules deposited on living cells[72] (Scale bar = 10 μm). (c) Fluorescent images of freeze-dried linseed oil capsules at different excitation wavelengths[75]. (d) A photograph of air-containing polyelectrolyte capsules in aqueous solution after centrifugation[76].

2.5.3 Hollow Capsule Formations

The stepwise depostition procedure offers versatility of building capsules with different composition and functionality. Pure polymers, organic/inorganic components can be introduced into the shell formations, with particular active functional sites.

2.5.3.1 Polymeric Capsules

In most cases, pure polymers (polyelectrolytes) were used to fabricate capsules on various templates. After core removal, hollow capsules could be produced with different diameters. One of the typical examples is the capsule composing of poly(allylamine hydrochloride) (PAH) and poly(sodium 4-styrenesulfonate) (PSS) templating on melamine formaldehyde (MF) resin particles (diameter = 8.7 μm)[77].

Such capsules are thin spherical shells when suspended in aqueous solution. After drying, creases and folds can be found as a consequence of capsule shell collapse caused by water evaporation. At the same time of colloidal template dissolution process, capsules undergo a slight shrinking due to the elastic relaxation[78]. Atomic force microscopy (AFM) and small-angle neutron scattering (SANS) measurements revealed the mean thickness of capsules composing of PAH and PSS is 1~2 nm per single polyelectrolyte layer[77, 79], as shown in Figure 2.3.

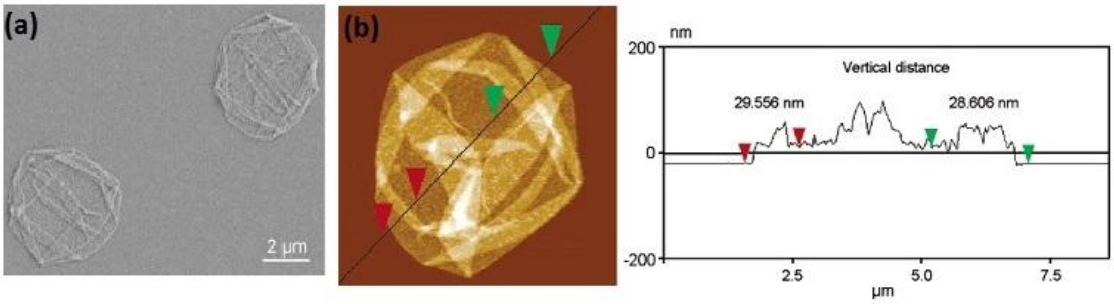

Figure 2.3 SEM (a) and AFM (b) image of $(PSS/PAH)_5$ capsules prepared on MF (4.6 µm)[80].

Besides the PAH and PSS, a lot of polymeric capsules have been fabricated and their properties have been widely studied. The choice of shell components plays an important role in the potential application of the LbL capsules. Interestingly, polymer capsules offer a kind of novel vesicles for post-loading drugs, dyes and other material. Typical cases have been demonstrated, for instance, the combination of biocompatible shell components and encapsulated pH sensitive materials inside make the capsules become good candidate for pH sensors inside different organelles[81] (Scheme 2.10 a); and the biodegradable components (e.g. chitosan[82] or poly-L-arginine and synthetic poly(hydroxypropyl)methacrylamide dimethylaminoethyl [83]) facilitate the deconstruction of capsule shells, resulting in the controlled release of encapsulated substances inside living cells (Scheme 2.10 b).

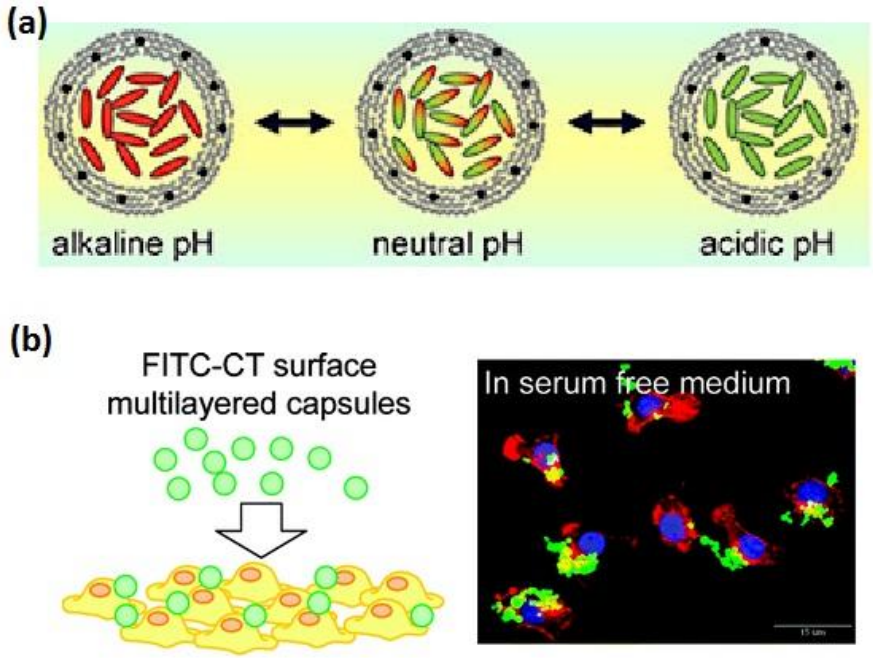

Scheme 2.10 Schematic representation of capsules for pH sensing (a) and drug delivery (b).
* (a) The capsule interior was filled with pH sensitive SNARF-1-dextran. Capsules demonstrated different fluorescent colours in acidic and alkaline pH[81]. (b) Biodegradable capsules containing basic fibroblast growth factor (bFGF) inside demonstrated the local and sustained release [82].

2.5.3.2 Inorganic Capsule

During the stepwise polymer deposition procedure, if charged inorganic components were added, after removal of the colloidal templates and organic components (bridging polymer multilayers) by calcination, hollow inorganic capsules can be obtained. One of the first examples is the hollow silica capsules obtained after calcination of silica nanoparticles (SiO_2)/polymer multilayer coated PS latex spheres[84], as shown in Figure 2.4. After twice deposition of SiO_2/PDADMAC mixture, individual SiO_2 nanoparticles can be found on the surface of the PS latex particle. After calcination, the PS core was removed and the SiO_2 nanoparticles were fused, resulting in a crosslinked uniform silica wall (cage) with a spherical morphology. The high-temperature treatment condensated the silica nanoparticles within single spheres and generated structural integrity for the hollow silica sphere. The sintered silica spheres can be redispersed in water after sonication, illustrating that this coalescence predominately occurred intra-individual SiO_2 nanoparticles, rather than inter-spheres.

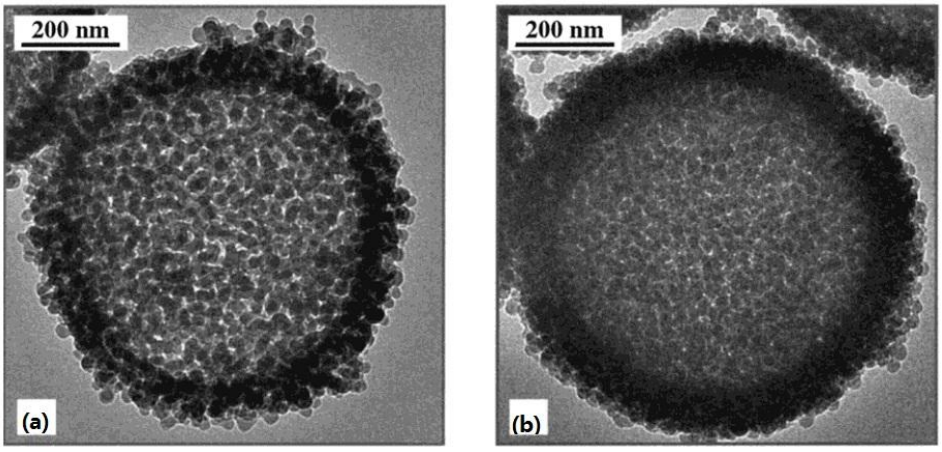

Figure 2.4 TEM images of calcined silica microspheres with deposition of two (a) and three (b) SiO_2/PDADMAC layers[84].

LbL assembly also provides a simple way to control the wall thickness and outer diameter of the hollow silica spheres. TEM images demonstrated a regular increase of silica sphere wall thickness (increment of 30 nm) and diameter (increment of 60 nm) with the increase of deposited silica nanoparticle layers. And it was obvious that the more silica particles deposited, the more uniform wall would be fabricated. According to the cross-sections TEM images, the average silica wall thickness was found to be 100-120 nm[84].

Due to the versatility of layer-by-layer assembly technique, other nanoparticles (Titanium dioxide, silica, magnetic, Laponite and luminescent semiconductors (CdTe)) with different composition, size and shape could also be used as building blocks for multilayers preparation on sphere templates (MF, PS)[85], offering numerous potential applications ranging from electrical, chemical as well as optical areas.

2.5.3.3 Composite Capsules

High temperature sintering of the inorganic/organic composite leads to the formation of hollow and porous inorganic cages. Due to the porous structure, these cage-like inorganic capsules lose the film-like properties (e.g. permeability), resulting in their limited application. However, if only the templates were removed by using selected solvents or other methods, composite capsules composing of inorganic particles and bridging polymeric multilayers can be obtained. Such inorganic/organic composite capsules exhibit combination properties of controllable permeability and mechanical

strength.

Considering the LbL assembly capsule fabrication procedure, there are two time points for introduction of the inorganic components, one is after the LbL deposition procedure, and another one is during the LbL assembly process.

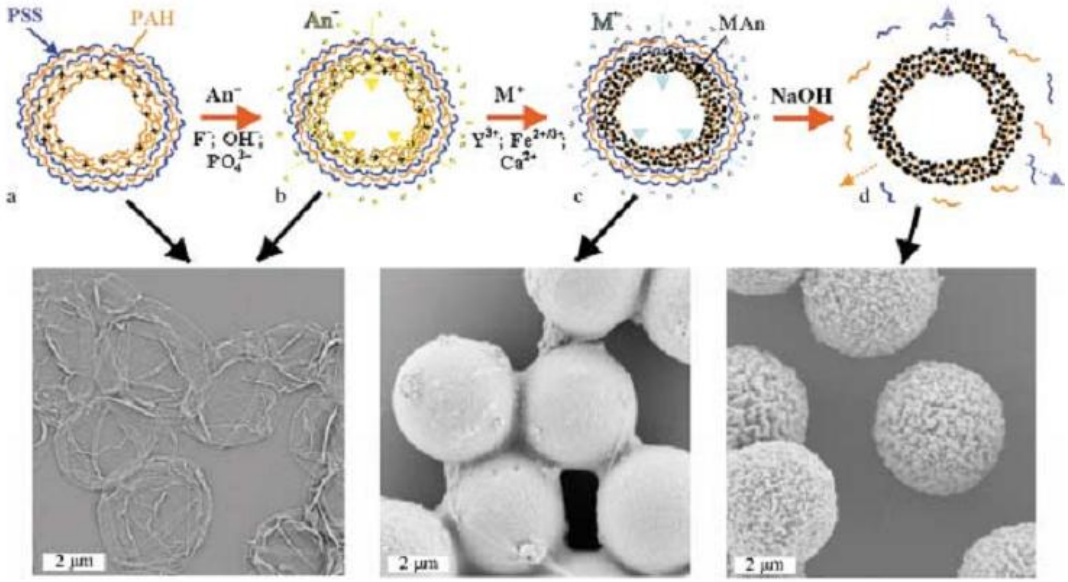

Figure 2.5 Preparation of composite hollow capsules.

* An^- = F^-, OH^-, or PO_4^{3-}; M^+ =Y^{3+}, $Fe^{2+}/^{3+}$, or Ca^{2+}; MAn=YF_3, Fe_3O_4, or hydroxyapatite; below: SEM images of the YF_3 capsules at different preparation stages[86].

For the former, a clear example has been done by Sukhorukov and co-workers[86], as shown in Figure 2.5. Generally, hollow PAH/PSS capsules with an inner PAH/citrate layer were built up firstly. Then the citrate ions were placed by other anions (precipitating agent) by exposing PAH/citrate–PAH/PSS capsules to a mixture containing 0.01 M NaOH, 0.1 M H_3PO_4, or 0.1 M HF. After anion replacement, water insoluble iron (II, III) oxide (Fe_3O_4), hydroxyapatite and yttrium fluoride (YF_3) particles were deposited on the inner capsule surface, respectively. Finally, PAH/PSS shells were removed by treating the resulting PAH/inorganic–PAH/PSS polyelectrolyte capsules with alkali solution for 24 h. Raman microscopy and UV-Vis spectroscopy results indicated that only the inner PAH layer existed after polymer dissolution, and the survived inner PAH layer maintained the connection of the inorganic particles. Such versatile approach generate a kind of capsules with higher mechanical stability (compared to the pure polyelectrolyte ones), and good shape persistence after drying. In addition, due to the variety of deposited inorganic particles, the composite capsules

could be endowed with various potential applications, such as YF_3 shells can be used as adsorbents for rare earth ions, the magnetic active Fe_3O_4 shells can be used in delivery systems, and the capsules with calcium hydroxyapatite shells can find applications as novel biomaterials. Most importantly, comparing with the inorganic capsules, these composite capsules possess a polymer layer, which would facilitate control of the encapsulation and release of the encapsulated substances.

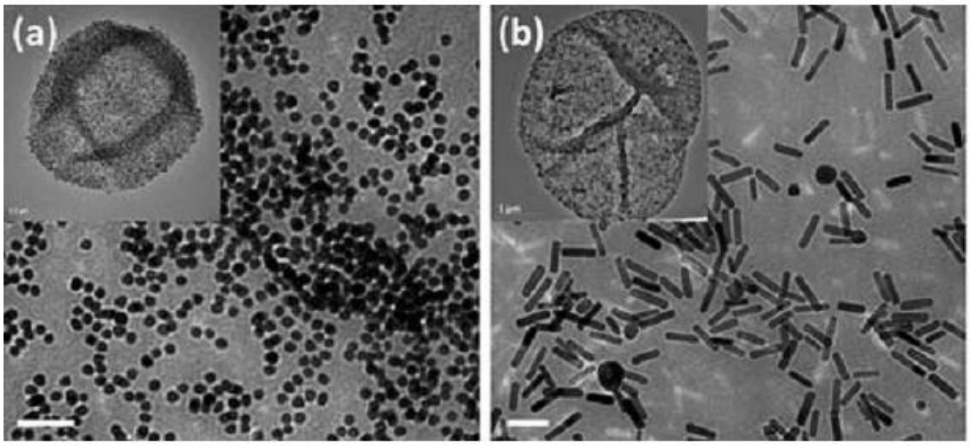

Figure 2.6 TEM images of composite capsules with (a) GNPs and (b) GNRs embedded inside the multilayer shell of hollow $(PSS/PAH)_4$ capsules[5].

Besides the method of inorganic deposition on fabricated hollow capsule, charged inorganic particles (gold, silver, iron, etc.) can also be introduced during the LbL process *via* the direct electrostatic assembly[18, 87-89]. After removal of core templates, hollow capsules with nanoparticles absorbed in the multilayer shells can be obtained. Typical examples of nano-size gold particles loaded hollow capsules are presented. As shown in Figure 2.6, TEM images demonstrated the polyelectrolyte capsules with (a) gold nanoparticles (GNPs), (b) gold nanorods (GNRs) incorporated in the multilayer $(PSS/PAH)_4$ shell.

The integration of polymer multilayer shells and nanoparticles allows the production of capsules with important functionalities, such as labeling, adjusting the permeability/opening of the capsule shell, targeting, etc. For example, by modifying the capsule shells with gold nanoparticles, site specific release of the loaded contents could be performed with the help of near infrared laser light[19]. Details of the application of such composite capsules will be discussed in Section 2.6.2.1.

2.5.4 Cargo Substance Encapsulation

2.5.4.1 Encapsulation Strategies

The most straightforward method to encapsulate cargo substances originates from incorporating these substances with the templates (cores), which accomplishes entrapment during microcapsule fabrication procedure, also known as *active loading*[90]. After template removal, desired cargo substances are trapped inside capsules directly, a schematic illustration is shown in Scheme 2.11. For instance, encapsulation of bioactive compounds are successfully achieved in porous $CaCO_3$ microparticles[20, 90]. By co-precipitating with or adsorbing on $CaCO_3$ particles, protein and dextran are easily to be loaded into porous $CaCO_3$ microparticles (~ 4.75 μm), and then the protein/dextran-filled particles can be used as templates for polyelectrolyte deposition. By treatment with EDTA solution, shell-like structures with loaded macromolecules inside are obtained. Practically, this approach allows an encapsulation efficiency of 80% for protein (66 kDa)[91]. Generally, loading of such macro-substances in porous $CaCO_3$ particles is affected by their properties, such as molecular weight and solubility. As suggested, materials with amorphous property or long needle shapes are not suitable for fabrication of spherical templates; their molecular weight, water solubility as well as affinity to carbonate surface (holes) determines the encapsulation efficiency due to diffusion-limited permeation of the multilayers[10, 20]. Promisingly, this approach can easily be applied to encapsulate macromolecules at neutral pH, which benefits the engineering of a series of micro-containers for bioactive substances with widely ranges in the field of biotechnology, biochemistry and medicine areas.

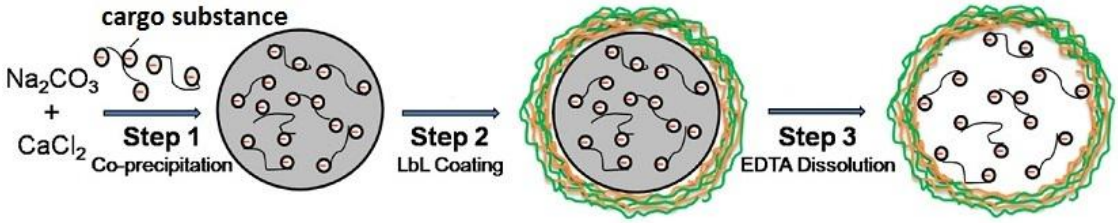

Scheme 2.11 Active loading of cargo into the preformed hollow capsules [92].

Comparably, a second method for encapsulation is developed, known as *passive loading*, to which the cargo substances were introduced after capsule fabrication[90]. Mainly, two kinds of strategies are developed to achieve such passive loading, either by

diffusion or in-situ precipitation/generation. For the former, the desired substances are incubated together with the hollow capsules, and then the porous network-like structure of capsule formations allows the selective diffusion of cargo substances into capsules driven by physicochemical differences (e.g., substance concentration, solvent components) between the capsule interior and environmental medium. Scheme 2.12 showed the schematic representation of this concept. The method has been applied for encapsulation of urease[93], dextran[26], DNA and protein[94]. Comparing with active loading, this approach allows a lower encapsulation efficiency of water soluble substance in aqueous system[95].

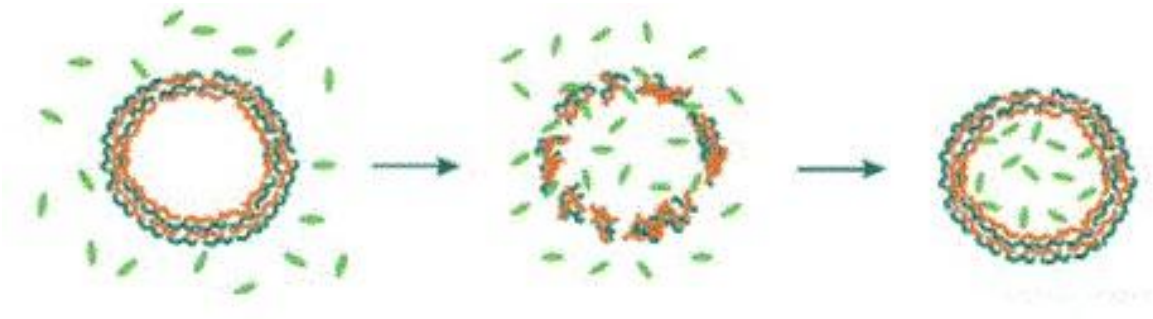

Scheme 2.12 Passive loading of cargo into prepared capsules[30].

Different from diffusion, other methods have been developed such as substance precipitation/generation within capsules, which are driven by ionic polarity gradient, complexation, chemical reactions, etc. General idea of this method has been presented in Section 2.5.3.3. A classical example of photochemical microreactors has been demonstrated as the *"ship in bottle"* synthesis of copolymers in capsules, involving monomer and initiator permeation through capsule shells followed by photoreactions inside capsules[96]. Specially, other two strategies based on spontaneous deposition of water-soluble substances *via* bounding to charged oligomers[63] or controlled precipitation into capsules *via* variable solubility [97] are also developed. These approaches realize encapsulation of substances with low molecular weight.

2.5.4.2 Sealed Encapsulation

Theoretically, the LbL capsules are normally permeable for molecules with a molecular weight below 5 kDa[30]. Considering the porous structure of capsules, an adjustment to decrease capsule shell permeability is required, in order to achieve the cargo substance encapsulation[19]. Many strategies have been developed to accomplish a better

encapsulation in the purpose to achieve longer storage duration.

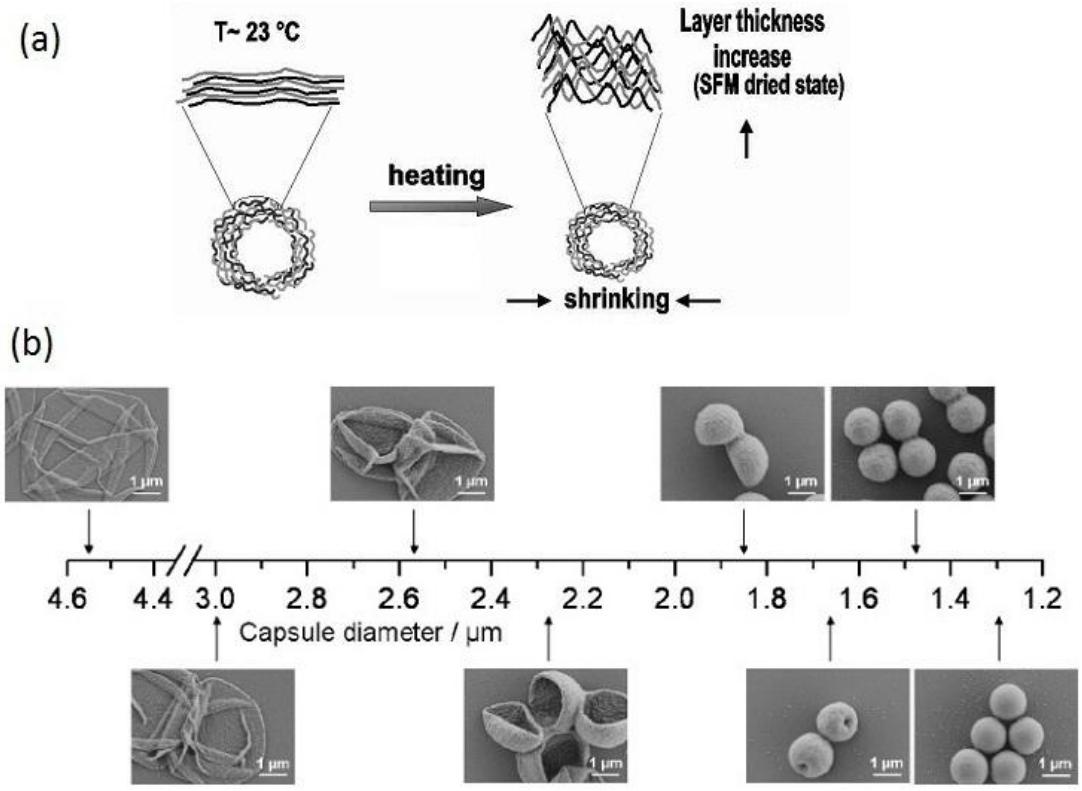

Figure 2.7 Schematic illustration (a) and SEM (b) images of heat shrinkage.

* (a) Configurational arrangements of the $(PSS/PAH)_5$ capsules before and after heating. The reduction of the capsule diameter is accompanied by an increase of the thickness of the layer[77]. (b) SEM images of $(PDADMAC/PSS)_4$ capsules shrunk to different sizes as a function of diameter after temperature treatment. The first image shows an initial capsule with a diameter of 4.55 µm[98].

Typically, after cargo substance loading, either active or passive, heat treatment can be applied to adjust the shell permeability through the so called heat-shrink process. After incubated at elevated temperature, the building block polymers consequently change ones' two-dimensional arrangement with a low entropy state into a more coiled arrangement with increased entropy[77], as shown in Figure 2.7 a. This polymer chains re-arrangement decreases shell permeability, as a result of capsule size decrease accompanying with shell thickening and densification[98] (Figure 2.7 b). For $(PSS/PAH)_5$ capsules, after heating at 70 ℃ for 2h, a remarkable heat-induced size decrease can be observed (1 µm decrease of the diameter). Meanwhile, AFM revealed the accompanied increase of capsule shell thickness, changed from 41 ± 1nm to 53.3 ± 0.8 nm[77].

Interestingly, not all the capsule systems undergo a heat-shrinking process when heated; it was suggested that the heat-dependent change in size was governed by the so called *'odd-even effect'*, which associated with the capsule internal electrochemical properties as reported by Köhler and co-workers. The microcapsules composing of poly(diallyldimethylammonium chloride) and poly(styrene sulfonate) (PDADMAC/PSS) were studied as typical examples (Figure 2.8). After heating, capsules with an even number of multilayers (PSS with negative charges as the outmost layer) showed a heat induced shrinking accompanied by a increase of shell thickness; in contrast, capsules with an odd number of multilayers (PDADMAC with positive charges as the outmost layer) swelled to 5-fold of their initial size followed by their rupture[98]. And further research work revealed the heat-dependent behavior in water was mainly controlled by the charge amount of the outer polyelectrolyte layer, where the surface potential will influence the water mobility in the internal layers, and then to induce the swell or shrinking of capsule shells[99, 100].

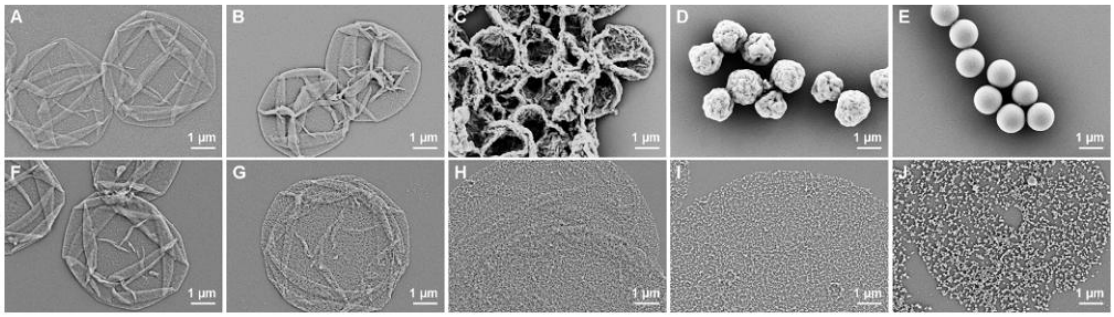

Figure 2.8 SEM images of dried PDADMAC/PSS capsules after 20 min incubation at different temperatures.

***** The first row shows $(PDADMAC/\ PSS)_4$ capsules (A) before and after heating at (B) 35, (C) 40, (D) 50, and (E) 70 ℃. The second row presents $(PDADMAC/\ PSS)_4$-PDADMAC capsules (F) before and after heating at (G) 35, (H) 40, (I) 55, and (J) 70 ℃ [99].

And, it is worth mentioning that the this odd-even effect becomes less pronounced with increasing number of deposited polyelectrolyte multilayers[101]. It should be noted that not all the cargo substance can undergo a heating procedure, thus development of other strategies for encapsulation of heat-sensitive materials is urgently necessary.

Crosslinking approach has been developed as an alternative way for sealed encapsulation. Basically, crosslinkable polymers, either natural or synthesized, have been introduced as building blocks for capsule preparation. Chemical crosslinkers or

external triggers are used to bond related functional groups of the individual polyelectrolytes. For example, the frequently-used crosslinker EDC (*N*-(3-Dimethylaminopropyl)-*N′*-ethylcarbodiimide hydrochloride) is applied to crosslink the polyelectrolytes containing amino groups and carboxylic acid groups through amidation reactions. Consequently, stabilities of the capsules have been largely improved[102] as evidenced by steady multilayer shells in extreme pH conditions[103] and storage of macromolecules (500 kDa) at high pH[27]. Besides chemical crosslinkers, photo-active groups are also applied to crosslink the multilayer capsules *via* light triggered reactions, typical examples are given as the phtotosensitive diazoresin-based microcapsules, in which the enzyme is successfully encapsulated after photolysis reactions[104]. One should notice, after crosslinking of the functional groups (mainly the ionic groups), pH responsive ability of these stabilized capsules will be greatly reduced or eliminated, depending on the degree of reacted ionic groups.

Other methods that can tighten or strengthen the multilayer structures without consuming the ionic groups have also been developed to help encapsulation. One of the typical examples has been demonstrated by Bédard and co-workers. Remote controlled capsule shrinkage based on length reduction of azobenzene molecule photoisomerization leads to decrease of shell permeability, resulting in retention of dextran (10 kDa)[16]; details can be also found in Section 2.6.1.2.

2.5.5 Modulated Release

Basically, polyelectrolytes are primary building blocks for multilayer capsules. Therefore, any external parameters (stimuli) that can influence on these polyelectrolytes will make their contributions to modulate release. Generally, such parameters could be classified into three categories: physical, chemical and biological. In this section, a brief overview of these three parts will be presented.

2.5.5.1 Physical approaches

For these physical parameters, capsule rupture should be the most intuitive manner to achieve release. Near-infrared (IR) laser, magnetic field and ultrasound have been used to disrupt the multilayer shell by direct mechanical deformation.

Incorporating noble metal nanoparticles (especially the gold and silver nanoparticles) in multilayer shells, (near-) IR laser light with different wavelengths (e.g., 830 nm[105], 532 nm and 1064 nm[106]) has been applied to break the capsule shell site specifically, leading to shell permeability change, deformation[19, 88] and controlled release in living cells[107, 108]. Theoretically, the composite capsules containing gold or silver nanoparticles exhibit a broad absorption at (near-) IR region (approximately 700 ~ 1000 nm), the incorporated nanoparticles absorb irradiation energy in this region and then release it in the form of light scattering or heat, benefiting deformation of capsule formations[18, 19]. In the meantime, the light in this region has unique properties, high transmission and low scattering to be specifically, would cause no severe damage objectives (human body, biological medium). Therefore, this strategy has found great interests in the field of biological and medical areas, by applying fabricated composite capsules which exhibited a preference to absorb the bio-friendly infrared light. Related issue such as mechanism and potential applications will be discussed in Section 2.6.2.1.

Ultrasound has been applied for capsule ruptures remotely. For the pure polymeric capsule without metal nanoparticles, ultrasound with high power and low frequency (e.g., 120 W, 20 kHz[109]; 500 W, 20 kHz[110]) has shown the ability to split the polyelectrolyte capsule shells into piece, which is based on the shear forces generated from acoustic cavitation in liquids under ultrasonic vibrations. The nanoparticles (Ag[109], Fe_3O_4[110] and ZnO[111]) incorporated in the multilayer shells help enhance and accelerate the effect. The strengthened effect was attributed to the low elasticity and high brittleness of the nanoparticle/polyelectrolyte shell as well as the resulted higher density gradient, which led to reflection and superposition of the acoustic waves[110]. For practical applications in biomedical areas, low frequency ultrasound at high power is not suitable, because the strong wave intensity might cause permanent damage to tissue or body. Therefore, development of ultrasound with low power which eventually approaches the allowed in medicine is a challenging task. In this regard, a case using the ultrasound with the parameters close to current medical care use, low-power ($\leq$ 3.2 W) and high-frequency (850 kHz) particularly, has been reported by Sukhorukov and co-workers[91]. As in their work, high frequency ultrasound was found capable to rapture the $(PAH/PSS)_4$ microcapsules, which led to gradually release of encapsulated protein (66 kDa) within 10 minutes. In the mean time, addition of gold nanoparticles in

capsule shells speeded up the release efficiency by up to 4 times, which was proposed as the resulted mechanical rigidity of the composite shells.

Capsules containing magnetic nanoparitcles can response to the outer magnetic field, facilitating a way to modulate capsules' permeability by employing outer magnetic field to rotate these particles. By treatment with an oscillating magnetic field (100-300 Hz, 1200 Oe) for 30 minutes, the gold-coated cobalt (Co@Au) nanoparticles (3 nm) embedded in shells were twisted, which consequently destroyed the integrity of PSS/PAH multilayer microcapsules, demonstrating as increased permeability to macromolecules[112]. Research works have also been done on the capsules containing magnetite (Fe_3O_4) nanoparticles. Upon applying outer magnetic field, nanocavity was found on the surface of capsules composing of Fe_3O_4 and PAH; extending the magnetic stimulus duration, nanocavities gradually became cracks on capsules and finally destroyed the intact capsules; moreover, controlled rupture in living cells (cancerous A549 cell line) offered a potential application of these magnetic capsules as effective drug delivery system[113]. Besides the increased shell permeability triggered by alternated magnetic field, a temperature increase was found after exposure of these magnetic capsules to magnetic field for long time. As reported by Katagiri[114], the heat originated from Fe_3O_4 nanoparticles under magnetic field cannot rupture the polyelectrolyte microcapsules, but caused phase transition of the outer lipid membranes, benefiting the release of encapsulated dye molecules (phenol red). It is also worth mentioning, the external magnetic field could also realize other functions of these magnetic capsules. Typical strategies such as targeted delivery and imaging *in vivo* have been demonstrated in other works[115, 116].

2.5.5.2 Chemical Approaches

Generally, fabricating capsules with pH-sensitive weak polyelectrolytes, the charges or ionization degrees along the polyelectrolytes could be controlled by varying the solution pH value. Therefore, the stability of formed multilayer shells is greatly influenced by environmental pH conditions. The examples of polyelectrolyte complexes containing weak polyelectrolytes is shown in Figure 2.9. Typically, PAH, as a weak polyelectrolyte with an apparent dissociation constant pKa = 8.7, has been widely used for capsule preparation and well studied[117]. When the PAH was mixed with equimolar strong polyelctrolyte PSS, the stoichiometric complex formation

PAH/PSS (1:1) showed a large change of the pKa value, shifting to 10.7 at alkaline region[117] (Figure 2.9 a). When the PAH was mixed with equimolar weak poly (methacrylic acid) (PMA, pKa = 6.8), the titration curve of stoichiometric complex formation PAH/PMA (1:1) was divided into two branches, either located in alkaline (pKa = 10.8) or acidic (pKa = 3.9) regions (Figure 2.9 b). The titration curve in alkaline region represented the protonation of PAH (amino groups); while that in acidic region represented the deprotonation of PAM (carboxylate groups) [118].

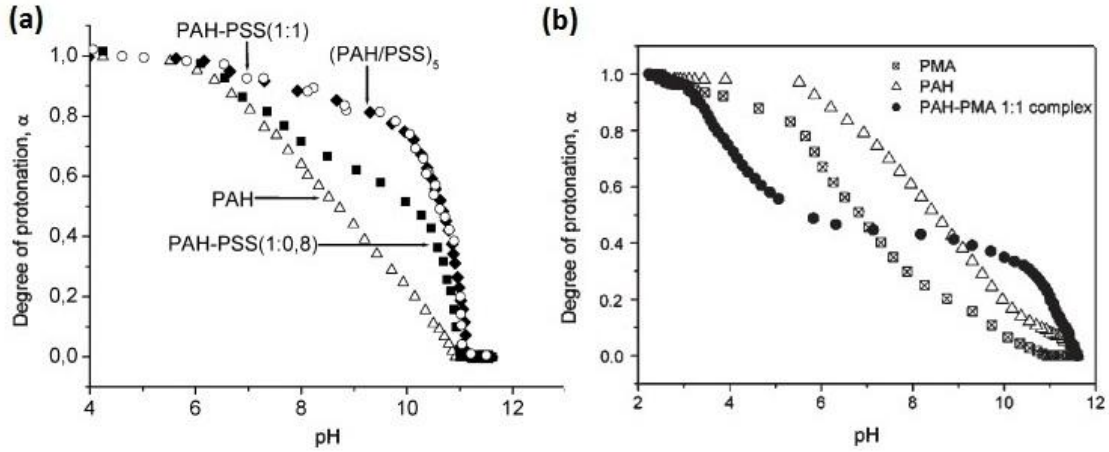

Figure 2.9 Potentiometric titration of PAH/PSS (a) and PAH/PMA (b) complexes.
* The protonation degree α is plotted versus the pH value [32, 117].

Similar shifts in pKa were also found in many cases, where the pKa shifted to alkaline region for polybases and shifted to acidic region for polyacids[119, 120]. Since the dissociation of polyelectrolyte and polyelectrolyte complex is pH dependent, thus the stability of polyelectrolyte multilayer/capsules could be tuned by outer pH, leading to swelling or even dissolution in different pH conditions. For example, the capsules composing of PAH and PMA were found stable in the pH range from 2.5 to 11.5. However, beyond this pH range, the dissociation of polyelectrolyte, either PAH or PMA, was suppressed, which resulted in capsule dissolution due to lack of electrostatic interactions between polyions[118]. Using such capsule stability changes triggered by pH, reversible swelling or irreversible dissolution, encapsulated substances were released in water directly[62] or in living cells[83].

Ionic strength is another parameter that can influence the morphology[47, 121], permeability [122] and stability[123] of multilayer capsules in aqueous solutions, by screening the charges along the polyelectrolyte molecular chains or forming defects in

multilayers; the effect of ionic strength on polyelectrolyte capsules can be easily judged by detecting the diffused cargo substance amount through the multilayers as a function of ionic concentrations[124]. It was found that the formed cavities mostly attributed to the permeability through multilayers. In the mean time, increasing the ionic strength proportionally promoted the permeability increase[124].

2.5.5.3 Biological Approaches

For the ones who care much about the materials science domain, bio-degradable polymers would be their first choices to achieve release due to possible capsule disassembly caused by polymer degradation. This strategy involves employing bio-degradable polymers to build up capsule systems and using biological stimuli to reduce shell integrity and release encapsulated substances. These stimuli mainly originate from enzymatic reactions or hydrolysis. Li and co-workers reported the first study of bio-degradable polyelectrolyte capsules[125]. As in their work, the enzyme (phospholipase A_2) caused hydrolysis reactions on the lipid/polyelectrolyte surface of lipid-coated polyelectrolyte multilayer capsules, which further adjusted shell permeability. Several biopolymers, such as DNA[126], polypeptides[127] and polysaccharides[128], are promising candidates to fabricate such capsules. De Geest and co-workers reported two bio-degradable capsule systems containing polypeptides and polysaccharide[83]. These capsules were decomposed by either enzymatic degradation of poly-L-arginine (pARG) component or hydrolysis degradation of carbonate ester of poly(hydroxypropylmethacrylamide dimethylaminoethyl) (p(HPMA-DMAE)). Degradation of the capsules inside cells is very attractive and practical important for drug delivery, especially for the targeted intracellular delivery[129]. Typical example has been demonstrated for the capsules composing of hyaluronic acid and poly(lysine) (HA/PLL), offering a potential drug delivery vesicle for intracellular use[130]. As shown in Figure 2.10, the bio-degradable microcapsules, both $(HA/PLL)_{4.5}$ as well as $(HA/PAH)_{4.5}$ capsules, were found to be internalized into endo/lyso- somatic vesicles within 2 hours, when they were cultured with macrophages. Then a rapid rupturing of these capsules due to degradation effect intracellular was observed, demonstrating as yellow/orange images representing the overlay of the colors of both capsules and cells in the same focus plane.

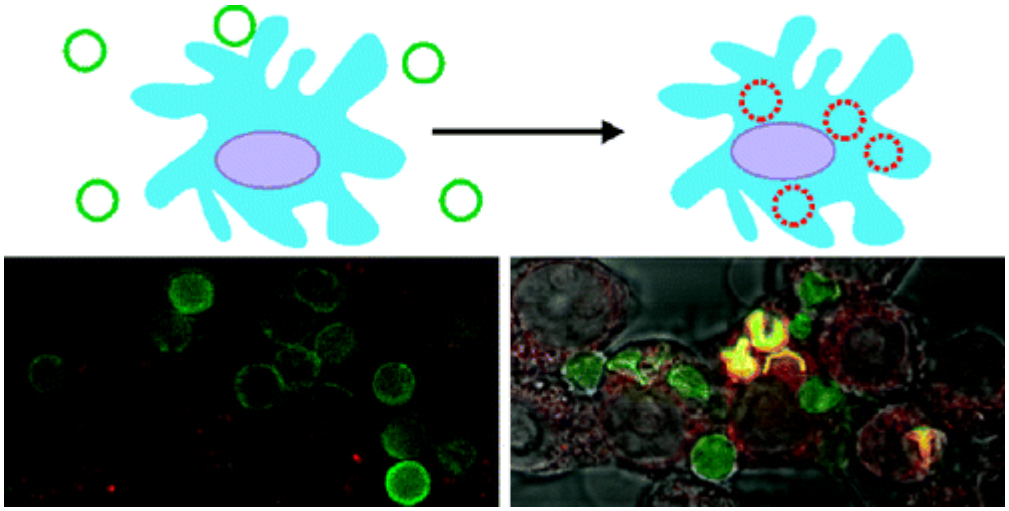

Figure 2.10 Schematic and confocal microscopy images of degradation of the bio-capsules in living cells. * The bottom panel showed confocal microscopy images of bio-degradable capsules after 2 h coincubation with RAW mouse mcarophages. Capsules were stained green fluorescent using HAFITC, while the cellular lysosomes are stained using LysoTracker Red. The left pane gives the overlay of the green and red channel, the right pane was the overlay of green, red, and DIC. Colocalization between the green and red channel is observed as a yellow/orange color[130].

Polyelectrolyte capsules containing glucose sensitive components (glucuronic acid[131], phenylboronic acid[132]) have been devoted to achieve release of encapsulated substance, e.g., insulin. However, no successful capsule decompose based on effect of glucose stimuli have been illustrated.

For all the biodegradable polyelectrolyte capsules inside cells, no external stimulus but the stimuli inside cells is required for their decomposition, providing them high potential for intercellular applications, e.g., gene therapeutics. However, no matter triggered enzymatically, hydrolyticly or by other manners, it is difficult to precisely control over the release of encapsulated substance, which will definitely limit the practical use of such biodegradable capsules.

2.6 Light Stimuli Responsive Capsules

Stimuli responsive capsules are demonstrating numerous functionalities, widely used as promising systems in various areas ranging from medicine, drug delivery to chemical synthesis and catalysis, etc[14, 15]. Polymers/polyelectrolytes are the main components of the capsules multilayers. Thus the capsule properties mainly depend on the properties of the polymers, such as their hydrophobic/hydrophilic properties, molecular weight,

chemical components and functional groups of the molecular chains. All these parameters endow the capsules with special functionalities when they are dealing with various outer stimuli. The classification, basic principles, building blocks, preparation, potential applications, as well as the recent development of stimuli-responsive capsules have been widely studied and reviewed[14]. The stimuli system is too huge and complicated to be discussed in this review. Here this section mainly focuses on the light addressable capsules and their potential applications, with the highlight in the UV responsive capsules and their potential applications.

Light stimuli responsive capsules are capable to affect their micro-/nano- structures come in the form of remote control triggered by external light (e.g., sun light) without requirement of direct contact or interactions. The development of such highly light sensitive vesicles is of great importance, especially in the fields of surface sciences and environmental applications, where sometimes lights would be the only available stimuli to drive the systems. Various strategies were applied to develop light addressable vesicles with different functionalities.

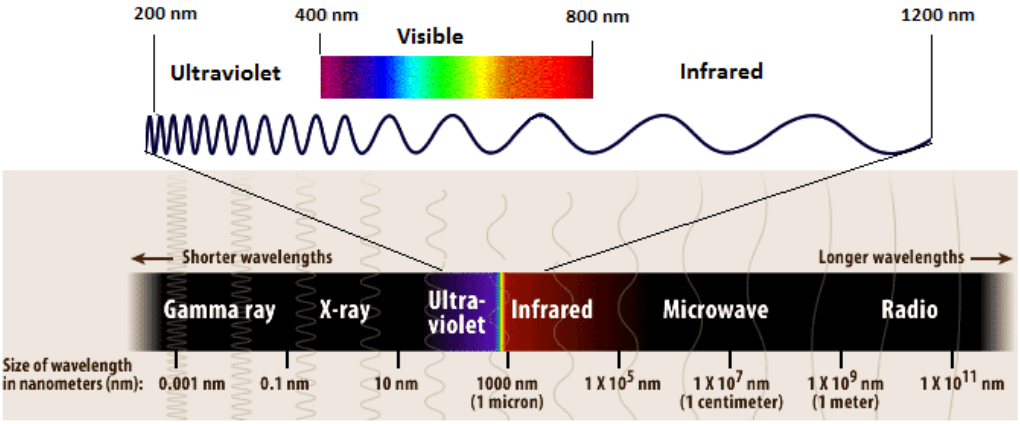

Scheme 2.13 The electromagnetic spectrum.

Light radiation with wavelength in the range of 200~1200 nm is the most studied type of remote trigger for polyelectrolyte capsules (as shown in Scheme 2.13). Mainly, there are two types of light sources commonly used for research, ultraviolet and infrared lights. Ultraviolet (UV) light, the electromagnetic radiation with a wavelength ranging from 10 nm to 400 nm, has been found large number of applications in agriculture, environment and cosmetics areas. UV sensitive vesicle is one of the optimized options for these applications due to the abundant existence of UV light in sunlight. Meanwhile,

Near-infrared (NIR) waves have been found greater interest in turbid medium (e.g., biological tissues or pharmaceutical solids) because of the deep penetration and low light scattering at specific wavelengths[19]. A lot of research works have been done on both UV and NIR lights, here the following section will summarize these work and discuss their underlying working mechanism and potential applications.

2.6.1 Light Induced Chemical Changes

The main chemical constituents of LbL multilayers are primarily of atoms of carbon, hydrogen, oxygen held together by covalent bonds. Upon irradiation of ultraviolet and/or visible light, sufficient energy is introduced to excite or reactive most molecule covalent bonds and atomic valence electrons. Thus the capsule multilayers are capable of absorbing irradiation at certain wavelengths. In the UV-Visible region (the abundant light), shorter wavelength (200 to 400 nm) near ultraviolet region (150 to 70 kcal/mol) is more energetic than the longer wavelength (400 to 800 nm) visible light (70 to 35 kcal/mol) [133] based on the Planck–Einstein equation ($E = hc / \lambda$). As consequence, UV light is most often used in the photochemical reactions.

For LbL capsule application, it has been reported that the UV irradiation causes chemical changes within the capsule multilayers, which led to structural rearrangement and capsule size change. One example has been reported by Katagiri and co-workers[134]. After 2 hours of UV irradiation (20 mW/cm^2) at a wavelength of 365 nm, capsules made of poly(sodium 4-styrenesulfonate) (PSS) and poly(diallyldimethylammonium chloride) (PDDA) were found a size shrinkage of 20% of their original. It was revealed that the UV absorbable aromatic groups can absorb the UV energy, and push chemical transition towards within the multilayers, resulting in the capsule shrinking. And this UV induced process was confirmed by the generation of product SO_4^{2-} ions. Thus it is inspired that UV absorbing chromophoric functional group are good alternative for introducing of UV sensitive properties to capsules. Several chromophoric groups will be discussed, with the emphasis on the chemical groups used in this thesis.

2.6.1.1 Benzophenone

Benzophenone (BP) is an organic compound with the UV absorbable phenyl rings linked by a carbonyl (C=O) group. Basically, the UV absorption of benzophenone and derivates is discrete but extremely complicated owing to the thermal distribution of molecules over many levels of low-lying torsional modes. Principally, BP has two UV absorption bands around 220~300 nm (attributed to the π-π* transition) and 300~380 nm (attributed to n-π* transition), respectively[135]. BPs in different solvents (e.g., ethanol and cyclohexane) with different solvent affinity exhibit a slight difference of UV absorption spectrum, as shown in Figure 2.11[136].

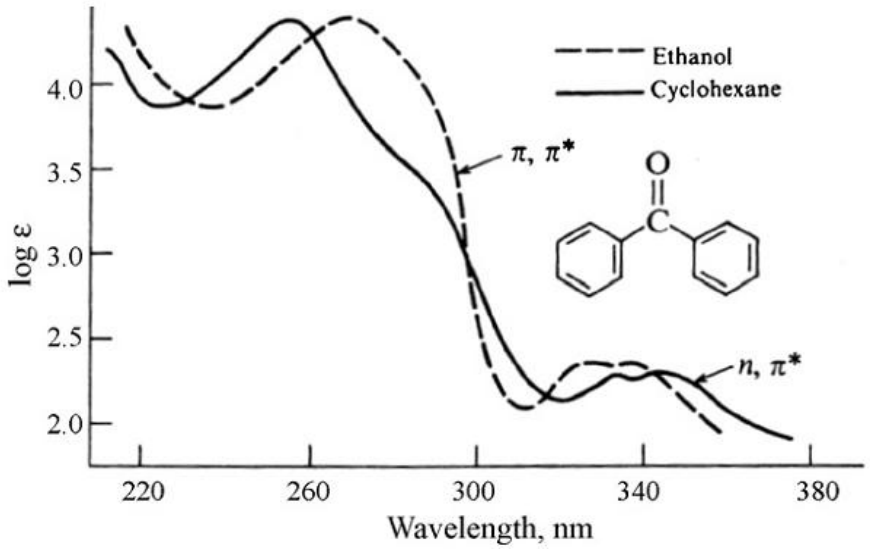

Figure 2.11 UV absorption spectra of BP in ethanol (dotted line) and in cyclohexane (solid line)[136].

Two of the advantages of BPs are their better stability when compared with other chromophors (e.g. diazo esters, aryl azides, and diazirines) and their preferential reactivity with unreactive C–H bonds, even in the presence of water and bulk nucleophiles[137]. These two advantages combine to produce highly efficient and remarkable site specified molecule covalent modifications, which make BPs become of great usefulness in chemical and biochemical applications. Generally, the BP related molecule covalent modification process can be illustrated as shown in Scheme 2.14. First, upon exposure to UV irradiation, electromagnetic energy pushes the electron transition from a nonbonding sp^2-like n-orbital on oxygen to an antibonding π*-orbital of the carbonyl group. Then the electrophilic electron-deficient oxygen n-orbital interacts with weak C–H σ-bonds, leading to a hydrogen abstraction (H–abstraction) in

order to complete the half-filled n-orbital. When amines or similar heteroatoms are proximal to the excited carbonyl, a recombination occurs, resulting in generation of a new C–C bond[137].

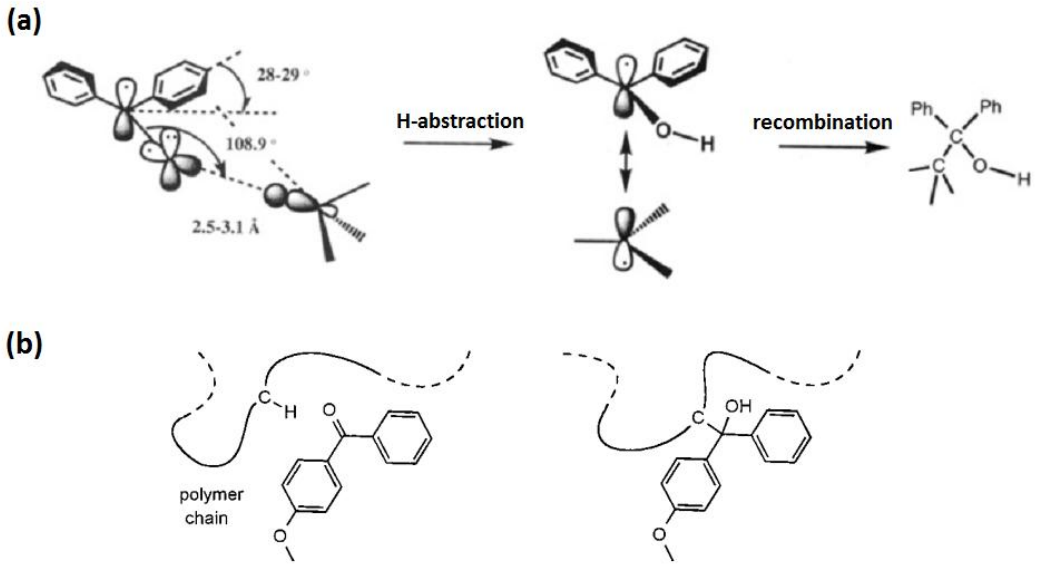

Scheme 2.14 Geometric (a) and schematic (b) representations of the photo-crosslinking *via* hydrogen abstraction of benzophenone derivatives[137, 138].

This basic C–C generation process induced by UV irradiation *via* hydrogen abstraction offers a simple but effective way to remotely crosslink the nearby molecule chains. This distinct crosslinking method endows BP and its derivates great interesting as the subject of optical spectroscopy and photochemistry. From 1980s, BPs have been used as photo initiators in UV-curing applications such as inks, imaging; and the biocompatible BP compounds have been approved as chemical UV absorbers used in products such as makeup and perfumes[139, 140]. In addition, BPs have been used as photoactivatable reagents to functionalize specific C–H bonds remotely in steroids, and further to map chains conformations in various systems, such as micelles and membranes[141, 142]. In biological applications, BPs have been introduced in site-specific photo-crosslinking proteins (e.g. p-benzoyl-L-phenylalanine) to identify and sense the protein-peptide interactions in living cells[143, 144].

To the best of our knowledge, the application of BPs in LbL assembly multialyer system is rare. One research work reported the preparation of the photo-crosslinking multilayer structure composing of benzophenone modified polyelectrolyte. Upon UV

irradiation, a highly stable film can be obtained through BP associated chemical transition[145]. Another research work reported nano-scale hollow particles (~500 nm) made of benzophenone modified poly(allylamine hydrochloride). After UV irradiation (190 mW/cm^2, 3 min), a decreased shell permeability was found, which allowed a controlled release of encapsulated substance (rhodamine B)[146]. For modification of polyelectrolyte microcapsule, BP compounds could be introduced into capsule layers as potential crosslinking sites, which could offer a novel way to crosslink the capsule shells through UV induced H–abstraction and further recombination reactions with adjacent un-reactive C–H bonds. This strategy and possible applications will be discussed in Chapter 4.

2.6.1.2 Azobenzene

Azobenzene (AZO) refers to a class of molecules that composed of two phenyl rings linked by an azo (N=N) double bond. The conjugated chemical structure owes AZO strong electronic absorption in both near-UV and visible light regions. The UV absorption spectrum of AZO and derivatives could be slightly different due to the different ring substitution patterns. But, generally the electronic absorption of AZO exhibits two absorption peaks, a low intensity peak in the visible region (attributed to the n-π* transition), and a more pronounced absorption peak in ultraviolet region (attributed to the π-π* transition), as shown in Figure 2.12 a [147].

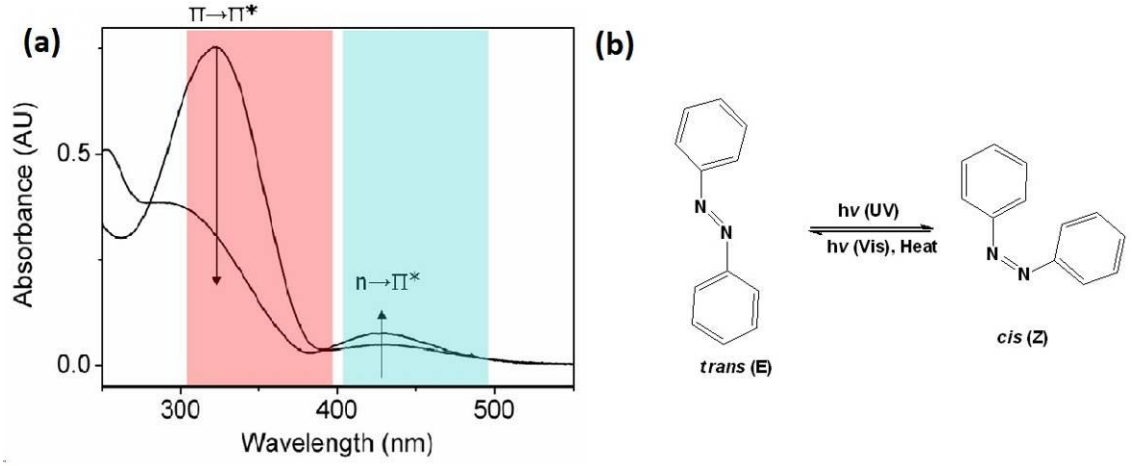

Figure 2.12 UV absorption (a) and schematic representation of reversible *trans-cis* photoisomerisation (b) of AZO molecules[147].

One of the most interesting properties of AZO is the efficient and reversible photoisomerisation behaviour. Normally, AZO exists in a stable *trans* state, upon irradiation at a certain wavelength, the two isomers can be switched from thermal stable *trans* state to metastable *cis* state *via* absorption of a photon within the absorption band. Reversibly, with the addition of proper thermal treatment or irradiation at a wavelength in the *cis* absorption band, the *cis* molecule will be converted back to the *trans* state (as shown in Figure 2.12 b). For the thermal isomerisation, an energy barrier is 90 kJ/mol. Besides, a length reduction of the AZO molecule from 9.0 to 5.5 Å is accompanying with the *trans-cis* isomerization[148, 149]. This *trans-cis* isomerization provides a novel method to facilitate the preparation of photoswichable materials.

It is still a debate on the mechanism of the *tran-cis* photoisomerization of azobenzene. Mainly, two theories have been developed: rotation around the azo bond with a reduced bond order in analogy to stilbenes, or inversion in the plane due to rehybridization of one AZO-nitrogen with small changes of AZO π bond, as shown in Scheme 2.15[150, 151].

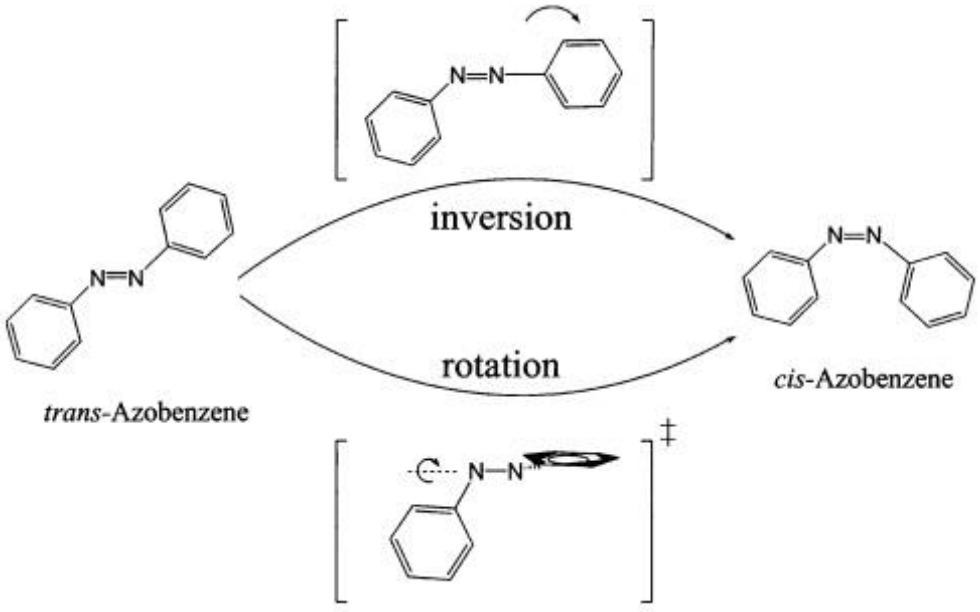

Scheme 2.15 Schematic illustration of *tran-cis* photoisomerization mechanism[150].

With different substituted chemical functional groups (e.g., $–NH_2$, $–NO_2$) extending from the phenyl rings, AZOs are coloured with yellow, orange or red, leading to the subtle shifting of their electronic absorption spectra. In particular, the configuration of pseudo-stilbene class with a pair of *'push-pull'* groups substituting the 4, 4' positions

results in a strongly asymmetric electron distribution, which shifts the absorption of *trans* and *cis* isomers, leading to the overlap of the two absorption regions[152]. An interesting idea would be using a single wavelength to induce a continuous cycling of the forward (*trans→cis*) and reverse (*cis→trans*) photoisomerisation in one system, which might be beneficial for many photoresponsive effects.

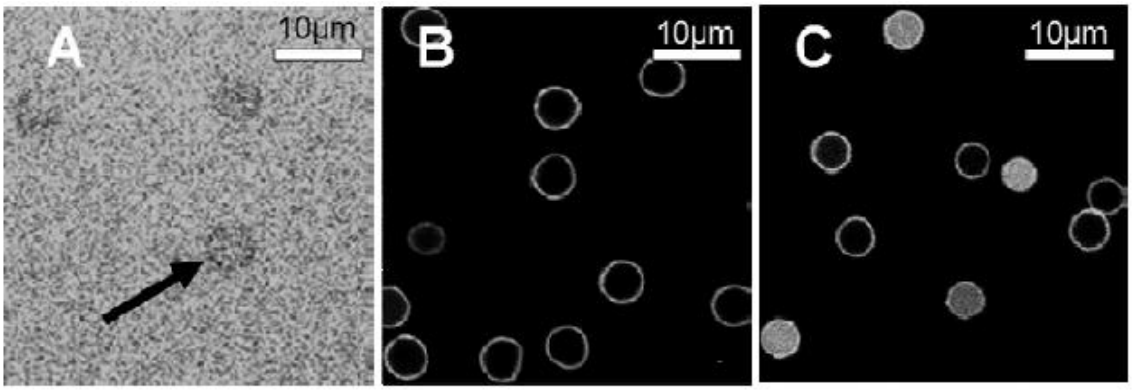

Figure 2.13 LCSM images of (PAH/PAZO)n/PVS capsules, showing the dye permeability with (c) or without (b) UV irradiation[16].

The AZO molecules are rigid and anisotropic, which make them become idea liquid crystal mesogens. However, for other applications, these robust and non-reactive moieties should be incorporated into other materials. Ionic attachment should be an advisable way to introduce the AZOs, due to the resulting homogenous and stable formations[153]. Many research works have been done to introduce small molecular AZO dyes, AZO-functionalized polymers and micelles have already been fabricated [154-157]. The incorporation of AZO chromospheres in LbL multilayers can demonstrate many novel photo-induced changes. Typically, multilayers containing the polyanion poly [1-4[4-(3-carboxy-4-hydroxyphenyl-azo)benzene-sulfonamido]-1,2-ethanediyl] (PAZO) have demonstrated unique photoisomerization effect of azobenzene groups. A light induced encapsulation strategy for microcapsule based on such photoisomerization was first illustrated by Bédard and co-workers[16]. In their work, $(PAH/PAZO)_n$/PVS including the photoactive AZO units were reported to shrink fabricated microcapsules and allow the encapsulation of macromolecules (AF488-Dextran) after irradiation under near-UV light (300-400 nm) (as shown in Figure 2.13). However, the reversible photophysical process of AZO was found somewhat diminished, as the results of irreversible change of the capsule permeability.

Azobenzene-related transitions not only cause the *trans-cis* molecular conformation change in plane, but also cause changes in molecular alignment in domain. Exposure to UV light, depending on mutual orientation of the interacting dipole moments between the counterpart molecules, the AZO molecules tend to form J styled (end-to-end) or H styled (plane-to-plane) aggregates, respectively (Scheme 5.2) [158]. In theory, the changes in molecular alignment can be easily monitored by UV-Visible spectroscopic measurements, illustrating as red- or blue- shift of corresponding maximum absorption. Consequently, these individual self-organized AZO moieties led to polymer chain motions in sub-domains or features, and then anisotropic orientation would further cause a phase separation of neighbouring areas. Several research works based on such photoresponsive micro-crystallization or phase separation have been developed to functionalize related optical storage and liquid crystal systems[159, 160]. For LbL polyelectrolyte capsule, strategy of UV controlled capsule behaviour based on azobenzene molecule re-alignment could be established to adjust their morphology and/or structure stability, which will be discussed in Chapter 5.

2.6.1.3 Diazonium

Diazonium compounds (salts) refer to a group of organic compounds containing a functional group $R–N^{+}{\equiv}NX^{-}$, where R could be organic residue (e.g. alkyl or aryl), and X is an inorganic or organic anion such as a halogen. The diazonium group ($–N^{+}{\equiv}N{:}$) has two different functionalized nitrogen atoms, the charge deficient one (connected to the phenyl moiety) is balanced with the counter ion X^{-}, and the other charge riched one containing a pair of unbonded electrons can react with the strong H donor (e.g., phenolic hydroxy group) to form a hydrogen bond[161, 162]. Diazonium group is very photosensitive, can be decomposed fast and readily when exposed to UV irradiation around 380 nm, which makes the diazonium groups ideally UV light triggered crosslinkable sites based on photolysis.

One of the typical examples of diazonium contained polyelectrolytes used for layer by layer assembly is the diazo-resin (also known as DAR), which has been synthesized in a polycondensation reaction of formaldehyde and diphenylamine-4-diazonium salt, as first reported by Cao et al[163]. DAR has a strong UV absorption around 380 nm which could be assigned to the π-π^{*} transition in the diazonium group[164]. Upon exposure to a 380 nm UV light, the diazonium group is activated to form phenyl cation and then be

substituted by nucleophilic groups, such as carboxylic, phosphate and sulfonate groups, providing a novel light triggered covalent bonding with other compounds[163-165]. Basically, upon exposure to UV light (~380 nm), the polyelectrolyte complexes composing of DAR and the cationic polyelctrolytes or other charged substances can undergo a chemical transition from weak ionic interaction to covalent bonding, leading to readily crosslinked complexes. This brilliant strategy has been accomplished in various systems to fabricate formations with different architectures and properties, such as composite ultrathin films containing magnetic particles [166], single-walled carbon nanotube[167] and DNA[168], DAR/pectin films for cell culture supports[169], as well as fancy "giant" hollow capsules (> 280 μm)[170]. Specially, a novel feature of the DAR contained capsules would be able to seal the capsules and to entrap the cargo substances for the possible application in the field of delivery, biosensors and controlled release.

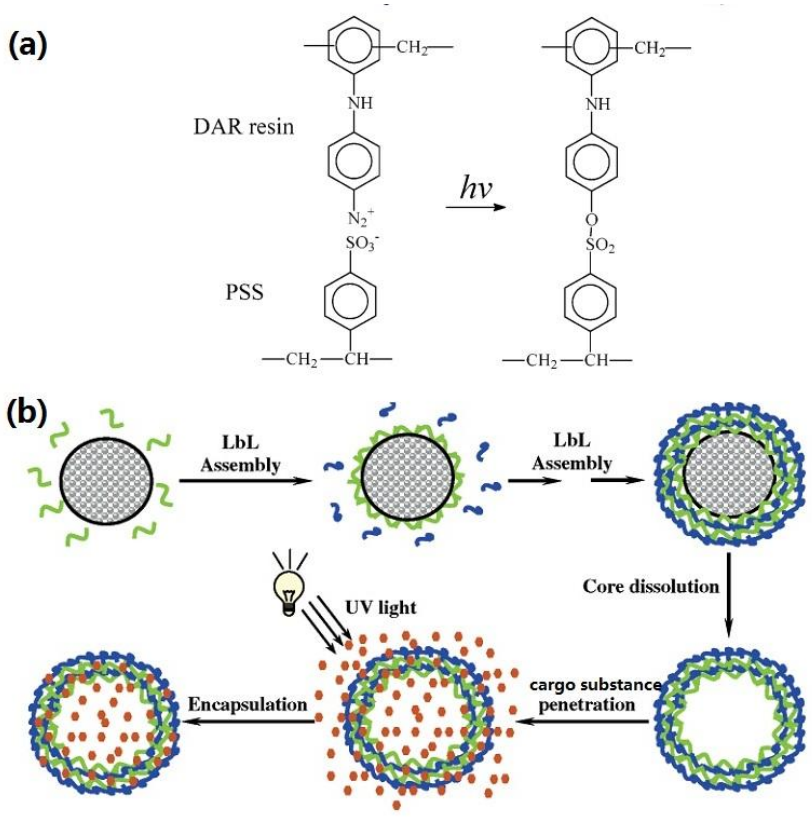

Scheme 2.16 Schematic illustration of substance encapsulation in DAR-based microcapsules[104].

Generally, after capsule fabrication and cargo substance penetration, the DAR-realted photolysis (Scheme 2.16 a) could decompose the diazonium group and converted ionic

groups ($–N_2^+$ and $–SO_3^-$) to covalent ester bond ($–SO_3–$), further provides tight crosslinking to seal the porous capsule shells, resulting in decrease of shell permeatbility and retention of cargo substances (Scheme 2.16 b). As presented in Zhu's work[104], the microcapsules composing of DAR and PSS could be demonstrated as a stable enzyme encapsulation technique, which was benefited from the DAR-related shell crosslinking triggered by UV light. And the encapsulated enzyme exhibited high (52.8 %) catalytic activity compared with the same amount of free enzyme, illustrating good preservation and sufficient transport rates for cargo substances.

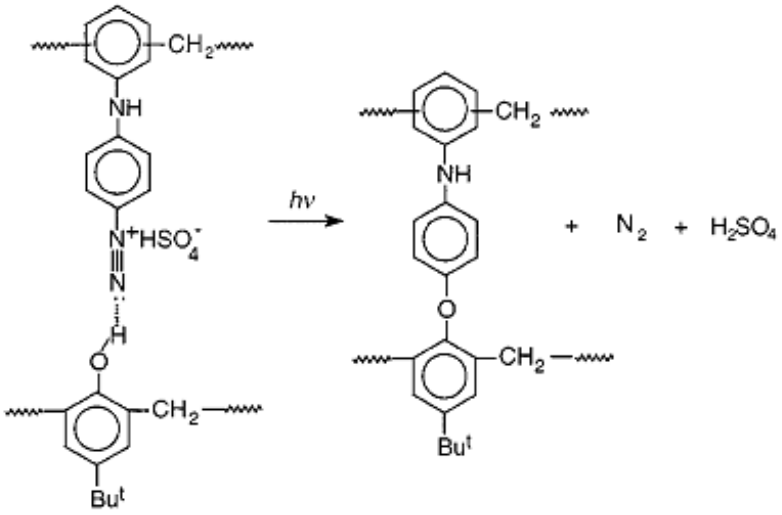

Scheme 2.17 The photoreaction of diazo-resin (DAR) and phenol-formaldehyde resin (PR) in a self-assembled film[162].

As mentioned above, one of the two nitrogen atoms carries a pair of unbonded electrons, which can react with strong H donors. Thus, the DAR is easy to build up multilayers with the other (non-charged) polymers/substances *via* H-bonding attraction between N^+N: of DAR and strong hydrogen donors (e.g., –OH) of counterpart polymers[162]. Typical examples have been presented by Cao[161, 162], basic mechanism was given in Scheme 2.17. In this new multilayer system, it was the H–bonding not the electrostatic interactions that pushed forward the polymer deposition. And it was reported that after UV irradiation, the covalent bonds formed in the multilayers as a consequence of diazonium group decomposition. Specially, it was confirmed to be a very useful method to fabricate stable ultra-thin film from a precursor film formed *via* H–bonding. Although there is no UV responsive microcapsule based on such strategy reported by our colleagues, it still would be a promisingly method to fabricate stable multilayer

capsules composing of DAR and other components *via* H–bonding and further photolysis.

2.6.1.4 o-Nitrobenzyl

Other chemical compounds could also cause related chemical transitions within the multilayers, which would also benefit the functionalization of capsules. Here, the o-Nitrobenzyl derivative will be discussed as an example, which could be introduced into UV-responsive LbL capsule.

Unlike other chemical groups, which are photo-crosslinkable and re-alignmentable, o-Nitrobenzyl (ONB) and derivatives would be the most popular and well studied type of photoremovable protecting groups. Different form the BP, AZO and diazonium groups discussed above, o-Nitrobenzyl is a class of light mediated chemical bond cleavable (or removable) groups, providing a simple and efficient method for the remote cleavage of substrate molecule chains. Normally, a photoresponsice initiator (ONB) is used to couple hydrophilic and hydrophobic chains to generate a photo-responsive amphiphilic block copolymer [171]. After exposure to near-UV light (> 320 nm), a rapid ester cleavage occurs, leading to decoupling of the substrate system, and providing full activity of the two separated molecule chains, as shown in Scheme 2.18.

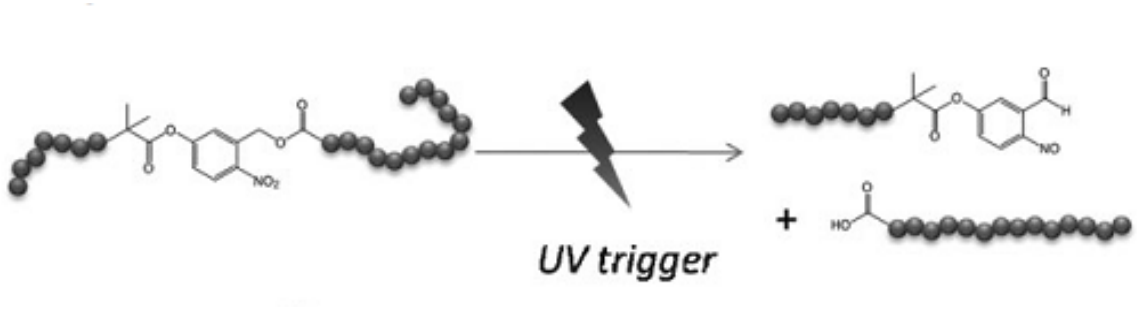

Scheme 2.18 Photocleavage of ONB-coupled amphiphilic copolymer triggered by UV light[171].

Photocleavable ONB and derivates have been widely used in protein mapping and organic synthesis areas. Thompson and co-workers reported a convenient method to build up large molecule proteins with sufficient photo-removable groups to inhibit its biological function without using the highly specific cite-directed manner[172]. For drug delivery system applications, various systems have been studied. Interaction with light induced deconstruction of the self assembly vesicles have been demonstrated with

various architectures, including nanoparticles[173], micelles[174] and liposome[175]. The use of ONB derivatives allows for spatial and temporal control of such vesicle deconstruction, facilitating possible light (UV specifically) triggered application such as imaging, sensing and most importantly, delivery. For delivery system, Meier and co-workers reported a potential light-triggered nanocarrier system trough self assembly of a photocleavable amphiphilic block copolymer. After exposure to UV light, this amphiphilic carrier disintegrate, generating small micellar-like structure, and simultaneously release their encapsulated substances[171, 176].

Another outstanding feature of ONB is its ability to be cloven by bio-friendly near-infrared (NIR, 700-1000 nm) irradiation[177]. With the ability of cleavage triggered by both UV and NIR light, ONB could be a very useful chemical group to trigger release the encapsulated cargos. However, to date, no work has been associated with LbL capsules. Strategically, if the ONB was introduced into polyelectrolyte chains to build up multilayer capsules, both UV and NIR light can be used to adjust the capsule permeability selectively and even to deconstruct the shell formation gradually from the outer layer to inner layer with the breakage of the polyelectrolyte chains. Thus, these UV and NIR responsive ONB capsules would serve as smart, triggerable vesicles that can be applied to release encapsulated substances when directly exposure to sunlight, or to release the encapsulated substances in living cells or organs under irradiation of NIR lasers.

2.6.2 Light Induced Local Heating

How to release the encapsulated substances in specific sites without affecting their activities is still a challenging task. As one of the strategies to solve this stated problem, light induced local heating for remotely activation of the release of encapsulated materials using light is recently developed. After exposure to light at a certain wavelength, metal and/or metal oxide nanoparticles inside the capsule shells could absorb the radiation energy, and then generate local heating as the consequence of energy release.

For example, if a spherical gold nanoparticle (GNP) is much smaller than the light wavelength (3~80 nm)[178], an electromagnetic frequency will predominantly generate a local surface plasmon resonance (LSPR) oscillation at the surface of GNPs. The

oscillation of LSPR decays by release its energy in the form of light scattering or heat[179]. The generation of heat affects the local environment, and facilitates the enlargement of holes on capsule shells (Scheme 2.19-2). Furthermore, continuous treatment of intensive laser lead to the deconstruction of the capsule shells (Scheme 2.19-1). Thus, the light induced release can be achieved by the process of 1) multilayer melting caused by local heating as a result of conversion of absorbed light to heat, and 2) multilayer swell or deconstruction caused by increased thermal stresses within the capsule shell [180].

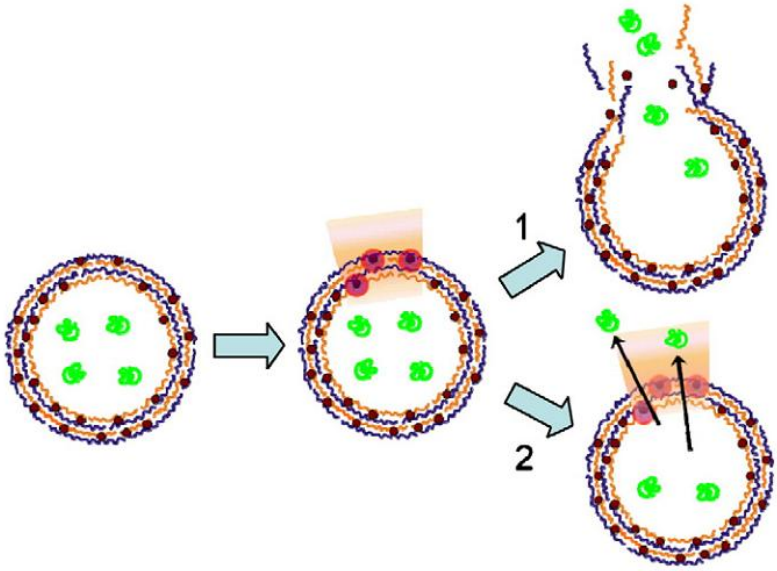

Scheme 2.19 Two possible release scenarios of encapsulated material by the laser nanoparticle interaction.

* (1) Upon illumination, the nanoparticles produce a large amount of heat that breaks the capsule wall open. (2) During illumination, the nanoparticles produce a small quantity of heat sufficient to exceed the glass transition of the polymer complex of the capsule, decreasing the shell's permeability until illumination is stopped. The increased permeability allows for encapsulated material to be released from the capsules without the shell being damaged [147].

2.6.2.1 Gold and Silver Nanoparticles

The most popular and well studied type of metal particles used in biomedical application is gold nanoparticles (GNPs). Gold nanoparticle synthesis, physical-chemical properties as well as the combined applications with biological and biocompatible ligands in various areas including sensing, diagnostics, therapy have been widely studied and summarized[178].

Predominantly, GNPs can absorb light in the visible range (400~800 nm). Due the LSPR effect, GNPs in the 10 nm size range have a strong absorption maximum around 520 nm in water. Increase the size to 40 nm, the absorption shifts to 530 nm due to the red shift effect. For biological applications, a desirable optical light region ranging from 700 nm to 1000 nm is preferred. In this radiation window, light has a high transmission and low scattering of biological medium[181], which would facilitate the site specified release without causing severe damage to surrounding medium, especially for biological applications. For this reason, strategies were developed to shift the light absorption position of GNPs to, the so called "biologically friendly window", near infrared (NIR) region.

One way of tuning the red shift is to change the shape of gold nanoparticle, for example from spherical to rod-shaped. As shown in Figure 2.14 a, changing the shape of gold particles from spherical to rod-like shifted the maximum absorption from 530 nm to 1050 nm[182]. Interestingly, nanoparticles with rod-shape have two resonances: one along the short axis, another one along the long axis. The plasmon oscillation of the nanorod strongly depends on its aspect (length to width) ratio; with increase of the nanorod aspect ratio, the long-axis LSPR effect pushes red-shifting from the visible to NIR with the accompanied increase of oscillator strength[183]. Thus, the tuning of red-shifts can be easily controlled by adjusting the shape or aspect ratio of gold nanoparitcles *via* the seeded growth method[184, 185].

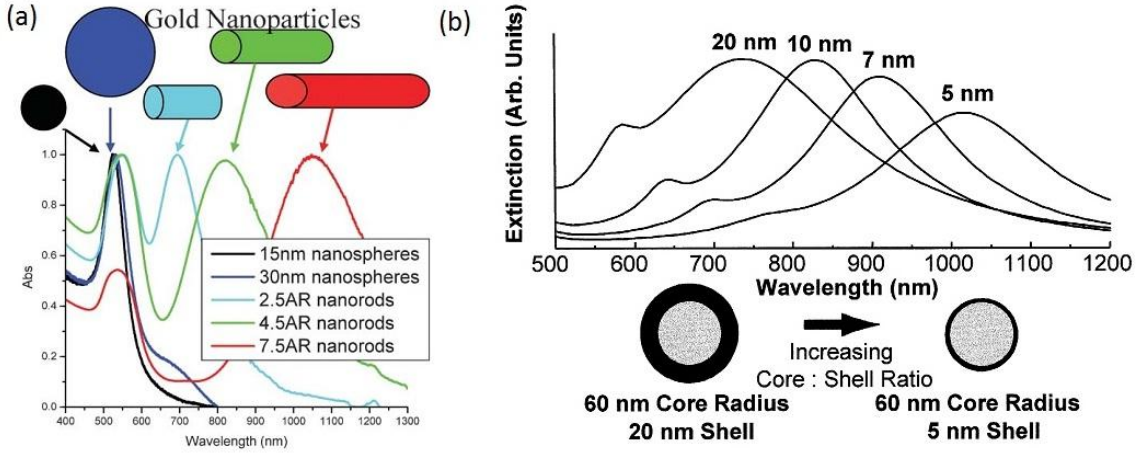

Figure 2.14 UV-Vis spectra of gold nanoparticles of various sizes and shapes.

* (a) Detected gold nanoparticles- absorption of various sizes and shapes[182]. (b) Theoretically calculated optical resonances of metal. Theoretically calculated optical resonances of metal nanoshells (silica core, gold shell) over a range of core/radius thickness ratios[186].

Metal nanoshells offer another method to red-shift the absorption position[186], as shown in Figure 2.14 b. Decreasing the nanoshell thickness deposited on the silicon particle surface, the absorption shifts from the visible to NIR region due to increased coupling between the inner and outer shell surface plasmons. The LSPR could be tuned *via* controlling the ratio of shell thickness to core radius. The integrity of the gold nanoshell and the substrate particle perform as a strong light absorber in NIR region, offering a good approach for thermal therapeutics applications. After exposure to NIR light (820 nm, 35 W/cm^2), the human breast carcinoma cells incubated with gold nanoshells exhibited a local cell death effect. Likewise, tumour tissue treated with gold nanoshells exhibited an irreversible local damage after exposure to low doses of NIR light (820 nm, 4 W/cm^2)[187].

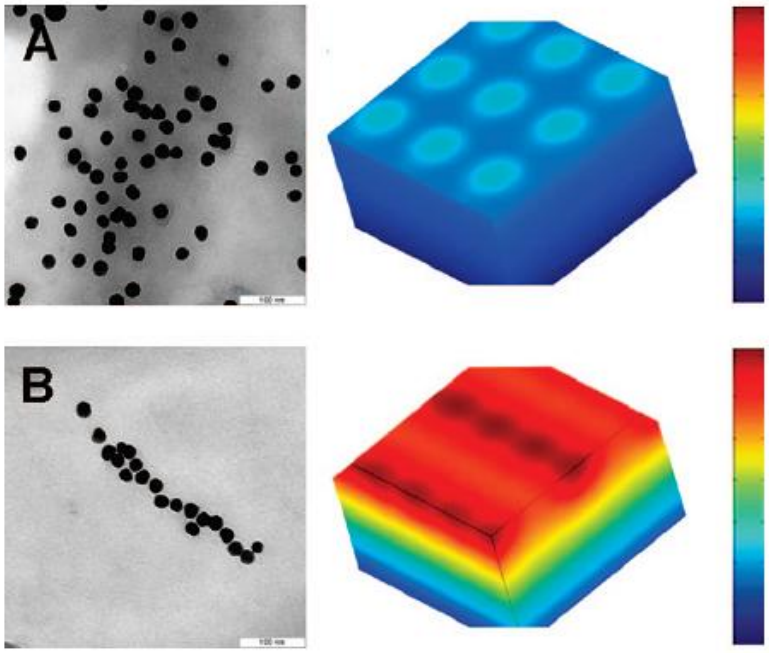

Figure 2.15 Modeling the temperature distribution for non-aggregated (top) and aggregated gold nanoparticles (bottom).

* Nonaggre-gated nanoparticles do not possess absorption in the near-IR part of the spectrum. For 20 nm nanoparticles, the absorption coefficient is about 0.02 at 830 nm, so the temperature rise at 50 mW of incident power is less than 1 degree. For a single line of four aggregated nanoparticles, a temperature rise of 7 K can be produced (red). TEM images of uniform distribution and aggregatesof nanoparticles are shown on the left side of corresponding simulations. The scale bars for the TEM images are 100 nm[19].

The third method of red-shifting the LSPR is to control the distribution of gold nanoparticles in the multilayer shells. Usually, the colloidal gold naonparticles applied

in the LbL process are single ones. To control the distribution state, gold nanoparticles could be aggregated by pre-mixing the dispersive gold nanoparticle suspension with oppositely charged mixing components (molecules or NaCl solution) [19, 44]. Upon aggregation, gold nanoparticles assemble to form bigger clusters. Due to the inter-particle plasmon coupling effect, these gold clusters exhibit a maximum absorbance above 600 nm. It is also found that different mixing components can result in different gold aggregates with string-like or ball-like morphologies. And it seems that the ball-like aggregated gold clusters show a more pronounced absorbance (~700 nm) than the string-like ones. Controlling the distribution state of gold nanoparticles not only develop an absorbance at longer wavelength, but also generate a bigger surface area for the laser illumination. Exposure to laser illumination at 830 nm, aggregated gold nanopaticles was estimated to get a 5 times increase of absorption coefficient [188], and a linear assembly of four gold nanoparticles can produce up to 7 K of temperature rise in comparison with less than 1 K of a single nanoparticle[19], as demonstrated in Figure 2.15.

Light induced local heating as the consequence of absorption of light in surface plasmon region can be developed as novel strategies to affect the capsule shells. NIR pulsed lasers with different wavelengths has been applied to investigate the capsule deconstruction effect. Modulated NIR pulse lasers (1064 nm) with different intensity (30~700 mJ/cm^2 per pulse) were used to investigate the shell rupture effect of polymeric multilayer capsules cooperating with one or more layer of densely packed GNPs. After a 5 min of continuous 1064 nm laser irradiation, a moderated laser dosage (30 mJ/cm^2) started to break the capsules, further increase the laser dosage to 50 mJ/cm^2, no capsule outline cannot be discerned[106].

The NIR illumination with a wavelength at 840 nm showed a sophisticated optical opening of the inner capsules of the shell in shell microcapsules, which triggered the release of encapsulated substance (fluorescent labeled dextran, 150 kDa) into a larger container, realizing a novel way for bioreactions application in a confined volume[105]. Using the gold nanoparticles and NIR LSPR, encapsulated substances, for example drug, biomolecules, can be easily delivered to the living cells. Parak et al. demonstrated the capsule shell rupture caused by moderate intensity (2.3 mW) NIR laser (830 nm) induced heating of the gold sulfide/gold nanoparticle in the shells[107]. The

disintegration of capsule wall led to release of the encapsulated substance in living breast cancer cells without causing significant cell damage (Figure 2.16).

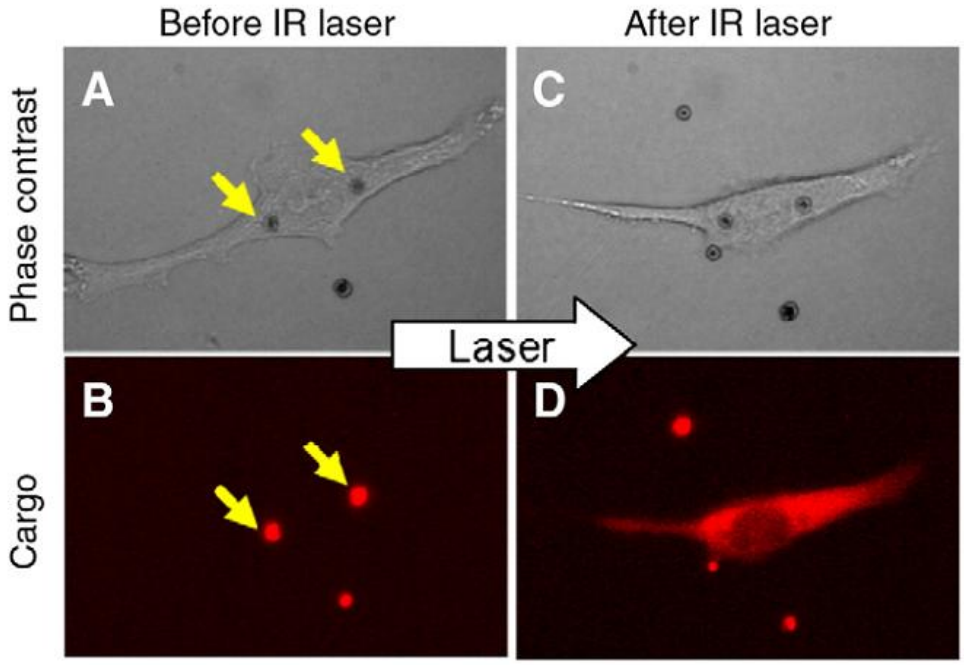

Figure 2.16 NIR laser induced release in living cells.

* Before irradiation, capsules were ingested by living cells with no uncontrolled release of the encapsulated cargo (A, B); upon exposure to NIR laser (830 nm), light induced heating of the gold nanoparticles in the capsule shells lead to rupture of the capsule shells, released the encapsulated cargo (C, D) [107].

As another kind of noble metal, silver is also used as remote triggers for laser illumination applications in the form of nanoparticles. Mainly, the silver nanoparticles have absorption bands in the visible region (380-500 nm); typically, silver nanoparticles in the 10 nm size range have an absorption maximum around 390 nm[189]. Similar as gold nanoparticles, the changes of particle size[190], shape[191], as well as junction[192] also have effect on the absorption spectra of silver nanoparticles, and further to push forward the red-shift progress. Particularly, silver nanoprisms (with 100 nm in width and 50 nm in height) with high sensitivity (200 nm/RIU)[193], have been used as sensors for Alzheimer's disease research[194] and single-particle assays study [190].

2.6.2.2 Titanium Oxide Nanoparticles

Nanosized titanium dioxide (TiO_2) and related titanium composites have been well studied due to their excellent catalytic and oxidative properties. TiO_2 nanoparticles have been widely used as approved inorganic UV absorber in sunscreen cosmetics due to their strong UV absorption in UV region around 360 nm[195]. Many attempts have been made to prepare TiO_2 and/or composites with enhanced UV absorption or red-shift the light absorption to visible region. These methods, such as doping (with transition metals[196], non-metal carbon[197], sulfur[195]) and coupling (with semiconductor[198]), have improved the UV-Visible absorption of TiO_2 and related composites, making them become better candidates in surface science and environmental applications, where light (mainly UV light) would be the only available external stimulus. Sasaki et al., reported the fabrication of self-assembled multilayer films composing of TiO_2 nanoparticles/nanosheets and polyelectrolytes on various substrates[199]. After UV irradiation, bridging polymers between the nanoparticle and/or nanosheet layers could be decomposed, resulting in inorganic multilayer films. Katagiri et al., reported a UV-responsive organic-inorganic hybrid capsules composing of binary inorganic oxide system (SiO_2/TiO_2) and polymeric bridging multilayers[200]. These hybrid capsules showed strengthened mechanical integrity resulting from the inorganic component. In addition, exposure to UV light, these capsules showed a UV induced rupture due to the existence of UV absorption of TiO_2 component at low irradiation intensity (up to 20 mW/cm^2). Besides the UV-Visible responsive properties, capsules composing TiO_2 nanoparticles possess improved mechanical integrity resulting from the incorporated metal components, which may offer them with mechanical properties in solid-state applications.

3. Materials, Methods and Instruments

3.1 Materials

Poly(methacrylic acid) (PMA, 100 kDa) was purchased from Polysciences Inc. (USA). Nafion® perfluorinated resin (aqueous dispersion), Poly(allylamine hydrochloride) (PAH, 70 kDa), Poly[1-[4-(3-carboxy-4-hydroxyphenylazo) benzenesulfonamido]-1,2-ethanediyl, sodium salt] (PAZO, ~100kDa), Poly(diallyldimethylammonium chloride) (PDADMAC, 100-200 kDa, 20 wt. % in H_2O), Poly(styrenesulfonate sodium salt) (PSS, 70 kDa) were purchased from Sigma-Aldrich.

9-Bromo-1-nonanol, Calcium chloride dihydrate ($CaCl_2$ $2H_2O$), N,N′-Dicyclohexylcarbodiimide (DCC), 4-(Dimethylamino) pyridine (DMAP) , Diphenylamine-4-diazonium salt (Variamine Blue RT Salt), Ethylenediaminetetraacetic acid (EDTA), 4-Hydroxybenzophenone, R-Limonene, Paraformaldehyde, Sodium carbonate (Na_2CO_3), Sodium sulfite (Na_2SO_3), Zinc chloride ($ZnCl_2$) were purchased from Sigma-Aldrich.

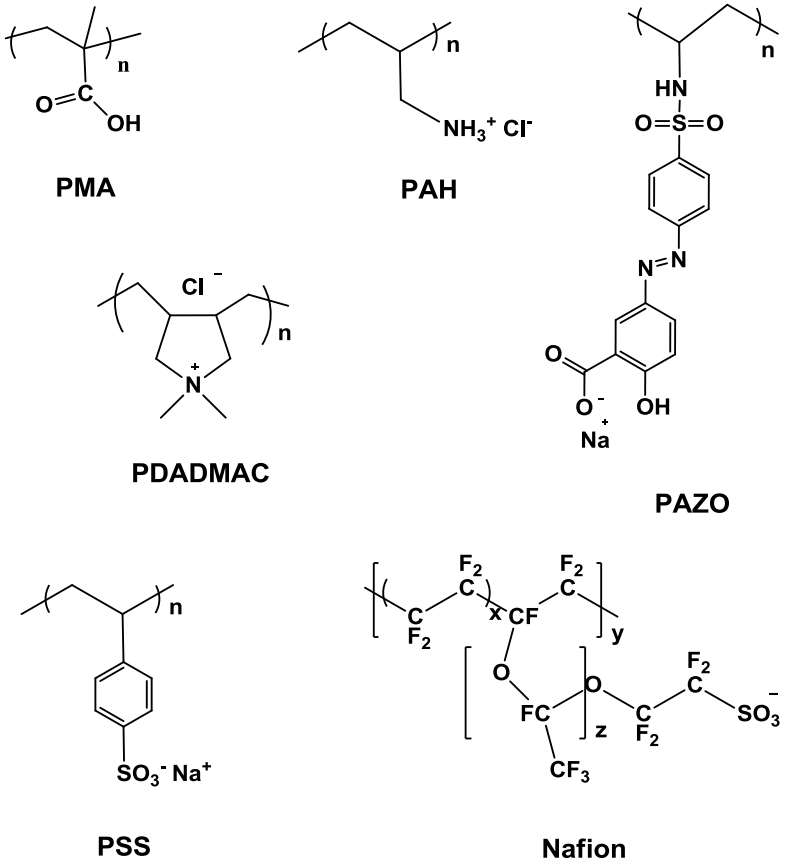

Scheme 3.1 Structural formulas of polyelectrolytes used for capsule preparation.

Monodisperse silica particles (SiO_2, 4.99 ± 0.22 μm, 5% weight dispersion) were purchased from Microparticles, GmbH (Germany).

Gold nanoparticles suspension (20 nm, ~7.2×10^{11} particles/ml, and stabilized in 0.1 mM PBS, reactant free) was purchased from Sigma-Aldrich.

Alexa Fluor®488 labeled- dextran (AF488-dextran, 10 kDa) was purchased from Invitrogen. Bovine serum albumin (BSA, 66 kDa), Fluorescein, Rhodamine B (RhB), Rhodamine B Isothiocyanate (RBITC), Tetramethylrhodamine isothiocyanate–Dextran (TRITC-Dextan, 500 kDa), were purchased from Sigma-Aldrich.

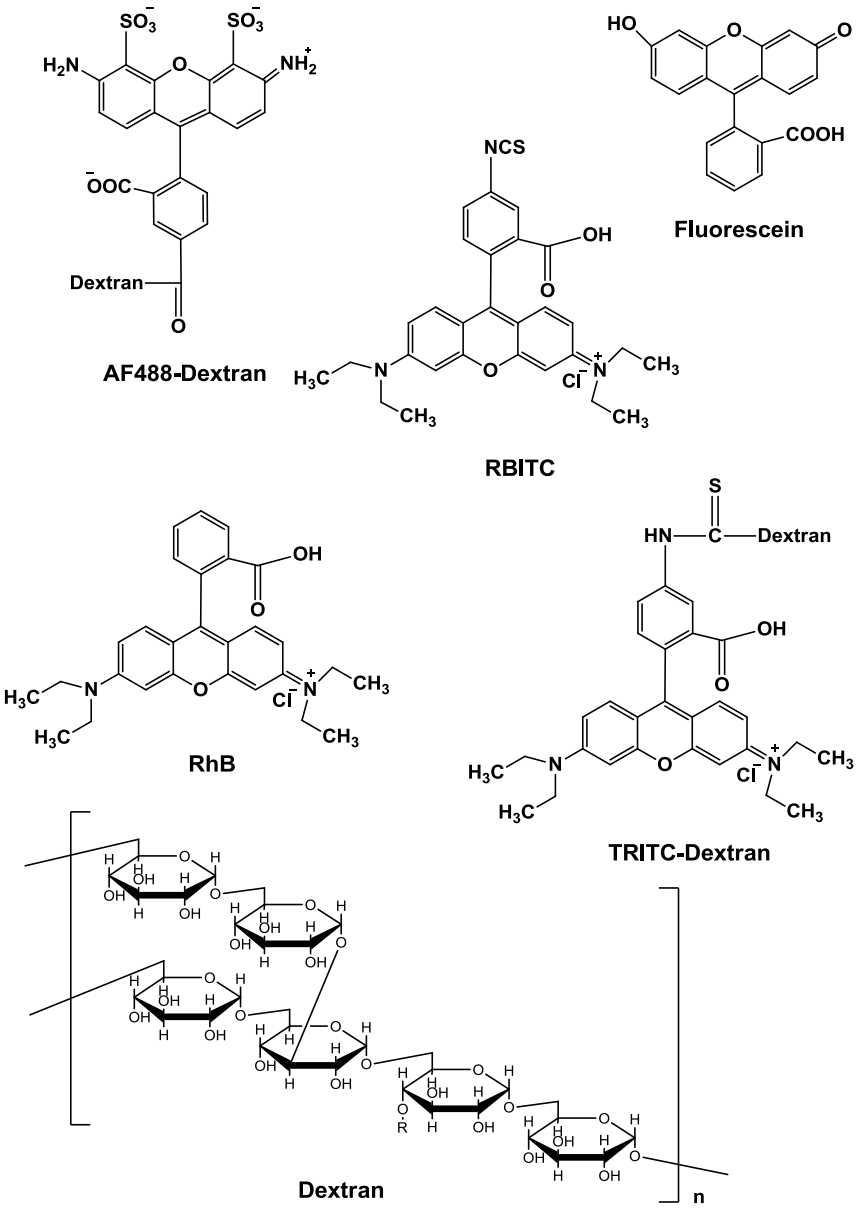

Scheme 3.2 Structural formulas of fluorescent polymer and monomers.

Ammonium fluoride (NH_4F), Ammonium hydroxide (NH_4OH, 28% NH_3 in H_2O), Hydrofluoric acid (HF, 48 wt. % in H_2O), Hydrogen peroxide (H_2O_2, 30%), Sulfuric acid (H_2SO_4, >95%) and other chemicals were purchased from Sigma-Aldrich.

All the chemicals were used as received without further purification. All solutions were prepared with water from three stage Millipore Milli-Q 185 water purification system (Millipore, USA) with a resistivity higher than 18.2 Ω·cm. All the commercial available polymer/polyelectrolytes used to prepare polyelectrolyte/multilayer capsules were illustrated in Scheme 3.1. All the bought fluorescent polymer and monomers were presented in Scheme 3.2.

3.2 Polymer Synthesis and Fluorescence Labelling

3.2.1 Synthesis of Benzophenone-Substituted Poly(methacrylic acid)

The synthesis process of benzophenone-substituted poly(methacrylic acid) (PMA-BP) was shown in Scheme 3.3. First, 4-(9-Hydroxynonyloxy) benzophenone was synthesized in the same way as previously reported[145]. Then, Benzophenone-Substituted Poly(methacrylic acid) was synthesized. Briefly, PMA (2.0446 g, 23.75 mmol) was dispersed in 30 ml Dimethyl sulfoxide (DMSO), 4-(dimethyl-amino) pyridine (DMAP, 1mmol) and 4-(9-hydroxynonyloxy) benzophenone (2.5 mmol) were added at 0 ℃. The mixture was then stirred for 1 hour and N, N′-dicyclohexyl carbodiimide (DCC, 2.5mmol) was added in three times in 30-min interval. After 6 hours, the reaction was left overnight and the solution temperature was increased to room temperature gradually. After the reaction, the insoluble substance was filtered and the filtrate was concentrated under vacuum. The filtrate was re-precipitated to large amount of acetone and dried under vacuum.

The product of PAM-BP was confirmed by the ^{1}H NMR spectrum (D_2O, 600MHz, Brucker) (as shown in Figure 13) : δ (ppm) 1.13-1.15 (t, –C**H**$_3$), 2.19 (s, –C**H**$_2$–), 3.59-3.63 (m, O=C–O–C**H**$_2$–, –C**H**$_2$–O–BP), 2.78-3.01 (m, – (C**H**$_2$)$_6$–), 4.68 (s, **H**$_2$O) , 7.82-7.99 (m, H of **BP** group). The degree of benzophenone substitution was calculated from rationalizing and comparing the integration values of single protons from the methylene groups (O=C–O–C**H**$_2$–, –C**H**$_2$–O–BP) (Figure 3.1, peak c; representing the

portion of BP) against that of the methyl groups (Figure 3.1, peak b; representing the portion of PMA backbone), and it was determined to be ~50 %.

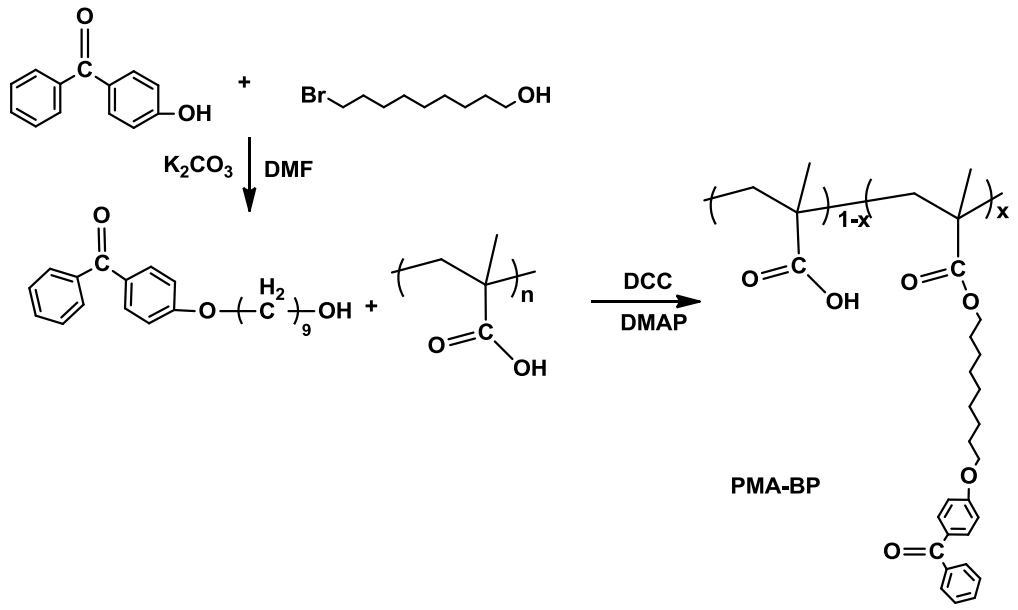

Scheme 3.3 Synthetic scheme of benzophenone-substituted poly(methacrylic acid), PMA-BP.

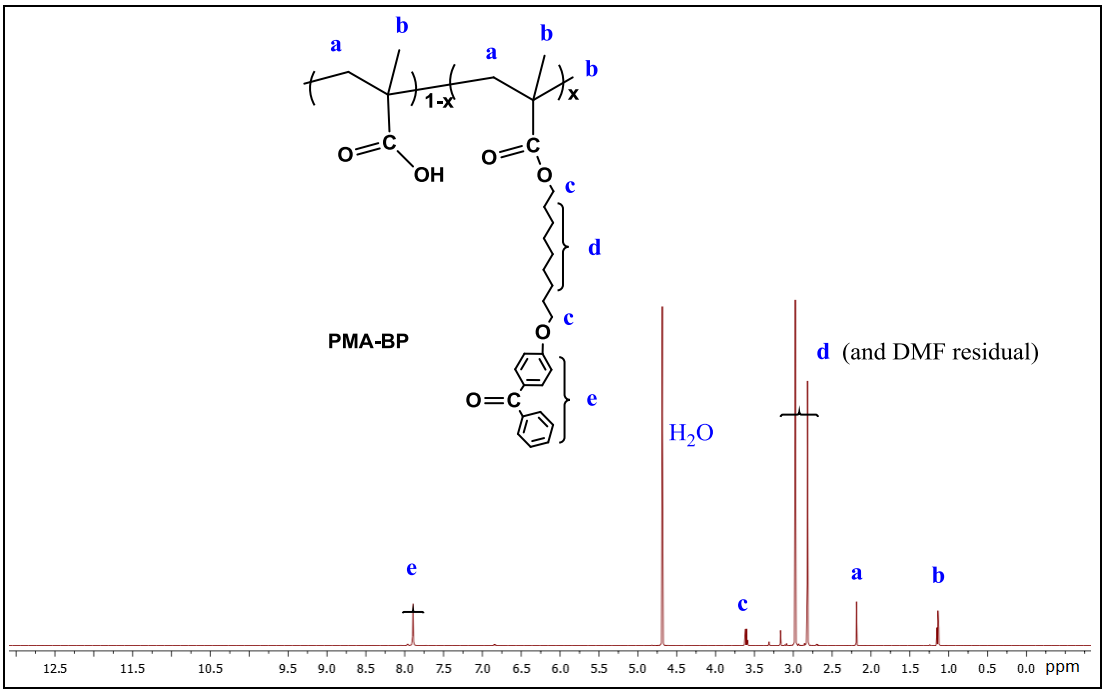

Figure 3.1 ^{1}H NMR (D_2O, 600MHz) spectrum of PMA-BP.

3.2.2 Synthesis of diazo-resin

Diazo-resin (DAR) was synthesized through a polycondensation reaction of diphenylamine-4-diazonium salt with paraformaldehyde, following an electrophilic

mechanism, as reported by Cao et al (Scheme 3.4)[163]. Briefly, 4.7 g (0.016 mol) of diphenylamine-4-diazonium salt and 10 ml of concentrated H_2SO_4 was added to a 50 ml flask. Then 0.5 g (0.167 mol) of paraformaldehyde was added in several batches at ~ 0 ℃ (ice cooled). The reaction was left stirring for 4 hours at this temperature. Then the resulting mixture was dissolved in 25 ml of cold water (0~5 ℃), and precipitated out with 2.2 g of $ZnCl_2$. After purification and drying in vacuum, a yellow-green powder (as a ½ $ZnCl_2$ complex) was obtained and used for capsule preparation. All the operation was carefully performed in the dark.

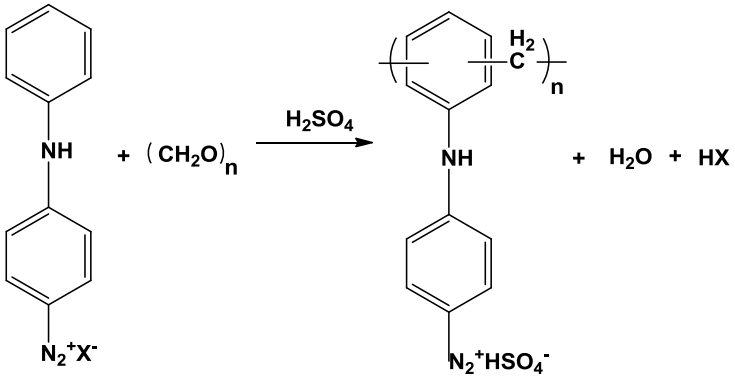

Scheme 3.4 Preparation of diazo-resin[163].

3.2.3 Preparation of Fluorescently Labelled PAH

Rhodamine B isothiocyanate labeled PAH (RBITC-PAH) was prepared as a fluorescent polyelctrolyte. Briefly, 100 mg PAH was dissolved in 40 ml borate buffer (pH was adjusted to 9.0 with 0.1M NaOH). And then a solution of 4.32 mg of RBITC dye (in 5ml ethanol) was added to the PAH solution (at a molar ratio of 1:100, dye: amino group) under vigorous stirring for 12 hours. To remove unbound dye, the mixture was dialysed against water (resistivity 18.2 MΩ·cm) in a dialysis membrane (Carl Roth GmbH + Co. KG, Germany) with a cutoff 14 kDa for one week in fridge after reaction (~ 4 ℃). The resulting RBITC-PAH was freeze-dried and kept in dark for further study.

3.3 Methods

3.3.1 Capsule Preparation

Multilayers were assembled on the templates by using the layer-by-layer technique as described previously[66]. Prior to the assembly, SiO_2 particles (4.99 ± 0.22 μm,

Microparticles GmbH) were first cleaned with a solution of 25 % NH_3 : 30 % H_2O_2 : H_2O (1 : 1 : 5) for 15 min at 75 ℃ to ensure a better attachment of the first polymer layer to the SiO_2 surface[26], and then washed 3 times with pure water (resistivity 18.2 MΩ cm). Oppositely charged polyelectrolytes (normally 2 mg/ml in 0.5 M NaCl) were alternatively deposited on the SiO_2 templates with 15 min of shaking, followed by three wash steps. To avoid aggregation, polymer coated particles were ultrasonicated 10 second after each wash step. After the polymer deposition steps, the SiO_2 templates were dissolved with a 0.2 M NH_4F and HF buffer solution at pH=4.5[33]. Hollow microcapsules with desired multilayer numbers were obtained after several wash steps.

For $(PAH/PMA\text{-}BP)_4$ microcapsule preparation, the PMA-BP solution (2mg/ml in a mixture of 1:1 methanol and H_2O, 0.5 M NaCl) was adjusted to pH=6 to ensure a 90% charged solution.

For $(Nafion/DAR)_4$ microcapsule preparation, negatively charged Nafion was deposited on templates as the first layer, then followed by the positively charged DAR. One should notice, the commercial product Nafion (Nafion® perfluorinated resin) does not form true solution, it only disperses in water[201]. When the templates (SiO_2 microparticles) were immersed in Nafion dispersion, the hydrophobic effect here became the main driving force to finish the deposition of the 1st Nafion layer. After that the electrostatic interactions between opposite charges take back the predominant role for LbL assembly. For the DAR solution, no salt was added because the DAR is a ½ complex of $ZnCl_2$, and fresh made solution was used for each capsule preparation procedure.

For UV controlled protein release study, BSA was used as the model protein. To fabricate protein encapsulated microcapsules, BSA was co-precipitated with $CaCO_3$ micro-particles by mixing 0.33 M $CaCl_2$, Na_2CO_3 and 2 mg/ml BSA solution in 1 : 1 : 1 proportion[20]. And then BSA encapsulated particles were used as templates for polymer deposition. $CaCO_3$ component removal was performed with treatment with 0.2 M EDTA solution followed by several wash steps.

For the capsule sample containing gold nanoparticles (20 nm, Sigma), RhB encapsulated microcapsules were deposited with additional two gold layers and one polyelectrolyte bilayer. For gold nanoparticle deposition, the capsules were re-dispersed

in the pre-aggregated gold nanoparticles suspension[19]. After wash steps, RhB encapsulated capsules with the structure of RhB-(Nafion/DAR)$_4$-(Au/Nafion/DAR/Au) were obtained.

3.3.2 Multilayer Film Preparation

Quartz slides were carefully cleaned as the way of SiO_2 particles clean procedure mentioned above (Section 3.3.1). LbL deposition was carried out by hand. The slides were alternately immersed in oppositely charged polyelectrolyte solutions for 8 min each, followed by 3 min of wash. All the light sensitive multilayers were carefully prepared in dark.

3.3.3 Polymer-coated Oil Droplets Preparation

R-Limonene was used here as a model oil for this study. To encapsulate limonene, ultrasonication technique was used to fabricate limonene emulsion as the following two steps. Scheme 3.5 showed the preparation procedure schematic. First, a 'pre-emulsion' was prepared by homogenizing 20 % Limonene and 80 % aqueous surfactant solution (20 mM SDS). This oil and surfactant mixture was blended using an ultrasonic processor (Vibra-Cell™, Sonics & Materials, Inc. USA) for 2 min (20 kHz, 750 Watt × 40 %). And then 1 portion of pre-emulsion was sonicated with 2 portion of PDADMAC solution (2 wt. %) for 2 min (20 kHz, 750 Watt × 40%). After the two emulsion process, stable limonene emulsion oil droplet suspension was obtained, and these droplets were used as spherical templates for further alternative polyelectrolyte deposition steps.

After centrifuged at 8000 rpm for 5 min, the water phase of secondary emulsion was removed by inserting a syringe needle through the oil phase. And then the remaining oil droplets were treated with equal volume of the PAZO and PDADMAC (2 mg/ml in 0.5 M NaCl, pre-heated to 30 ℃) alternatively, and the mixture was shaken for 10 min. To prevent aggregation, the first two polymer deposition steps were followed by removal of water phase without wash steps. Then the resulting intermediate product was consecutive treated with PAZO and PDADMAC, followed by 3 wash steps.

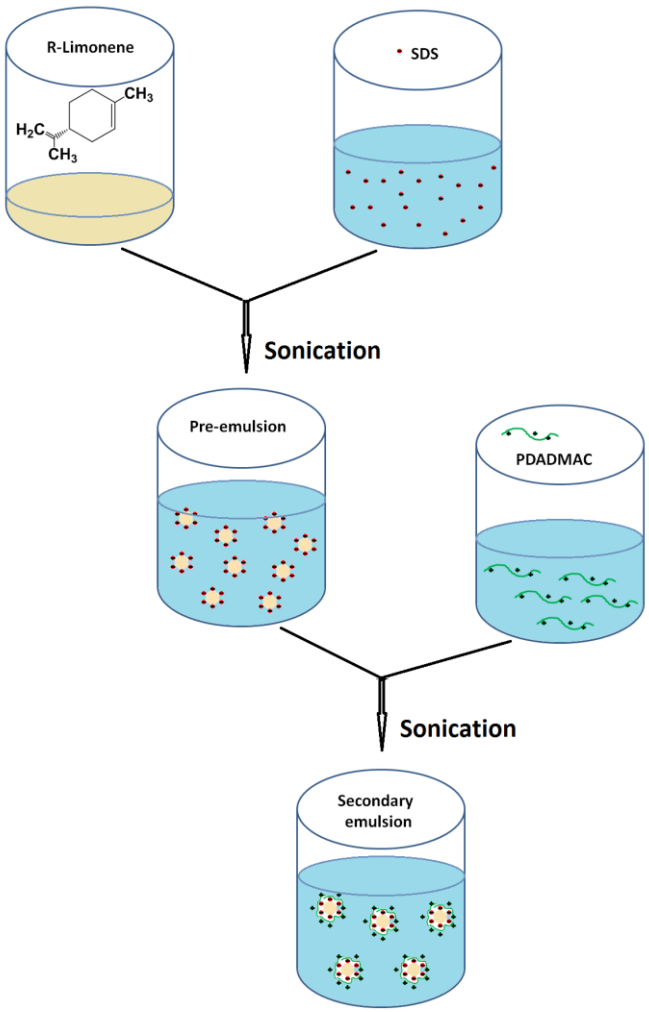

Scheme 3.5 Preparation of limonene emulsion.

3.3.4 UV Irradiation

Samples with different multilayer components were treated with different UV sources. Briefly, microcapsules containing benzophenone groups, $(PAH/PMA\text{-}BP)_4$, were irradiated with a mercury lamp (UVACUBE 100, Honle UV Technology) with the effective working wavelength ranging from 200 nm to 600 nm; and the other microcapsules containing azobenzene or diazonium groups, $(PDADMAC/PAZO)_4$, $(Nafion/DAR)_4$, DAR_8, $(PDADMAC/PAZO)_4\text{-}(DAR/Nafion)_2$ and polyelectrolyte coated limonene droplets were treated with a UV lamp (OmniCure® 2000, Lumen Dynamics Group Inc.) with the effective working wavelength ranging from 320 nm to 500 nm. In particular, for the $(PDADMAC/PAZO)_4$ capsules, an optical filter (# 011FG09-25, LOT-Oriel Ltd) was used to cut off the visible light, leaving UV

irradiation only. For visible light irradiation, a dichroic longpass filter (# NT69-864, Edmund Optics Inc) was used to cut off UV light.

The irradiation intensity was detected by using a ILT1400 radiometer (International Light Technologies Inc.)

The samples were dispersed in pure water in a cuvette, and exposed to UV lights directly. The dispersions were continuously stirred with a magnetic stirrer during UV irradiation. To reduce temperature increases, an ice bath was applied to ensure that the temperature change of the capsule suspension is less than 5 ℃.

For the multilayer films, polymer-coated quartz slides were placed above a water-ice bath, and be irradiated with the same irradiation system as their corresponding microcapsules, respectively.

3.3.5 Heat Treatment

In order to investigate the effect of local heating on microcapsules during the UV irradiation period, heat treatment was carried out to monitor capsules' heat-related behaviour as a function of temperature. Briefly, capsule suspensions were incubated for every 1h in water bath at different temperatures ranging from 25 ℃ to 90 ℃. After thermal incubation, these capsule samples were observed under SEM, and their size and distribution was statistic analysed.

3.3.6 Capsule Stability and Permeability Study

Capsule stability and permeability studies were investigated by using Confocal Laser Scanning Microscopy (CLSM) measurements with a Leica TS confocal scanning system (Leica, Germany) equipped with a 63x/1.4 oil immersion objective.

For the pH sensitive $(PAH/PMA\text{-}BP)_4$ and $(PAH/PMA)_4$ microcapsules, they were visualized by the incorporation of a rhodamine labeled polymer (RBITC-PAH)[20] during capsule preparation, their stability at different pH conditions were investigated. Briefly, the pH of capsule suspensions was carefully adjusted with addition of 0.1 M HCl and 0.1 M NaOH, the images of these capsules were captured and the diameter of the capsules was determined by the Image-Pro Plus 6.0 (Media Cybernetics, USA)

software. For permeability study, irradiated $(PAH/PMA\text{-}BP)_4$ microcapsules were re-suspended in fluorescent polymer solution (AF488-Dextran, 10 kDa, 1mg/ml). Then the gradual polymer penetration progress was captured with confocal laser scanning microscope.

For other microcapsules, $(Nafion/DAR)_4$, DAR_8 and $(PDADMAC/PAZO)_4$-$(DAR/Nafion)_2$ to be specifically, their shell permeability was demonstrated as a time dependent fluorescent polymer/molecule penetration progress, which was quantified as the relative fluorescent intensity inside capsules by using a Leica Microsystems (Heidelberg GmbH).

3.3.7 UV Induced Fluorescent Molecule/Polymer Encapsulation

To detect the feasibility of encapsulation in fabricated microcapsules, fluorescent molecules and polymers were used as model cargo substances for the studies. Briefly, fabricated microcapsules were re-dispersed in these fluorescent solutions for ~ 2 h with shaking. Later, the mixtures were treated with UV irradiation for certain time, washed several times to remove free fluorescent substances in water, and observed with a Leica TS confocal scanning system (Leica, Germany) equipped with a 63x/1.4 oil immersion objective. For confocal observation, capsules were centrifuged and washed twice with water to remove free dye polymers before each set time point.

Quantification of encapsulated fluorescent substance amount was also studied. The fluorescence intensity of each sample was determined with a fluorescence spectrometer (Perkin Elmer LS 55), and normalized with the standard solutions (either RhB or AF 488-Dextran) with known concentrations.

Specially, for DAR contained microcapsules, $(Nafion/DAR)_4$ and DAR_8 to be specifically, 150 µl of microcapsule suspension (containing 1.5×10^7 capsules) were re-suspended in 1.5 ml dye solution (RhB, 100 µg/ml) for 2 hours with shaking. The capsule-dye mixtures were exposed to UV light (55 mW/cm^2) directly for 10 min. After irradiation, capsules were collected, and washed at least 5 times with water. And then, 400 ul of water was added to re-disperse the dye encapsulated capsules. At a set experimental time, 50 µl of a capsule suspension containing RhB was taken out, centrifuged and the supernatant was carefully collected. The precipitated capsules

containing RhB were re-suspended in same volume of water, and were broken after 5 freeze-thaw cycles incorporating with 5 min of ultrasonic treatment[202].

For complex microcapsules, $(PDADMAC/PAZO)_4$-$(DAR/Nafion)_2$, capsules were re-dispersed in excess amount of AF 488-Dextran solution (300 μg/ml, 2 ml). After shell sealing triggered by the first 10 min of UV irradiation, capsules were collected, and washed several times with water to remove free polymers. A portion of the sample (containing 6.7×10^6 capsules) without further UV irradiation was taken to quantify the encapsulated polymer amount.

3.3.8 UV Triggered Substance Release

Basically, UV irradiation triggered the release of two substances, BSA and AF488-Dextran to be specifically.

For quantification of released protein from $(PDADMAC/PAZO)_4$ microcapsules, a portion of protein encapsulated capsule suspension was taken out at a set UV irradiation time, centrifuged, and the supernatant was used for the protein quantification with a commercially available assay bioassay kit (BCA Protein Assay Kit 33227, Pierce) according to a bicinchoninic acid (BCA) assay method based on reactions of copper ions in working reagent and peptide bonds of BSA, as reported by Smith et al [203]. The absorbance at 570 nm was measured in micro-plate reader (BIO-RAD, model 550).

For quantification of released fluorescent polymers (AF488-Dextran, 10 kDa) from complex microcapsules, 1 ml of capsule stock suspension (containing 1×10^8 capsules) was re-suspended in 2.0 ml AF488-Dextran solution (300 μg/ml) for 2 hours with shaking. The capsule-dye mixtures were exposed to UV light (50 mW/cm^2) directly for 10 min. After irradiation, capsules were collected, and washed several times with water to remove free polymers. The resulting suspension was then split into two portions (diluted to 3 ml for each), one was treated with additional UV irradiation up to 7 hours, and the other part was kept in dark. Then, additional UV treatment up to 7 hours was applied to trigger the release of encapsulated fluorescent polymers. After a set UV experimental time point, 400 μl of capsule-dye mixture (containing 6.7×10^6 capsules) with/without additional UV treatment was taken out, centrifuged, the supernatant was carefully collected, and the precipitate was added with equal volume of pure water. The

fluorescence intensity of each sample (in supernatant or in precipitate) was determined with a fluorescence spectrometer (Perkin Elmer LS 55), and normalized with the standard fluorescent polymers solutions with known concentrations.

3.3.9 Remote Instant Release of Encapsulated Small Molecule

Remote release of the encapsulated small molecular dye was carried out by using a laser setup, as presented in earlier research work[204]. The fluorescent dye RhB was used as the model substance. Briefly, the pre-aggregated gold nanoparticles[19] were incorporated in multilayers after capsule preparation and molecule encapsulation with addition of a polyelectrolyte layer, resulting in the $(Nafion/DAR)_4$-GNP/DAR/GNP microcapsules. A laser diode operating (see Section 3.4.4) at 840 nm with incident power of up to 100 mW was applied to break the microcapsules. The fast release of encapsulated dyes was acquired with Leica TS confocal laser scanning system.

3.4 Instruments

3.4.1 Atomic Force Microscopy

Atomic force microscopy (AFM), also known as scanning force microscopy (SFM), scans within a fraction of nanometer with very high resolution, offering an advanced tool for imaging, measuring and manipulating. AFM is based on measurement of atomic forces (e.g., Van der Waals, Capillary, chemical bonding, electrostatic forces), providing information by "feeling" the sample surface.

Figure 3.2 shows the basic principle of AFM (a) and the instrument used in this thesis (b). AFM is a member of Scanning Probe Microscopy (SPM) family, who employ sharp probes to scan across sample surfaces. As shown in Figure 3.2 a, a silicon-based cantilever with a sharp tip (several nanometers) performs scans. The tip feels the interactions/forces between tip and specimen, and leads to a cantilever deflection according to Hooke's law[205]. A laser beam pointed at the tip detects the deflection and reflects it to the position detector (an array of photodiodes). A computer processes the collected data and reconstructs the detected surface. Piezoelectric components are used to fabricate the moving stage and cantilever, facilitating desired tiny but accurate and precise scanning.

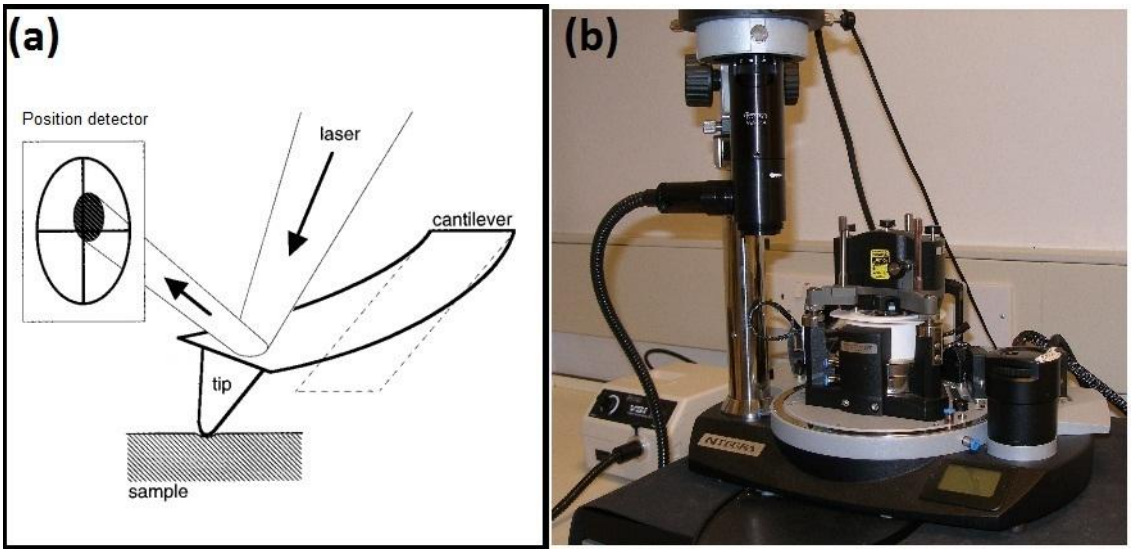

Figure 3.2 Schematic (a) and photographic (b) images of AFM instrument.

* Image (a) is reprinted from [206].

Generally, AFM is commonly applied to detect surface morphology, providing information such as roughness, material distribution, thickness, etc. AFM also allows the analysis of biological specimens, imaging biological molecules and possible interactions. Besides, AFM can be used to manipulate a surface by scratching it or creating desired nano-structures on the surface.

In this work, the thickness of the microcapsules $(PAH/PMA\text{-}BP)_4$ before and after UV irradiation was determined by an AFM system (Ntegra Therma, NT-MDT, Russia), where a drop of the diluted capsule suspension was placed onto a silicon wafer and air-dried at room temperature. The single-shell thickness of a capsule was then estimated as the half-height of the flat region of a dried collapsed capsule.

3.4.2 Confocal Laser Scanning Microscopy

Confocal laser scanning microscopy (CLSM, also known as Laser Scanning Confocal Microscopy) is a non-destructive technique frequently used for acquiring in-focus optical images with depth selectivity. Compared with traditional wide-field microscopy, CLSM allows point-by-point information collecting with desired depth and high resolution three-dimensional image reconstruction.

Since the first introduction originally patented by Marvin Minsky in 1957, tremendous explosion in the popularity of confocal microscopy have been achieved, demonstrating

as great interest growth of applications in biological fields which rely on imaging both opaque and non-opaque specimens. For the early studies, the principle of confocal microscopy involved employment of both the laser scanning method and the three-dementional detection of the biological specimens with fluorescent labeling. Then it was developed into a fully mature technology, which could be considered as an integration of electronic systems, including optical microscope, computer, and laser systems with selective wavelengths and beam scanning assembly. By applying of spatial filtering techniques, these modern confocal microscopes are able to eliminate the light or glare which is out-of-focus due to their thickness exceeds the immediate plane of focus, resulting in numerous applications for routine investigations on molecules, cells, as well as living tissues. For observation, the samples are often labeled with fluorescent dyes/markers to make selected objects visible.

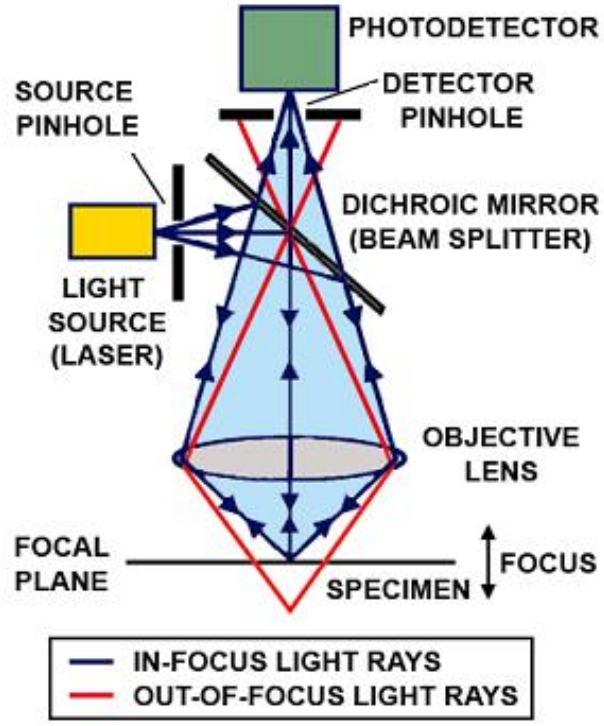

Scheme 3.6 Schematic illustration of CLSM setup and its light path[207].

Scheme 3.6 presents a typical schematic representation of CLSM setup and related light path. In a confocal laser scanning microscope, a laser beam emitted from the laser source passes through a source pinhole, is reflected on a dichroic mirror and then is focused within/on specimen surface through the objective lens. The scattered/reflected/emitted light by sample is then collected by the objective lens and

then is separated by a beam splitter. Selected light signal with suitable wavelengths passes through the detector pinhole and then is detected by a photodetector and transformed into data points by a computer.

One of the primary advantages of CLSM is its ability to acquire relative thin (0.5~1.5 μm) optical sections through fluorescent specimen which has a thickness up to 50 μm. Technically, out-of-focus light that is not coming from focused point is obstructed by the detector pinhole, permitting one to obtain images with desired plane/section depth. Therefore, sample information from different plane depths can be obtained with sequential image acquisition after adjustment of interested sample Z-positions by raising or lowering the microscope stage or objective lens. Image information is restricted to a well-defined plane, and its quality is greatly improved due to reduction of background fluorescent signals. In particular, once a series of optical images (two-dimensional) with desired depths (normally Z-series) has been collected, a three-dimensional representation of the specimen can be packed by assembling a stack of these two-dimensional images from successive focal planes. This approach facilitates analysis of the specimens with complicated interconnected structures, and helps investigate inter-relationships between different structures and functions, typical examples are cells and tissue.

In this work, Confocal laser scanning microscopy graphs were captured with a Leica TS confocal scanning system (Leica, Germany) equipped with a 63x/1.4 oil immersion objective. Capsule sample suspension was deposited on a thin glass slide (22×40 mm, thickness no. 1.5, VWR) and covered by a cover glass (18×18 mm, thickness no. 1, VWR). The samples were fluorescent labeled in advance.

3.4.3 Contact Angle Measurement

Contact angle measurement exhibits the ability of a liquid (water, organic solvent) spreads on a solid, demonstrating as measurement of the outline tangent of a liquid droplet deposited on the solid surface. The contact angle measurement tells the information of a surface, such as surface energy and wettability.

The contact angle measurement instrument used in this work is shown in Figure 3.3. The principle of this instrument is quite simple. Briefly, when a drop of liquid is

deposited on a solid surface, the detector captures its image with the help of illumination. The angle between outline tangent of the droplet at its located solid surface is calculated and named as contact angle (θ). A surface with a better liquid affinity shows a more spread liquid shape, resulting in a smaller θ value. For example, a hydrophilic surface (low surface energy) shows a fast water spread, great water wettability and a small contact angle.

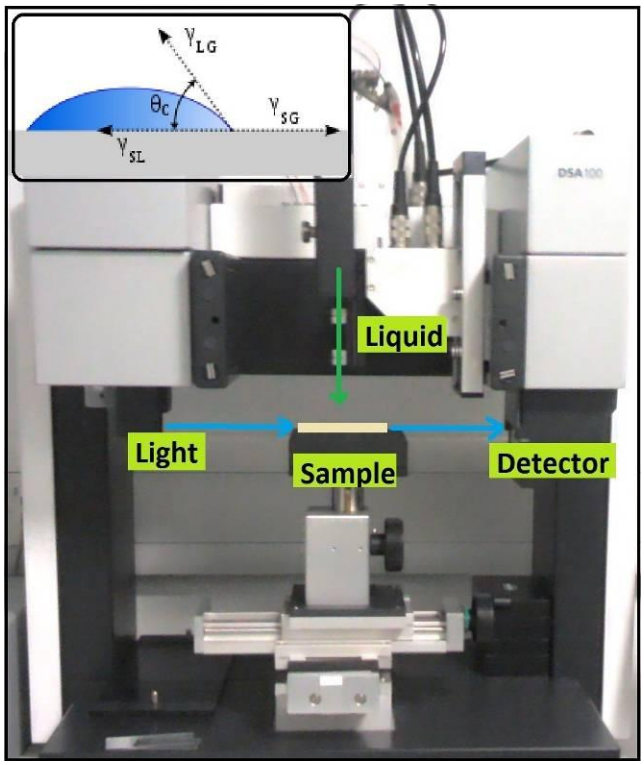

Figure 3.3 Contact angle measuring instrument.

* The inset shows the contact angle schematic.

Measuring the contact angles can be performed static and dynamic according to the sessile and captive drop method. The sessile drop method is the commonly used approach for characterization of surface energies. Measuring the contact angle of droplet profile by using a goniometer (by eye or software) allows one to analyze the contact angle visually, and this method is called the static sessile drop method. In comparison, a dynamic sessile drop method requires adding liquid dynamically or titling the surface. Without increasing the interfacial area of contacted two phases (liquid/solid), the maximum angle is defined as advancing angle, while the smallest angle is defined as receding angle when the liquid is removed or the surface is titled.

The difference between the two angles is defined as contact angle hysteresis. This hysteresis shows a possible range of contact angles could reach.

In this work, static sessile drop method was used to evaluate the water wettability of obtained multilayer films, and to judge their hydrophilicity. Generally, contact angle measurements of water (15 μl) on multilayer films containing DAR were captured using a Drop Shape Analysis System (Krüs, DSA100, Germany).

3.4.4 Continuous Laser Irradiation

The laboratory-made laser setup used in this work is shown in Figure 3.4. The main idea is similar to confocal laser scanning microscope, irradiating the sample in the focused plane. Briefly, the laser beam is launched in Z direction, passes through a 100× objective and is focused on the sample slide. A white light source working together with a XYZ moving stage helps locate and focus on the capsule samples. A detector (CCD camera) connected to a computer provides direct view of focused capsules and laser spot, also records the laser induced capsule breakage progress.

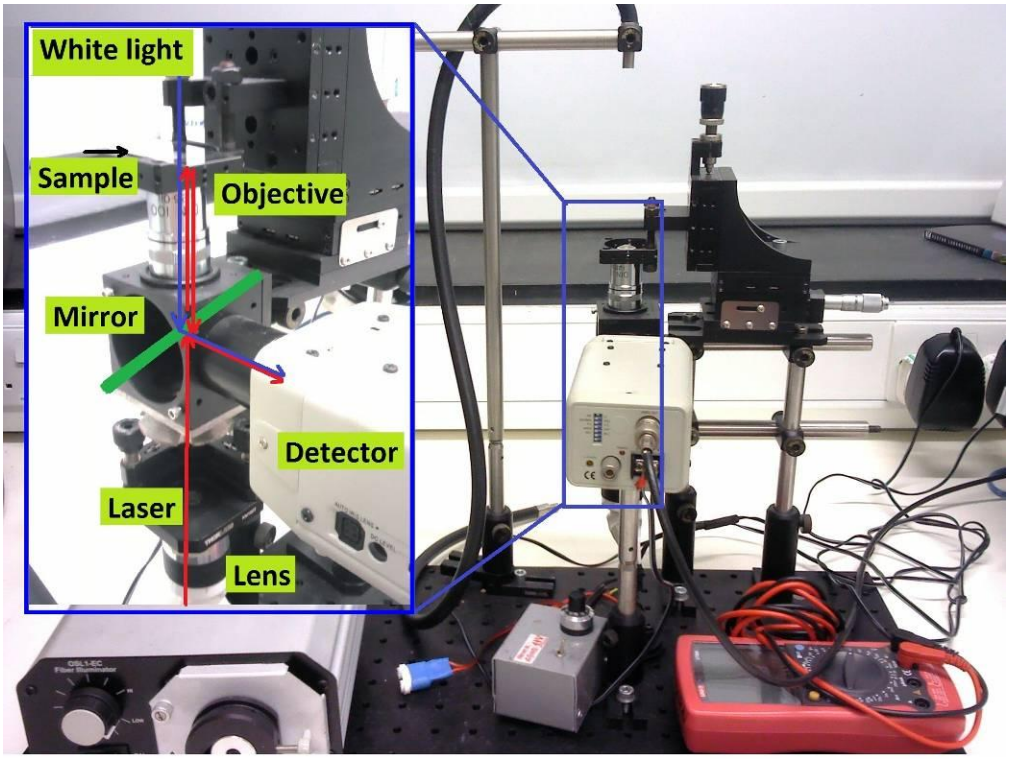

Figure 3.4 Laser irradiation setup.

In this work, remote instant release of the encapsulated small molecular dye was carried out by using this laser setup, as presented in earlier report[204]. The capsule suspension was dropped on a thin glass slide (22×40 mm, thickness no. 1.5, VWR), covered by a cover glass (×18 mm, thickness no. 1, VWR) and then sealed by using nail polish in order to prevent the sample to dry out. A laser diode operating at 840 nm with incident power of up to 100 mW was applied to break the gold nanoparticle incorporated microcapsules. The fast release of encapsulated dyes was acquired with Leica TS confocal laser scanning system right after laser treatment.

3.4.5 Dynamic Light Scattering

Dynamic light scattering (DLS) is one of the most popular methods used to determine size and distribution of particles, emulsions or molecules, which are dispersed/dissolved in liquid. Theoretically, when a monochromatic light beam, such as a laser, hits onto a solution/suspension, the Brownian motion of particles/molecules causes the incoming light to be scattered at different intensities. This intensity fluctuation is related to the size of the particle. Therefore, it is possible to calculate the spherical particle size distribution and describe these particle motions in liquid medium, measuring these changes and using the Stokes-Einstein relationship:

$$\mathrm{r} = \frac{k_B T}{6\pi\eta \cdot D}\Delta m \tag{3.1}$$

Where r_{is} the radius of particle, k_B is Boltzmann's constant, T is the temperature, η is viscosity, and D is the diffusion constant.

DLS was used to determine the size of fabricated emulsion and polymer-coated oil droplets in aqueous solutions. For measurements, a small volume of sample solution was transferred to a transparent cuvette, diluted with water and placed in the thermostated cavity of a Malvern Nano ZS zetasizer (Malvern Instruments Ltd, UK).

3.4.6 Electron Microscopy

Generally, electron microscope creates images of specimens at sub-nanometre resolution by using electron beams. Comparing with traditional optical microscope, it allows a much higher magnification (up to 10,000,000×) and greater resolving power

(50 pm resolution), because the electrons accelerated by electrostatic/electromagnetic lenses have wavelengths great shorter (100,000 times) than visible light photons. Electron microscopes are often used as an integral part of laboratories for study on a wide range of specimens ranging from inorganic to biological samples, presenting various sample surface information. Moreover, electron microscopes have been applied in industry applications for quality control.

3.4.6.1 Scanning electron microscopy

Scanning electron microscope (SEM) generates the images of sample surfaces by using a focused beam of high energy electrons to scan the surface of specimens. SEM produces images by collecting emitted secondary electrons from the sample which is excited by primary focused electrons. In a SEM, the electron beam scans across the surface in a raster pattern, various detected signals with beam position are used to build up images of the located area, giving the information about the surface composition, structure and topography, etc. SEM allows a high resolution better than 1 nanometer. A SEM instrument used in this work is presented in Figure 3.5.

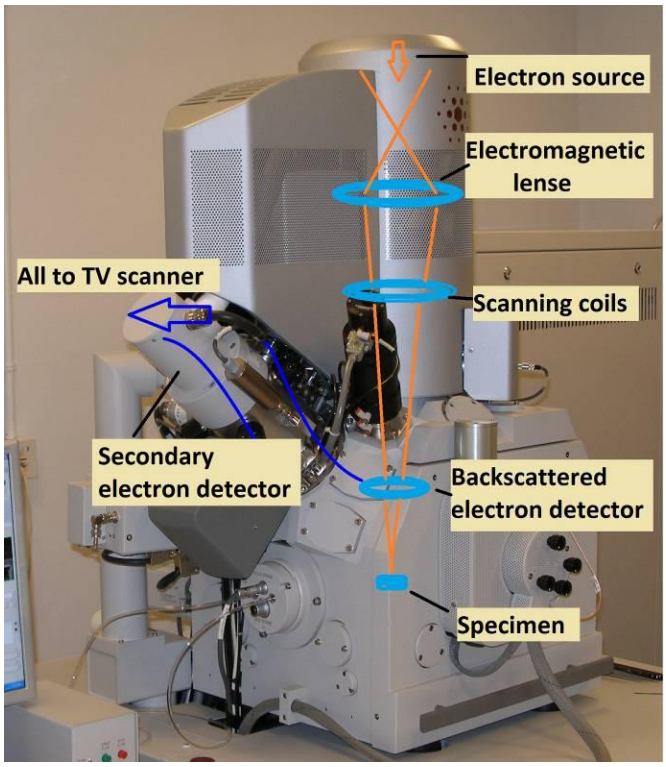

Figure 3.5 SEM instrument.

For conventional SEM observation, SEM relies on electron interactions at the surface, therefore specimens should be electrically conductive or semi-conductive, and electrically grounded in order to avoid electrostatic charge accumulation at the surface. Nonconductive specimens are usually coated with an ultrathin layer (nanometers thick) of electrically conducting material; gold and graphene are the two commonly used ones, being deposited onto the specimens either by low-vacuum sputter coating or by high-vacuum evaporation. However, such coating method sometimes may cover some detail information of the delicate samples, due to the nano-scaled thickness of coating layer. Specimens can be observed in vacuum with different vacuum degrees. In order to prevent electron beam penetration into sample, low accelerating voltages are normally used. For example, a voltage in the range of 1~5 kV is preferred for biological samples, even though the SEM can be operated up to 30 kV.

In this thesis, morphology observation of all the samples (microcapsules and polymer-coated oil droplets) with and without UV irradiation were observed by SEM. Briefly, sample suspension was dropped on a glass wafer, air-dried, and coated with gold before SEM observation (FEI inspect-F). Images were taken at various magnifications, with an accelerating voltage approximately to be 10 kV and spot size to be 3.5 at a working distance about 10 mm. Statistical analysis of capsule size and distribution was done by using Image-Pro Plus Version 6.0 (Media Cybernetics, Inc.).

3.4.6.2 Transmission electron microscopy

Different from SEM, TEM relies on transmission rather than surface processes, involving a high voltage electron beam transmission through an ultra-thin specimen and interactions within specimen and electrons. The electron beam is accelerated by an anode, focused by electrostatic and electromagnetic lenses, and then strike on specimen. The electrons that partially passed through specimen give information about the structure of specimen. The resulting information is then magnified by a series of objective lens until it is recorded by the viewing screen. A TEM instrument used in this work is presented in Figure 3.6.

TEM generates two-dimensional, black and white images with significant high resolution. Specially, high resolution transmission electron microscopy (HRTEM)

allows the resulted images with high resolution at 50 million times of magnification, owing to correction of the spherical aberration. Consequently, TEM is able to examine the detail of a specimen, for instance to determine a single column of atoms. TEM has been applied as an indispensable tool for widely applications in scientific fields.

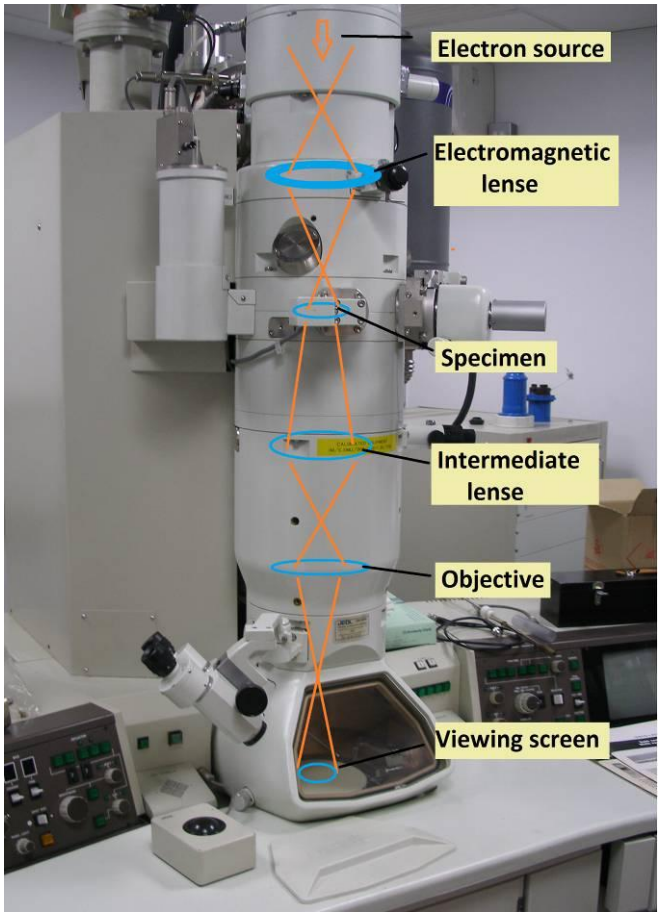

Figure 3.6 TEM instrument.

For TEM measurements, a high-resolution TEM (JEOL 2010) operating at 200 kV was used. Diluted capsule suspension was deposited on a carbon-coated copper grid, and air-dried for several hours. Then the copper grid was installed to a sample holder and placed into the vacuum chamber of TEM for observation.

3.4.7 Fluorescence Spectroscopy

Fluorescence spectroscopy (also known as fluorometry) analyzes fluorescence from a sample by using a fluorescence spectrometer. This technique is complementary to UV-Vis spectroscopy, in which light absorption deals with electronic transitions from

ground state to excited state, while here measures transitions from excited state to ground state.

Scheme 3.7 shows the light path of fluorescence spectrometer used in this thesis. Specially, in an emission mode, the excitation light beam (generated by high energy pulsed Xenon source) hits the Ex. Mono (monochromator), becomes desired single wavelength. The obtained monochromatic light passes the slit and strikes on sample, generating excited sample molecules. The excited molecule emits their energy in the form of fluorescent light. Part of the light passes through the Em. Mono (another monochromator) and be detected by the emission detector.

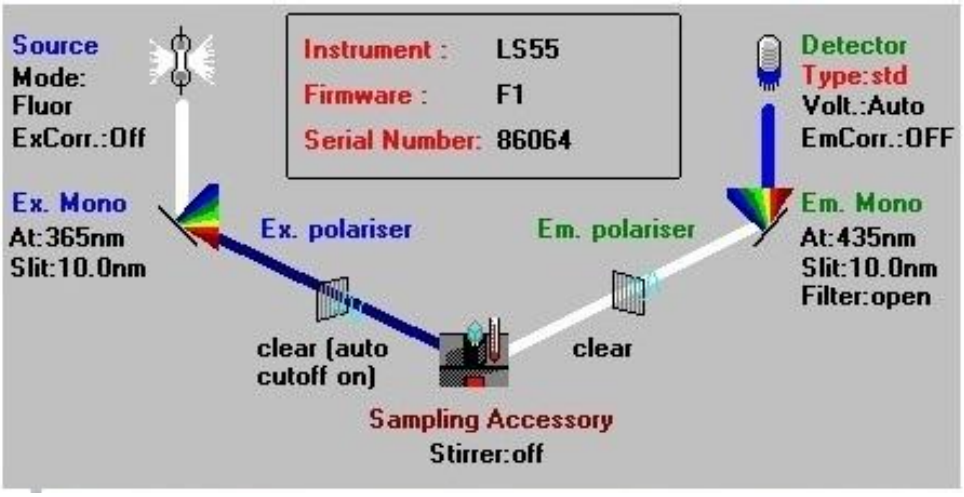

Scheme 3.7 Light path of fluorescence spectrometer.

This technique requires using a light beam to excite electrons in sample molecules and causes them to emit light. Typically, in an *emission spectrum*, the excitation light used to excite the molecules is kept as a single wavelength, and then emission through a wavelength region excited by this monochromatic light is recorded. Contrarily, to obtain an *excitation spectrum*, the emission light is set as a constant, while the excitation light is measured in a wavelength range. A fluorescence spectrum gives information of the maximum emission/excitation location and related fluorescent intensities.

In this work, the quantification of encapsulated and released fluorescent substance was carried out using the fluorescence spectrometer (Perkin Elmer LS 55). The slit width was 10 nm. Specifically, for samples containing AF 488-Dextran, the excitation and

emission wavelengths used are 496 nm and 518 nm; for samples containing RhB, the excitation and emission wavelengths used are 553 nm and 627 nm, respectively.

3.4.8 Fourier Transform Infrared Spectroscopy

Fourier Transform Infrared Spectroscopy (FTIR) is a technique that can be applied to indentify the chemical samples due to the information of chemical bonds (functional groups) presenting in the detected infrared spectrum. The chemicals could be organic or inorganic in their status of solid, gas and even the liquid, although the interference from water is not favoured.

The main purpose of the FTIR absorption spectroscopy is to measure light absorption of the sample at each wavelength. Generally, a monochromatic light is used to irradiate the sample, the light absorption by the sample is measured, and then the similar process is repeated for each light with different wavelengths. As shown in Figure 3.7, a light source containing the full spectrum of wavelengths is used to shine into a Michelson interferometer, which contains a several stationary mirrors and a moving mirror. Once the light shines into the interferometer, each wavelength is blocked periodically, thus monochromatic light is separated and passes the sample at different rates. Afterwards, the collected the raw data of light absorption is processed by a computer and used to generate a spectrum. The data processing requires a algorithm named *Fourier transform*, thus this method was called *"Fourier transform spectroscopy"* when the technique was developed by employing of light containing different wavelengths to irradiate the sample at first time.

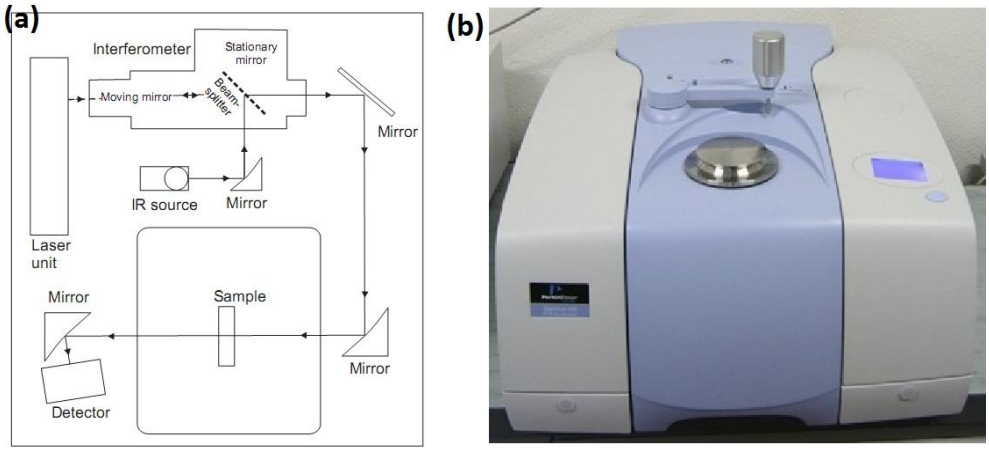

Figure 3.7 Schematic illustration (a) and photographic image (b) of FTIR setup.

Theoretically, this spectrum gives the information of related molecular bond vibrating at different frequencies, due to the various bonds existed in the sample. Technically, the infrared spectra of pure compounds/chemicals with known components are used as gold standards or "fingerprint" to interpret chemical components of the samples. Therefore, the chemical bonds in a sample can be determined when comparing the obtained infrared spectrum with the infrared spectra of known compounds. Sometimes, the FTIR spectrum is not adequate enough to indentify an unknown sample, thus other characterization tools such as UV-Visible spectroscopy, nuclear magnetic resonance (NMR), mass spectrometry, X-ray diffraction, etc., are also needed for investigations. Moreover, due to the proportional dependent relationship between FTIR absorption intensity and sample concentration, FITR spectroscopy can be also used for quantitative analysis.

In this work, FTIR spectra of vacuum dried microcapsule samples with and without irradiation were obtained using an infrared spectroscopy (FTIR spectrometer 100, Perkin Elmer). All data were collected at a spectral resolution of 4 cm^{-1} ranging from 4000 cm^{-1} to 600 cm^{-1}.

3.4.9 Nuclear Magnetic Resonance Spectroscopy

Nuclear magnetic resonance (NMR) is a physical phenomenon which occurs when the nuclei of certain atoms are immersed in a static magnetic field and exposed to a second oscillating magnetic field, in which the nuclei absorb and emit electromagnetic radiation. NMR spectroscopy is the use of the NMR phenomenon to study molecules' information (e.g. chemical, structural), which is based on resonant frequencies of the nuclei present in the sample. This information is also known as chemical shift (δ, in ppm).

NMR is a very powerful but theoretically complex analytical tool, it can be used to study any sample containing nuclei possessing spin theoretically. Briefly, the resonance frequencies in the same magnetic field are influenced by neighbouring NMR active nuclei, depending on the bonding electrons that connect the nuclei. This dependence is known as spin-spin or "J" coupling. Such coupling permits one to indentify the connections between atoms on a molecule.

NMR spectroscopy is routinely used by chemists to investigate properties of organic molecules, with the help of NMR active nuclei (e.g., ^{1}H, ^{13}C, ^{31}P, ^{15}N, ^{29}Si). ^{1}H NMR and ^{13}C NMR spectroscopies are the two most frequently used types. From them, one can get the information about the number of chemically non-equivalent nuclei (H or C) and the environment of nuclei (e.g. attached atoms, hybridization state). Comparably, they are different. ^{1}H NMR spectrum is much more sensitive (^{13}C nuclei is only 1 % as intense as ^{1}H) and can be acquired more quickly than ^{13}C NMR (^{13}C signals spread over a much wider range). Specially, in a ^{1}H NMR spectrum, one can determine how the atoms combine to form a unique molecular structure, by quantifying information from peak intensities. However, the integrals are not used in a ^{13}C NMR spectrum.

One important thing needs to be concerned about in the course of routine use of NMR is the signals deriving from possible contaminants, for example water and solvents, which would mislead to signal identification. Helpfully, the ^{1}H and ^{13}C chemical shifts of the commonly used solvents, usually presenting as extra peaks, have been collected by Gottlieb and co-workers [208], providing great assistance to the practicing chemists.

In this work, NMR measurement was applied to characterize the substitution ratio of Benzophenone-substituted Poly(methacrylic acid). ^{1}H NMR spectrum was obtained by using a Bruker spectrophotometer (D_2O, 600 MHz).

3.4.10 Quartz Crystal Microbalance

A quartz crystal microbalance (QCM) is applied to measure the mass variations of thin films on a specified surface by measuring the changes in frequency of a quartz crystal resonator. A typical schematic representation of QCM setup is given in Scheme 3.8. A common QCM setup mainly contains frequency sensing equipment, an oscillation source, a measurement and recording device.

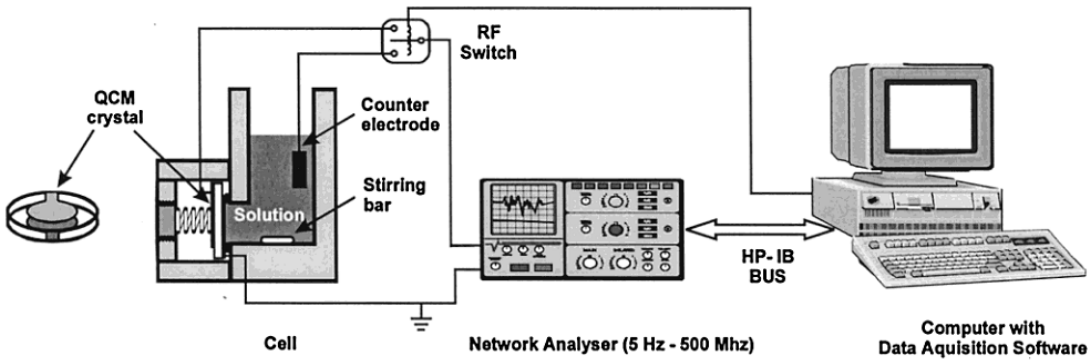

Scheme 3.8 Schematic illustration of QCM setup[209].

The measurement of QCM is based on the piezoelectric effect. Generally, a piezoelectric effect is defined as electric polarization produced by applied mechanical strain. Conversely, applying of electric field on a substance produces mechanical deformation, demonstrating as shrink or expansion. For example, upon applying a potential to quartz crystal by two electrodes mounted on the across sides, the crystal starts vibrating. Generally, when an alternating current with proper frequency is applied (normally 8 or 10 MHz for quartz), the crystal will vibrate in its fundamental resonant mode. The resonant frequency change of the crystal mainly depends on its mass change, increasing the mass on crystal surface causes a decrease in resonant frequency. Theoretically, in the case of ideal mass layers (very thin film), a linear relation between mass variation and frequency shift which derivate from Sauerbrey equation[210] is used to determine mass change:

$$\Delta f = \frac{-2 f_0^2}{A\sqrt{\mu\rho}} \Delta m \qquad (3.2)$$

Where f_0 is the resonant frequency (Hz), Δf is frequency change (Hz), Δm is mass change (g), A is piezoelectrically active crystal area (cm^2), ρ is density of quartz (2.648 g/cm^3), and μ is shear modulus of quartz crystal (2.947×10^{11} g/cm s^2).

The QCM technique can be used in different environmental conditions, such as under vacuum, in gas phase and more recently in liquid environments. It is very useful to monitor substance deposition progress (rate, mass change, layer thickness), to evaluate

the affinity of molecules to a functionalized surface, and it could also be used to investigate possible interactions between to substances occurred on the crystal surface.

QCM was applied to monitor the stepwise assembly process in this thesis. Briefly, the crystal resonator (#151218-10, International Crystal Manufacturing CO, INC.) was immersed alternatively in polyelectrolyte solutions for a period of 15 min, carefully washed, and air dried; then the frequency shifts were recorded using the experimental setup described by Krause[209]. All the measurements were carried out at 30 ℃ in a thermal stable incubator (Digi Therm™, Tritech Research, Inc.) in the duration of approximately 17 min for 200 total scans.

3.4.11 UV-Visible Spectroscopy

An Ultraviolet-Visible (UV-Vis) spectroscopy demonstrates light absorption or reflectance in the ultraviolet (200 to 400 nm) and adjacent visible (400 to 800 nm) regions. In this wavelength range, sample molecule adsorbs the energy of light and undergoes an electronic transition to a higher energy orbital. The UV-Vis spectrophotometer is used to record the possible absorption, together with its intensity (absorbance). Likewise, the UV-Vis spectrophotometer can also be used to record the intensity of light that reflected from a sample.

A typical example of light path of the UV-Vis spectrophotometer used in this thesis is given, as shown in Scheme 3.9. Generally, two light sources, a D_2 (deuterium) lamp and a tungsten lamp, are used to generate ultraviolet light and visible light for UV-Visible spectrophotometer, respectively. The light beam reflects from mirrors and hits a monochromator. The monochromator separates the light beams into single wavelengths by applying diffraction grating, which allows only selected monochromatic light successfully pass through a slit. The monochromatic light with specific wavelength hits a CBM (common beam mask) and then is conducted to a CBD (common beam depolarizer), at where it is split into two equal beams. One of the resulting beams is conducted to pass through a sample cuvette, the other is allowed to pass through a reference cuvette. A detector is used to measure and compare the intensities of these light beams.

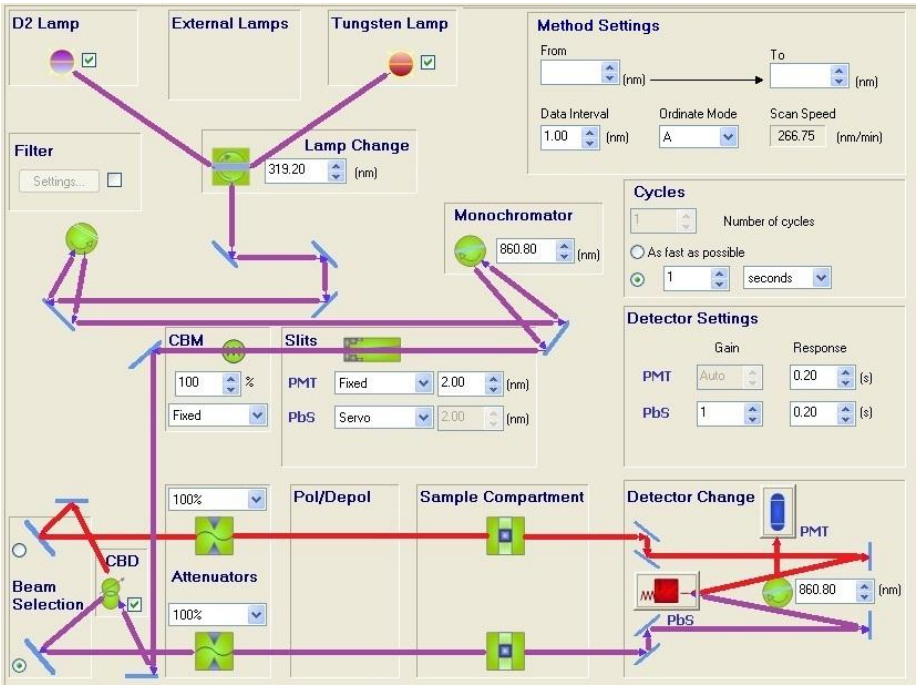

Scheme 3.9 Light path of UV-Vis spectrophotometer.

Similar as other absorption spectroscopy, for example FTIR, the goal of the UV-Vis is to measure how well a sample absorbs light at each wavelength. Practically, in order to detect the absorption of single wavelength, a scanning monochromator in the UV-Vis spectrophotometer employs the diffraction grating to allow a "step-through" of each wavelength. The absorption of each wavelength in UV-Vis range corresponds to the excitation of outer electrons, promotes them from ground state to an exited state. Generally speaking, the transitions involving π (multiple-bond), σ (single bond), and n (n-caused by lone pairs) electrons and charge transfer electrons are most discussed types. Normally, most absorption spectroscopy of organic samples, locating in an experimentally convenient region from 200 to 700 nm, is attributed to the electronic transitions of *n* or π electrons to the π^* excited state; thus, unsaturated groups in the molecule are required, which could provide the π electrons.

UV-Vis spectroscopy is frequently applied in analytical chemistry, where the determination of different compounds could be made quantitatively. Typically, measurements of transition metal ion solutions (e.g., Au, Ag) and organic compounds (e.g., DNA, protein and chromophores) have been carried out.

In this work, a UV-Vis spectrophotometer (LAMBDA 950, Perkin Elmer) was employed to investigate the UV absorption of the polyeletrolyte discussed here.

Aqueous solution measurements were made using quartz spectrophotometer cuvettes (sigma, S10C). For multilayer films, another detector suitable for film measurement was used. Films were placed in the sample chamber directly.

4. UV CrossLinkable Microcapsules Made of Weak Polyelectrolytes Containing Benzophenone

4.1 Introduction

4.11 Background

Light-addressable vesicles demonstrate a novel channel to activate material delivery remotely, with emphasis on either encapsulation or release. However, the development of an intelligent or smart delivery system would be more complicated in practice, where more complex functionalities or multi-functionalities are required to satisfy different external stimulus triggers (i.e., enzymes, temperature, pH, ionic strength)[29]. Therefore, the integration of two or more stimuli-responsive functionalities in one vesicle system has important implications.

As a practical matter, LbL assembly would be a promising technique to achieve the goals due to its simplicity and versatility[11]. The step-by-step polymer deposition of the capsule preparation process facilitates the modification of the fabricated capsules, providing opportunities to engineering a novel class of capsules with desired structures and properties. Specially, if the multilayer shells are composed of weak polyelectrolytes, the resulting capsules will automatically have a pH-responsive property. Consequently, LbL assembly offers a relatively simple and effective way to introduce a pH-responsive property at the very beginning of the capsule fabrication. In return, the pH-responsive property allows the control of the shrink-swell behaviours of capsule shell reversibly as a consequence of the dissociation equilibrium of the weak polyelectrolyte complex. Thus, a controlled release could be achieved through the controllable shell thickness or permeability, as well as the deconstruction of the capsule by adjusting the acidity of the surrounding solution.

It has been shown that, by responding to a certain UV wavelength, capsules are able to alter their shell thickness, permeability, and multilayer arrangement[16, 134]. In particular, chemically stable benzophenone (BP) is widely used as a photoactivatable reagent to functionalize or reconstruct the remote C−H bonds in flexible molecular chains. The highly efficient and good site-specific covalent modifications of macromolecules make

BP a promising candidate for capsule modification. Upon irradiation at a certain wavelength, BPs react with unreactive C−H bonds predominantly[137]. The introduction of BP groups in the multilayers will therefore endow the LbL capsules with novel UV responsive properties. In addition, microcapsules or multilayers composed of weak polyeletrolytes are sensitive to outer pH stimuli. It is possible to adjust reversibly the fabricated capsule's shrink-swell behaviour by altering the environmental pH values[211, 212].

4.1.2 Aim and Objectives

The general aim here is to fabricate UV responsive multilayer capsules for potential cargo encapsulation use. Specially, for capsules composed of weak polyelectrolytes, the chemical and physical properties of polyelectrolyte capsules could be controlled and altered by UV light remotely, while preserving the pH-responsive properties of the weak polyelectrolyte multilayers. In return, the external pH stimulus can be used to adjust the shrink-swell of the UV crosslinked capsules through the control over dissociation equilibrium of the weak polyelectrolyte complex.

Therefore the main objectives of this chapter are:

1) To design and fabricate multilayer microcapsules composed of weak polyelectrolytes (PAH, PMA) with UV-absorbable benzophenone groups.

2) To investigate the UV induced capsule shell crosslinking effect, for example the possible morphology change, thickness change, and permeability changes (molecule encapsulation).

3) To study the pH response (shell stability) of the UV crosslinked capsules, in normal pH range (pH = 3~11) and extreme pH conditions (pH = 2 or 12).

4.2 UV Induced Capsule Shrinking

The UV response properties of these fabricated capsules were studied. In this work, the UV irradiation intensity used was approximately 5 mW/cm^2, and the UV treatment duration was 0~2 hours. The structural formulas of these polyelectrolytes used for capsule fabrication were given in Scheme 4.1.

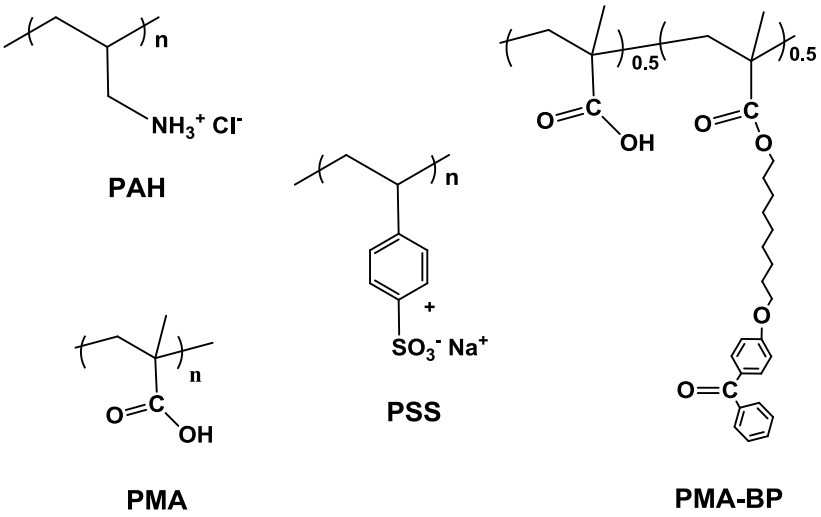

Scheme 4.1 Structural formulas of the polyelectrolytes used in this chapter.

$(PAH/PMA\text{-}BP)_4$ capsule suspensions were exposed to the UV light under a power of 5 mW/cm^2 for different irradiation durations. As shown in Figure 4.1, the size change of these capsules before and after UV irradiation was obvious. Before the irradiation, the capsules showed round and flat morphologies on the silicon wafer with an average diameter of 5.12 μm (Figure 4.1 a).

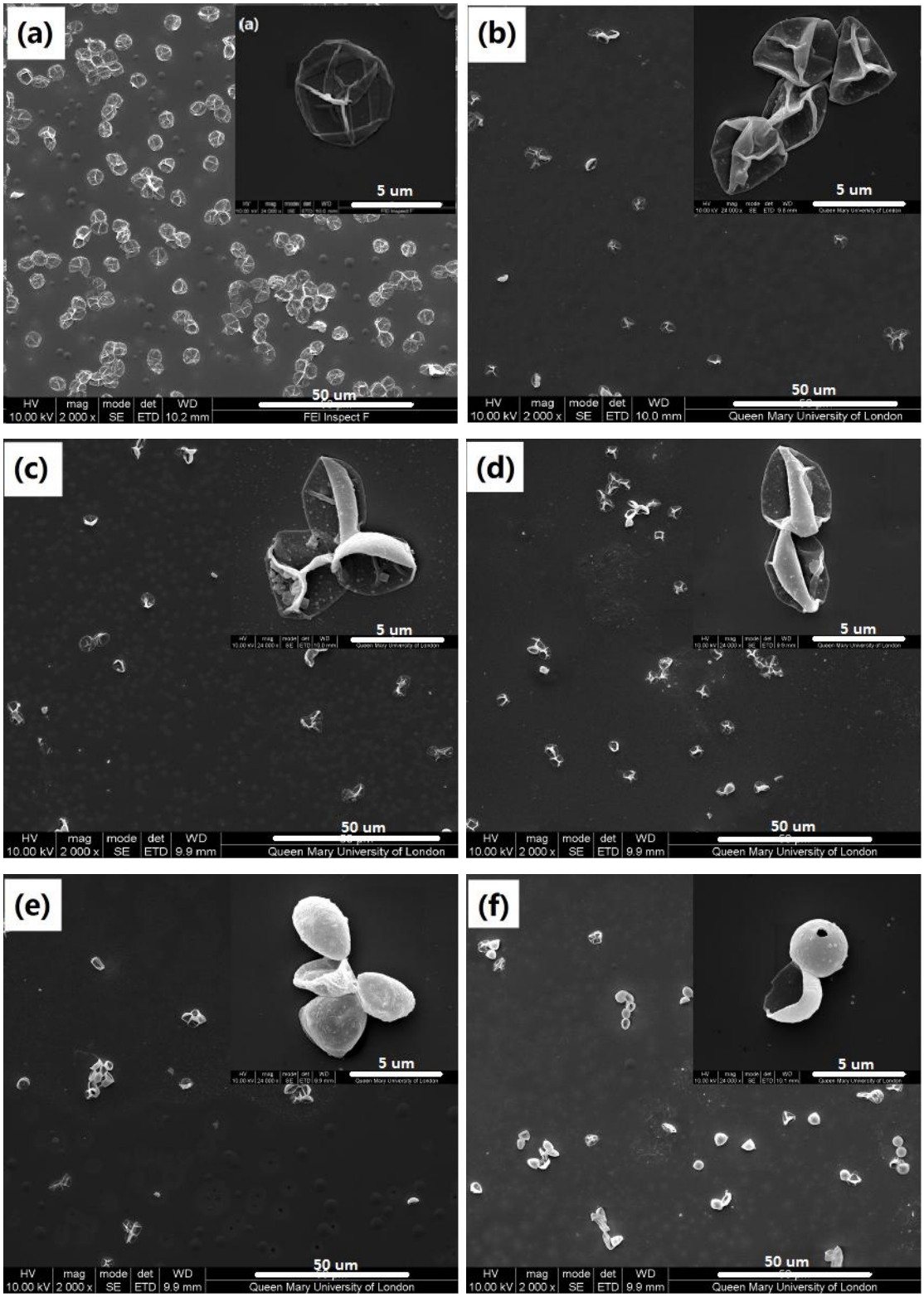

Figure 4.1 SEM images of $(PAH/PMA\text{-}BP)_4$ capsules before (a), and after UV irradiation for 15 (b), 30 (c), 60 (d), 90 (e), and 120 min (f).

After being placed under the UV light, the capsule shrinkage happened immediately. For only 15 minutes, the average diameter was decreased to 4.54 μm (Figure 4.1b).

With the increase of UV irradiation time, the capsule size continued to decrease. After 120-minute UV irradiation, a significant reduction in the capsule diameter could be found, i.e, the capsule size reduced to 3.65 μm (i.e., a reduction of ~30% in diameter) (Figure 4.1 f). Further increasing the UV irradiation period to 3 hours did not show obvious size decrease. With the shrinkage of capsule, the capsule shell appeared thicker and stronger, which resulted in a three-dimensional spherical capsule appearance under the SEM observation (Figure 4.1 f). The capsule change in diameter and shell thickness could be verified by the AFM results, as shown in Figure 4.2 and TEM results in Figure 4.3. After 2 hours' UV irradiation, the $(PAH/PMA\text{-}BP)_4$ capsule shell thickness was almost doubled, changed from ~35 nm to ~70 nm. Furthermore, the irradiated capsules shrunk to diameters below 4 μm, consistent with the SEM results.

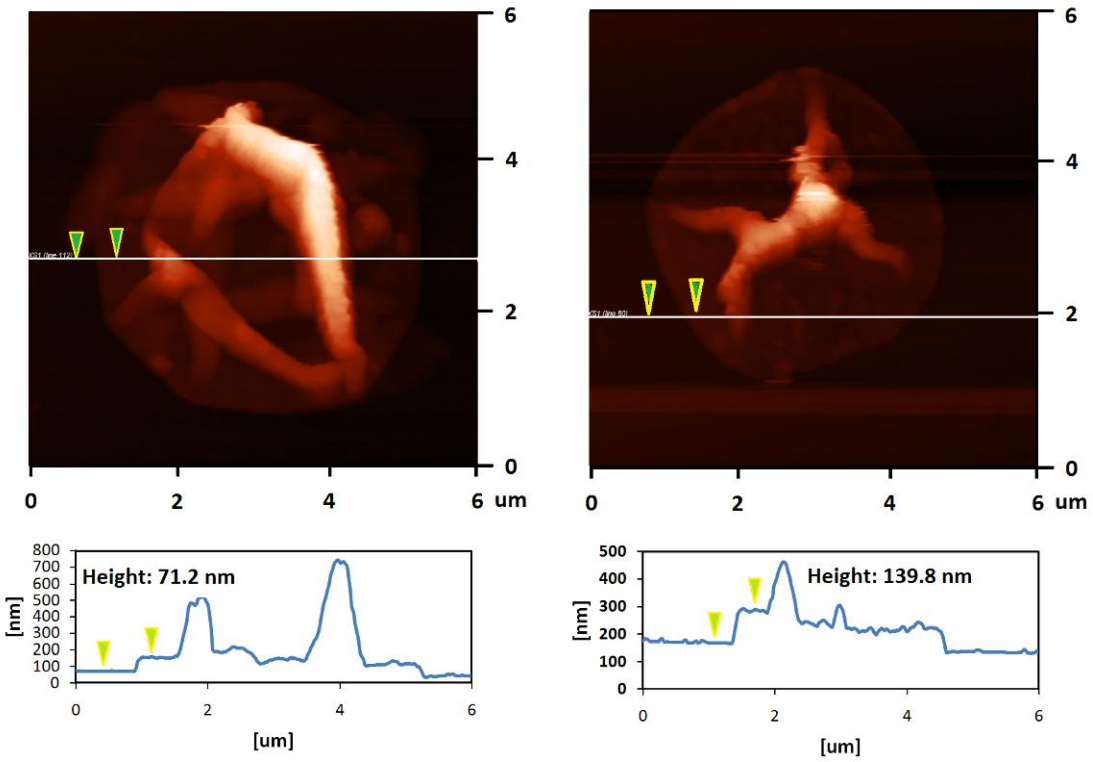

Figure 4.2 AFM images (top) and cross-section profiles (bottom) of $(PAH/PMA\text{-}BP)_4$ capsules before (left), and after UV irradiation for 120 min (right).

*The height (single shell thickness×2) of the dried collapsed capsules changed from 71.2 nm to 139.8 nm.

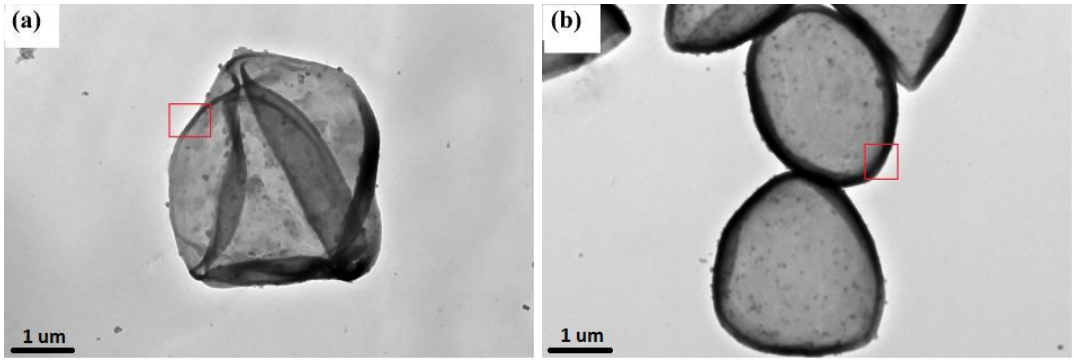

Figure 4.3 TEM images of $(PAH/PMA\text{-}BP)_4$ capsules before (a) and after UV irradiation for 120 min (b). * Shell thickness changed from 34 ± 3 nm to 72 ± 9 nm (Capsule shell thickness and distribution was expressed as mean ± SD of at least 4 capsules per sample and 10 locations per capsule randomly measured, as shown in the red rectangle)

In order to investigate the main reason that caused the shrinkage of $(PAH/PMA\text{-}BP)_4$ capsules, PAH/PMA-BP multilayer films were made as previously described, and UV-Visible spectroscopy was used to detect the possible UV absorbance change happened in the films.

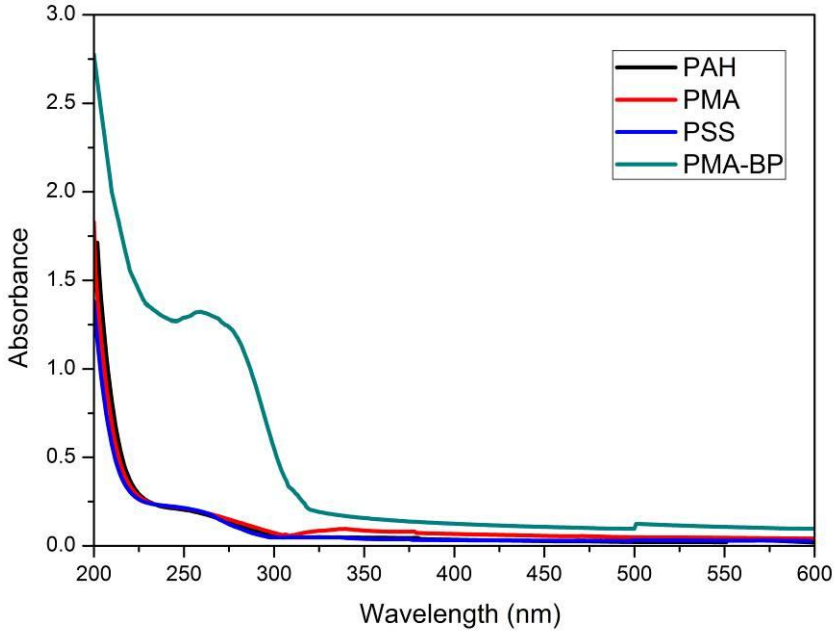

Figure 4.4 UV-Vis spectra of polyelectrolytes.

As shown in Figure 4.4, for the polyelectrolytes used in the experiment, PMA-BP showed a UV absorbance peak at 265 nm wavelength, which could be attributed to the π-π* transition of the benzophenone groups in the polymer chains, totally different

from those of PAH, PSS, and PMA polymers. When the electrostatic reactions happened between PAH and PMA-BP polymers, the maximum absorption peak changed slightly, shifting to 275 nm, as shown in Figure 4.5. With the increase of the number of PAH/PMA-BP layers (e.g., from 8 layers to 64 layers), the intensity of maximum absorption peak became more pronounced (increased from 0.054 to 0.383 a.u.), which indicated the increasing amount of benzophenone groups deposited on the planar substrate.

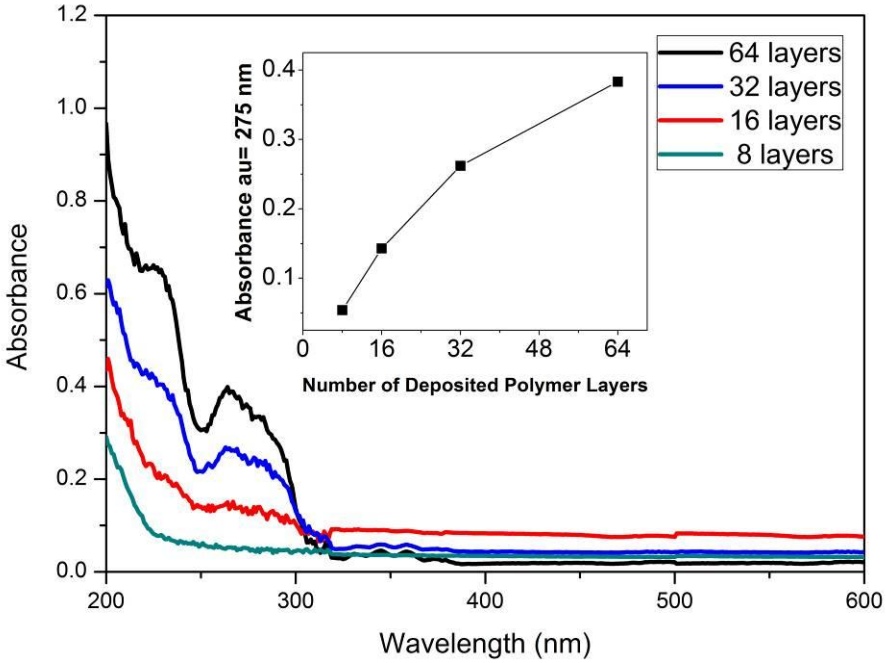

Figure 4.5 UV-Vis spectra of PAH/PMA-BP multilayer films.

* The inset showed the increase of absorbance at 275 nm with increase number of deposited polymer.

When the multilayer films were exposed to UV lights, the intensity of absorption peak at 275 nm decreased with the irradiation times, as illustrated in Figure 4.6, which showed the UV-Vis spectra of 64 multilayer of PAH/PMA-BP film on a quartz slide as a function of UV irradiation time. Under UV irradiation, benzophenone groups were excited, and tended to absorb photons from the nearby unreactive C–H bonds, leading to the generation of a new C–C bond and crosslinking within the multilayers[137].

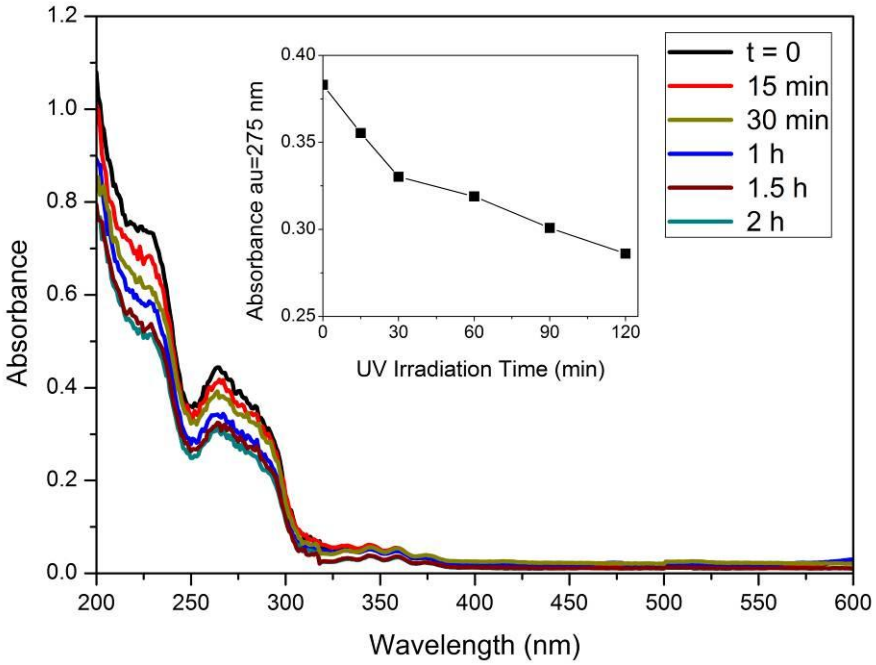

Figure 4.6 UV-Vis spectra of PAH/PMA-BP 64-layer film.

* The inset showed the decrease of absorbance at 275 nm with increase of UV irradiation time.

Fourier transform infrared (FTIR) spectra analysis of 0~2 hour irradiated (PAH/PMA-BP)$_4$ capsules confirmed this chemical transition (Scheme 4.2). As shown in Figure 4.7, the FTIR spectra of the samples containing the BP groups exhibited a decrease in the C=O carbonyl group peak at 1603 cm^{-1}, which could be attributed to the deformation of BP radicals after UV irradiation. In addition, the decrease in the aromatic ring at 1512 cm^{-1} also verified this BP-related chemical change. However, a broad peak that corresponds to the generation of hydroxyl group (–OH) accompanied with BP deformation in the region 3400~3500 cm^{-1} was too weak to be observed.

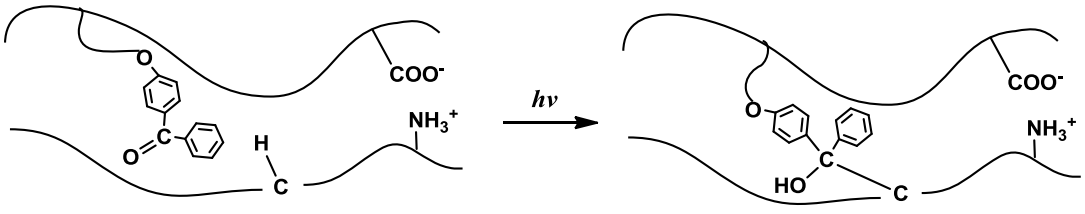

Scheme 4.2 Schematic representation of crosslinking reaction in the capsule shells.

* The photo-crosslinking won't influence the electrostatic interactions between polyanion and polycation.

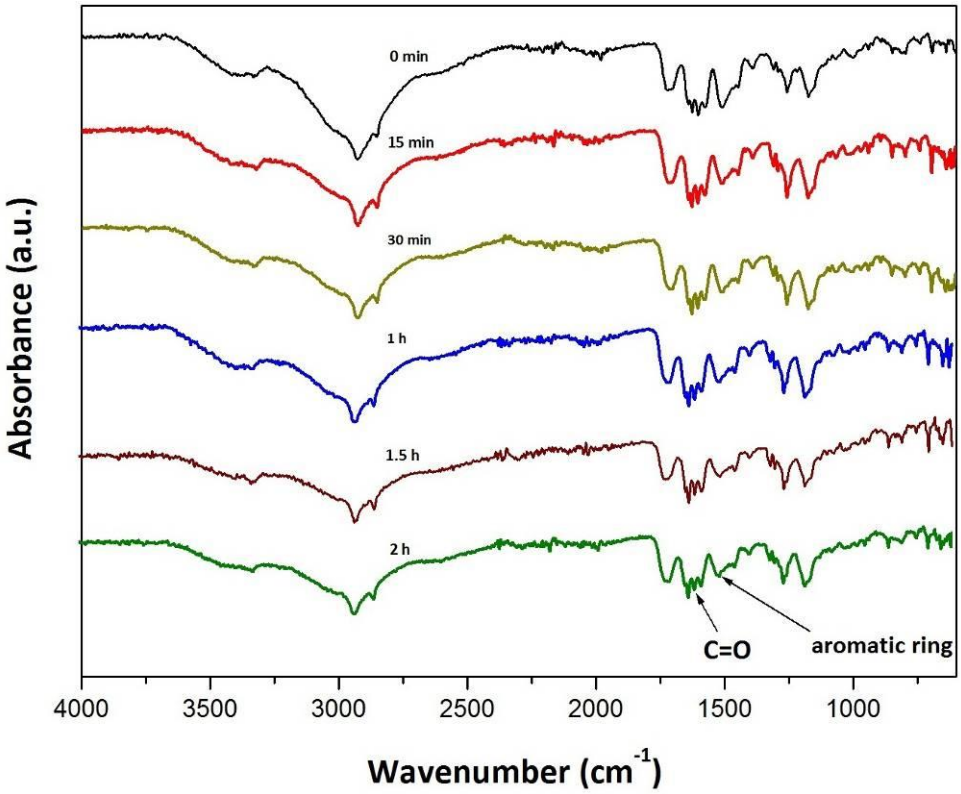

Figure 4.7 FTIR spectra of PAH/PMA-BP samples before (black line) and after (other lines) UV irradiation.

* The 1603 cm^{-1} and 1512 cm^{-1} are the benzophenone's carbonyl group (C=O) and aromatic ring skeletal stretch vibrations, respectively.

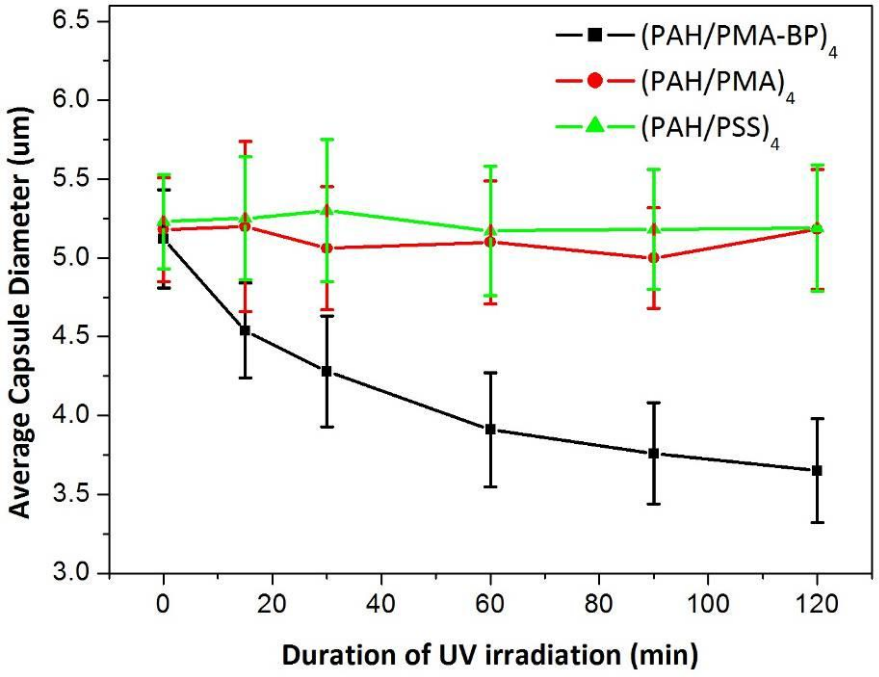

Figure 4.8 Size changes of three different kinds of capsules after UV irradiation.

* The UV irradiation was fixed at 5 mW/cm^2. Capsules diameters and distributions were expressed as mean ± SD of at least 35 capsules per sample random measured of SEM images.

Capsules without BP groups were introduced in other two capsule systems for the study. As found in the control groups, other capsules without BP group such as $(PAH/PMA)_4$ and $(PAH/PSS)_4$ capsules cannot absorb UV energy at a wavelength between 250 and 600 nm, and exhibit no capsule shrinkage. As shown in Figure 4.8, capsules with BP groups shrunk from 5.12 ± 0.31 μm to 3.65 ± 0.33 μm upon 2 hours of UV irradiation. While the $(PAH/PMA)_4$ and $(PAH/PSS)_4$ capsules without BP group showed no obvious shrinkage (Figure 4.9).

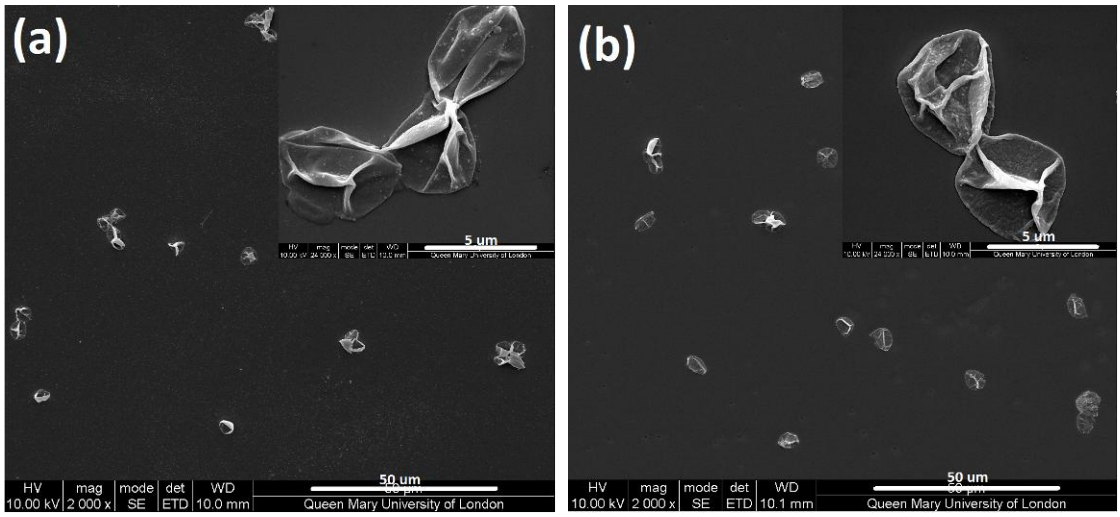

Figure 4.9 SEM images of $(PAH/PMA)_4$ (a) and $(PAH/PMA)_4$ (b) capsules after UV irradiation of 2 hours.

It has been reported that PSS possesses a maximum UV absorption ~220 nm. Theoretically, exposure PAH/PSS to UV light will cause a size shrinkage. As reported by Katagiri, after 2-hour irradiation under a power of 20 mW/cm^2, PAH/PSS shrunk to less than 50 % of their original diameter[134]. However, no obvious PAH/PSS capsule shrinkage could be found in our experiments (Figure 4.8 and Figure 4.9). The low UV power (only 5 mW/cm^2) used in our study could be one explanation. Another reason may be attributed to the limitation of our UV source. As the UV source is selected predominately to suit the chemical transition of BP groups in this work, a mercury lamp (UVACUBE 100, Honle UV Technology) was used, which only emit a small fraction of UV light at wavelength smaller than 250 nm (i.e. < 10%). Consequently, the contribution from the most expected spectral range to cause effect on PSS (i.e., around 220 nm) is small and may well resulted in no apparent shrinkage of PAH/PSS capsules in our condition after 2 hours of irradiation. It should be noted, however, that the PAH/PSS capsules were only used as control to contrast the BP-related capsule change.

4.3 UV Triggered Fluorescent Polymer Encapsulation

Besides the environmental influencing factors (e.g., pH, ionic strength), the permeability of capsules mainly depends on their shell density. Shrinkage is one of the effective methods to increase shell density. Different strategies such as light induced morphology change[134] and heat treatment[26] were used to alter the shell density. Both however suffer certain limitation: for instance the former shrinks the capsules through a length reduction of azobenzene molecule caused by *trans* to *cis* photoisomerization, while the latter cannot deal with temperature sensitive materials such as DNA and protein. Different from the physical contraction caused by in-plane molecule photoisomerization or heat treatment, benzophenone related shrinking requires a stable chemical covalent bonding within multilayers, which leads to a re-conformation of the neighbouring polymer chains, and benefits a new method of engineering steady delivery systems.

In this sub-experiment, the fluorescent polymer AF488-labeled dextran (AF488-Dextran, 10 kDa) was chosen for the encapsulation study due to its strong fluorescence resistance to photobleaching, and most importantly, good visualization characteristics to demonstrate the changes in permeability of the microcapsules during long periods of irradiation. As shown in Figure 4.10, Confocal Laser Scanning Microscopy (CLSM) images illustrated the fluorescent polymer encapsulation of $(PAH/PMA\text{-}BP)_4$ capsules in the presence of a AF488-Dextran. Due to the photobleaching, encapsulation can only be viewed after a short irradiation duration, consequently 15 minute of irradiation result was used as an example here. Before UV irradiation, all the capsules were suspended in the fluorescent polymer solution (the green back ground) for 1 hour, and the fluorescent dextran can permeate into the hollow capsules (Figure 4.10 a). However due to the porous structure of capsule shells, hollow capsules can't hold the dye inside (Figure 4.10 b), only very few amount of the dye was stuck in the capsule shells. Upon UV irradiation, the capsule shell of the hollow capsules obtained photo crosslinking, became shrunk and closed or decreased the porosity of the shells to keep the dye inside (Figure 4.10 c).

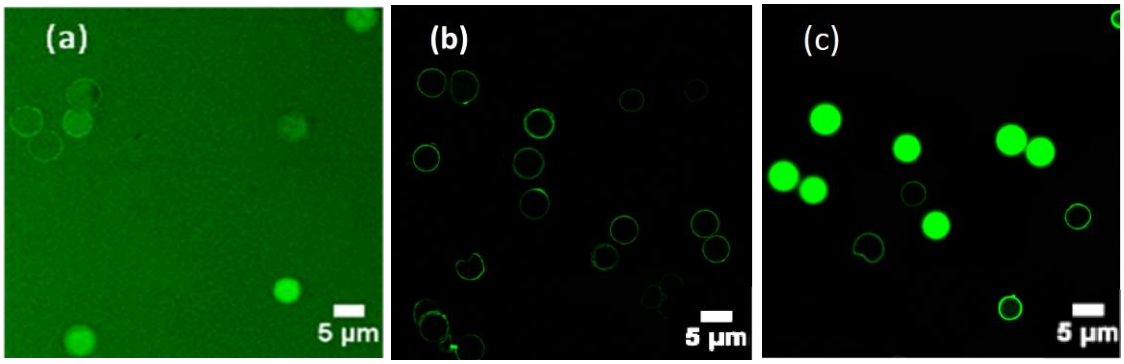

Figure 4.10 CLSM images illustrating the dye encapsulation of $(PAH/PMA\text{-}BP)_4$ capsules in the presence of a AF488-Dextran.

* Before UV irradiation, the fluorescent polymer (green) can permeate into the hollow capsules (a), can't be hold if washed directly (b), but can be encapsulated in the capsules after 15 min irradiation, even after 3 wash steps (c).

4.4 UV triggered Capsule Permeability Change

The fluorescent polymer encapsulation limits our study to short irradiation durations due to the photobleaching effect. For longer irradiation periods, we will use the suspensions of already-irradiated capsules to examine the dye penetration effect, which again can demonstrate the capsule permeability changes caused by UV lights. As shown in Figure 4.11 and Figure 4.12, $(PAH/PMA\text{-}BP)_4$ capsules were first irradiated for 2 hours, and were then suspended in AF488-labeled dextran solution. Throughout the dye permeation experiments, aliquots of the sample solutions were taken after certain incubation time, and then illustrative images were captured to represent typical examples of different dye permeation status (hollow, half-filled, filled). At the beginning, there was no dye permeation into the capsule shells, capsules showed black shadow images under the microscope (Figure 4.11 a). With the increase of time, dye polymers started to penetrate capsule through the shell network structure or defects. Extending the UV irradiation time to 3 hours, it was obvious that the dye polymers had already penetrated into part of the capsules, as the color of the capsules gradually became dark grey (Figure 4.11 b). When the time reached 4 hours, a part of the capsules were filled with fluorescent polymers. A clear example was presented in Figure 4.11 c, which demonstrates an intermediate state of permeability, i.e., about 40 % capsules were filled with fluorescent polymers and showed bright green images. Compared with Figure 4.10 a (1 hour in dextran solution), it was obvious that the UV

crosslinking strengthened the capsule shells and decreased the porosity of the shells, resulting in a much stronger shell structure to resist dye penetration.

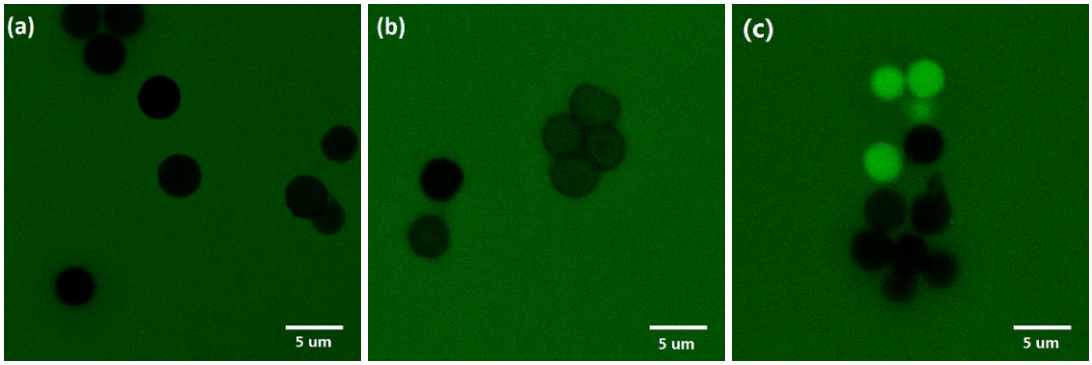

Figure 4.11 CLSM images illustrating the dye permeation of 2 hours-irradiated $(PAH/PMA\text{-}BP)_4$ capsules in the presence of a AF488-Dextran for 0 hour (a), 3 hours (b) and 4 hours (c) .

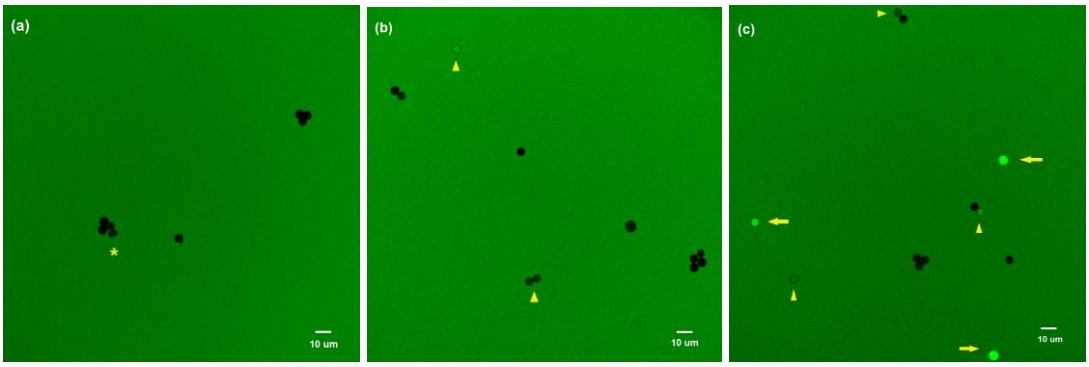

Figure 4.12 CLSM images (at low magnification) illustrating the dye permeation of 2 hours-irradiated $(PAH/PMA\text{-}BP)_4$ capsules in the presence of a AF488-Dextran for 0 hour (a), 3 hours (b) and 4 hours (c). * Typical dye permeation status, hollow (black shadow image), half filled (Δ) and filled (→), were demonstrated. (The symbol * represented a capsule with defect). Scale bars measured 10 μm.

4.5 Capsule Stability and pH Response

Fabricating multilayer capsules with pH sensitive weak polyelectrolytes, the charges or ionization degrees along the PAH (pKa = 8.6) and PMA (pKa = 6.8) molecular chains could be controlled by varying the solution pH value. It has been shown that after LbL assembly, pKa values of the electrostatic absorbed PAH-PMA multilayers could be shifted by approximately 2~3 pH units to the alkaline (pKa, PAH =10.8) or to the acidic (pKa, PMA=3.9) region, respectively[32]. Therefore, after capsule preparation, electrostatic interactions between the polyanion and polycation could be influenced by the outer pH environments. Here we described the pH-dependent behaviours of weak polyelectrolyte microcapsules, $(PAH/PMA)_4$, $(PAH/PMA\text{-}BP)_4$, as well as irradiated $(PAH/PMA\text{-}BP)_4$ capsules.

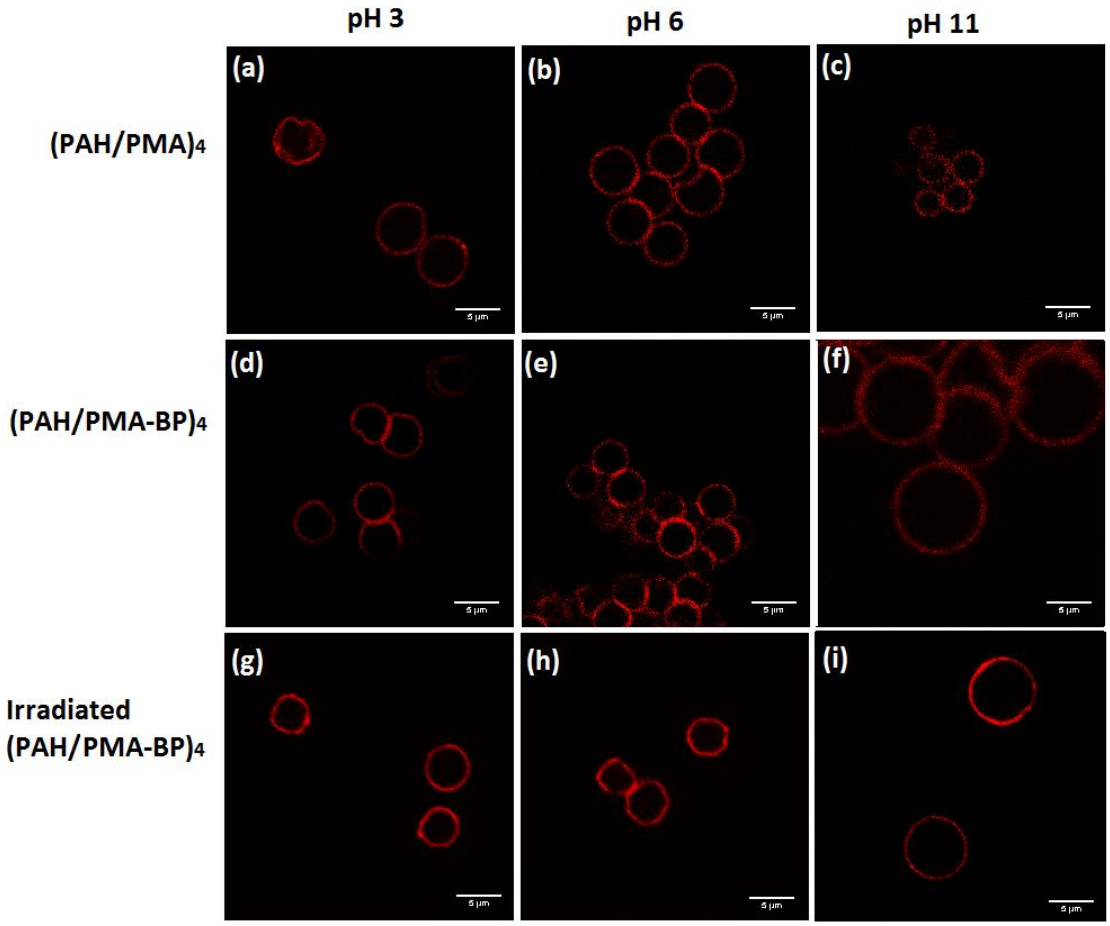

Figure 4.13 CLSM images of different capsules at pH3, pH6 and pH11.

* The scale bar measured 5 μm.

As shown in Figure 4.13 (1st row), the stability of $(PAH/PMA)_4$ capsules in different pH solutions depended on their dissociation behaviour, similar to those reported in Mauser's work[32]. At pH=6, both PAH and PMA were highly charged, all the capsules are stable with a diameter of 5.0 ± 0.30 μm (Figure 4.13 b). By decreasing the pH value, PAH was fully charged, but more and more carboxylate ($–COO^-$) groups of the PMA were protonated. At pH= 3 (i.e., below the pKa of PMA in PAH-PMA multilayers), only a small amount of carboxyl (–COOH) groups were dissociated, resulting in PAH with excess amount of uncompensated ammonium ($–NH^{3+}$) groups. The electrostatic repulsion between the positive charges of PAH caused a swelling of the shell structure. If the electrostatic repulsion played a predominant role here, the remaining electrostatic interactions between the minority ionic pairs of PAH and PMA would not be strong enough to stabilize the shell structure. However, at pH= 3, uncharged PMA molecules provided a hydrophobic association, which helped the capsule shell survive and

exhibited only a slightly size increase to 5.35 ± 0.29 μm in diameter (Figure 4.13 a). Likewise, PMA became fully charged at pH=11, while most of the PAH got deprotonated. Without a hydrophobic interaction, electrostatic repulsion of the negative charges became the dominate interaction, resulting in the dissolution of the shell (Figure 4.13 c). Adjusting the capsule suspension pH value to 12, capsule dissolution occurred immediately, no image could be captured. As for the $(PAH/PMA\text{-}BP)_4$ capsules (2^{nd} row), the stability of the capsule system composed of PMA-BP was a slightly different. Due to the existence of ~50 % esterified PMA segment, the total amount of PAH in PAH/PMA-BP capsules was only half of that in PAH/PMA capsules in order to obey the rule of charge balance. Thus, an increase in pH will lead to a more pronounced effect on the PAH/PMA-BP system (Figure 4.13, 2^{nd} row), exhibiting an early swelling state of capsules at pH=11. At high pH, the excess amount of uncompensated carboxylate groups of PMA segment would cause the dissolution of the shell, but the existence of the esterified PMA segment (~50 % of PMA-BP) played a role in stabilizing the shell structure in basic conditions. As shown in Figure 4.13 f, an immediate dissolution was depressed, resulting in swollen capsules in diameter of 9.71 ± 0.60 μm.

Stabilizing the pH sensitive multilayers in extreme pH conditions is a challenging task. Crosslinking might be an effective method to solve this problem. By crosslinking the functional groups of the individual polyelectrolytes with chemical crosslinkers, this strategy provides good protection against the dissolution of polyelectrolyte multilayers[213, 214]. For instance, if we use a crosslinker, e.g., EDC, to crosslink the functional groups ($–NH_2$ and –COOH) of PAH/PMA capsule shells, the multilayer system will become stable in extreme pH condition. In the meantime, these capsules also became rigid and would not respond to the outer pH anymore as the charge sites of the multilayers were consumed and became amide bonds (–NH–CO–)[32]. Here we introduced the photoactive BP groups to crosslink the PAH/PMA capsule. As shown in Scheme 4.1, UV irradiation caused a recombination of BP and unreactive C–H bond[138], providing crosslinking sites within multilayers. Unlike the amidation reaction of –COOH and $–NH_2$ groups, UV crosslinking not only stabilized the capsules, but also maintained ionizable groups. As shown in the Figure 4.13 (the 3^{rd} row), at pH=6, 15-minute irradiated capsules were stable with a size of 4.30 ± 0.29 μm (Figure 4.13 g), which was consistent with the SEM results. By decreasing the pH value, capsule got a

slight swelling and the size increased to 4.55 ± 0.24 μm (Figure 4.13 h). Increasing the pH value to 11, the capsule size was increased to 6.79 ± 0.54 μm (Figure 4.13 i). Comparing with the un-irradiated $(PAH/PMA\text{-}BP)_4$ capsules, the UV-crosslinked capsules still possessed a pH-responsive property but was not as extreme as the un-irradiated ones.

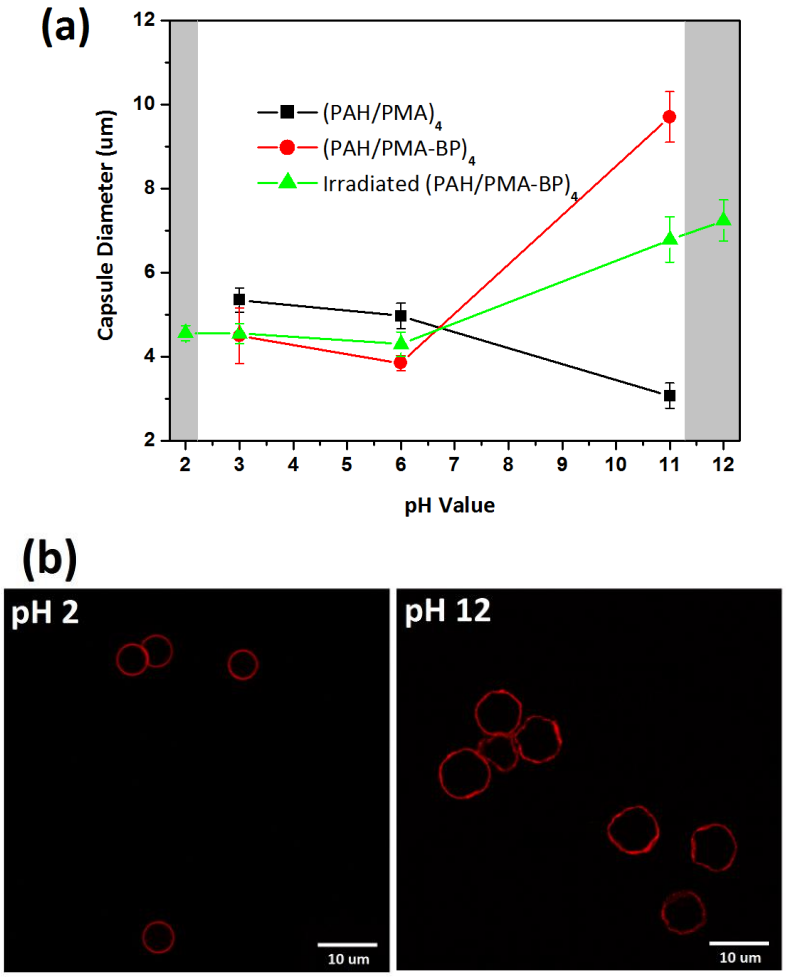

Figure 4.14 Diameter of microcapsules as a function of pH (a), and LCSM images of $(PAH/PMA\text{-}BP)_4$ at pH2 and pH12 (b).

*The gray areas indicate the regions where the un-irradiated capsules are dissolved. (Scale bar: 10 μm)

Besides the relatively normal pH ranges from 3 to 11, capsules in extreme pH conditions were also investigated, as shown in Figure 4.14. Adjusting the capsule suspension to a pH value beyond the pKa values of the PAH/PMA multilayers, capsule without irradiation cannot survive due to the lack of electrostatic interactions (Figure 4.14 a). However, the UV irradiated capsules were still stable after suspending in a solution of pH=2 for 1 week. Comparing with the capsules in pH=3 solution, there

appears to have no obvious size change of the irradiated $(PAH/PMA\text{-}BP)_4$ capsules at pH=2, i.e. an average diameter of 4.56 μm. However at pH=12, the irradiated capsules continued to swell to a diameter of 7.24 μm.

Response to environmental pH stimulus allows controlling the structures of delivery systems. As a consequence, the release of encapsulated cargos from pH-activated carriers could be adjusted. pH sensitive carriers such as nano-/micro- spheres, hydrogels and liposomes have been widely studied and developed[215]. For examples, the pH-responsive organic-inorganic hybrid spheres composed of sandwich-like organoclay layers controlled release of ibuprofen and eosin at different pH (4-9) due to the pH-induced protonation of amino groups[216]. The PEGylated siRNA nanoparticle showed rapid release of the encapsulated siRNA at pH 5.5, which could serve as novel delivery system for treatment of liver diseases[217]. In this chapter, it is expected that these $(PAH/PMA\text{-}BP)_4$ microcapsules with UV responsive properties and pH dependent stability could provide a novel way for controlled drug delivery systems, in which UV light could be used to encapsulate chemicals and drugs without heating, and the UV caused shrinkage as well as the pH dependent stability could be used to modulate cargo release. Nevertheless, one should notice, the extreme pH conditions investigated here might be not suitable for applications in biological media such as human skin and internal tissue, organ. However, modifying the permeability of polyelectrolyte multilayer shell through benzophenone-related crosslinking without consumption of ionic groups would offer an optional approach for the researchers to fabricate crosslinked (or sealed) vehicles or delivery systems for biological uses, where such vehicles would respond to subtle pH changes and thus to be activated.

4.6 Conclusions

In this chapter, the fabrication and characterization of UV responsive $(PAH/PMA\text{-}BP)_4$ capsules from two weak polyelectrolytes with enabling pH response were reported. The capsule properties were found tuneable by the exposure to UV light. i.e., the capsules can shrink about 30 % in diameter with nearly doubled shell thickness upon 2 hours of irradiation at a wavelength of 275 nm. Such UV-triggered shrinkage modified the capsule permeability, providing a novel method for the entrapment biologically active compound avoiding heating. In addition, $(PAH/PMA\text{-}BP)_4$ capsules exhibited tuneable

pH responsive properties. It was demonstrated that the capsule size and stability can be controlled reversibly by varying the solution pH values. It was shown that after UV irradiation, crosslinking happened in the capsule shells, increasing the capsule stability in extreme pH conditions. The increased stability didn't consume the functional groups of weak polyelectrolytes, which kept the capsule's pH-responsive capability. These $(PAH/PMA\text{-}BP)_4$ microcapsules with UV responsive properties and pH dependent stability could provide a promising way for delivery systems. As shown in Scheme 4.3, a schematic illustration of this UV responsive microcapsule system composing of weak polyelectrolytes was demonstrated.

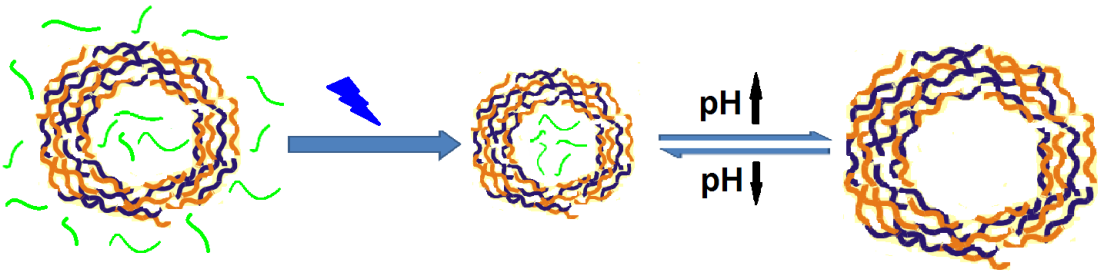

Scheme 4.3 Schematic representation of the two-channel controllable microcapsule system.

5. UV-induced Microcapsule Disruption Based on Azobenzene Re-alignment

5.1 Introduction

5.1.1 Background

One of the most challenging tasks and the ultimate purposes to develop delivery systems is to modulate the release of encapsulated cargo materials[218]. Strategies such as heat treatment and light-induced morphology change were used to alter the shell density and integrity, and then to influence capsule permeability [16, 26, 219] . As one of the most interesting parts of stimuli-responsive capsules, photo stimuli responsive capsules are able to affect their micro-/nano- structures come in the form of remote control triggered by external light (e.g., sun light, infrared laser) without requirement of direct contact or interactions[220]. The development of such highly light sensitive vesicles is of great importance, especially in the fields of surface sciences and environmental applications, where sometimes lights would be the only available stimuli to drive the systems. Various strategies were applied to develop such light addressable vesicles with different functionalities[220]. One of the classical examples is the laser induced local heating[19], which has been widely studied to deconstruct the capsule shells, demonstrated good site specificity, and can be used as promising delivery system for biological and clinical applications. However, the requirement of specific laser wavelength and site-directed energy supply will definitely limit its application. For practical uses, the abundant existence of UV light in sunlight may offer a new kind of natural triggers for such applications. One of the key points is how to trigger the shell disruption or capsules breakage by using UV light directly.

Polyelectrolytes are basic components for LbL capsule fabrication. Diverse polyelectrolytes have been used to build up capsules. Different combinations of the oppositely charged polyelectrolytes with active functional groups endow their capsules with unique architectures and properties, which affect their further applications. An ideal strategy here for controlled release would be achieved by UV light induced polyelectrolyte microcapsule breakage due to the activation of UV responsive

component in polyelectrolyte shells. A kind of novel UV responsive compounds that access the needs is the azobenzene (AZO). AZO derivates refers to a class of molecules that composed of two phenyl rings linked by an azo (N=N) double bond. Theoretically, the conjugated chemical structure owes AZO strong electronic absorption in both UV (π-π* transition) and visible light (n-π* transition) regions, leading to efficient and reversible *trans–cis* photoisomerisation behaviour by switching the treatment between UV irradiation and visible light irradiation or thermal treatment[221]. For LbL assembly, polyanions with the AZO chromophore in the side chains were employed to make multilayers with counterpart polyelectrolytes. It has been reported that incorporation of the robust AZO chromophores into various polycations could influence its photoresponse (e.g. micro-crystallisation and phase separation) due to their mobility and preference of dipolar azo units to form aggregates[222], exploring intensively functionalities for optical storage[160] and liquid crystal alignment[159]. Specifically, for PDADMAC/PAZO system, when the UV light triggered a photoisomerization reaction, a UV spectral change towards longer wavelength side (also known as red shift) accompanied with a decrease in the π-π* band intensity occurred, which was interpreted by the formation of J aggregate[223]. As a consequence of J aggregate, these individual end-to-end self-organized AZO moieties led to polymer chain motions in sub-domains or features, which further exhibited as phase separation of adjacent domains due to anisotropic oriented average aggregate directions[18]. This kind of AZO motion based phase transitions have found interesting applications to photo-control over the matrix and vesicle destruction[18, 224].

5.1.2 Aim and Objectives

The aim here is to break the multilayer capsule shell integrity by using the UV light remotely, and thus to realized the UV triggered cargo substance release. The general idea is based on UV light controlled capsules disruption through J-styled aggregation of AZO moieties in these multilayer shells.

Therefore the main objectives of this chapter are:

1) To design and fabricate polyelectrolyte multilayer microcapsules $(PDADMAC/PAZO)_4$ containing azobenzene molecules.

2) To investigate the UV induced capsule shell disruption, for example the UV-dosage dependent capsule morphology change (swelling and breakage).

3) To study on the underlying mechanism of UV induced capsule shell disruption. And to study the feasibility of UV triggered cargo substance release from the multilayer capsules.

5.2 UV Induced Capsule Breakage

The UV response properties of these fabricated capsules were studied. In this work, the UV intensity used was approximately 55 mW/cm^2, and the UV treatment duration was 0~3 hours. Specially, for UV triggered protein release, UV irradiation was also carried out with the intensity of 27 mW/cm^2. The structural formulas of these polyelectrolytes used for capsule fabrication were given in Scheme 5.1.

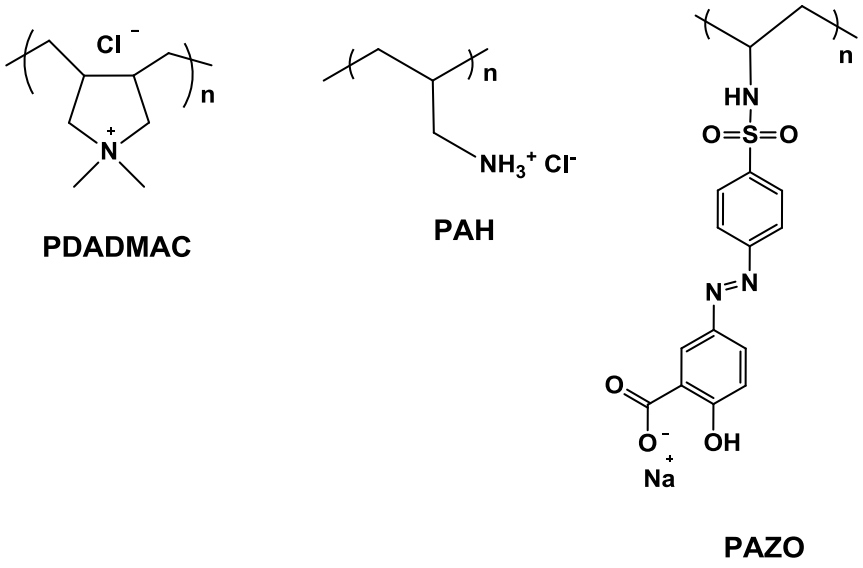

Scheme 5.1 Structural formulas of the polyelectrolytes used in this chapter.

The experimental results showed that exposure of the PDADMAC/PAZO microcapsule suspensions to UV light led to breakage of the capsules. Figure 5.1 illustrated the breakage of the $(PDADMAC/PAZO)_4$ capsules as a function of time. In this sub-experiment, capsules exposed to the UV light with intensity of 55mW/cm^2 were demonstrated as an example of UV induced capsule breakage. Before irradiation, the capsules were flat with creases and folds with an average diameter of 5.12 μm (Figure 5.1 a). After 10 min of UV irradiation, part of the hollow shells started to swell, and an

increase in the average diameter of the capsules from 5.12 μm to more than 7 μm was observed (Figure 5.1 b). In the meantime, capsule debris (white dots) appeared around the swollen capsules, which indicated the starting of shell disruption. Further extending UV irradiation time, capsules continued to increase in size, which led to complete disruption of the shell formations. After 60 min of irradiation, almost 70% capsules were broken; typical example of the broken capsules after 60 min of UV irradiation was shown in Figure 5.1 c. When the irradiation time reached 120 min, no intact capsules survived, only the split capsule debris and some needle-like formations were observed on the silica wafer (Figure 5.1 d).

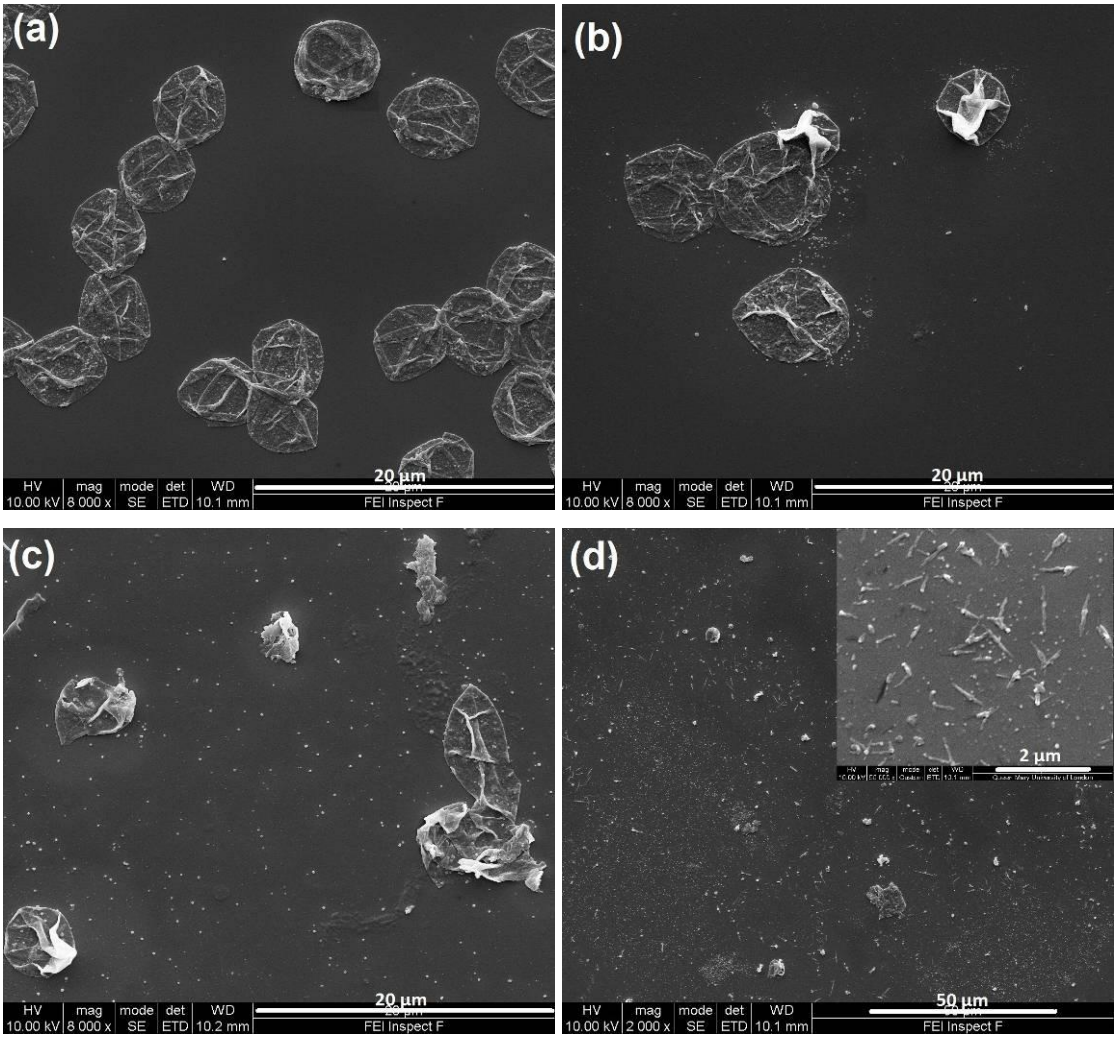

Figure 5.1 SEM images of $(PDADMAC/PAZO)_4$ capsules after UV irradiation of 0 (a), 10 min (b), 60 min (c) and 120 min (d).

* The inset represented needle-like formations.

During all the irradiation process, ice bath was used to keep the whole capsule

suspension in a thermo-stated environment. However, due to the existence of UV absorbable material PAZO, local heating effect based on UV energy absorption in the polyelectrolyte shells was unavoidable. Previous works of Sukhorukov's group have already revealed the temperature-dependent behavior of hollow polyelectrolyte multilayer capsules, which resulted in either capsule shrinkage[225] or swelling[201, 226]. In particular, for PDADMAC contained capsules, it was proven that the unbalanced energy of multilayer system originated shell swelling[226]; and for PAZO contained capsules, the heat treatment showed no significant influence on capsule size change[16]. Since the capsule swelling and disruption phenomena were also found in our work, careful attention to the local heating related behavior of the PDADMAC/PAZO system was required to illustrate the UV induced capsule disruption. Briefly, $(PDADMAC/PAZO)_4$ suspension were incubated in water bath for 1 h at each temperature point ranging from 20 ℃ to 90 ℃. After thermal incubation, the capsules were observed under SEM, and the possible capsules morphology and size changes were analyzed. As shown in Figure 5.2, it was obvious that the heat treatment barely showed any dramatic influence on capsule morphology. At 20 ℃, capsules were flat with a diameter distribution of 5.12 ± 0.328 μm. Increase of the temperature did not show any significant influence, either on capsule size or shell roughness. As the SEM images shown in Figure 5.2, a typical example of capsules after incubated at 90 ℃ was given. Unlike the effect of UV irradiation, such capsules had an average diameter of 5.008 ± 0.368 μm, and all of them kept their shell integrity after heating, almost no broken one could be found, indicating that these $(PDADMAC/PAZO)_4$ capsules had high thermal stability, and the local heating was not the main reason caused capsule breakage.

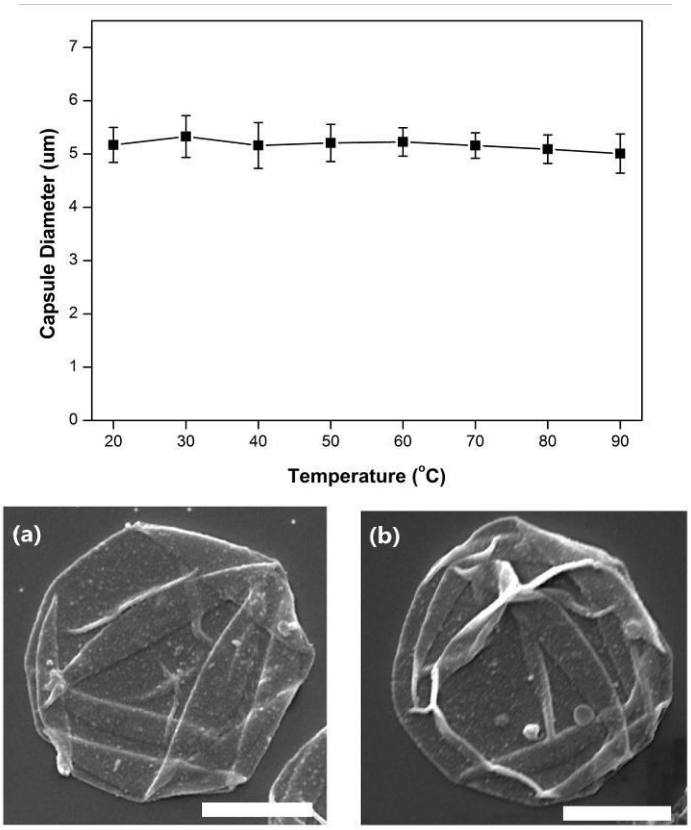

Figure 5.2 Quantification of the $(PDADMAC/PAZO)_4$ capsule diameter after heat treatment.
* The lower panel: SEM images represented the capsules incubated at (a) 20 ℃ and (b) 90 ℃. The scale bars measure 2 μm. Capsule diameter and distribution were quantified by randomly averaging the diameters of at least 35 capsules per sample from the SEM data.

Here in this experiments, $(PAH/PAZO)_4$ capsules, containing a more flexible polycation PAH with positive charges on the side chains, were used as control groups. However, a gradually capsule breakage process as happened to PDADMAC/PAZO system was not observed over 2 hours. Contrarily, UV irradiation caused a capsule size decrease slightly. As shown in Figure 5.3, after 2 hours of irradiation, $(PAH/PAZO)_4$ capsules diameter gradually decrease from 4.96 ± 0.273 μm to 4.20 ± 0.383 μm. On the other hand, almost all the capsules were intact without any obvious damage. Interesting, light-induced capsule shrinkage has also been observed in the LbL multilayer system containing azobenzene compounds, as reported by Bédard and co-workers[16]. In their work, $(PAH/PAZO)_3$PAH/PVS capsules were built up with PAZO, PAH and poly(vinylsulfonate) (PVS). It was believed that the UV induced *trans* to *cis* isomerisation of azobenzene that caused a significant shrinkage in their capsule system, demonstrating as significant size decrease, apparent shell morphology changes as well as shell permeability decrease.

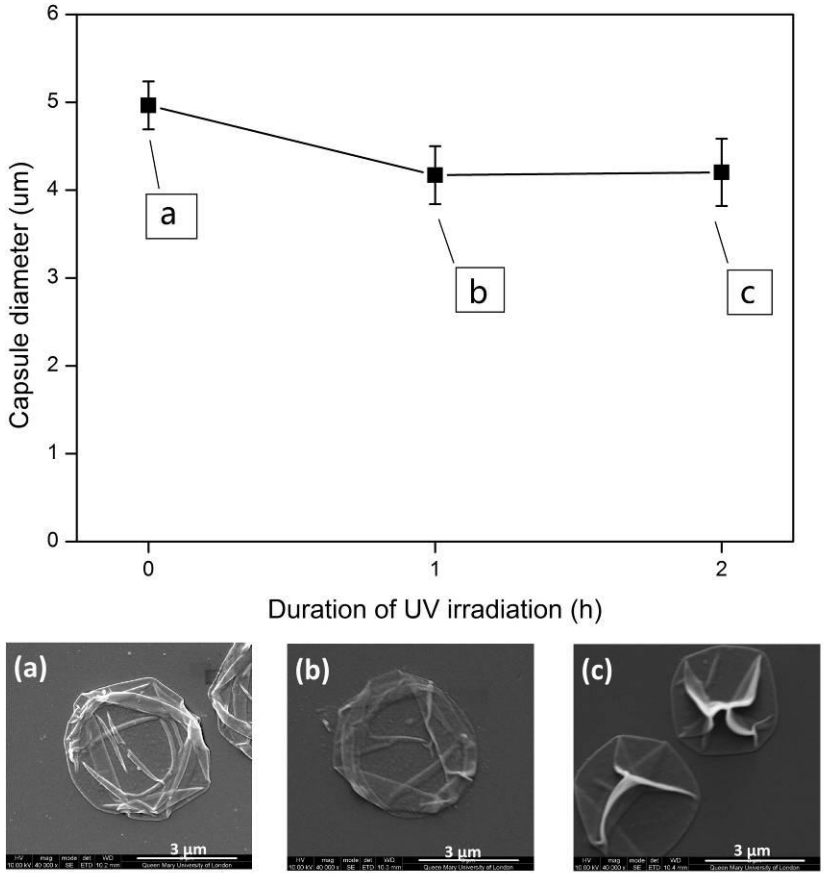

Figure 5.3 Quantification of the $(PAH/PAZO)_4$ capsule size before and after UV irradiation. Lower panel: SEM images represent the capsules before irradiation (a), after irradiation for 1 hour (b) and 2 hours (c).

Comparing these above three capsule systems containing PAZO, one might obviously presuppose that different properties of the positively charged counterpart polyelectrolytes should be associated with the different UV responsive behaviour, such as capsule disruption and shrinkage. Preliminary investigation has already found significant influence of polycations on the azobenzene molecular orientation in films and on the photoisomerization kinetics[227]. In our experiments, similar influences were recorded by UV-Vis spectroscopy.

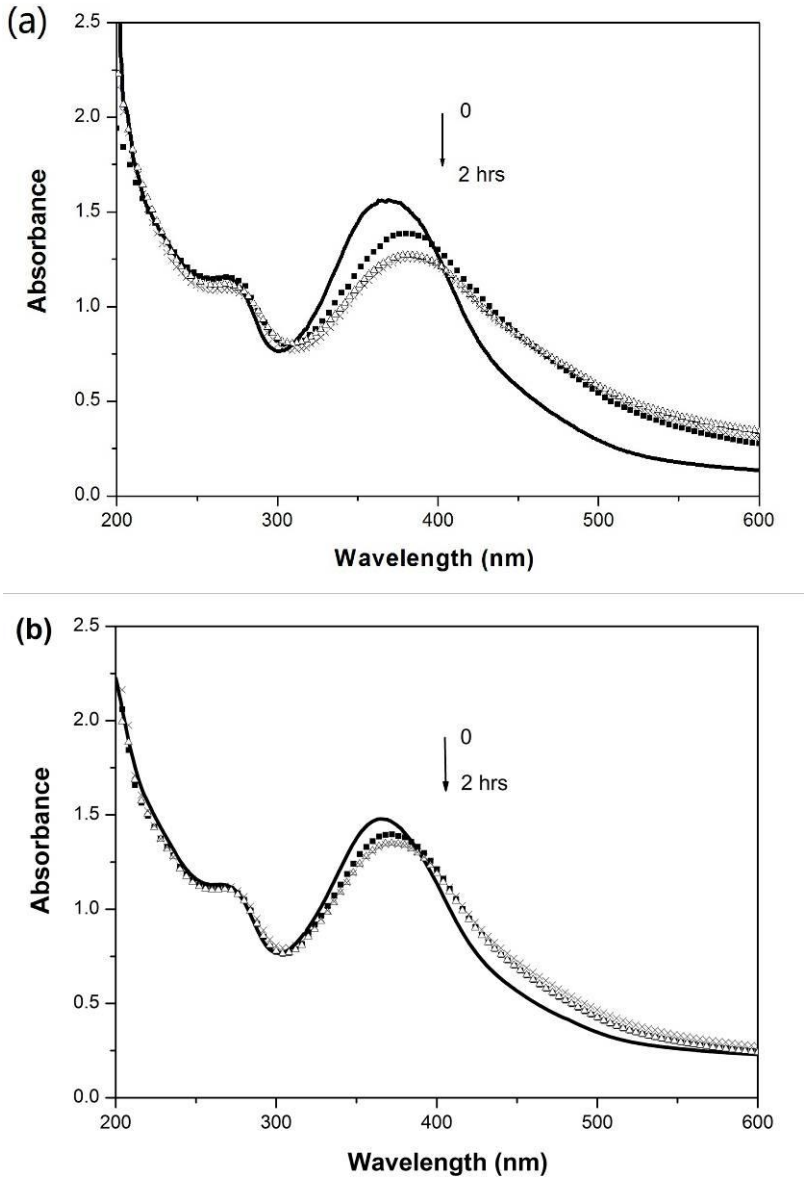

Figure 5.4 UV-Vis spectra of (a) $(PDADMAC/PAZO)_4$ and (b) $(PAH/PAZO)_4$ microcapsule suspensions before (–), and after UV irradiation for 30min (···), 60min (Δ) and 120min (×).

As shown in Figure 5.4, the UV-Vis absorption spectra, obtained from the two kinds of microcapsules containing azobenzene groups in the multilayer shells were given. For both of the fresh fabricated $(PDADMAC/PAZO)_4$ and $(PAH/PAZO)_4$ microcapsule aqueous suspensions, a strong absorption at ~366 nm was found, which was assigned to the π-π* transition of *trans*-azobenzene, and the absorption detected at ~268 nm was due to a transition that roughly parallel to the short axis of the *trans*-azobenzene chromophore[223]. As a consequence of photoisomerization reaction induced by UV light, the spectra of the two kinds of microcapsule suspensions showed a decrease in the π-π* band maximum intensity. But this band did not disappear even after 2 hours of

irradiation, indicating that the photoisomerization did occur but was not completed. Similar phenomenon was also observed in Stroeve's work[223], and reasonable interpretation was attributed to steric hindrances against *trans* to *cis* conversion[228] and hindrances of tight AZO aggregate formations[229].

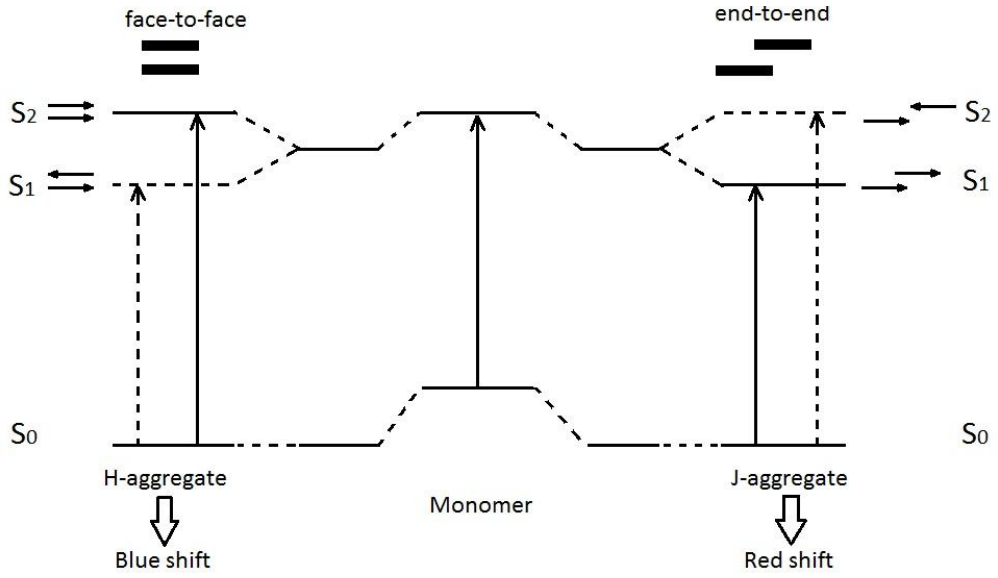

Scheme 5.2 Shematic representation of the relationship between azobenzene arrangement and the spectral shift based on molecular exciton theory.

* The azobenzene molecules aggregated in a face-to-face way (parallel) to form H-aggregates or in an end-to-end way to form J-aggregates.

UV absorbance spectra change on isomeriaztion is one of the most well known phenomena as photochromism, demonstrating as the AZO molecular conformation change in plane qualitatively. However, one must notice, the photoisomerization also causes changes in dipole moment. Depending on mutual orientation of the interacting dipole moments between the counterpart molecules, AZO moieties tend to form end-to-end or plane-to-plane aggregates, also known as J or H aggregates (Scheme 5.2), respectively[230]. Theoretically, such aggregate formations can be easily monitored by spectroscopic measurements. As shown in Figure 5.4, exposing the capsule suspensions to UV light, another spectral change occurred. Specifically, a time dependent red shift in the maximum absorbance was clearly visible. For $(PDADMAC/PAZO)_4$ capsules, after 30 min of irradiation, the maximum absorption peak was centered at 381 nm, demonstrating a red shift by 15 nm caused by UV light. Further exposing to UV light for 1 hour, an additional red shift by ~2 nm was found at 383 nm. After that, increasing the UV irradiation period to 120 min did not show significant red shift any more. In

comparison, the maximum absorption position of $(PAH/PAZO)_4$ microcapsule suspension was located at ~371 nm after 30 min of irradiation. After 2 hours of irradiation, the maximum absorption was observed a total red shift by 7 nm and subsequently receding to a constant value of ~373 nm. These phenomena can be interpreted as azobenzene aggregation in the form of J aggregates, as suggested by Stroeve[223]. It should be noted that the decrease of absorption intensity in PDADMAC/PAZO system was more pronounced, which illustrated the mobility of AZO moieties was higher than that in PAH/PAZO system[223], further facilitated AZO orientation when the capsules were exposed to UV light.

The differences caused by polycations in PAZO contained systems were also supported by FTIR studies. As shown in Figure 5.5, for both of $(PDADMAC/PAZO)_4$ and $(PAH/PAZO)_4$, weak shoulder peaks were assigned to the N=N stretching vibration in *trans* azobenzene, which appeared at ~1400 cm^{-1}[231, 232]. Additional, a medium peak at 1042 cm^{-1} was found in the spectrum of $(PAH/PAZO)_4$, which was attributed to the C–N out-of-plane bending[233, 234]. For $(PDADMAC/PAZO)_4$, after 2 hours of UV irradiation, no significant difference in FTIR spectra can be found. This result was in accord with UV-Vis spectra, where no clear band assigned to *cis* isomer can be observed, indicating the re-orientation was preferred in the PDADMAC/PAZO system. For $(PAH/PAZO)_4$ capsules, UV irradiation not only caused the disappearance of N=N and C–N peaks, but also induced a generation of NH_4^+ ions signals at 3054 cm^{-1} and 3144 cm^{-1}. These new ions were converted from $–NH_3^+$ of PAH segment, as suggested by Katagiri and co-workers[134]. According to their work, chemical transitions caused by 120 min of UV irradiation at 20 mW/cm^2 can result in structural rearrangement and capsule shrinkage. Considering Bédard's work, it can be concluded that the chemical transitions and/or azobenzene molecule conformation changes should be the main reason to drive $(PAH/PAZO)_4$ capsule shrinkage. However, the $(PDADMAC/PAZO)_4$ capsules didn't demonstrate similar UV induced shell shrinkage due to the lack of such chemical and conformation transitions.

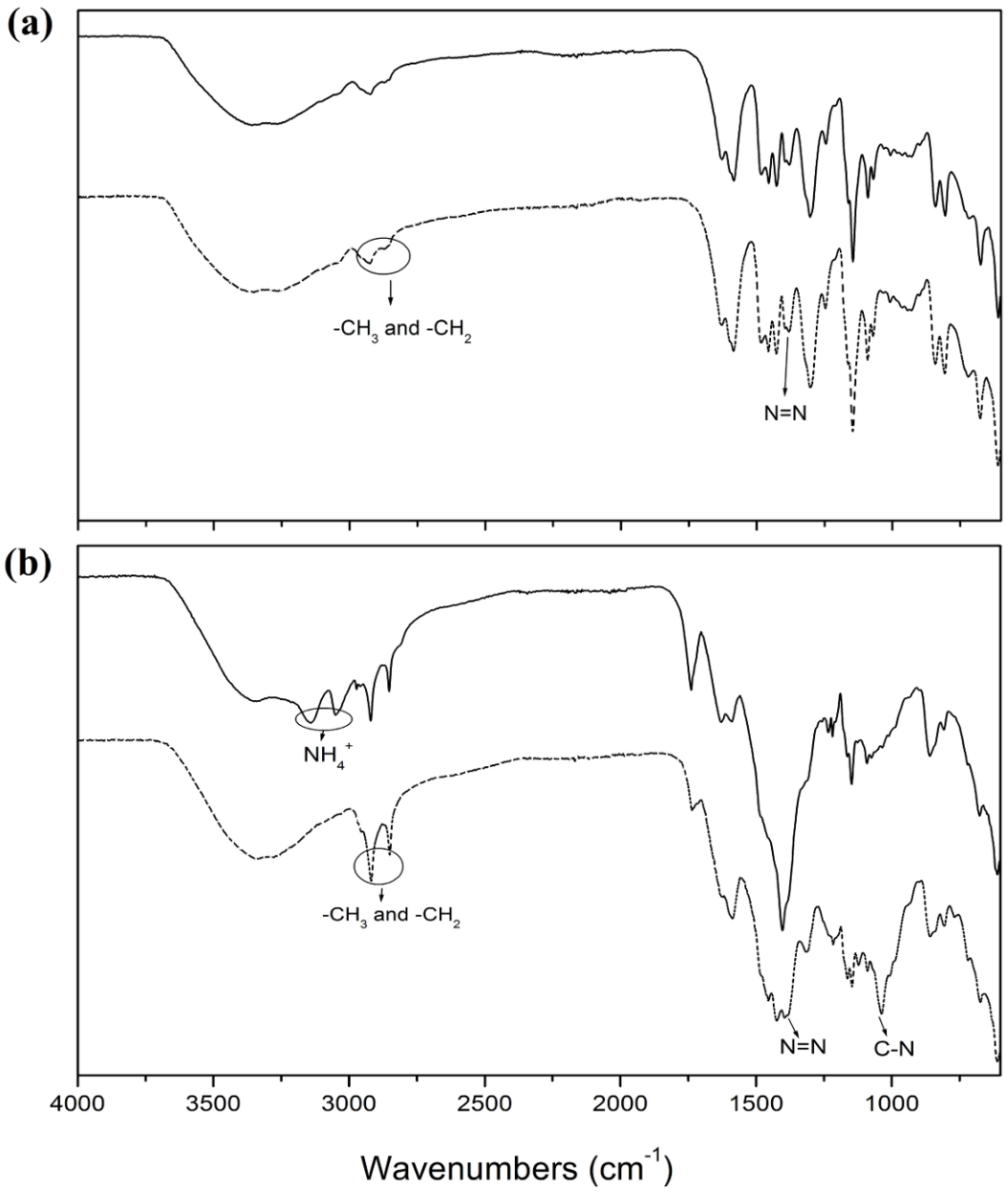

Figure 5.5 FTIR spectra of $(PDADMAC/PAZO)_4$ (a) and $(PAH/PAZO)_4$ (b) microcapsules before (dot lines) and after 2 hours of UV irradiation (solid lines).

A remarkable feature is that the azobenzene related aggregates caused by photoisomerization have been used as triggers to adjust the functions of Langmuir Blodgett films, typical applications are electrical conductivity switching[235] and liquid crystal alignment[236]. Moreover, it was reported that the aggregates or clusters of azobenzene derivatives induced by UV irradiation can lead to *"catastrophic"* destruction of the shell-like formations, which have been developed as strategies to build up photosensitive liposomes[164] and polymersomes[204] for drug delivery use. As

mentioned above, a significant red shift was observed with the $(PDADMAC/PAZO)_4$ microcapsule suspension as the consequence of UV irradiation. Considering the distinct different capsule morphology changes occurred in these two capsule systems containing PAZO, the authors proposed that these significant end-to-end J aggregates as in-line effected by PDADMAC were the main reason that caused the gradually capsule breakage process in our $(PDADMC/PAZO)_4$ capsule system.

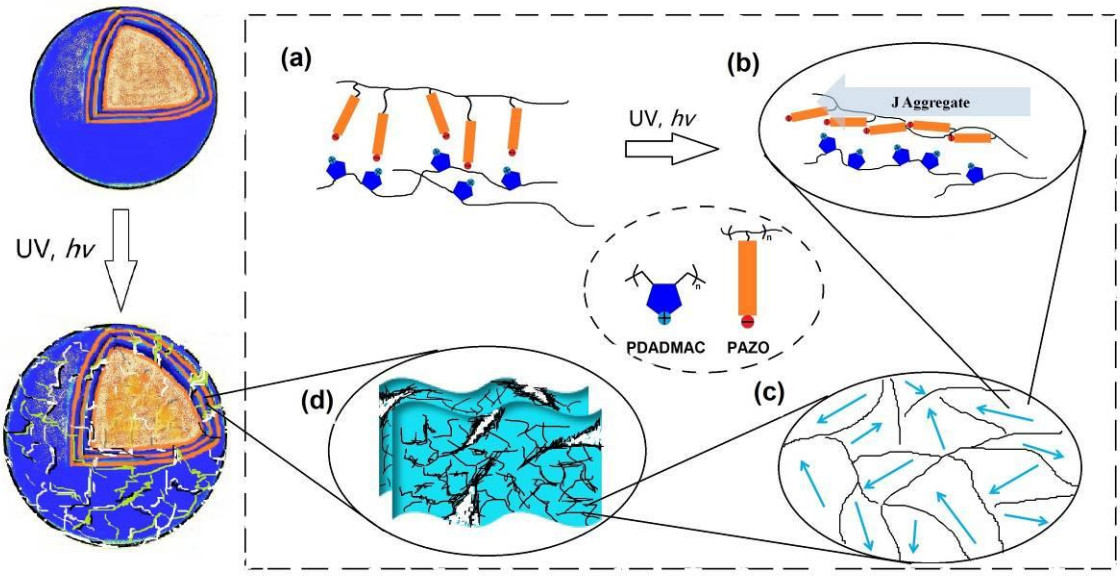

Scheme 5.3 Schematic illustration of $(PDADMAC/PAZO)_4$ microcapsule disruption induced by UV irradiation.

As suggested, in the case of PDADMAC/PAZO film, layer-by-layer polyelectrolyte deposition was not as regular as other polyion pairs, interdigitation of the polyion chains were found instead of proper deposition; moreover, the patchy structures with 60 nm of aggregates were confirmed by TEM investigation[223]. In the case of LbL microcapsules, as schematic illustrated in Scheme 5.3, such aggregates directly exhibited as apparent rough shell surface consisting of various domains with anisotropic AZO moieties (Scheme 5.3 a). Combining results of UV-Vis spectroscopy, one may draw a conclusion that it was the combination of PDADMAC and PAZO led to aggregation of PAZO segment in the progress of polymer deposition, which further facilitated the large extent of J aggregates when capsules were exposed to UV light (Scheme 5.3 b). Such aggregates in many cases have been proposed as a chiral "pinwheel" structure composing of a trimer or tetramer, and they were preferred to form readily in presence of water *via* strong noncovalent aromatic-aromatic

interactions[237]. Further studies described such extended aggregates in several assemblies as a mosaic or lattice of the small "unit" aggregates having a surface area of ~20 Å[238] (Scheme 5.3 c). The numerous formations of such mosaic aggregates in one microcapsule led to presence of stress raisers between the neighboring aggregates, which became the breaking points in progress of further aggregate assemblies (Scheme 5.3 d). When the integrity of the microcapsules was lost on irradiation and the aggregate formations were not flexible enough to retain the spherical shell structures, the capsule gradually started to be split on the local scale, demonstrating as capsule swelling phenomena. Further accumulated tearing effect led to the visualized capsule breakage.

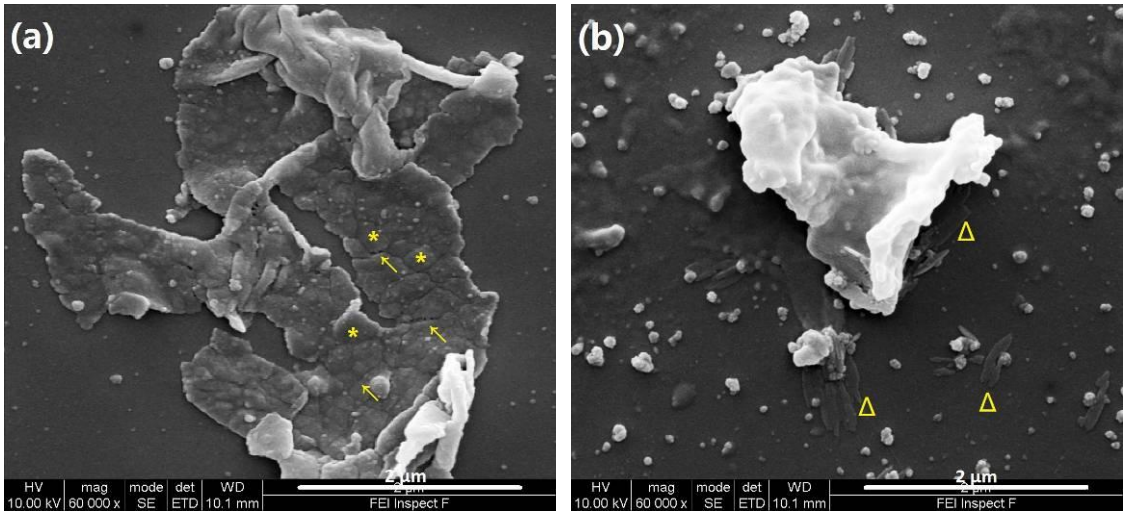

Figure 5.6 SEM images of $(PDADMAC/PAZO)_4$ microcapsule debris after UV irradiation of 60 min (a) and 120 min (b).

* The symbols represented macro-mosaic formations (*), related stress raisers (↖) and lamellar-like formations (Δ), respectively.

The hypothetical capsule disruption mechanism was supported by SEM studies. Typical images of the macro-mosaic like aggregates (symbol: *) and related stress raisers (symbol: ↖) in one microcapsule were given, as shown in Figure 5.6 a. With the increase of irradiation time, more and more capsules became broken, resulting in more and more debris formations. The photoisomerization induced aggregation also occurred in these capsules debris, leading to further re-orientation within these pieces. Such re-orientation caused generation of small lamellar- and needle- like formations[53]. As shown in Figure 5.6 b, after 2 hours of irradiation, split capsule debris was observed accompanied by lamellar-like formations (symbol: Δ) nearby. And in the solution,

numerous needle-like structures were also observed, as the ones deposited on silicon wafer (Figure 5.1 d).

Different external triggers with their abilities to affect microstructures of fabricated capsules have been applied to break multilayer capsules. For example, ultrasound radiation, with either high (850 kHz[91]) or low (20 kHz[111]) frequency, can tear the microcapsules into pieces through the generated cavitation; IR laser can trigger a instant capsule shell breakage[106]. Unlike the UV triggered gradually capsule swelling-disruption process in this work, these two methods demonstrated rapid and powerful abilities to break fabricated LbL capsules. Moreover, ultrasound and IR laser both showed great potential application in biological media, where encapsulated cargo drugs could be released rapidly. However, one should notice, our capsule system here offered another possible way to liberate the cargos with slow release rate. And most importantly, the release speed could be adjusted by the UV intensity as well as the number of capsule layers (see section 5.4).

5.3 Irreversible Effect on Capsule Disruption

In theory, azobenzene-related aggregates, either in J or H form, are reversible. After irradiation, a *cis* to *trans* isomerization can be achieved through thermal treatment or exposure to visible light (> 400 nm). As for the PDADMAC containing multilayers, it was found a much higher intensity of recovery when the samples were left in dark or heated[223]. A strategy based on reversible *trans* to *cis* photoisomerization was applied to realize reversible control of formation and disruption of bilayer vesicles composing of azobenzene modified amphiphillic molecules[239].

However, for capsules composing of PDADMAC and PAZO, the UV induced capsule swelling was not reversible. As shown in Figure 5.7 a, capsules showed swollen but relatively intact morphologies after 1 hour of UV irradiation with UV intensity of 10 mW/cm^2. Later, subsequent visible light irradiation (>400 nm, 5 mW/cm^2) did not show any reformation or shrinkage of the swollen capsules, even after 2 hours or irradiation (Figure 5.7 b). These results confirmed the back-isomerizaiton, if there was any, cannot push backwards of capsule shell changes. And these results further provided a clear indication that capsule disruption was based on stress destroy

originated from azobenzene moieties assemblies, as presented in our hypothesis (Scheme 5.3).

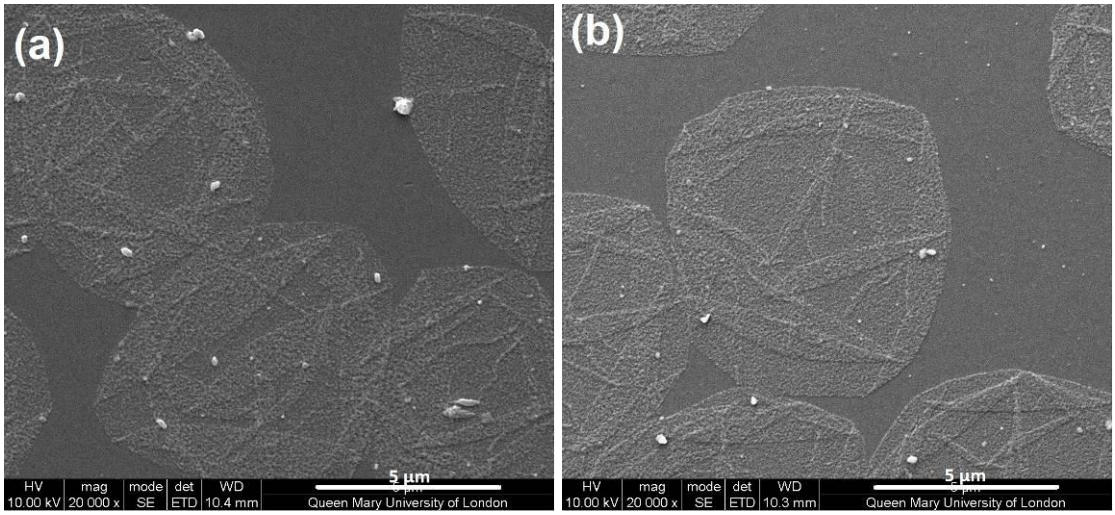

Figure 5.7 SEM images of $(PDADMAC/PAZO)_4$ capsules after 1 hour of UV irradiation (a), and after additional 2 hour of visible-light irradiation (b).

5.4 UV-regulatable Protein Release

The organized J aggregates within the capsule multilayers induced by UV lights led to the disruption of PDADMAC/PAZO shells, which could offer a promising strategy for the controlled release of the encapsulated substances, especially for the applications where the abundant UV light (e.g., sunlight) could be used. To determine the feasibility, UV induced protein release experiments were studied (for experimental section see Section 3.3.8).

Here the bovine serum albumin (BSA, 66 kDa) was used as the model substance. To quantify the protein release, the initial encapsulated protein amount of the sample for BCA test should be calculated first. For every BSA encapsulated capsule suspension (2 ml), the initial BSA concentration in the capsule preparation procedure was 2 mg/ml, its volume used was 1ml, and the encapsulation effect was detected to be 80%, which showed good accordance with pervious work[91], thus the encapsulated BSA total amount was 1.6 mg. To measure the protein release, the BSA-capsule suspension was diluted to 20 ml, which referred to the working samples. Then for protein release test, 0.5 ml of working sample was taken out after UV irradiation. If there was no protein release, every portion used for protein quantification contains 40 μg of BSA protein in capsules.

As shown in Figure 5.8, BSA encapsulated PDADMAC/PAZO capsules with different layers (two and four bilayers) were irradiated with different UV power, 55 mW/ cm^2 and 27 mW/cm^2, respectively. Generally, the protein amount released in the supernatant of all the measured samples increased slowly during all the irradiation times. From the first beginning of 80 min, the protein amount increased from ~3.5 μg to ~14 μg, and there was almost no difference could be found among the four samples. After that, the difference between samples irradiated with different UV powers gradually became significant. As one can see clearly, BSA was released faster with the increase of UV power. Meanwhile, two-bilayer capsules demonstrated a faster protein release rate than that of the four-bilayer capsules, which could be attributed to the faster breakage of relatively thin shells. As for the non-irradiated capsules, a time-dependent protein release behavior was detected. No pronounced difference between the microcapsules with different multilayers could be found during the short incubation time. After 3 hours of stirring in water, a maximum BSA amount approximately to be 6.4 μg escaped from the network shell structures was determined, which was only 16% of the encapsulated BSA amount in microcapsules. Comparing with the irradiated ones, it was obvious to raise the idea that the UV irradiation exhibited pronounced effect on cargo substance release. And most importantly, this UV induced release was found to be controllable through adjusting UV energy and architecture of these microcapsules.

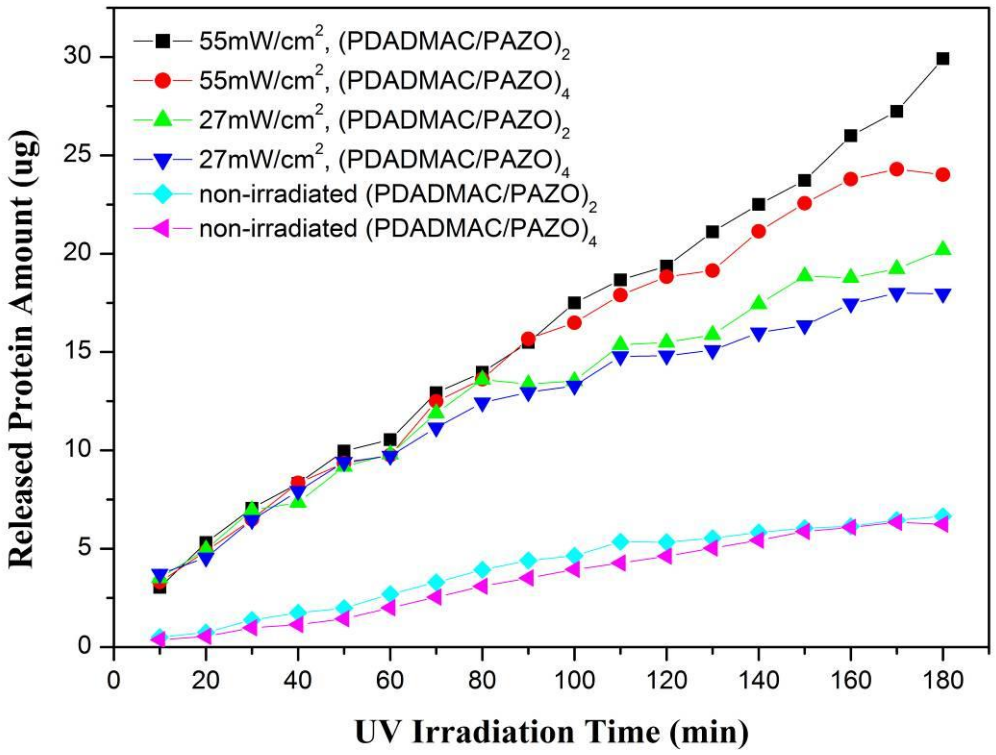

Figure 5.8 UV induced protein release as a function of irradiation time.

For the hollow capsules, 2 hours of irradiation was enough to break all of them (Figure 1 d). However, in the protein release experiments, the protein release from the $(PDADMAC/ PAZO)_2$ capsules was only 75% (30 μg) even after 180 min of irradiation with intensity of 55 mW/ cm^2. It should be noted that after UV irradiation the samples were centrifuged, and the supernatant was used for BCA test. It may be proposed that a certain amount of protein would adsorb on the debris formed during irradiation. If the debris was big enough, the adsorbed protein would precipitate with the pieces, leading to a smaller protein amount in supernatant. And another possible explanation might be attributed to the electrostatic interactions between the encapsulated BSA and the deposited PDADMACADMAC layers. These negatively charged BSA and the positively charged PDADMAC polymers may interact with each other *via* direct attachment or by diffusion[240], which prevented the breakage of the multilayer shells, resulting in the slow release of the encapsulated BSA.

5.5 Oil Encapsulation and UV Triggered Release

As mentioned above, microcapsule swelling-breakage originated from the UV induced re-alignment of azobenzene molecules has triggered a UV-dosage dependent protein

release, illustrating great potential for externally triggered release from microcapsules. The initial encapsulated BSA macromolecules were active-loaded into these capsule shells, by co-precipitating with the formed $CaCO_3$ particles. These resulting micro-scaled $CaCO_3$ particles containing BSA provided stable solid supports for following stepwise polyelectrolyte deposition. Differently, LbL assembly process was carried out on metastable templates in this section, and further cargo substances encapsulation and controlled release behaviors were also studied. Briefly, the UV sensitive PDADMAC/PAZO multilayers were deposited on oil droplets, limonene to be specifically, which were prepared by using emulsion technique previously (Section 3.3.3). Generally, we are aiming to control the evaporate rate of limonene by coating with UV responsive polymers, proposing a possible method for the sunlight triggered release in cosmetic application.

R-limonene is a stable scent ingredient with orange-like smell extracted from citrus fruit. Upon exposure to sunlight and moist air, limonene evaporates and oxidizes to produce oxidation products which act as skin and respiratory irritants and sensitizers.

In this section, the oil droplets of R-limonene were obtained though a two-step emulsion approach, as schematic illustrated in experimental section (Scheme 3.5, Section 3.3.3). A pre-emulsion was prepared by treating a mixture of limonene (O, oil phase) and surfactant solution containing negatively charged SDS (W, water phase) with sonication. As shown in Figure 5.9, the two-phase mixture was turned into a homogeneous oil in water (O/W) milky-white emulsion (Figure 5.9, b). Then, a secondary emulsion was obtained by sonicating the pre-emulsion with positively charged PDADMAC, as shown in Figure 5.9 c.

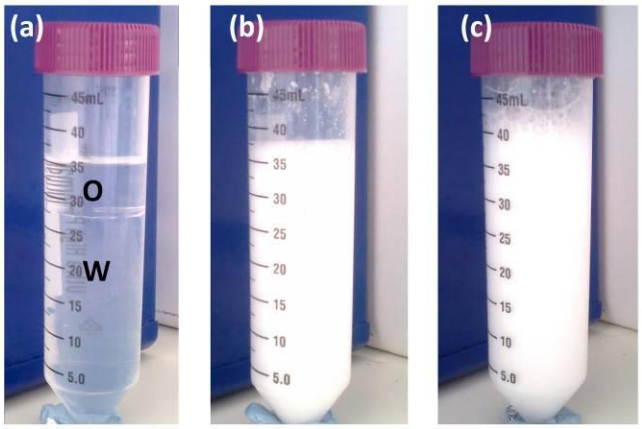

Figure 5.9 Preparation of limonene emulsion.

These oil droplets in pre-emulsion showed good dispersity under optical microscopic observation, and exhibited an average size of 1616.7 nm determining by DLS (Figure 5.10). Exposure the mixture of pre-emulsion and PDADMAC to sonication led to a slightly size decrease, DLS presented an average size of 1589.8nm of the secondary emulsion (Figure 5.11).

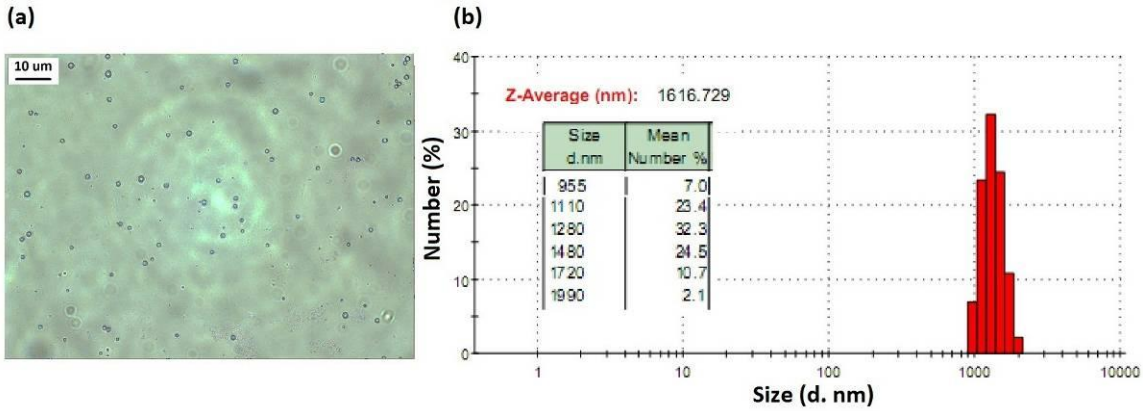

Figure 5.10 Characterization of pre-emulsion: (a) optical image and (b) average size and distribution.

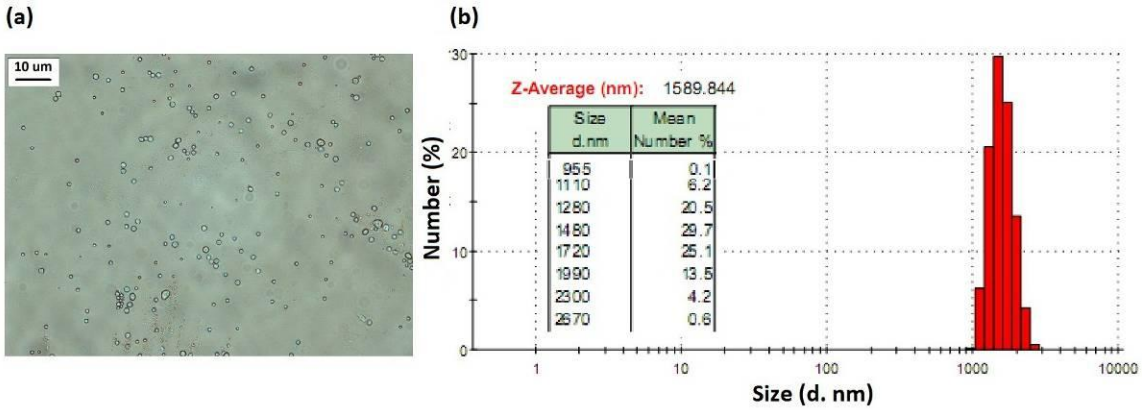

Figure 5.11 Characterization of secondary emulsion: (a) optical image and (b) average size and distribution.

The obtained secondary emulsion (positively charged) was used for further LbL polyelectrolyte deposition, starting with the negatively charged PAZO. After LbL assembly, five double layers of PDADMAC/PAZO-coated R-Limonene were obtained (as shown in Figure 5.12), named as L-$(PD/PAZO)_5$, and used for further study. These encapsulated limonene droplets were visualized as a yellow suspension, because of the color of PAZO (Figure 5.12 a).

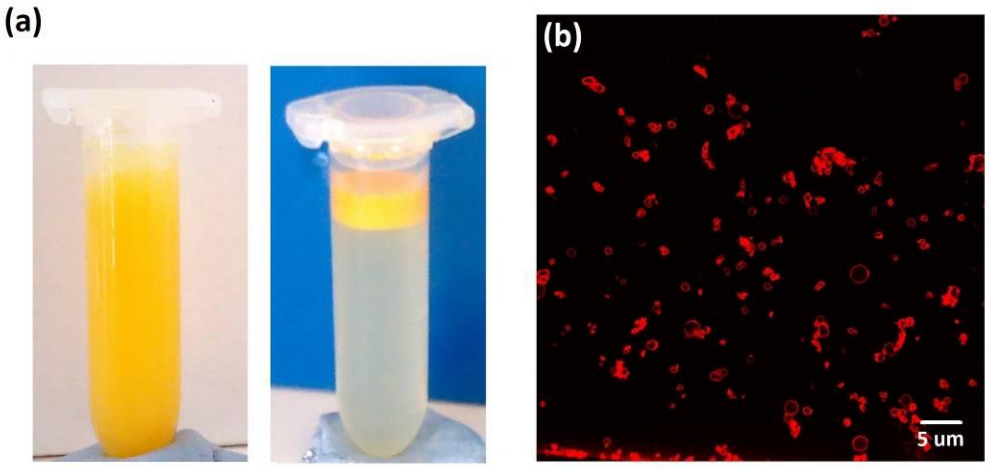

Figure 5.12 Prepared L-(PDADMAC/PAZO)$_5$ suspension (a) before (left) and after centrifugation (right), and CLSM images of [L-(PDADMAC/PAZO)$_2$ (RBITC-PAH /PAZO) (PDADMAC/PAZO)$_2$] with fluorescent dyes in the multilayer (b).

Confocal Laser Scanning Microscopy (CLSM) measurement was also performed for observation of these coated droplets, as shown in Figure 5.12 b. Encapsulated limonene [L-(PDADMAC/PAZO)$_2$ (RBITC-PAH/PAZO) (PDADMAC/PAZO)$_2$] were visualized by incorporating rhodamine labeled polymer (RBITC-PAH) during capsule preparation process. CLSM image confirmed the successful encapsulation of limonene droplets by exhibiting the red polymer layers, and also showed good accordance with the result of droplet size distribution obtained from DLS data.

After encapsulation, the average size of L-(PD/PAZO)$_5$ was determined to be 1338 nm, with the distribution ranging from 955 nm to 1990 nm, judging from DLS data, as shown in Figure 5.13. This size change should be attributed to the vigorously shaking in fabrication process, which split big oil droplets into small ones.

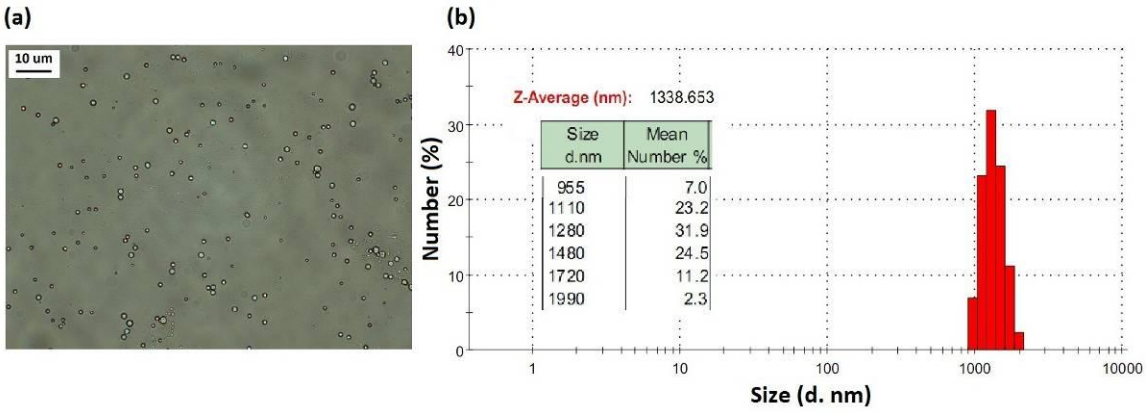

Figure 5.13 Characterization of L-(PD/PAZO)$_5$: (a) optical image and (b) average size and distribution.

UV irradiation of the encapsulated limonene was carried out with intensity of 55 mW/cm^2. UV irradiation caused the deconstruction of the polymeric shells, resulting in the release of limonene. As shown in Figure 5.14 (a-e), after irradiation, the outline of droplets under optical microscope exhibited a gradually increase tendency with the increasing of irradiation time. It can be explained that the released hydrophobic oil droplets tend to aggregate together to form bigger droplets in water. In the mean time, a lot yellow/orange colored debris was found in the suspension due to the disruption of multilayer shells.

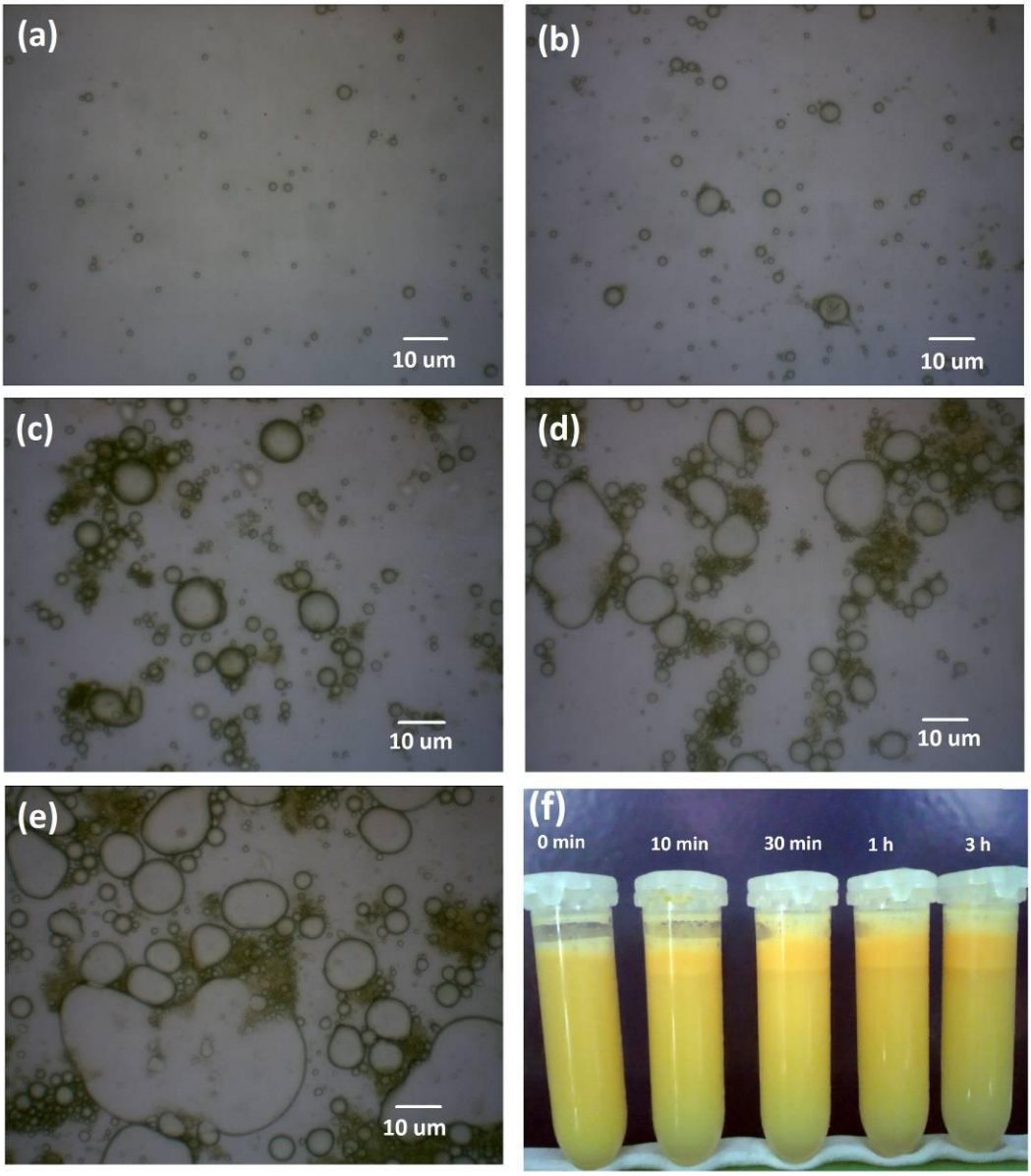

Figure 5.14 Optical images of oil droplets after UV irradiation and the creaming of encapsulated limonene.

* Image a to e showed the optical images of oil droplets after UV irradiation for 0 min, 10 min, 30 min, 1h, and 3 h respectively.

Besides the UV induced release of limonene from multilayer shells, creaming phenomena was observed as a function of irradiation time when exposure to UV light, as shown in Figure 5.14 f. These irradiated L-$(PD/PAZO)_5$ samples were collected and placed into tubes. It was clear that no creaming can be found in the non-irradiated sample. On the contrary, creaming was found in all the irradiated samples. It seemed that the amount of creaming depended on the duration of irradiation, indicating a UV-dosage dependent disruption of the polyelectrolyte multilayers.

UV irradiation induced multilayer deconstruction not only acted as the creaming of the encapsulated limonene, but also demonstrated as the precipate of the polymer shells. A typical example was shown in Figure 5.15. Broken shells and/or hollow shells started to precipitate in the 3 h-irradiated sample. While in the 30 min-irradiated sample, there was no obvious precipitate can be found. The formation of polymer precipitation provided another evidence for the UV induced changes in the limonene suspensions.

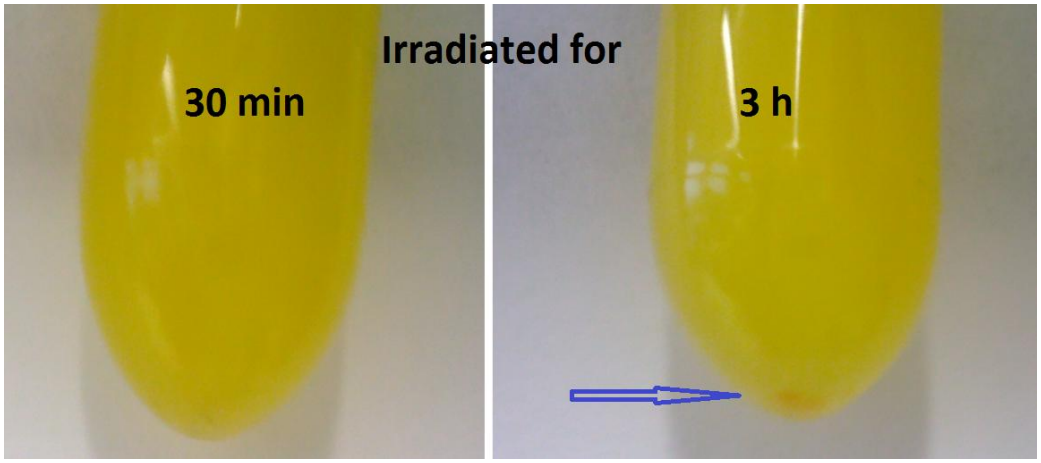

Figure 5.15 Polymer shell precipitation after UV irradiation.

* The blue arrow showed the formation of polymer precipitate.

SEM images revealed the UV induced breakage process of L-$(PD/PAZO)_5$ shells. After UV irradiation, these diluted samples with different irradiation time were dropped on glass slides, dried, and observed under SEM. After limonene evaporation, polymeric shells were left. Different from the multilayer on solid templates, these shells fabricated on oil seemed not uniform and possessed rough surfaces (Figure 5.16 a, b). Before irradiation, the PDADMAC/PAZO shells were relatively intact, and showed clear outline. It was obvious that more and more PDADMAC/PAZO shells became rough and broken with the increase of UV irradiation time. After exposure to UV light, these

shells underwent a process of swell (Figure 5.16 c, d and e, f) and breakage (Figure 5.16 g~j) gradually.

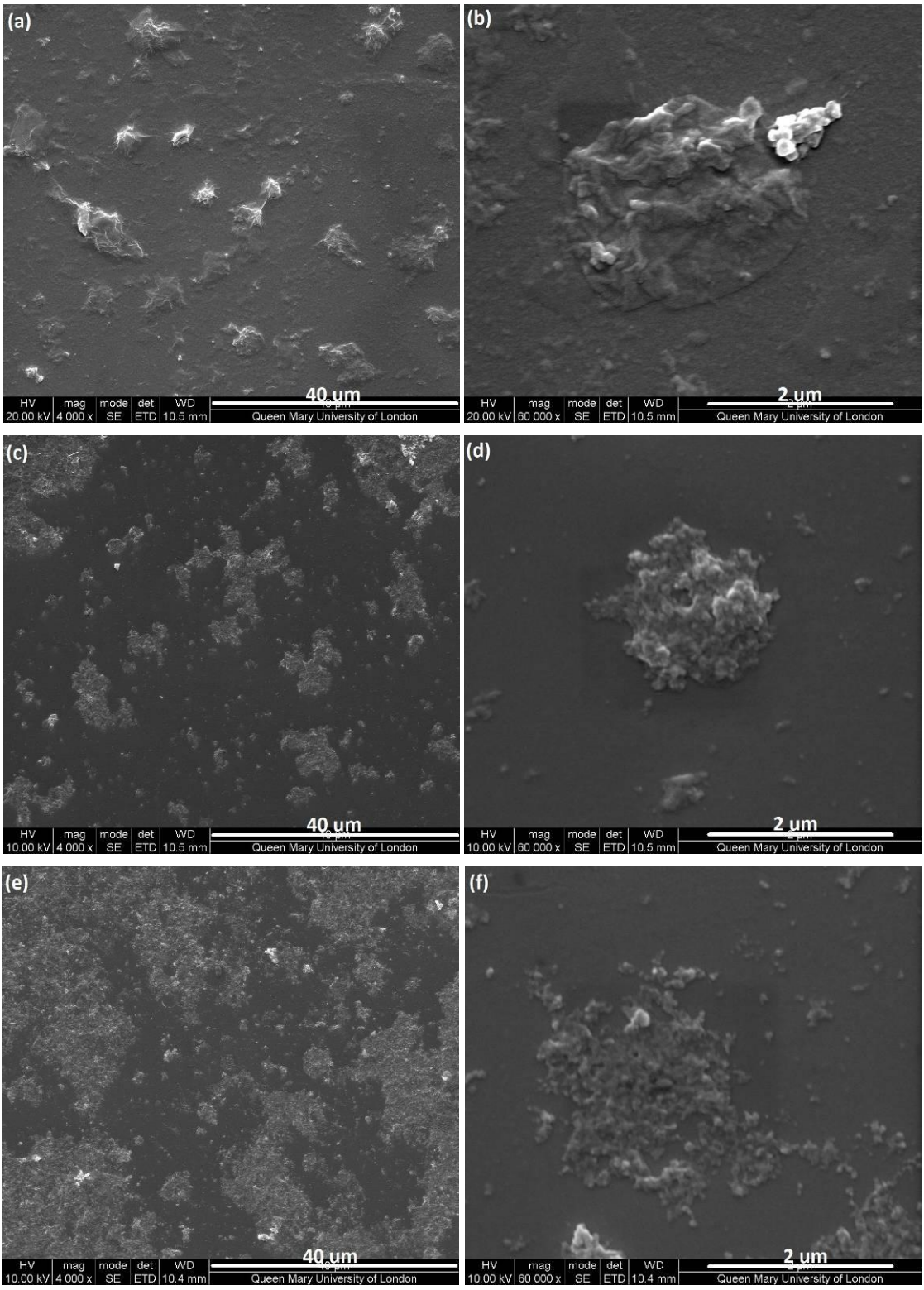

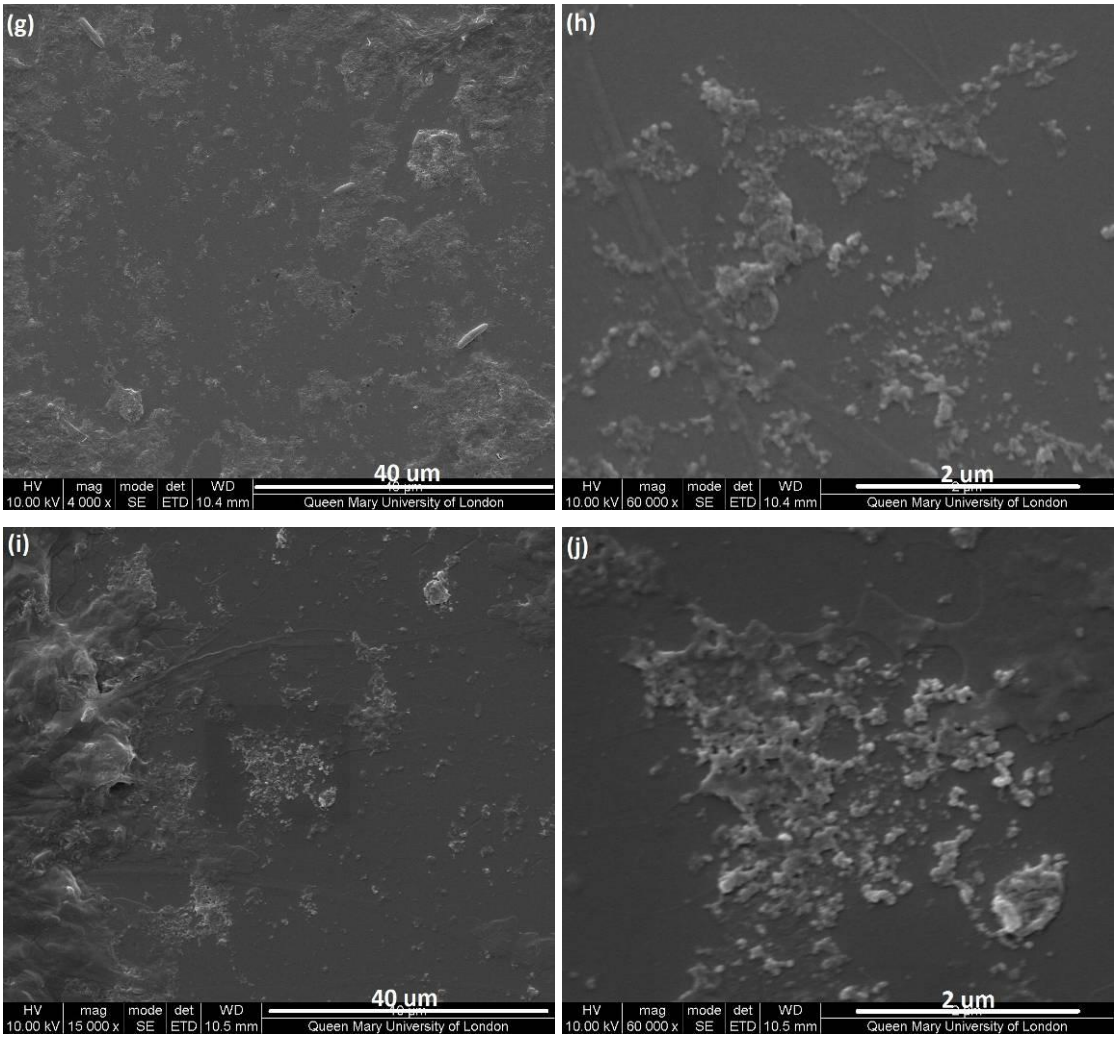

Figure 5.16 SEM images of L-$(PD/PAZO)_5$ polymeric shells before (a, b) and after UV irradiation of 10 min (c, d), 30 min (e, f), 1 h (g, h) and 3 h (i, j).

5.6 Conclusions

In this chapter, a novel class of UV responsive polyelectrolyte microcapsules was successfully fabricated by alternative deposition of PDADMAC and PAZO on SiO_2 microparticles. Upon exposure to UV light, the AZO moieties in the multilayers tended to be self-organized in the form of J aggregates due to the influence of the polycation PDADMAC. SEM studies revealed that the re-orientation of AZO within shell formations led to great damage of capsule integrity, illustrating as a progress of capsules swelling and further disruption. Upon 2 hours of UV irradiation, no intact capsules can be found, and the capsule debris was further split into needle-like formations. Moreover, this UV induced microcapsule disruption process was proved to be irreversible, even when the capsules were exposed to the visible light. In addition,

such UV induced capsule disruption based on J aggregated was employed to modulate the release of encapsulated BSA and R-Limonene, which demonstrated a convenient way to controllable release of the encapsulated substance by adjusting UV intensity and microcapsule architecture. Promisingly, this PDADMAC/PAZO microcapsule system showed great application for many environmental and photochemical uses, where sometimes the UV light could be the only available stimuli to drive these micro-vesicle systems. As shown in Scheme 5.4, a schematic illustration of this UV triggered microcapsule swelling-disruption was given.

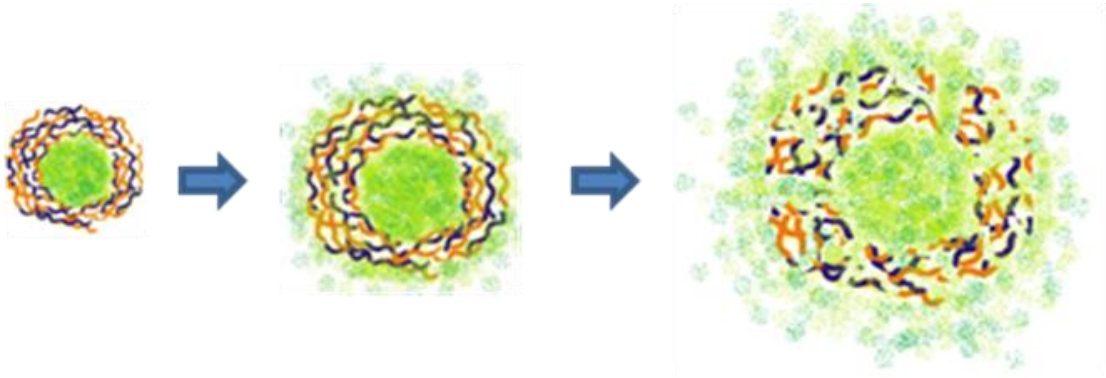

Scheme 5.4 Schematic representation of UV triggered AZO-microcapsule swelling-disruption.

6. Polyelectrolyte Microcapsules Made of Diazo-resin for Encapsulation

6.1 Introduction

6.1.1 Background

Molecule encapsulation into polymer based capsules with controlled release properties has attracted increasing interests during the past decades. Ideally, such encapsulation should provide efficient loading and essential protection for cargo substances together with time and site specific release. Most importantly, effective encapsulation should offer a way to modulate substance entrapment in the capsules which could benefit a long enough storage with a desired release properties[241]. Generally, polymeric micro- and nano- capsules made of LbL assembly had been intensively explored to achieve substance encapsulation. However, small molecules encapsulation remains a bottleneck and could be achieved such procedures as heat-treatment[26] and crosslinking[219] within the multilayers to decrease the shell porosity, strengthen the capsule walls and thus to decrease shell permeability. Many efforts have been devoted to provide solutions for the problems of how to encapsulate large molecules effectively into microcapsules without losing their activities. However, small molecules, such as drugs, dyes, and other bioactive substances that have a molecular weight below 1 kD are small in size and relatively difficult to be encapsulated by the porous polyelectrolyte complex made capsule shells[242]. Therefore, the encapsulation for such small molecules remains of great challenging due to possible requirements in drug delivery and microreactors applications.

As mentioned above, many efforts have been devoted to provide solutions for the problem of how to encapsulate large molecules effectively into microcapsules without losing their activities. However, for small molecule encapsulation, it is still a challenging task. Interestingly, an effective loading of small molecule rhodamine 6G (Rh6G, positively charged) into microcapsules templating on melamine formaldehyde (MF) was demonstrated[240]. Unfortunately, driving force for such Rh6G encapsulation was based on electrostatic interaction of the oppositely charged Rh6G and PSS/MF complex (negatively charged), which would definitely limit the encapsulation of non-

charged or negatively charged molecules. And the existence of MF residue in capsules might influence on the further bio-applications. Another example of small molecule encapsulation was reported as precipitation of molecules from supersaturated solutions[97]. However, the nucleation and precipitation in the capsule interior were conducted by controlling the pH of outer environments, which might affect the activities of some pH sensitive substances, unfortunately.

To encapsulate desired cargo substance with small molecular weight requires a denser network structure with less and small pores. A promising approach named shell sealing could be used to adjust capsule properties. That is, after capsule fabrication, a controllable crosslinking could be employed to covalent bond the assembled polyelectrolytes due to the chemical reactions of functional groups. A kind of novel crosslinkable polyelectrolytes that access the needs is the diazo-resin (DAR). DAR has a strong UV absorption around 380 nm which could be assigned to the π-π* transition in the diazonium group[164]. Upon exposure to a 380 nm UV light, the diazonium group could be activated to form phenyl cation and then be substituted by nucleophilic groups, offering a novel light triggered crosslinking based on photolysis[163, 164]. In addition, DAR is easy to form LbL film *via* H–bonding attraction between N^+N: of DAR and strong hydrogen donors (e.g., –OH) of counterpart polymers[162]. These entire charming advantages make the DAR ideal candidate to build up UV-crosslinkable microcapsules for encapsulation.

On the other hand, the properties of microcapsules mainly depend on the shell composition. Therefore, the selection of counterpart polyelectrolyte become of great importance. It was suggested that a very hydrophobic multilayers would contain less water and should therefore be less permeable for water soluble substances than the hydrophilic ones[10]. Thus, Nafion, which consists of a perfluorinated backbone and contains sulfonic acid groups in short side chains[243], would be an optimal polyanion to build up multilayer capsules with DAR. On the other hand, polyelectrolytes having diazonium groups, such as positively charged DAR discussed in this chapter, can react with Na_2SO_3 to form diazo-sulfonate ($–N=N–SO_3^-$) under mild conditions, resulting in charged reversed DAR to negatively charged polymer[53, 56]. New strategy to seal the porous capsule multilayer systems is therefore inspired by externally triggered reactions within the DAR single component microcapsules made of positively and negatively

charged forms of DAR. Practically, after UV induced photolysis, interacted ion charges, such as diazonium and diazo-sulfonate here, are eliminated, leaving the crosslinked diazo-resin backbones to form rigid and more internally hydrophobic phenyl ring-rich multilayers in DAR single component capsule system. Thus, aim of this work was to explore the possibilities to reduce capsule permeability *via* UV-induced charge group modification. Strategically, the use of DAR components with both charges as well as the polyelectrolyte Nafion[244] as layer constituents for capsules fabrication would endow the prepared capsules with minimal shell permeability.

6.1.2 Aim and Objectives

The aim here is to prepare novel capsule systems containing diazonium groups and to use them as potential microcontainers for small molecule encapsulation. The basic idea is that the ionic bonds of counterpart ions could be converted to covalent chemical bonds through DAR-related photolysis upon direct exposure to UV light. And this chemical transition could provide a remote controlled method to seal the multilayers and further to influence permeability the fabricated microcapsules.

Therefore the main objectives of this chapter are:

1) To design and fabricate multilayer microcapsules $(Nafion/DAR)_4$, DAR_8 containing diazonium groups. To synthesize UV sensitive DAR, and use it to fabricate microcapsules with Nafion and charge reversed DAR.

2) To investigate the parameters corresponding to the UV induced capsule shell sealing, for example chemical transitions within multilayers, and the change of shell hydrophilicity.

3) To study the possibilities of cargo substances (macro-/small- molecules) encapsulation in these UV sealed microcapsules.

6.2 Fabrication of DAR-contained Microcapsules

6.2.1 A New Route to Fabricate Single Component Microcapsules

The single component DAR microcapsules were built up based on Laschewsky's *coating by multiple polyelectrolyte adsorption-surface activation* (CoMPAS) method[53]

with minor adjustment, as shown in Scheme 6.1. Generally, unlike the charge reversal activation performed on the film surface directly, the positively charged DAR polymers were converted into negatively charged ones by treatment with equal moles of an ice-cooled mixture of Na_2SO_3 and Na_2CO_3 firstly; then these oppositely charged polymers were used as polyanion and polycation for layer-by-layer assembled microcapsule preparation. This improved method benefited a simple way to fabricate single component multilayer capsules through a traditional route as alternating deposition of "positively" and "negatively" charged polyelectrolytes.

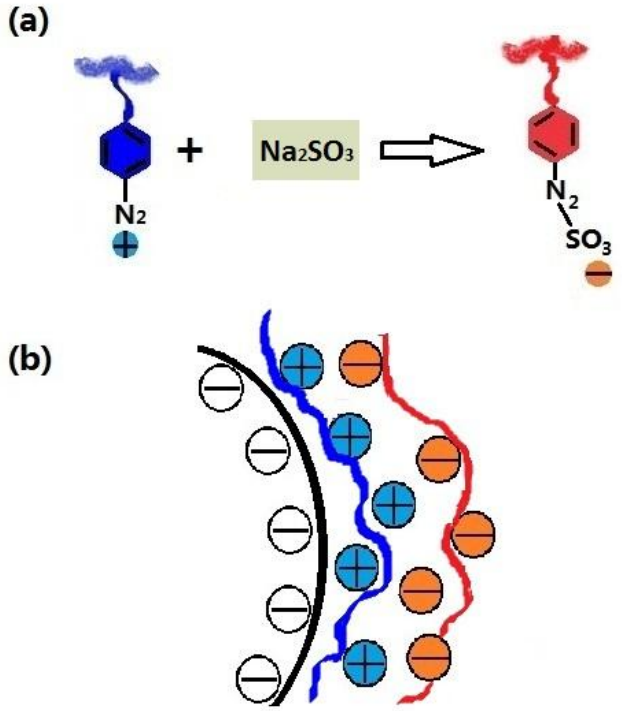

Scheme 6.1 Schematic illustration of single component DAR microcapsule preparation procedure.
* The charges of DAR polymers were reversed firstly (a), layer-by-layer assembly was carried out by alternating deposition of oppositely charged DAR polymers (b).

The key factor for fabrication of single component microcapsules is the charge reversal step, either on the multilayer surface or in the polyelectrolyte solution strategically. As shown in Scheme 6.1 a, upon exposure to alkali sulfite, the aromatic diazonium salt groups ($–N_2^+$) underwent a diazo coupling reaction, which converted them into diazo-sulfonate ($–N_2–SO_3^-$). This reaction occurred very fast with an obvious colour change, from dark green to yellow/orange in this work, could be finished within few seconds[245]. The most commonly used sulfite is sodium sulfite (Na_2SO_3)[245], as the one used in our experiment. The pH of the reaction system would greatly influence the coupling

reaction. As suggested, the reaction only led to generation of dark decomposition product phenylhydrazine at lower pH, therefore the sodium carbonate (Na_2CO_3) was added to buffer the reaction mixture at low temperature[245].

It was suggested that the DAR had a strong absorption at ~ 380 nm[164]. In this work, the original DAR aqueous solution (positively charged, $DAR^{\oplus}$) was found a strong absorption at 372 nm (Figure 6.1, solid line), which originated from the π-π* transition of the diazonium group[164]. By treatment with a mixture of Na_2SO_3/Na_2CO_3 at low temperature, a charge reversed DAR solution (negatively charged, $DAR^{\ominus}$) was obtained, characterized as a significant red-shift by 28 nm located at 400 nm, accompanying with a maximum absorption intensity decrease in UV-Visible spectroscopy (Figure 6.1, dot line). This pronounced change was attributed to formation of diazo sulfonate groups, which was found a maximum absobance at longer wavlength[56].

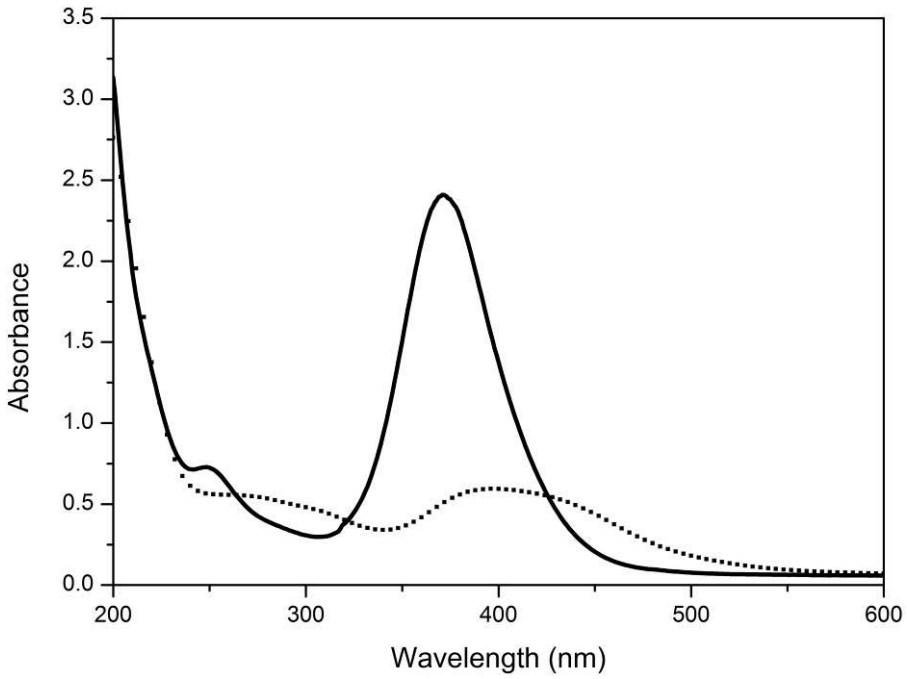

Figure 6.1 UV-Vis absorption spectra of DAR (solid line) and charge reversed DAR (diazo sulfonate, dot line) solutions.

6.2.2 Fabricated DAR-contained Microcapsules

After LbL assembly driven by electrostatic interactions of polyions, monodisperse hollow $(Nafion/DAR)_4$ and DAR single component microcapsules (DAR_8) with four double layers were obtained, as shown in Figure 6.2, respectively. Under SEM

observation, these capsules were flat with creases and folds. Specially, a unique pattern of creases and folds that different from other ordinary microcapsules were observed in $(Nafion/DAR)_4$ microcapsule system. Compared with the SEM images of DAR single component microcapsules, these special patterns should be attributed to the existence of Nafion component, which made capsules more hydrophobic internally and apparently looking more elastic once collapsed upon drying.

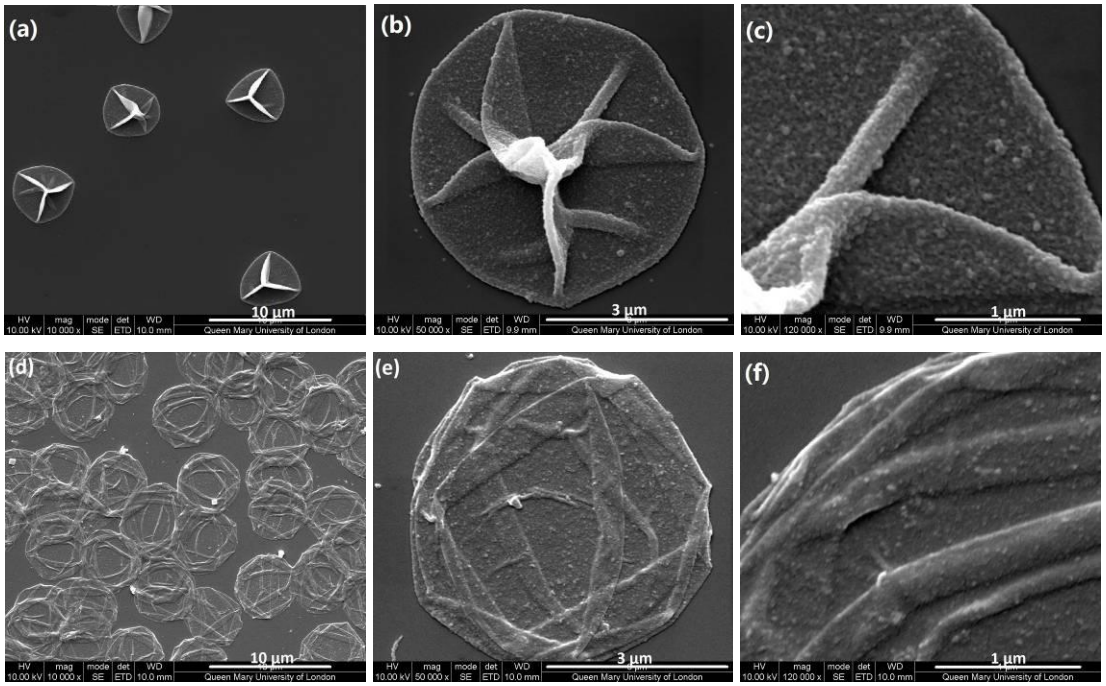

Figure 6.2 SEM images of DAR contained microcapsules at various magnifications.
Top panel: $(Nafion/DAR)_4$ microcapsules, bottom panel: DAR single component microcapsules.

The stepwise assembly processes of the two kinds of microcapsules were monitored by using quartz crystal microbanlance technique (QCM). The mass increase due to the polyelectrolyte adsorption was estimated from the QCM frequency shift according to the Sauerbrey equation[210] as follows:

$$\Delta f = \frac{-2 f_0^2}{A\sqrt{\mu\rho}} \Delta m \tag{6.1}$$

where the area of the gold coated crystal (A) was 0.205cm^2, the density of the crystal (ρ) was 2.648g/cm^3, and the shear modulus (μ) was 2.947×10^{11} g/cm s^2, and the resonant frequency of the crystal (f_0) used in this work was 10 MHz. Thus, the mass change due to the polymer adsorption on the electrode can be estimated as follows:

$$\Delta \mathrm{m}(ng) \approx -0.905468 \Delta F(Hz) \tag{6.2}$$

Taking into account the polyion film density adsorbed on the electrode, assumed to be $1.2 \pm 0.1 \mathrm{g/cm}^3$[246], the thickness of adsorbed film can be estimated as follows:

$$\Delta \mathrm{d}\,(\mathring{A}) \approx -0.368076 \Delta F(Hz) \tag{6.3}$$

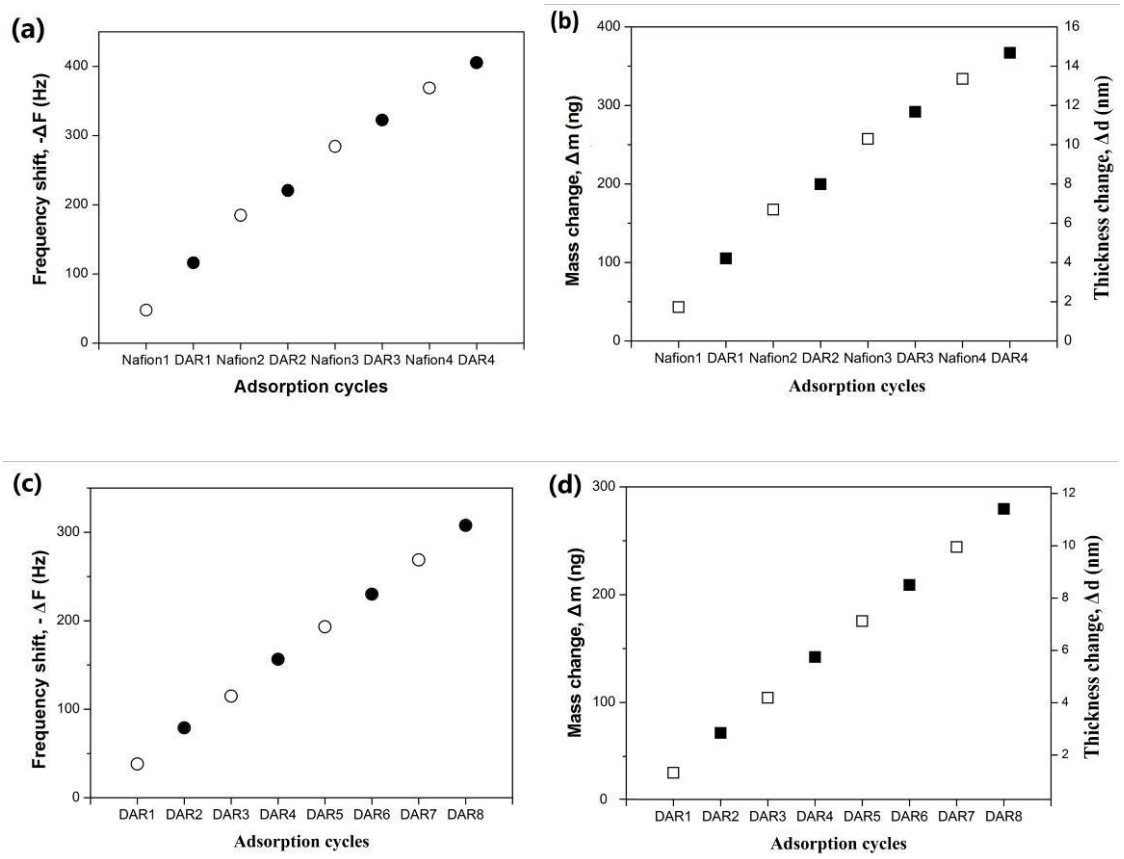

Figure 6.3 Frequency shift (-ΔF) due to alternatively polyelectrolyte adsorption (a, c), and estimated film mass (Δm) and thickness (Δd) changes (b, d).
Top panel: $(\mathrm{Nafion/DAR})_4$ system; Bottom panel: DAR_8 system.

Since there are two different microcapsule systems involved here, the results will be presented in two parts:

(Nafion/DAR)$_4$. As shown in Figure 6.3 a, QCM monitored a linear relationship (R^2= 0.9895) between frequency shift, -Δf, and the number of polyelectrolyte deposition cycles, due to the alternate adsorption of aqueous Nafion and DAR. The average frequency decrease were found to be 56 Hz for Nafion and 45 Hz for DAR, which meant that 5/9 of the bilayer mass was composed of Nafion and 4/9 of DAR. After 4

bilayers deposition, a total mass increase of 367.03 ng was found on a surface of 0.205 cm^2, which was accompanied with a thickness increase of 14.92 nm for 4 Nafion/DAR bilayers (Figure 6.3 b). To be specifically, an average thickness of one Nafion layer was estimated to be about 2 nm. Such relatively thin polyelectrolyte layers revealed that almost no free $–SO_3^-$ ions dissociated from Nafion were present in the internal multilayers, which would affect water uptake and proton conductivity of the multilayer system[225] (will be discussed later, see Section 6.4).

(DAR)$_8$. As shown in Figure 6.3 c, a better linear relationship (R^2 = 0.9998) between frequency shift, -Δf, and the number of polyelectrolyte deposition cycles was observed by QCM measurements, due to the alternate adsorption of aqueous DAR with two kinds of charges. The average frequency decrease were found to be 37.38 Hz for $DAR^{\oplus}$ and 39.56 Hz for $DAR^{\ominus}$, which meant almost equal moles of oppositely charged DAR deposited on the crystal surface. After 4 bilayers deposition, an average mass increase of 69.9 ng was estimated from one double layer ($DAR^{\oplus}/DAR^{\ominus}$), accompanying with a thickness increase of 1.4 nm for each single layer (Figure 6.3 d).

6.3 UV Induced in-situ Covalent Bonding within Capsule Shells

The UV responsive properties of these fabricated capsules were investigated. In this work, the UV intensity used was approximately 55 mW/cm^2, and the UV treatment duration was 10 min. The structural formulas of these polyelectrolytes used for capsule fabrication were given in Scheme 6.2.

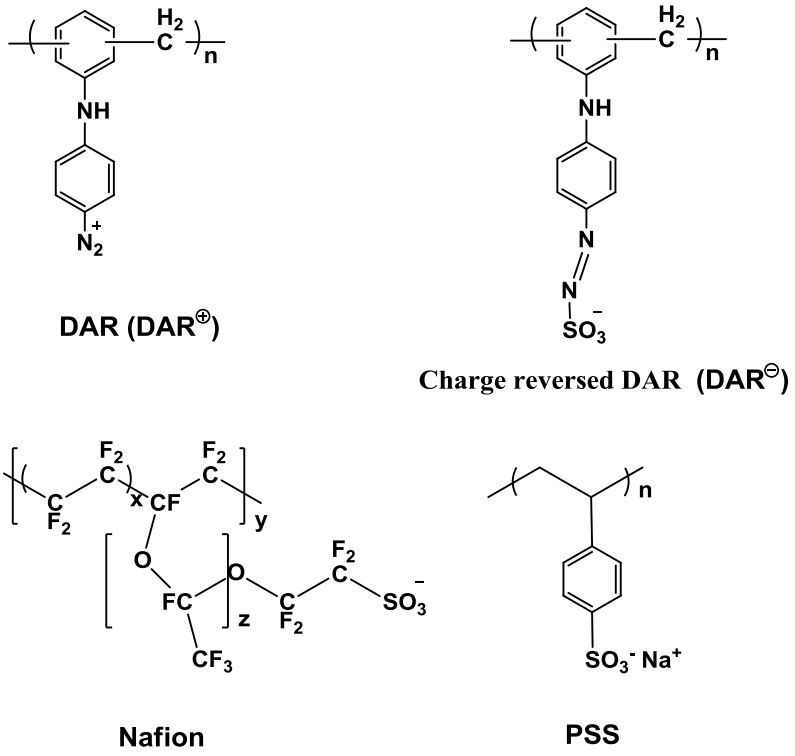

Scheme 6.2 Structural formulas of the polyelectrolytes used in this chapter.

The diazonium group was reported as a good leaving group and it would be cleaved forming phenyl cation under UV irradiation with a suitable light source. Thus, upon irradiation it could be substituted by nucleophilic groups resent in polyanions, such as carboxylic, phosphate and sulfonate groups[163]. Therefore, in this work, UV irradiation led to photolysis within the interacted ion pairs of Nafion/DAR and $DAR^{\oplus}$/$DAR^{\ominus}$, which exhibited as the decomposition of diazonium group (and formation of a sulfonate covalent bond), as shown in Scheme 6.3. Different from the other UV-related transitions, as reported by Katagiri[134] and Sukhorukov[16, 219], this DAR related transition from ionic bonds to covalent ester bonds required no polymer chain re-arrangement or re-conformation within the multilayers, thus there was no obvious capsule size decrease can be found in this work and somewhere else[104].

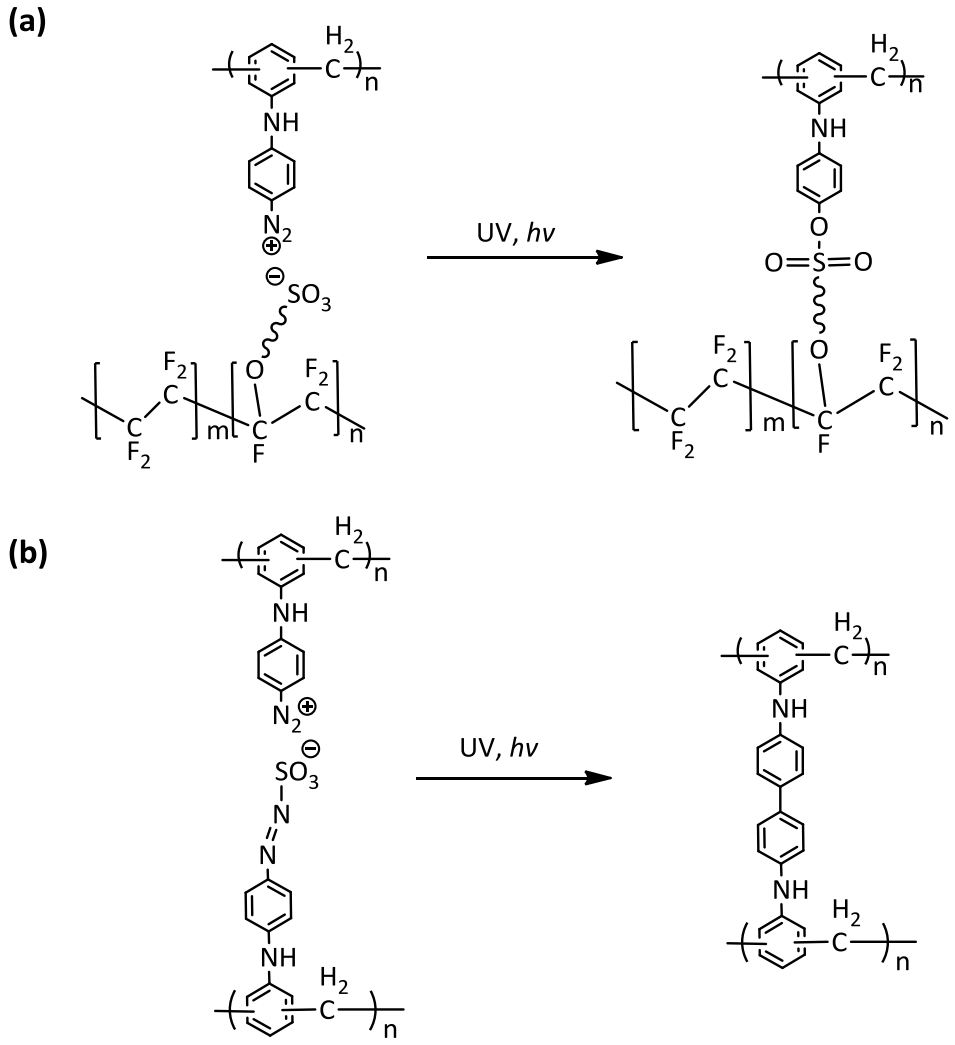

Scheme 6.3 Photolysis reactions of (a) Nafion/DAR and (b) DAR single component multilayer systems.

The process of UV-induced DAR decomposition can be easily monitored by the observation of absorbance change in UV-Vis spectroscopy. As shown in Figure 6.4, for both of these two kinds of DAR contained microcapsules, the remarkable decreases in the intensity of ~ 380 nm absorption band were followed, indicating of the reactivation of diazonium groups during UV irradiation.

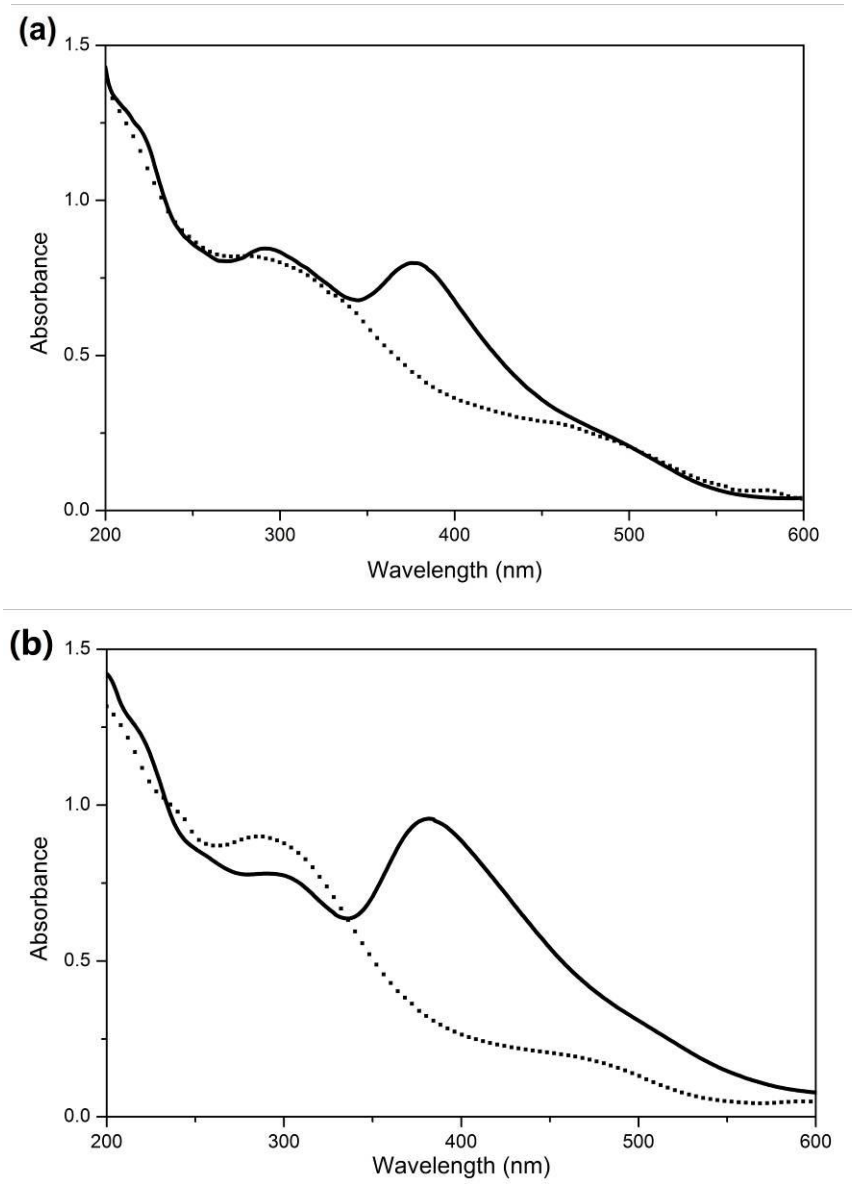

Figure 6.4 UV-Vis absorption spectra of $(Nafion/DAR)_4$ (a) and DAR_8 (b) capsules before (solid line) and after (dot line) UV irradiation.

In particular, comparing with DAR aqueous solution (Figure 6.1, solid line), assembled DAR_8 microcapsule suspension was observed an absorption centred at 382 nm accompanying with a red-shift by 10 nm and a signal intensity decrease (Figure 6.4 b, solid line). Both of the two changes could be explained as a consequence of deposition of charge reversed DAR (diazo-sulfonate). However, this shifting towards longer wavelength was not as pronounced as that of the pure $DAR^{\ominus}$ solution, indicating that the $DAR^{\ominus}$ was only the partial component for the single component multilayers[56]. After 10 min of UV irradiation (Figure 6.4 b, dot line), the absorbance at 382 nm decreased dramatically due to the photoreactions occurred within paired charges. In the

mean time, a concomitant increase was observed at about 290 nm, similar results can be found elsewhere [56, 165, 169].

Diazonium is well known as a kind of good leaving group activated by UV (~ 380 nm wavlenght), which could rapidly react with nucleophilic groups presenting in polyanions, such as carboxylic, phosphate and sulfonate groups[247]. In this work, upon exposure to UV light, the paired diazonium/sulfonate and diazonium/diazo-sulfonate groups underwent a chemical transition process. Specially, one should notice that for DAR single component system this photoreaction process in water is quite complex involving diazonium group decompositon followed by generation of cationic intermediates[165] and isomerization of diazo-sulfonate[248]. As a concequence, the electrostatic interacted charges were eliminated and new covalent bonds were generated instead upon exposure to UV light. Technically, this UV induced photolysis within DAR contained microcapsules can be also confirmed by FTIR results. As shown in Figure 6.5, for both of the $(Nafion/DAR)_4$ and DAR_8 microcapsule systems, absorption peaks around 2222 cm^{-1}, 2169 cm^{-1} and 1580 cm^{-1} were observed in the FTIR spectra before irradiation (Figure 6.5 a, c), which were originated from the asymmetric stretching of $–N_2^+$[164] and symmetric stretching of –C=C– in phenyl group conjugated with the diazonium group[237].

For $(Nafion/DAR)_4$, after 10 min of irradiation with an UV source (50 mW/cm^2), the absorption at 2222 cm^{-1}, 2169 cm^{-1} and 1580 cm^{-1} disappeared completely (Figure 6.5 b), indicating the fast decomposition of the diazonium groups. However, a new absorption peak at 1162 cm^{-1} corresponding to the generation of sulfonate group coupled with the phenyl group[164] was overlapped by the strong $C–F_2$ stretching of Nafion[230].

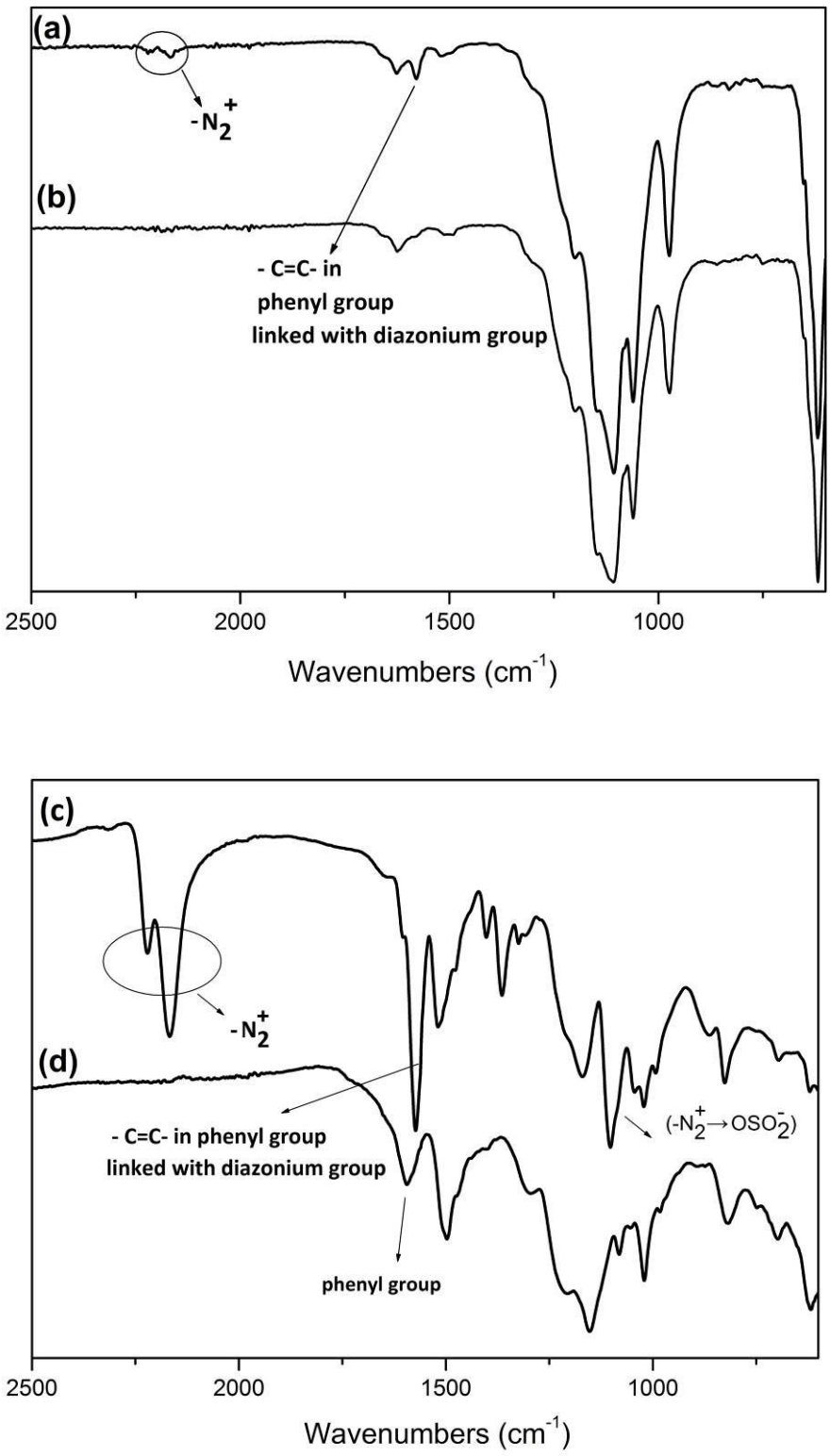

Figure 6.5 FTIR spectra of (top panel) $(Nafion/DAR)_4$ and (bottom panel) DAR_8 microcapsules before (a, c) and after (b, d) 10 min of UV irradiation.

Similar results were also found in DAR_8 microcapsule system, demonstrating as a complete disappearance of diazonium group signals and partially decreased absorption

of –C=C– in phenyl group. Specially, the peak at 1364 cm^{-1} was originated from the stretching of $–SO_3^-$ conjugated with the azo bond; and the peak at 1106 cm^{-1} corresponded to the N–O stretching of the complexes of diazonium and sulfonate groups ($–N_2^+ \rightarrow OSO_2^-$)[249]. Similar stretching in the FTIR spectra of Nafion/DAR system was covered by $C–F_2$ signal. With the fast decomposition of the diazonium group, the peak representing normal absorption of phenyl ring at 1595 cm^{-1} was observed due to the missing of previous dominating peak (phenyl group linked with diazonium group) in the nearby region[250]. In the mean time, the absorption peaks at 1364 cm^{-1} and 1106 cm^{-1} disappeared, for both of which should be attrributed to the elimination of diazonium and diazo-sulfonate groups in the progress of photolysis (Figure 6.5 d).

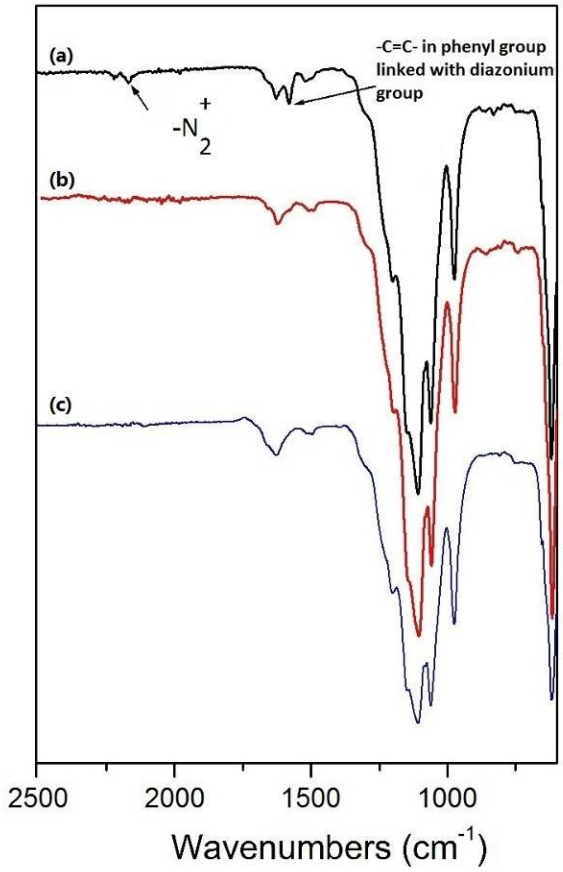

Figure 6.6 FTIR spectra of $(Nafion/DAR)_4$ capsules before (a), and after UV irradiation with UV lamp (b) and sunlight (c).

This DAR related photolysis occurred very fast, e.g., could be almost completed within 50 s with a 80 W medium mercury lamp at a distance of 13 cm[163]. In this work, no further change can be found when extending irradiation duration to 20 min (data not

shown). In addition, this UV induced photolysis reaction in our work was very sensitive to natural sunlight. Exposure of these DAR contained capsules (in quartz cuvette) to sunlight for 6 hours with UV intensity ranging from 431 μW/cm^2 to 1.848 mW/cm^2 (detected with 30 min intervals by using a ILT1400 radiometer, International Light Technologies Inc.) can also cause a similar chemical transition within multilayers, indicating that the gradually accumulated sunlight energy eliminated the absorption peaks at 2169 cm^{-1} and 1580 cm^{-1}. A typical example of the DAR contained microcapsules with UV irradiation of UV lamp and sunlight, (Nafion/DAR)$_4$ to be specifically, was shown in Figure 6.6.

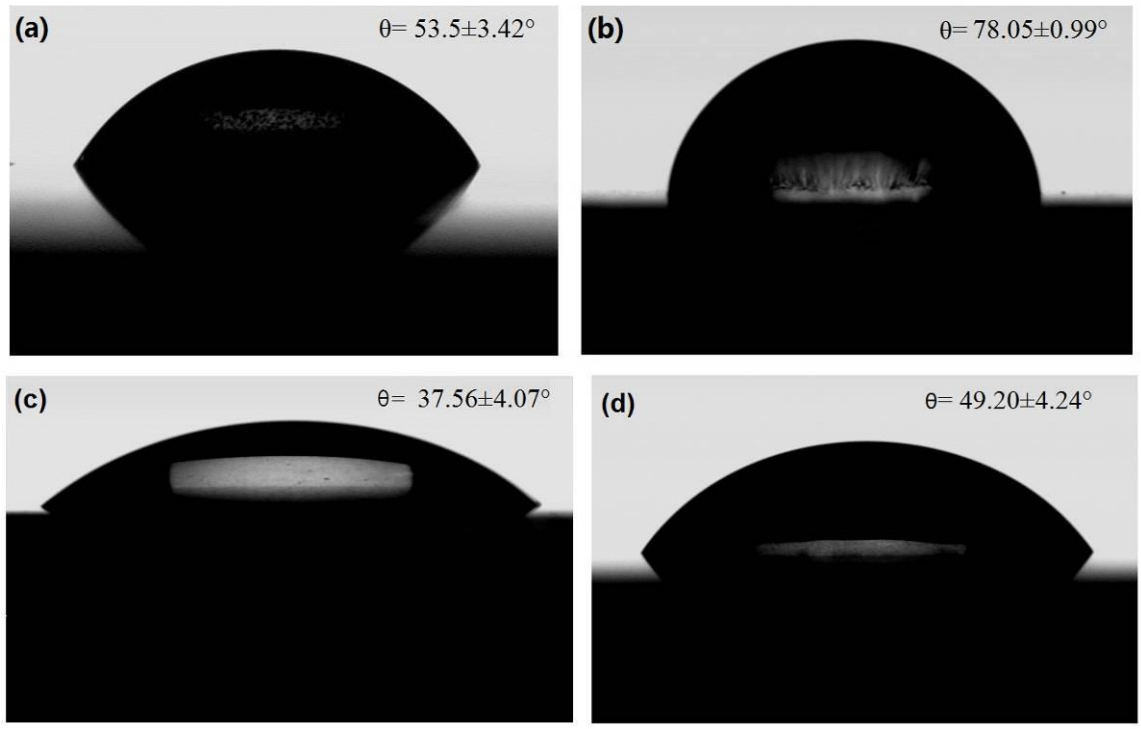

Figure 6.7 Photographs of water droplets on (Nafion/DAR)$_4$ (a, b) and DAR$_8$ (c, d) multilayers before (left) and after (right) UV irradiation.

UV induced chemical transitions not only converted the electrostatic interactions (diazonium/sulfonate, diazonium/dizao-sulfonate) into covalent bonding, but also changed the water permeability of the multilayers, demonstrating as a decreased multilayer film wettability directly. As shown in Figure 6.7, typical water droplet shapes and corresponding contact angles on the multilayers were given.

For (Nafion/DAR)$_4$ multialyers, an average water contact angle of 53.5 ± 3.42 ° was detected before UV irradiation, and then the UV treatment resulted in a remarkable

reduction of surface water wettability, demonstrating as observed an average water contact angle of 78.05 ± 0.99 °(Figure 6.7 a, b). Similarly, the UV irradiation decreased the surface water wettability of DAR single component multilayer system, as a clear change of average water contact angle from 37.56 ± 4.07 °to 49.20 ± 4.24 °was detected before and after irradiation, respectively (Figure 6.7 c, d).

6.4 UV-induced Macromolecule Encapsulation

UV exposure triggered a chemical reaction in the DAR contained systems, either Nafion/DAR or $DAR^{\oplus}/DAR^{\ominus}$, converting electrostatic interactions to covalent bonds, where the polyelectrolyte molecules likely become compacted and the pore size in the multilayer wall was therefore reduced. Thus, the water permeability of the multilayer wall was decreased upon UV irradiation, due to the covalent cross-linking between paired diazonium/sulfonate or diazonium/diazonium sulfate groups, resulting in retention of encapsulated substances.

First, an attempt was made for the purpose of encapsulation of polymers with a large molecular weight. $(Nafion/DAR)_4$ capsules were studied here as typical examples to encapsulate the model cargo substance, fluorescent polymer AF488-Dextran.

As shown in the following Confocal Laser Scanning Microscopy (CLSM) images (Figure 6.8), 10 min of UV irradiation can crosslink $(Nafion/DAR)_4$ capsules, and can retain fluorescent polymers (AF488-Dextran, 10 kDa) for a long time (2 or more weeks), when compared with capsules without irradiation. As one can see clearly, right after UV irradiation, all the capsules were filled with fluorescent polymers, showing very strong fluorescent signal (more than 250 units, Figure 6.8 a). With increase of time, fluorescent polymers gradually penetrated through the capsule shell network structures or defects, demonstrating as part of the capsules became hollow under CLSM observation. However, besides the empty capsules, most of the irradiated capsule can retain the fluorescent polymers inside even after 2 weeks, which was confirmed by the high fluorescent intensity inside capsules (~200 units, Figure 6.8 f).

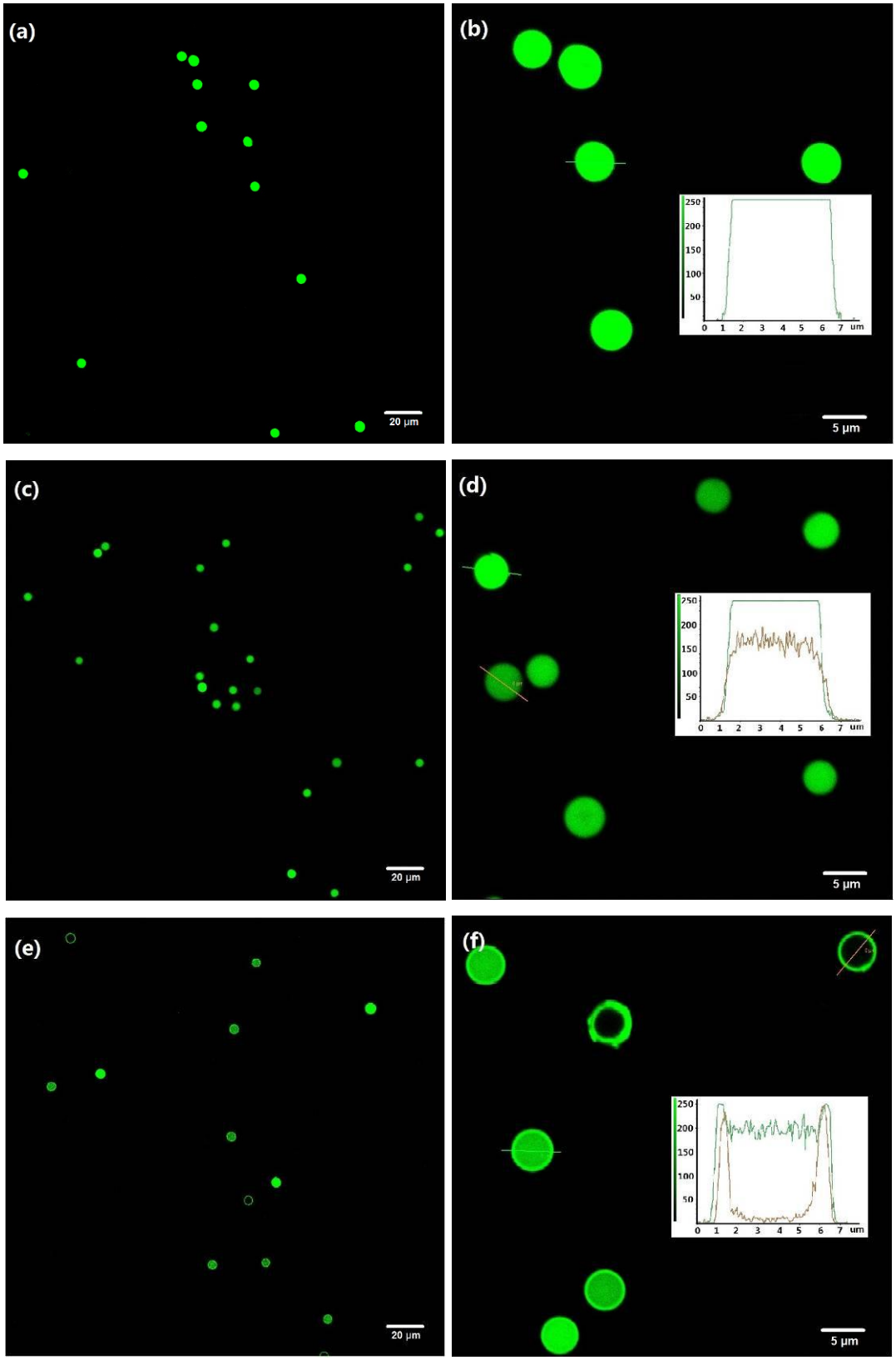

Figure 6.8 CLSM images of AF488-Dextran encapsulation in $(Nafion/DAR)_4$ microcapsules at various magnifications.

* These images were captured right after irradiation (a, b), and over 1 week (c, d) and 2 weeks (e, f) after irradiation. The line scan insets showed relative fluorescent intensity in capsules.

The substantial change in permeability of the capsule shells was further verified by the control groups, to which no UV irradiation was introduced. As one can see from the following images, without irradiation, fluorescent polymers cannot be retained inside capsules for as long as in the irradiated ones. Briefly, after 1 week, almost half of the dye polymers had already escaped, leading to weak fluorescent signals (~100 units, Figure 6.9 d); After 2 weeks, no fluorescent signal can be found, even doubled the emission laser power at high magnification (Figure 6.9 e, f).

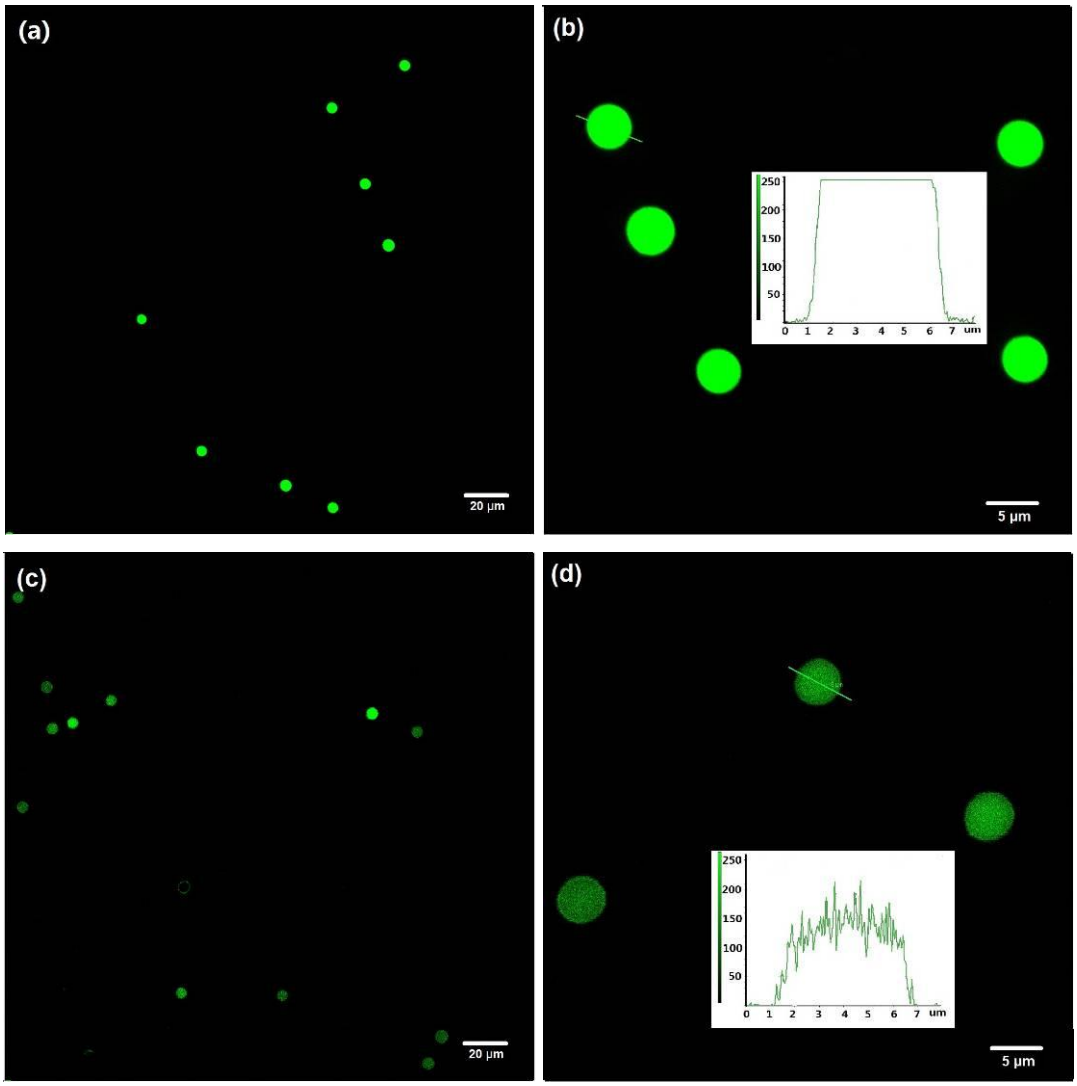

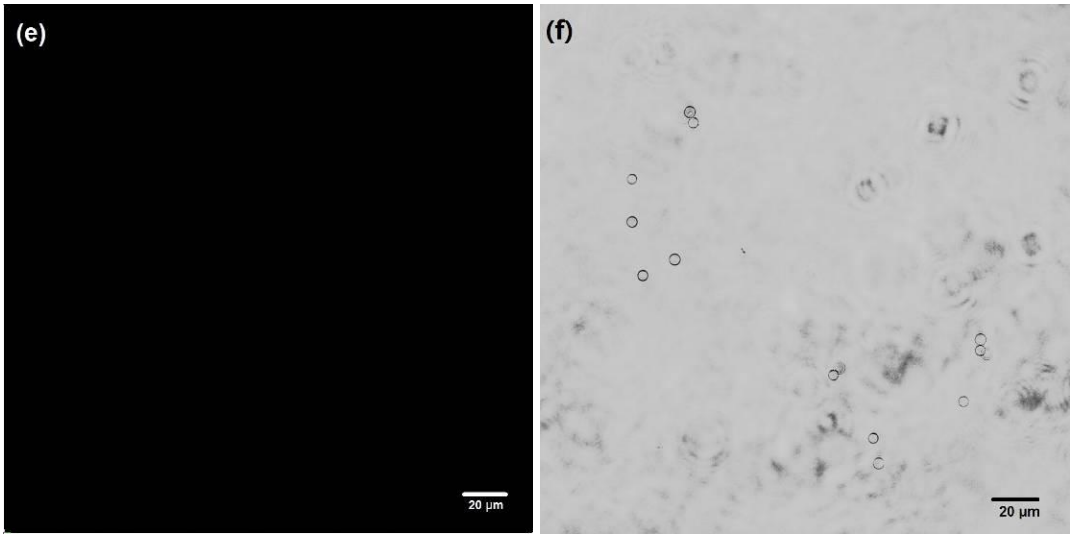

Figure 6.9 CLSM images of AF488-Dextran encapsulation in $(Nafion/DAR)_4$ microcapsules without irradiation at various magnifications.

* These images were captured after wash steps (a, b), and over 1 week (c, d) and 2 weeks (e, f) after wash steps. Image f presented corresponding capsules in bright field at high magnification. The line scan insets showed relative fluorescent intensity in capsules.

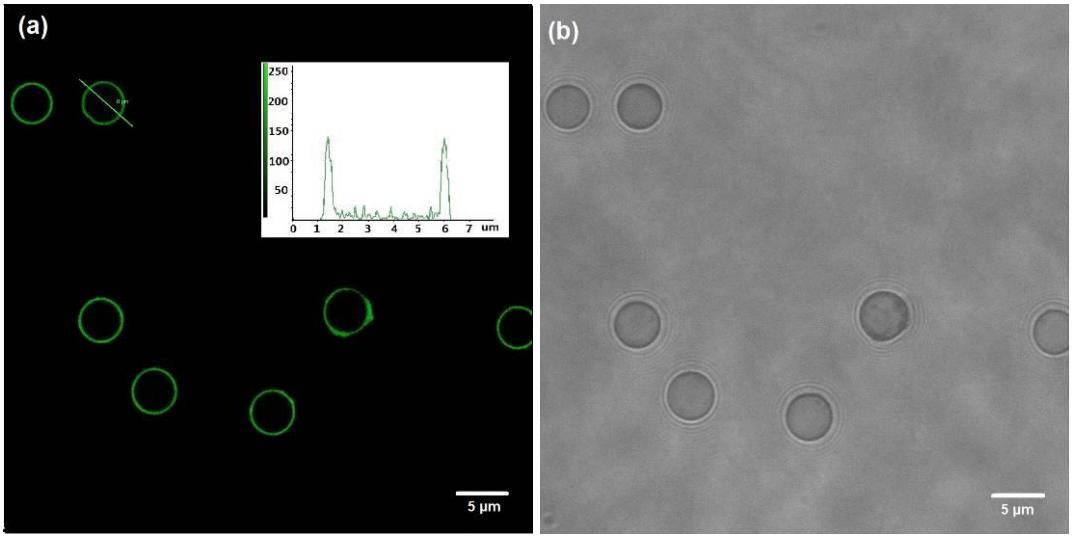

Figure 6.10 CLSM images of AF488-Dextran contained $(PSS/DAR)_4$ microcapsules without irradiation after wash.

* Image b showed the corresponding capsules in bright field. The line scan insets showed relative fluorescent intensity in the capsule.

As one can see clearly that the capsules without irradiation can also retain fluorescent polymers inside even after 1 week (Figure 6.9). Thus, it was assumed that the existence of Nafion, may have an effect on the permeability of $(Nafion/DAR)_4$ microcapsules. Here, $(PSS/DAR)_4$ microcapsule without fluorine (F) element were fabricated and studied. As shown in the following images, it was obvious that without irradiation, no

fluorescent polymers can be retained inside, only few of them can be trapped in the shells, leaving green ring-like images (Figure 6.10).

Since the significant difference of permeability for fluorescent polymer (10 kDa) between the non-irradiated $(Nafion/DAR)_4$ and $(PSS/DAR)_4$ capsules were observed, the authors proposed this could be attributed to the different multilayer composition of the two capsule systems. Nafion, as a classic example of the perfluorosulfonic polymers, was reported as the most common membrane polyelectrolyte used in direct methanol fuel cells due to its good chemical and thermal stability and high proton conductivity [201, 226, 239]. Here, in our experiments, this Nafion was used to build up $(Nafion/DAR)_4$ multilayer film. Comparing with the $(PSS/DAR)_4$ multilayer, $(Nafion/DAR)_4$ multilayer was found to be a more hydrophobic surface, as determined by the water contact angle measurement. As shown in Figure 6.11, a more hydrophilic surface with an average water contact angle of $39.65 \pm 1.80°$ for $(PSS/DAR)_4$ multilayers demonstrated when compared with that of the $(Nafion/DAR)_4$ multilayers (Figure 6.7 a). In theory, the water contact angle of Nafion terminating film should be very hydrophobic, close to $118°$ of Teflon[227]. Here, in this work, the water wettability of Nafion/DAR was great adjusted by the outmost DAR layer, although the underlying hydrophobic Nafion layer still had influence on the surface property due to the interpenetrated chains.

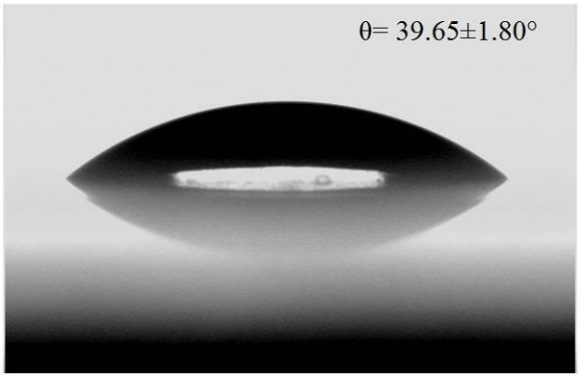

Figure 6.11 Photographs of water droplets on $(PSS/DAR)_4$ multilayers.

LbL assembly facilitates molecule encapsulation in microcapsules, especially for the large macromolecules have a molecular weight above 4 kDa[26, 66, 219]. As shown in above, the $(Nafion/DAR)_4$ allowed effective encapsulation of dye polymers with a molecular weight of 10 kDa, even without UV irradiation. In other words, these 10 kDa dye polymers were easy to go inside microcapsules, but slightly difficult to go outside.

The authors proposed this unique semi-one-way permeability as a result of the combination of high hydrophobicity and good film-forming property of Nafion layers. In bulk membrane, it was reported Nafion possessed a highly permeable to water due to very high water hydration effect of its $–SO_3^-$ groups, and the existence of interconnections between $–SO_3^-$ groups which facilitated rapid transfer of water through the Nafion[228]. In LbL films containing Nafion, such interconnected ionic channels were not expressed, because the $–SO_3^-$ charges were complemented with $–N_2^+$ of DAR, preventing rearrangement of fast ion channel formations[221, 229]. Therefore, the proton mobility of Nafion/DAR system mainly depended on free $–SO_3^-$ groups in the multilayer. However, as motioned above, QCM results revealed a thin layer structure of Nafion in the Nafion/DAR multilayer system (Figure 6.3), demonstrating the lack of free $–SO_3^-$ in the internal layers. As restricted by the counterions of DAR, no hydrophilic domain (mainly the dissociated $–SO_3^-$ groups) can achieve water uptake and assist proton conductance, leaving the very hydrophobic Teflon-like backbone structure of Nafion to play a dominant role. As a consequence, the water mobility was greatly reduced in the multilayer system, leading to a low permeability of the Nafion/DAR multilayer shells. After diffused through the capsule shells driven by concentration difference, the fluorescent polymers were trapped inside the shells due to the less water containing and less permeable hydrophobic Nafion membranes, which tended to shrink in aqueous solution.

6.5 UV-induced Small Molecule Encapsulation

However, the challenge is in encapsulation and securely storing of small active molecules. Many efforts have been devoted to altering the permeability of multilayer shells in the purpose of nanoscale encapsulation of bio-polymers, drugs and dyes. Such strategies as spontaneous deposition of water-soluble substances with charged oligomers[63] and controlled precipitation into capsules[97] were developed to achieve the goals. Here, in this work, we explored a novel method based on DAR contained capsule system to realize small molecule encapsulation without any chemical bonding to cargo substances or help of external adjustment, but only with the remote trigger of UV light.

Specifically, the dye molecule rhodamine B (RhB) with a molecular weight of 479 was used as a typical example of small molecules. And the DAR contained microcapsules, both $(Nafion/DAR)_4$ and DAR_8 were studied.

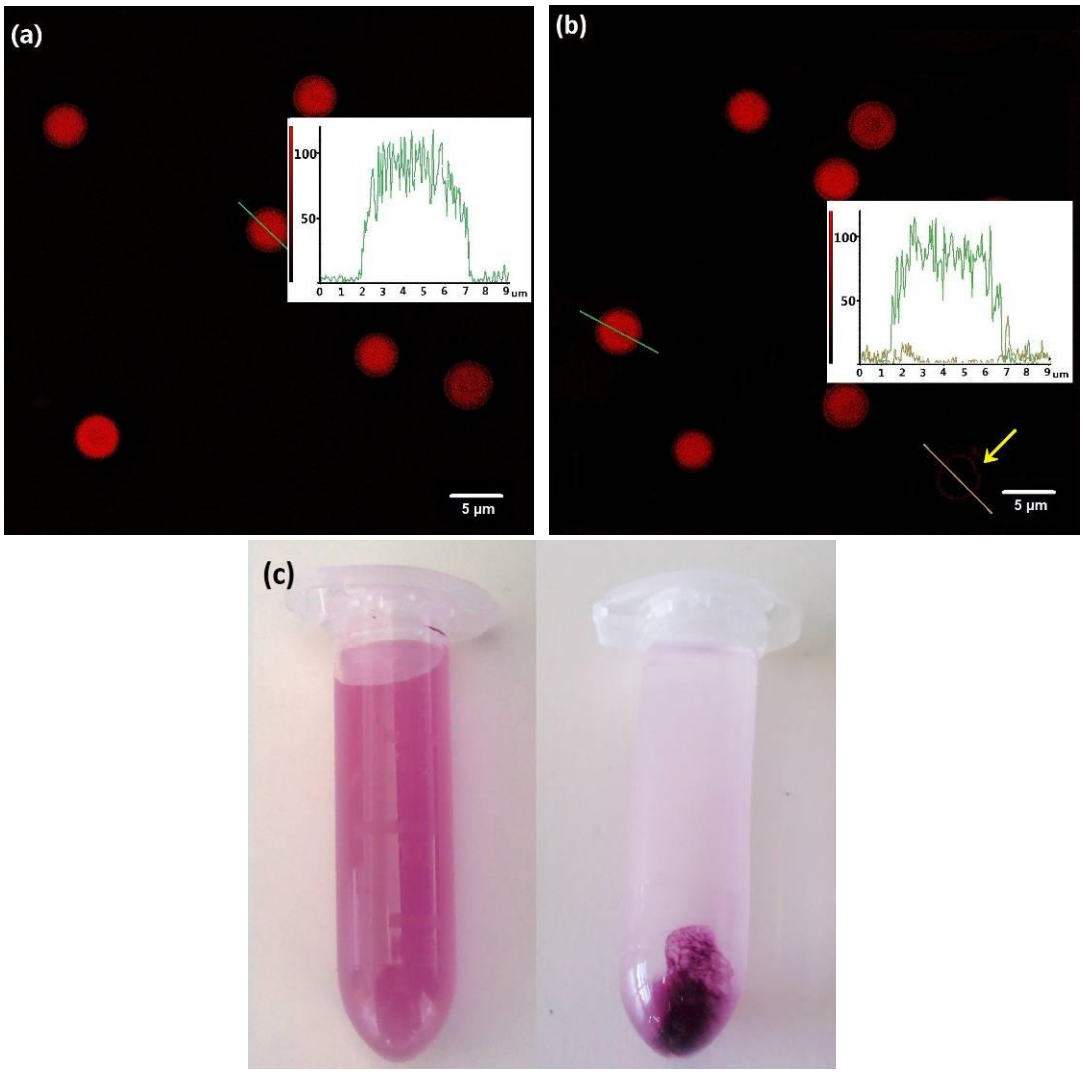

Figure 6.12 CLSM images of rhodamine B contained (a) $(Nafion/DAR)_4$ and (b) DAR_8 microcapsules after 10 min of UV irradiation. Image c presented the RhB encapsulated DAR microcapsules before (left) and after (right) centrifugation at 4500 rpm for 5 min.

* The line scan insets showed relative fluorescent intensity in capsules. The arrow represented a broken capsule, in which no RhB could be retained.

Generally, after 10 min of UV irradiation, the DAR-related photolysis covalent crosslinked the multilayers[104], and also converted the hydrophilic diazonium groups to the hydrophobic ester groups[251] (see Scheme 6.2). Accompanied by the elimination of paired charges, the network-like shell structures became denser with less and smaller pores, resulting in a great reduction of capsule shell permeability. As shown in the

Figure 6.12, after 10 min of UV irradiation, the DAR contained microcapsules, both $(Nafion/DAR)_4$ and DAR_8, acted like excellent micro-containers for the small RhB molecules, demonstrating as an average fluorescent signal intensity of ~ 89 units inside capsules and ~ 0 unit outside capsules. In the contrary, the capsules with defects can't entrap any dye molecule inside, exhibiting an empty cavity under confocal laser scanning microscopy (CLSM) observation (Figure 6.12 b, ~ 0 units inside capsules, as pointed out by an arrow).

As found in our work (section 6.4 and 6.5), the UV-induced shell sealing facilitated molecule encapsulation in fabricated microcapsules. Remarkably, small molecule RhB was successful encapsulated in these UV-sealed DAR capsules through diazonium-related photolysis. However, one should notice, small molecule encapsulation was not only attributed to the conversion of electrostatic interactions into covalent bonds, but also benefited from the capsule architectural property. To be specifically, the counterpart polymers (Nafion and $DAR^{\ominus}$) of DAR made their contribution to successful encapsulation (as discussed in section 6.3 and 6.4). On the contrary, the PSS/DAR microcapsules without such hydrophobic polymers in their shells can't encapsulate macromolecules (AF488-Dextran, 10 kDa, Figure 6.10) in their cavities. Moreover, UV irradiation can't decrease their shell porosity significantly, as confirmed by their limited ability to encapsulate macromolecules with molecular weight from 9.5 kDa to 186 kDa[104]. Similarly, the polymeric shells containing diazonium groups were only able to encapsulate macromolecular dextran (4 kDa)[252].

6.6 Modulated Long-term Release of Encapsulated Small Molecules

Theoretically, capsule shells were network-like structures, with a lot of pores in the multilayers. Sealing methods, e.g., DAR-related photolysis discussed here, could decrease the pore size and then to make the shells become semi-permeable or less permeable, resulting in the retention of loaded substances for certain time. In this work, two novel microcapsule systems containing DAR were used to achieve small molecule encapsulation, and to modulate the encapsulated substance release (for experimental section see Section 3.3.7). As one can see from Figure 6.13, the encapsulated RhB amount in the microcapsules with and without 10 min of UV irradiation normalized by capsule number was shown. For the $(Nafion/DAR)_4$ capsules, 690 fg RhB can be

retained in one $(Nafion/DAR)_4$ capsule, while there was no more than 1/3 of RhB content (204 fg) detected in the non-irradiated $(Nafion/DAR)_4$ capsules. This pronounced difference between the microcapsules with and without irradiation illustrated remarkable decreased permeability which was attributed to the DAR-related sealing effect on the capsules. As time went on, the RhB molecules gradually penetrated out the microcapsules. 11 days later, there was only 93 fg of RhB found in the non-irradiated capsules. This could be explained as that the charged dye molecules were trapped in the shells through electrostatic interactions with oppositely charged Nafion. However, in the irradiated capsules, there was 262 fg of RhB can be detected, which was almost triple of that in non-irradiated ones, confirming that most of the RhB molecules were retained by physical encapsulation instead of the chemical bonding. In addition, the sum of the RhB content in capsules and in supernatant roughly matched the total RhB amount encapsulated in per sample. From the two curves, it was confirmed that the DAR-related photolysis greatly 'sealed' the capsules, slowed down RhB molecules penetration. Similar results of the sealing effect can also be found in DAR single component microcapsule system, where 707 fg and 202 fg of RhB were found in irradiated DAR_8 microcapsules at Day 0 and Day 11 respectively, showing continuous gradual leakage from possibly not completely sealed capsules.

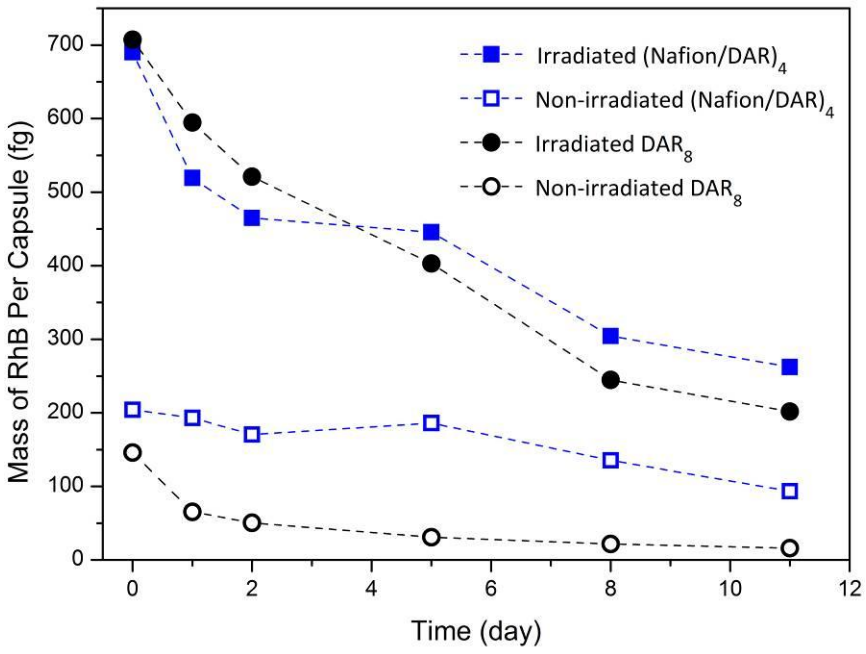

Figure 6.13 Mass of encapsulated RhB amount in per DAR contained microcapsule with and without UV irradiation.

Specially, one thing that worth mentioning for encapsulation should be the relatively small RhB amount found in the non-irradiated DAR_8 capsules when compared with the non-irradiated $(Nafion/DAR)_4$ capsules. As shown in Figure 6.13, at the beginning there was 156 fg of RhB found in non-irradiated DAR_8 microcapsules, then a very fast release occurred in a duration of 11 days, resulting in 10% (16 fg) of RhB retained inside capsules over 11 days. On the contrary, 11 days later, there was 45.6% of RhB can be found in the non-irradiated $(Nafion/DAR)_4$ capsules. As discussed in Section 6.4, in the Nafion/DAR system, Nafion played a predominant role in encapsulating of large molecule, due to its high hydrophobicity and good film-forming properties. Therefore, with the existence of Nafion, the $(Nafion/DAR)_4$ system was more hydrophobic and less water permeable after fabrication, exhibiting a good dye retention effect than DAR_8, even without UV irradiation.

Due to the possible bleaching effect of RhB, it might be not precise for fluorescent molecule amount quantification over a long time. However, the CLSM images of RhB encapsulated capsules over long duration after UV irradiation could provide us qualitative proof of the successful small molecules encapsulation. As shown in Figure 6.14, over two months after UV irradiation, there was still certain fluorescent signal could be detected in the UV-sealed $(Nafion/DAR)_4$ microcapsules, although the average fluorescent signal intensity was very weak (~ 38 units). Comparing with the CLSM images in Figure 6.12, these images were taken with an enhanced laser power, leading to low-contrast capsule images and quite noisy background with an average fluorescent signal intensity of ~ 20 units. On the other hand, no fluorescent signal can be visualized from the other capsules (non-irradiated $(Nafion/DAR)_4$ and irradiated/non-irradiated DAR_8) (data not shown), illustrating that almost all the encapsulated fluorescent RhB molecules were penetrated out these microcapsules during two months. Therefore, considering the RhB release curves in Figure 6.13, it could be concluded that the existence of Nafion in $(Nafion/DAR)_4$ microcapsules benefited a slow RhB permeability behavior, especially for the irradiated ones. At low magnification, almost all the irradiated $(Nafion/DAR)_4$ microcapsules containing RhB showed red dot-like images under CLSM observation, as shown in Figure 6.14 c. Specially, a broken capsules was pointed out in bright filed (Figure 6.14 d). This broken capsule, similar as other ones with defects in our work, cannot entrap any dye molecule in cavity, showed no corresponding fluorescent images under CLSM investigation (Figure 6.14 c). This result

confirmed the mobility of RhB molecules in capsule cavity, and further verified that the successful small molecular RhB encapsulation in DAR-related microcapsules was based on capsule shell sealing, rather than potential electrostatic interactions between polyions and RhB or chemisorption effect.

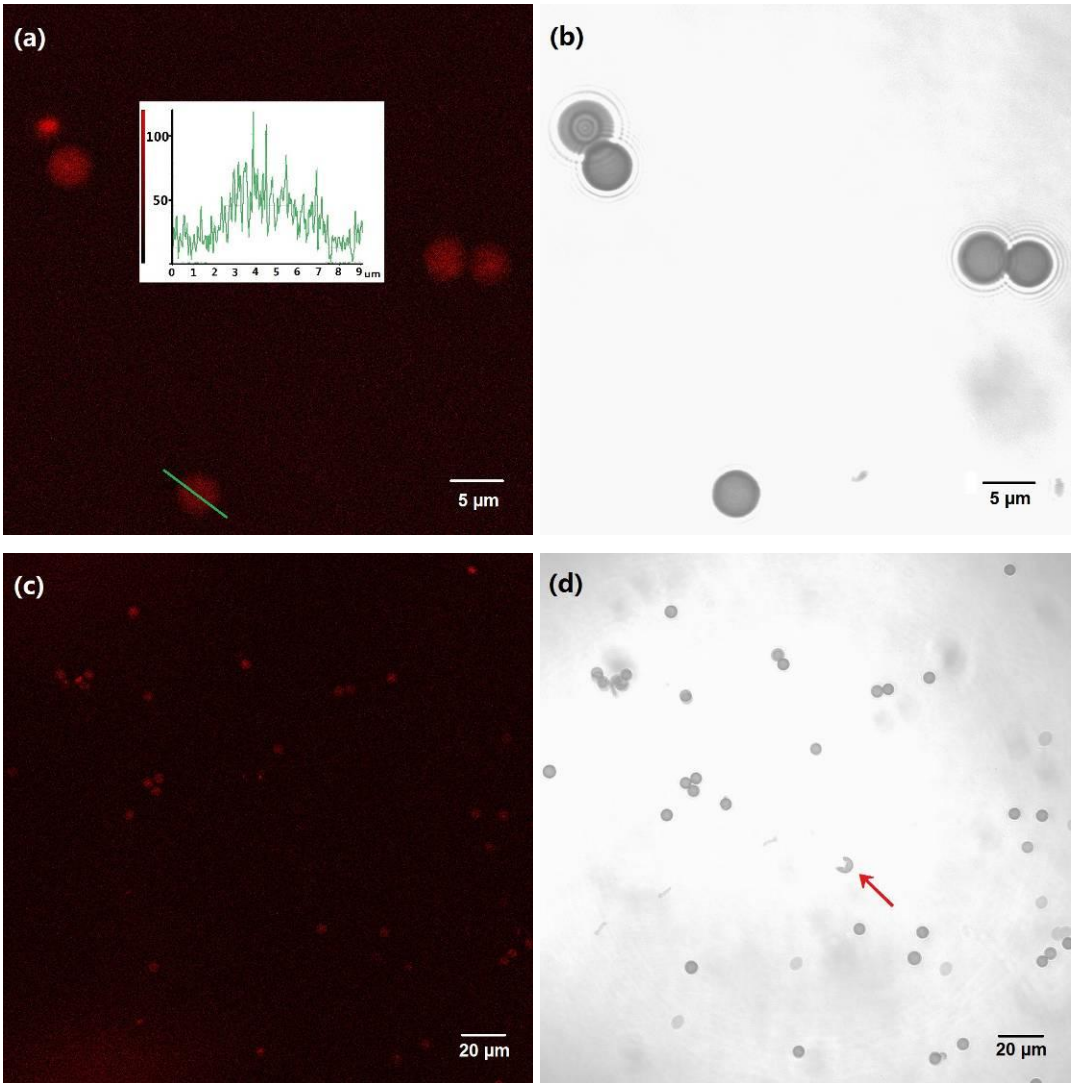

Figure 6.14 CLSM images of rhodamine B contained $(Nafion/DAR)_4$ microcapsules over 2 months after UV irradiation.

* The line scan inset showed relative fluorescent intensity in capsule. The arrow presented a broken capsule.

Besides the micro-scale LbL multilayer capsules as discussed in this thesis, other delivery systems with diverse architectures and release manners have been developed, in order to meet the urgent requirements in controlled small drug delivery field. For examples, the ultrathin (11 ± 2 Å) LbL film system composed of poly(b-amino esters)

(PBAEs) and poly(carboxy-methyl-b-cyclodextrin) (polyCD) complexes was proposed to control the release of small drugs (ciprofloxacin, flurbiprofen, and diclofenac). These drug molecules were non-covalent chemical interacted with cyclodextrins, and their release was modulated as zero-order release kinetics through hydrolytic top-down degradation of the film layers[253]. Unlike the LbL multilayer system, other hybrid delivery carriers (e.g. liposomal-, polymeric-, micelle-, dendrimeric- based and viral-like) based on nanoparticle platform have been developed as well[254]. The use of such nano-carriers for drug delivery includes many advantages, for example enhanced water solubility, specific accumulation and low nonspecific toxicity. And the most outstanding feature of these nano-carriers should be their great potential for clinic use, as several products of them have been become commercial available (e.g. liposomes: Doxil, Myocet, Daunoxome) or under approval of preclinical/clinical trials (e.g. micelle: Genexol-PM, NK911; Viral-like: HSP-DOX, CPMV-DOX)[254]. However, there are still some challenges existed such as limited drug encapsulation efficiency and uncontrolled drug release. To overcome these problems, careful considerations of carrier design (e.g. structural improvements) should be made. Strategically, LbL assembly approach would be a promising technique to solve the problem, by providing steady nano-scale shells with large hollow cavities to entrap small molecular drugs and modulate their release.

6.7 Infrared Laser Induced Instant Release of Encapsulated Small Molecules

A laser induced RhB molecule release double confirmed the physical encapsulation effect, for both of the $(Nafion/DAR)_4$ and DAR_8 microcapsules. In order to achieve laser induced cargo substance release, the pre-aggregated gold nanoparticles were introduced in capsule shells after capsule fabrication and dye encapsulation processes with the addition of a polyelectrolyte layer. Consequently, these capsules after gold modification looked not as monodisperse as initial ones; some cloud-like gold nanoparticle clusters were formed (symbol Δ, Figure 6.14 b), bridging the adjacent microcapsules (symbol *, Figure 6.14 b). The fluorescent intensity inside capsules became lower which might be attributed to the many wash steps during gold nanoparticle introduction. However, the purpose of this work was to observe the potential instant release of RhB triggered by IR laser qualitatively, thus the slightly changes in capsules could be acceptable.

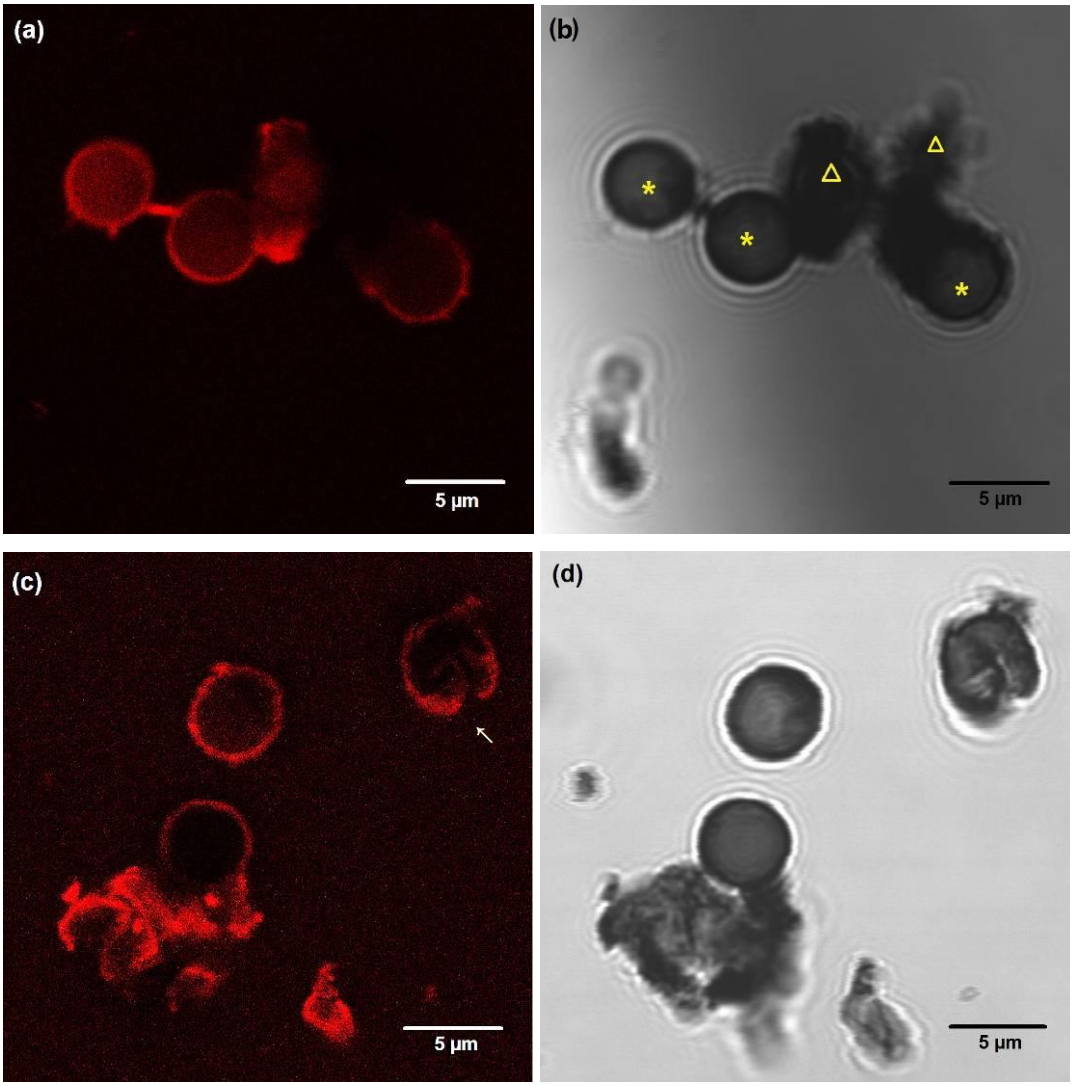

Figure 6.15 CLSM images of RhB-(Nafion/DAR)$_4$-(Au/Nafion/DAR/Au) microcapsules before (a, b) and after (c, d) laser irradiation.

* Images b and d presented capsules in bright field. The arrow presented a broken capsule, from which the fluorescent molecules were released. The symbol * presented the microcapsules, symbol Δ presented gold clusters.

As shown in Figure 6.15 (a, b), the laser induced Nafion/DAR microcapsules were used as a typical example here (for experimental section see Section 3.3.9). Before laser irradiation, the gold cooperated microcapsules showed red fluorescent images under confocal laser scanning microscopy observation. After irradiation for several seconds, laser generated local heating damaged capsule shells[224], promoted RhB molecule release. A typical example of the hollow broken capsule was given, as in Figure 6.15 (c, d). Compared with the initial ones, when the dye molecules were released, the microcapsule cavity became slightly dark, and local circumstance became fluorescent visible.

6.8 Conclusions

In summary, two kinds of novel UV responsive polyelectrolyte microcapsules containing DAR were fabricated by using layer by layer assembly. Upon direct exposure to UV light, the ionic bonds of counterpart ions were fast converted to covalent chemical bonds through DAR-related photolysis, which offered an externally controlled method to seal the multilayer capsules. These capsules were investigated as unique micro-containers for cargo substance encapsulation, which benefited from UV induced photolysis of the paired charges and the remaining hydrophobic backbones. Simply triggered by UV light, both of the two kinds of microcapsules exhibited excellent and efficient macro-/small- molecule encapsulation effect. When compared with the non-irradiated ones, the UV-sealed microcapsules exhibited a much higher RhB preservation, even over a long time (11 days) after UV irradiation. Specifically, without UV irradiation, the $(Nafion/DAR)_4$ microcapsules showed a better dye encapsulation effect, which could be attributed to the exsitence of Nafion. These two DAR contained microcapsule systems would be very promising micro-containers/vesicle for medical, biotechnological applications. And remarkably, such microcapsules also showed great application for many environmental and photochemical uses, where sometimes the abundant UV light could be applied as the efficient external trigger. As shown in Scheme 6.4, schematic illustration of this UV triggered capsule shell sealing based on DAR-related photolysis was shown.

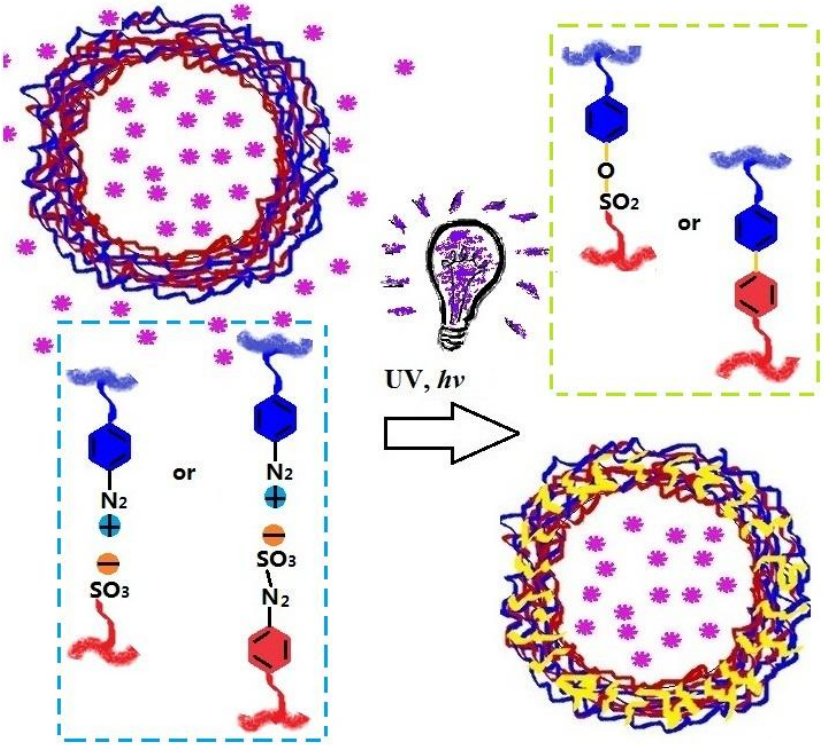

Scheme 6.4 Schematic representation of UV triggered capsule sealing based DAR-related photolysis.

7. Externally Triggered Dual-function of Complex Microcapsules

7.1 Introduction

7.1.1 Background

Numerous works have been done to provide solutions for diverse requirements in different fields ranging from biotechnology, pharmaceutics and chemical synthesis to catalysis perspectives. Delivery system originated from polyelectrolyte multilayer capsules has attracted increasing interests during the past decades. Generally speaking, different external stimulus have been employed to fabricate LbL capsule systems and to realize their functionalities, in order to meet their various requirements[29]. Typically, as earlier discussed in this thesis, UV light responsive capsules represent one series of the fast developed stimuli-responsive vesicles for potential applications in different areas. UV treatment allowed the functionalization of these fabricated capsules with accompanied changes in their morphologies, shell stability as well as permeability, benefiting from underlying chemical transitions. However, to the best of our knowledge, most of the research works concerning about UV responsive capsules have been focused on single functionality, with their emphasis on either encapsulation or release, triggering by remote UV light.

To develop multi-functional capsules system is of great importance, which sometimes can accomplish multi-functionalities, for example both the encapsulation and release, in one system just simply triggered by applying of only one external stimulus. Strategically, for multilayer capsules, it is not difficult to achieve this goal with introduction of different UV responsive chemical components (groups) in one system. In Chapter 5, the microcapsules composed of PDADMAC and PAZO demonstrated a novel UV induced swelling-disruption process, which was revealed as the J-styled aggregation of azobenene molecules. This gradually capsule breakage triggered by long term UV treatment (up to 3 hours) benefited an externally controlled release of cargo substances. On the other hand, in Chapter 6, the microcapsules containing diazonium groups exhibited an excellent ability to seal the multilayers, offering an excellent ability for molecule encapsulation via UV induced photolysis of paired ion charges, typical

example was demonstrated as high preservation of small molecule RhB (Mw=479). This UV induced sealing effect occurred very fast, e.g. 10 min was found enough to finish corresponding reactions. Therefore, cargo substance encapsulation and release triggered by single UV light can be integrated in one complex capsule system, as inspired by the completely different UV responsive behaviours of microcapsule systems discussed in above two chapters.

Ideally, with proper control over the balance of shell sealing and breakage (swelling and/or disruption), UV light with continuous wavelengths (containing the effective working wavelengths at ~ 365 nm and ~ 380 nm for azobenzene and diazonium group respectively) could push forward a UV dosage-dependent progress of capsule shell sealing and further breakage. Under a given UV irradiation condition, the fast shell sealing effect could be finished by in situ crosslinking of Nafion/DAR multialyers through a short-term UV induced photolysis; in the meantime, no obvious capsule breakage must be ensured in this duration. Further gradually breakage would be accomplished by re-alignment of azobenzene molecules in PDADMAC/PAZO multialyers triggered by long-term UV irradiation. Practically, this balance control can be easily achieved through adjustment of the ratio of two multilayer systems which might have different influence on built capsules. Regarding to the strengthened shell structures of Nafion/DAR capsules after sealing, which required combination of freeze-thaw and sonication treatments to break them (see Section 3.3.7), the multialyers containing a small percentage of crosslinking sites (diazaonium of DAR) would be preferred.

7.1.2 Aim and Objectives

The aim of this chapter is to realize dual-function of the LbL microcapsules triggered by the same UV stimulus, to achieve the both encapsulation and release to be specifically. By introducing UV sensitive chemical groups causing different potential response as building blocks, fabricated LbL capsules can be endowed with dual UV responsive properties in specific layers. One block is responsible for fast capsule sealing and the other for longer term capsule swelling and rupture. Therefore, the multi-function of these capsules could be activated selectively when exposed to external UV light with suitable wavelengths.

Therefore the main objectives of this chapter are:

1) To design and fabricate complex multilayer microcapsules $(PDADMAC/PAZO)_4$-$(DAR/Nafion)_2$ containing both azobenzene and diazonium groups.

2) To investigate the parameters corresponding to the UV induced capsule shell stability change, for example chemical transitions within multilayers, the capsule morphology changes based on rapid shell sealing (short-term, mins) and gradually shell disruption (long-term, hours).

3) To study the possibilities of cargo substances (macro-/small- molecules) encapsulation and successive release by these UV responsive microcapsules

7.2 UV–induced Capsule Sealing and Further Swelling

After layer-by-layer assembly, microcapsules containing both azobenzene and diazonium groups were obtained. As typical examples studied here, $(PDADMAC/PAZO)_4$-$(DAR/Nafion)_2$ were fabricated, to which four PDADMAC/PAZO and two DAR/Nafion layers were introduced.

As shown in Figure 7.1, the prepared microcapsules were flat with creases and folds under SEM observation, which were similar as the other ones found in this thesis. Without UV irradiation, these capsules showed uniform size distribution, with an average diameter of ~ 5 μm. At high magnification (× 120 k), the capsule exhibited an intact and relatively smooth surface (Figure 7.1 c).

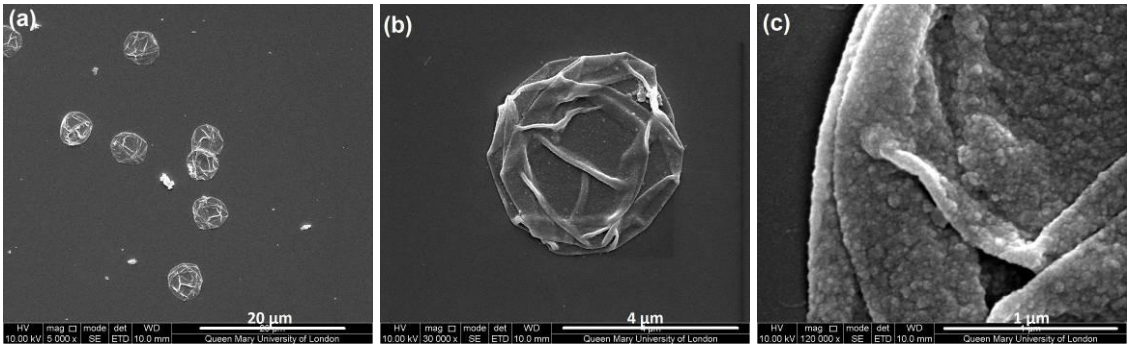

Figure 7.1 SEM images of fabricated $(PDADMAC/PAZO)_4$-$(DAR/Nafion)_2$ microcapsules.

The UV response properties of these fabricated complex capsules were studied. In this work, the UV intensity used was approximately 55 mW/cm^2, and the UV treatment duration was 0~3 hours. The structural formulas of these polyelectrolytes used for capsule fabrication were given in Scheme 7.1.

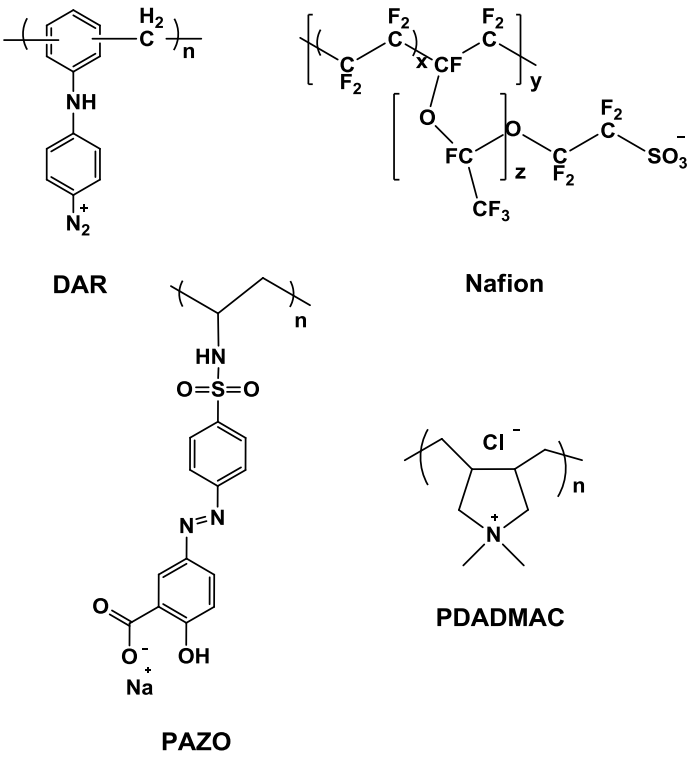

Scheme 7.1 Structural formulas of the polyelectrolytes used in this chapter.

With the constant UV irradiation intensity, these capsules exhibited a time-dependent swelling process after exposure to UV light, as shown in Figure 7.2 and Figure 7.3. After first 10 min of UV irradiation (Figure 7.2 1st row), no obvious size change could be found when compared with the initial capsules (Figure 7.1), and the shell formations seemed intact, no pore or crack could be found under SEM observation (Figure 7.2 c). Therefore, the first 10 min of UV irradiation could be chosen as the treatment to seal the outmost DAR/Nafion layers, which will be discussed later. Extending the UV irradiation duration to 20 min (Figure 7.2 2nd row), an obvious size increase was observed. More than 60% of the capsules increased their size to above 6 μm; however, there were still some capsules found at their initial size (Figure 7.2 d); in the mean time some tiny pores could be observed on the shells (Figure 7.2 f). After exposure to UV for 30 min (Figure 7.2 3rd row), most of the capsules swelled to ~ 7 μm, and obvious pores in the size of 30~40 nm were found (Figure 7.2 i).

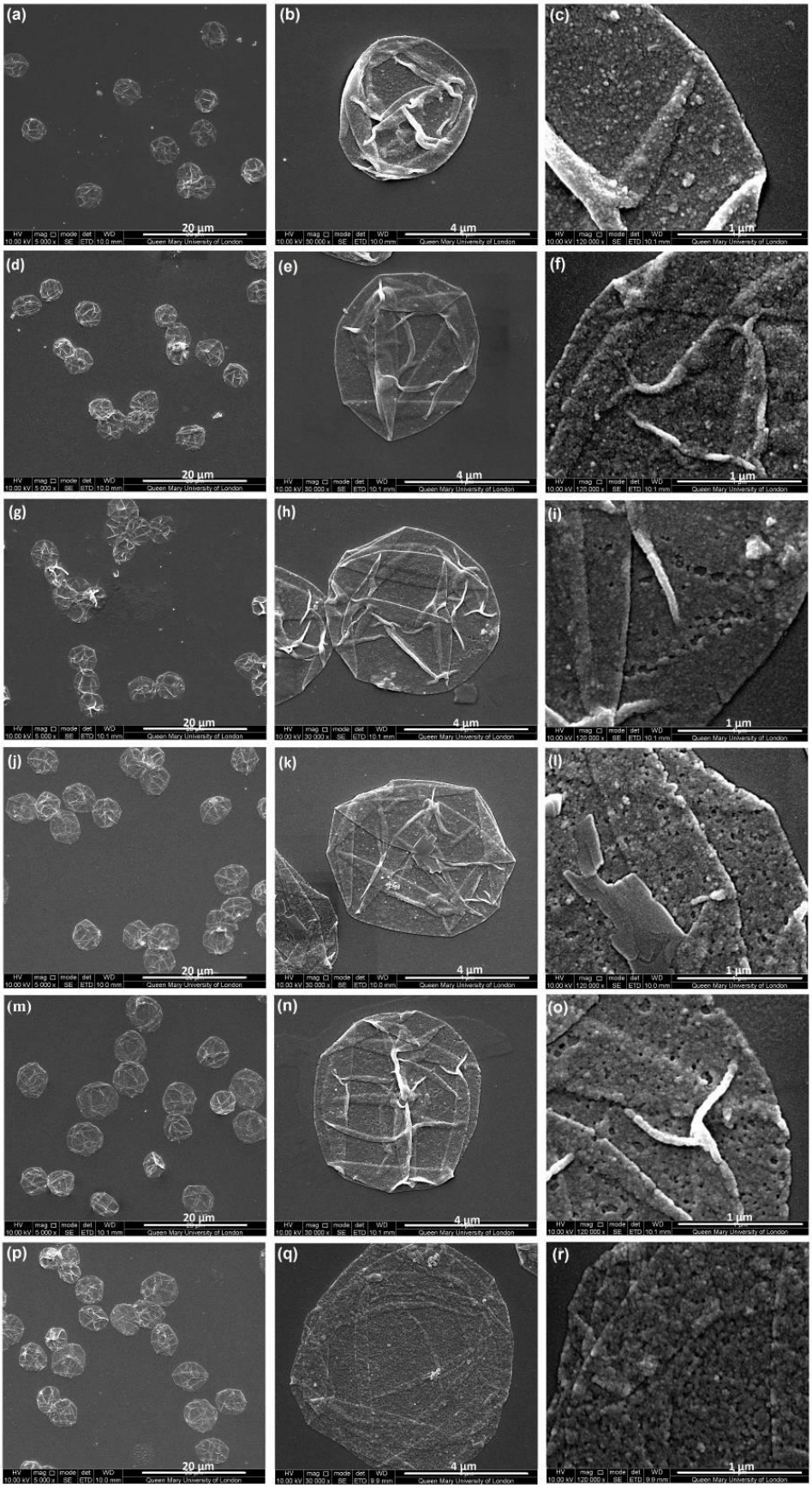

Figure 7.2 SEM images of complex microcapsules after UV irradiation of 10 min (1st row), 20 min (2nd row) 30 min (3rd row), 1 h(4th row), 2 h (5th row), and 3 h (6th row) at different magnifications.

When the UV irradiation time reached 1 hour (Figure 7.2 4th row), there was no significant further increase in capsule diameter could be found. However, the pores on the shells exhibited a size growth; some of them were found as large as 100 nm in diameter (Figure 7.2 l). Further extending the UV duration to 2 hours (Figure 7.2 5th row), a similar pore size increase tendency was found; more and more pores were emerged (Figure 7.2 o). After 3 hours of UV irradiation (Figure 7.2 last row), almost all of the capsules were swollen, some of them possessed a size of > 8 μm (Figure 7.2 q); as a consequence of continuous UV irradiation, numerous pores were found on the shell surfaces (Figure 7.2 r).

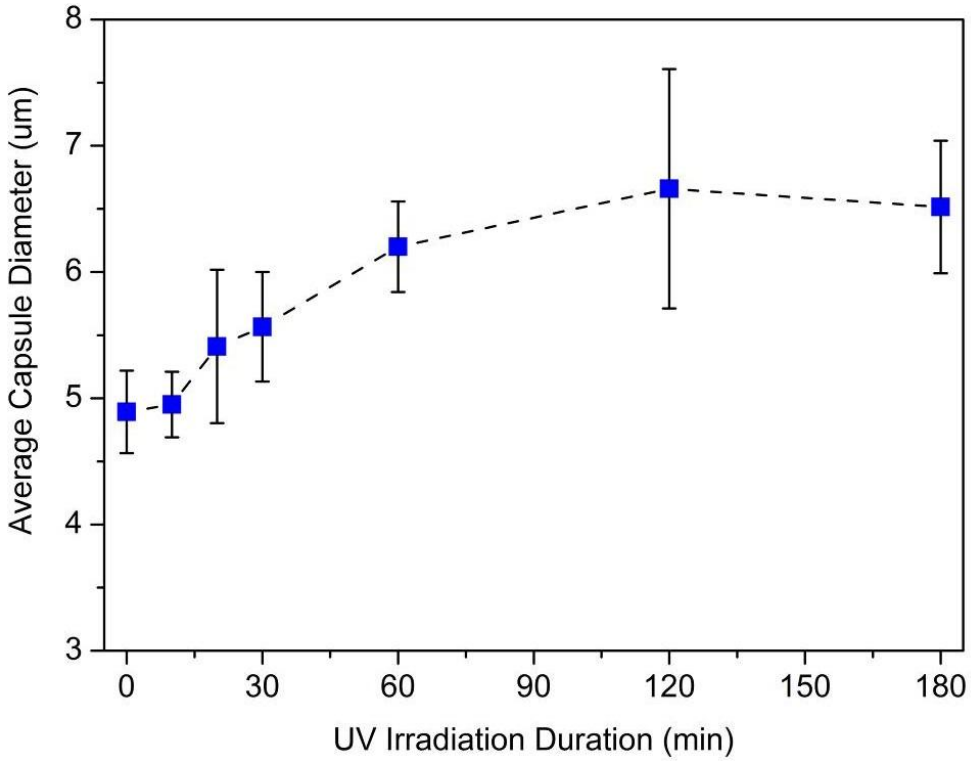

Figure 7.3 Size changes of complex capsules after UV irradiation.

* Capsule diameters and distributions were expressed as mean ± SD of at least 30 capsules per sample of random measurement of SEM images.

In general, as a result, 3 hours of UV irradiation caused remarkable capsule swelling (size change from 5 μm to 8 μm), and generated a lot of pores with the size more than 100 nm on their shells. Different from the UV induced capsule disruption found in $(PDADMAC/PAZO)_4$ system, the UV treatment didn't tear these capsules into pieces, as the spherical morphologies still can be watched under SEM observation. As demonstrated in Chapter 5, the UV irradiation triggered the azobenzene moieties to form end-to-end aligned J aggregates, which further led to an irreversible swelling-

disruption process. And this process was evidenced by the generation of lamellar- and needle- like formations. However, in this work, a few broken capsules (Figure 7.4 a, the symbol *) can be found, only few lamellar-like formations (Figure 7.4, the symbol ∆) can be found occasionally after 3 hours of UV irradiation.

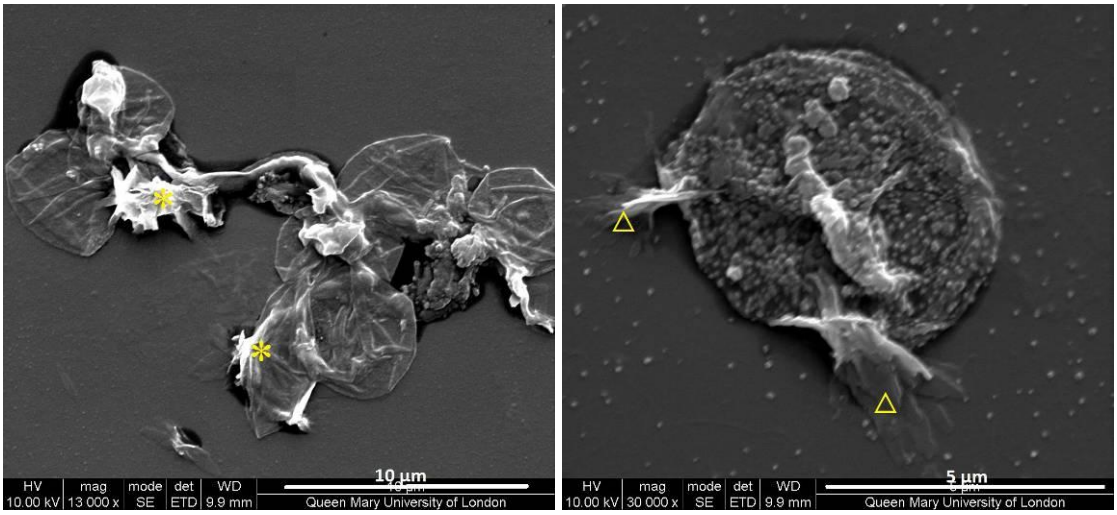

Figure 7.4 SEM images of broken complex microcapsules and lamellar-like formations after UV irradiation of 3 hours.

* The symbol * and ∆ showed the broken capsule and lamellar-like formations, respectively.

These changes in capsule morphologies were evidenced by the UV-Visible spectroscopy. As shown in Figure 7.5, the UV-Vis spectra of the complex capsules were demonstrated. Due to the analogical UV absorption curves and neighbouring maximum UV absorption peaks, the absorption of the complex multilayer capsules exhibited as a compromise of azobenzene and diazonium groups. Before UV irradiation, a strong absorption centered at 372 nm was found, which was contributed by the absorption of both azobenzene (π-π* transition at 365 nm) and diazonium (π-π* transition at 380 nm), and the weak peak detected at 270 nm was attributed to their parallel or concomitant adsorption[164, 223]. Exposure to UV irradiation, a fast absorbance decrease at maximum was observed, demonstrating as the consequences of photolysis of diazonium groups and possible photoisomerization reaction of azobenzene moieties. After 10 min of irradiation, the absorption intensity decreased to 50 % of the initial absorbance. Considering the SEM image of complex capsules after 10 min of UV irradiation (Figure 7.2, 1st row), potential chemical changes occurred during this period wouldn't cause capsule swelling.

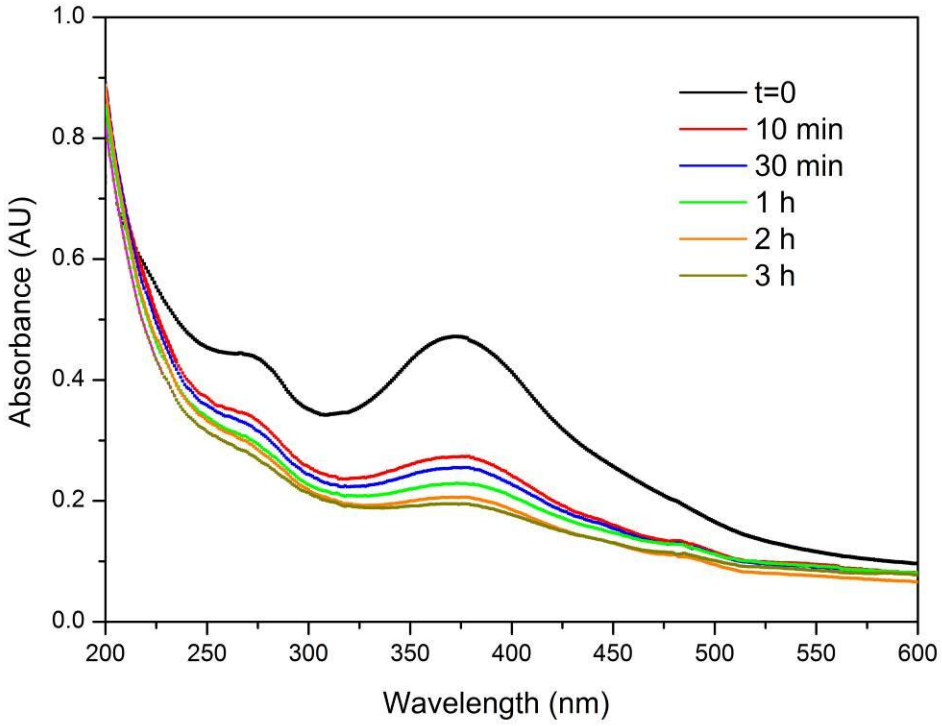

Figure 7.5 UV-Vis spectra of complex microcapsules upon exposure to UV light.

Practically, the DAR-related photolysis reaction occurred very fast, previous report has demonstrated a completed crosslinking effect with treatment of a 80 W mercury lamp at a distance of 13 cm within 50 s[163]. For the Nafion/DAR system, 10 min of UV irradiation was found sufficient enough to decompose all the diazonium groups and disappear the maximum absorption with a UV intensity of 50 mW/cm^2 (Figure 6.4 in Chapter 6). However, corresponding peak didn't disappear after 3 hours of UV irradiation in this work. This result should be attributed to the existence of PDADMAC/PAZO layers. As suggested, the photoisomerization azobenzene molecule couldn't be completed in this system due to the steric hindrances against this *tran* to *cis* conformation changes as well as possible hindrances of azobenzene aggregate formations[223, 255, 256] (the aggregate formations will be discussed in the following). Therefore, the remained absorption was assigned to that of PDADMAC/PAZO layers. Similar result was also found before (Figure 5.4 in Chapter 5), 2 hours of UV treatment didn't show the ability to disappear adsorption of azobenzene groups in PDADMAC/PAZO multilayers.

Theoretically, the UV triggered photoisomerization of azobenzene not only exhibited as *trans* to *cis* conformation change in plane, but also caused motions of azobenzene

moieties, exhibiting as re-alignment of azobenzene molecules. Consequently, J-styled (end-to-end) or H-styled (plane-to-plane) aggregates was preferred, depending on the mutual orientation of the interacting dipole moments between the counterpart molecules[158]. The generation of such aggregates can be easily monitored by UV-Visible spectroscopy, representing as blue shift for H aggregates and red shift for J aggregates. As found in $(PDADMAC/PAZO)_4$ capsule system (Chapter 5), a significant red-shift by 17 nm was observed, which was interpreted as the J aggregates of azobenzene molecules. In this work, besides the absorbance decrease, a time-dependent shift of maximum absorption towards longer wavelength was also found, as shown in Figure 7.5. Briefly, after 10 min of UV irradiation, the maximum absorption was located at 376 nm, exhibiting a red shift by 4 nm. Further exposing to UV light led to gradually red shift. Increasing the UV treatment duration to 3 hours a total red shift by 8 nm was visible at 380 nm. These results revealed that the J aggregates of azobenzene molecules were also formed in this complex multilayer capsules after UV irradiation.

The FTIR spectra of complex capsules before and after UV irradiation were exhibited in Figure 7.6, in order to demonstrate possible chemical changes in detail. Before UV irradiation, three absorption peaks representing the existence of diazonium groups were observed at 2222 cm^{-1}, 2162 cm^{-1} and 1577 cm^{-1} in the FTIR spectra, the former two showed the stretching vibrations of $–N_2^+$ and the latter showed the symmetric stretching of a phenyl group conjugated with the diazonium group.

After 10 min of UV irradiation, the peaks at 2222 cm^{-1} and 2162 cm^{-1} disappeared completely. With the disappearance of the peak at 1577 cm^{-1}, a new peak representing a normal absorption of the phenyl group, which was overlapped by signal of diazonium group before, was observed at 1590 cm^{-1}. All these changes should be explained as the UV induced decomposition of diazonium groups in the multilayers. In the meantime, another peak at 1111 cm^{-1} corresponded to the N–O stretching vibrational mode of complexes formed within DAR and adjacent polyanion also disappeared. Considering the existence of both Nafion and PAZO polymers surrounding DAR, this peak should be attributed to N–O stretching of complexes diazonium and sulfonate groups (in Nafion) $(–N_2^+ \rightarrow OSO_2^-)$[257] and also the complexes of diazonium and carboxylate groups (in PAZO) $(–N_2^+ \rightarrow OCO^-)$[165]. The disappearance of this peak also evidenced decomposition of diazonium groups under UV irradiation.

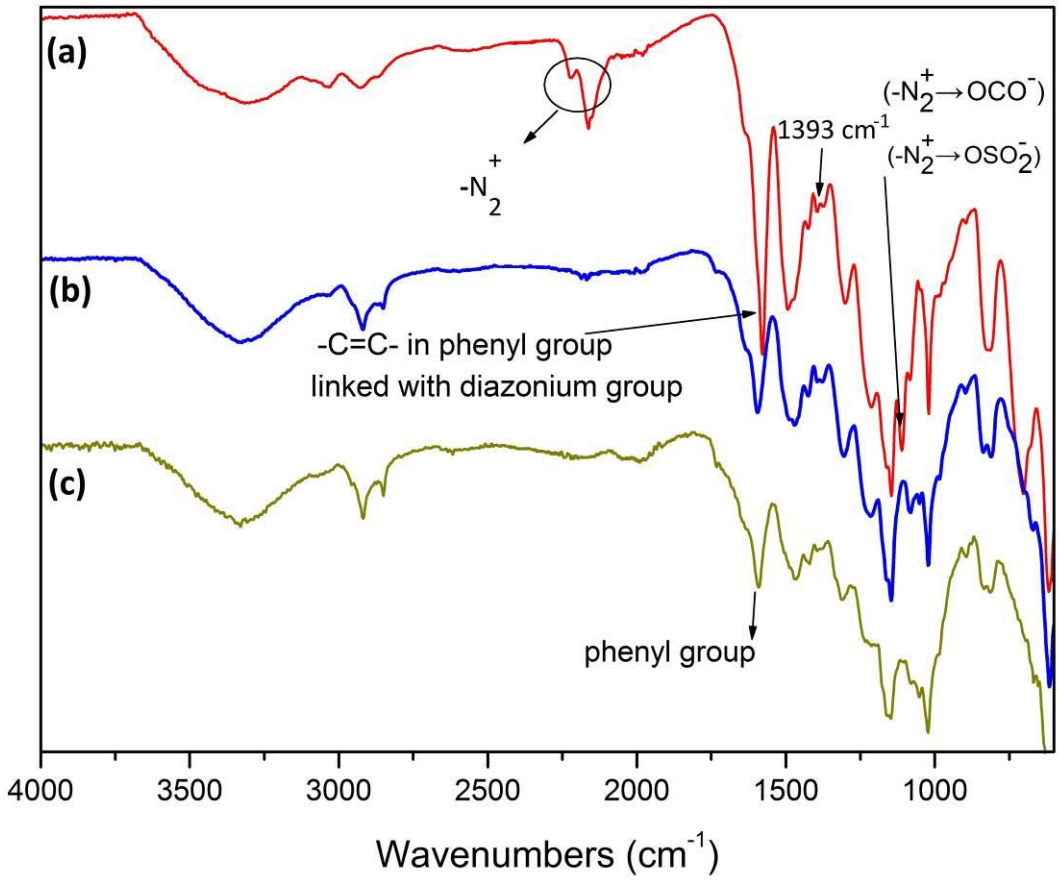

Figure 7.6 FTIR spectrum of complex capsules before (a) and after UV irradiation for 10 min (b) and 3 hours (c).

It should be pointed out here, a weak shoulder peak located at 1393 cm^{-1} was weakened after 10 min of UV irradiation. However, it is difficult to deal related signal identification. The reason is, on one hand, this weak peak could be assigned as association interaction (H-bonding) between the $–N_2^+$ and –OH within DAR and PAZO [162, 250]. On the other hand this peak could be originated from the signal of *trans*-azobenzene[231, 232]. For the former, UV irradiation was reported to be able to destroy the H-bonding between DAR and PAZO layers, convert it to stable ester bond (Ph–O–Ph), leaving stabilized layers against dissolution in polar solvent[250]. Whereas for the latter, it was reported that the UV irradiation can cause molecular conformation change in plane, which led to capsule shrinkage[16]. Therefore, any of these two chemical transitions, if there was any, could help the multilayer shells stable under UV irradiation, through possible inter-layer corsslinking between PAZO and DAR and/or capsule shrinkage attributed photoisomerization of azobenzene in plane. Unavoidable, the motion of azobenzene molecules would be suppressed to some extent consequently.

When the UV irradiation duration reached 3 hours, no obvious changes due to diazonium decomposition or azobenzene related photoisomerization could be observed. Combining the found red-shift effect in UV-Vis spectroscopy (Figure 7.4), the J aggregation would be the primary transition in this duration, although the degree of aggregation was found not as significant as that in pure PDADMAC/PAZO system (Chapter 5). Such end-to-end J aggregate of azobenzene has been found ability to break the integrate structure of film, shell-like formations [235, 258, 259]. And most importantly, it has been applied to break the $(PDADMAC/PAZO)_4$ microcapsules, as demonstrated in Chapter 5 schematic.

Generally, UV induced chemical changes in these complex capsule system is complicated, involving J-styled re-alignment of azobenzene molecules which mostly influenced by the interplay of PDADMAC polymers, and in-situ covalent bonding between paired diazonium and sulfonate groups. In this work, a polymer PAZO containing azobenzene groups on its side chains was used as polyanion for microcapsule preparation. The interplay of PAZO with its counterpart polymers was very important. As found in earlier work (Chapter 5), when the rigid polymer PDADMAC bearing the ionic charges in the backbone structure was used as polycation, the azobenzene molecular motion in domain was found predominately in a PDADMAC/PAZO multilayer system, where the rigid PDADAMC chains restricted the azobenzene molecule conformation change in plane and resulted in phase separation in nano-scale areas. Different from PDADMAC, the "soft" polymers showed different influence on fabricated multilayers with PAZO. For examples, when Polyethylenimine (PEI) was used as the polycation, a blue shift towards shorter wavelength of the maximum absorption in a UV-Vis spectroscopy was observed, when increasing the number of deposited PEI/PAZO bilayer on surface[223]; the multilayer microcapsules containing PAZO and relatively flexible counterpart polymers, $(PAH/PAZO)_3PAH/PVS$[16] and $(PAH/PAZO)_4$ (Chapter 5), showed capsule size decrease instead of capsule swelling when treated with UV light. Thus one should notice, as presented in the $(PD/PAZO)_4$-$(DAR/Nafion)_2$ structure, the diazonium of DAR not only interacted with the sulfonate groups of Nafion, but could also paired with carboxylate groups of PAZO. As a consequence, the interaction between the PDADMAC and PAZO was somewhat weakened, while the effect of DAR-related sealing was strengthened by the appearance of crosslinking between PAZO and adjacent DAR layers. Therefore, the UV-induced

red shift in complex capsules here was not as significant as that observed in the capsules composed of only PDADMAC/PAZO layers (Figure 5.4 in Chapter 5). In return, in the multilayer system of $(PDADMAC/PAZO)_4$-$(Nafion/DAR)_2$, the potential azobenzene molecular motion as J aggregates (together with possible *trans-cis* isomerization) occurred in the $(PDADMAC/PAZO)_4$ layers was not powerful enough to cause obvious phase separation or patch-like structures in macro-scale, which might be visualized as clear damage of shell integrity under SEM observation. Instead, the intrinsic chemical transition here primarily led to swollen microcapsules, with a lot of pores on the shell.

7.3 Macromolecule Encapsulation and Release Triggered By Continuous UV Light

Theoretically, 10 min of UV irradiation with an intensity of 55 mW/cm^2 can accomplish DAR-related photolysis reaction, which could convert the electrostatic interacted charges into covalent chemical bonds, as discussed in Chapter 6. This crosslinking within paired ionic groups provided adequate capability for molecule encapsulation; both small molecule RhB and macromolecule AF488-Dextran were studied. Here, efforts were devoted to encapsulate molecules in the complex capsules, in which the DAR/Nafion multilayers might provide potential sealing layers to achieve the goal (for experimental section see Section 3.3.7).

As the SEM images presented in Figure 7.1 and Figure 7.2, UV irradiation was found to have a significant effect on the morphology changes of complex capsules, exhibiting as a time-dependent swelling progress. In particular, no obvious capsule size increase or shell porosity change can be observed after the first 10 min of UV irradiation. Considering the DAR-related photolysis can be rapid completed within 10 minutes (as found in Chapter 6), thus the 10 min of UV irradiation was chosen here as a working duration to seal the complex capsules. Later, continuous UV treatment up to 7 hours was used to trigger possible release of encapsulated molecules.

In order to detect the feasibility, fluorescent polymers with different molecular weights, for example TRITC-Dextran (500 kDa) and AF488-Dextran (10 kDa), were used as cargo substances for this study. Briefly, the fabricated complex capsules were incubated in fluorescent polymer solutions for 2 hours with shaking. Then the mixture was

exposed to UV light (55 mW/cm^2) for 10 min. After that, the capsules were collected as washed for several times and observed under confocal laser scanning microscope.

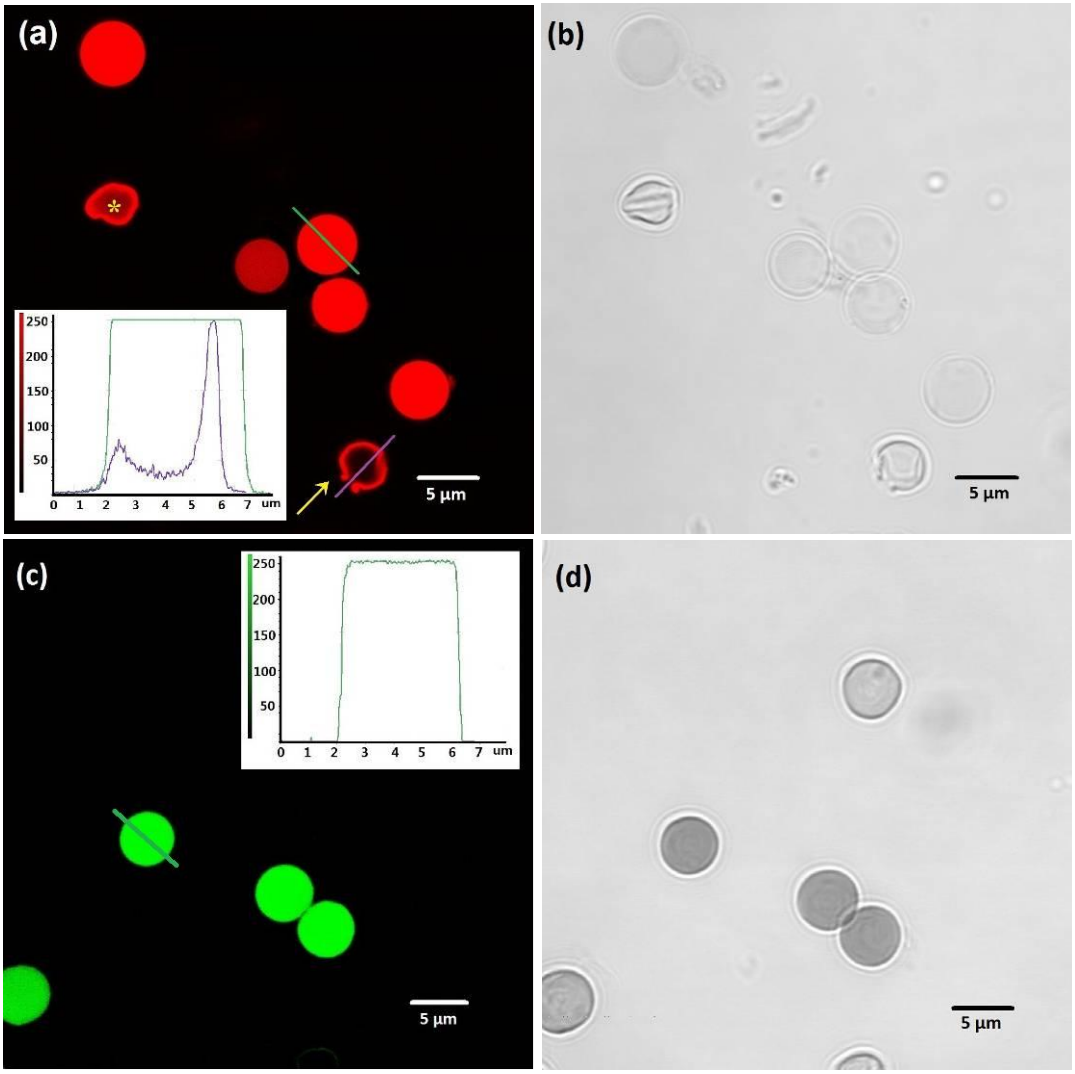

Figure 7.7 CLSM images of the (a) TRITC-Dextran and (b) AF 488-Dextran encapsulated complex capsules.

* Images b and d showed corresponding microcapsules in bright field. The symbol ↗ presented a broken capsule, the symbol * presented a capsule with defects on its shell.

As shown in Figure 7.7, bright images were observed, which demonstrated that 10 min of UV irradiation can crosslink the Nafion/DAR layers of complex micrcocapsules, and can successful retain the fluorescent polymers (both TRITC-Dextran and AF 488-Dextran) inside capsules. Very strong fluorescent signal intensity (more than 250 units) can be detected (Figure 7.7 a, c). Only a few broken capsule (symbol ↗) and defected capsule (symbol ∗) with hollow cavities can be found occasionally (Figure 7.7 a). It is

worth mentioning, in this work, the complex capsules were fabricated firstly, then incubated with fluorescent polymers. Thus it could be explained that the complex multilayer formations were permeable to these fluorescent polymers before UV treatment, even permeable for the polymers with high molecular weight of 500 kDa (TRITC-Dextran).

The UV triggered cargo release was also investigated in this work. Considering the long UV treatment duration would be applied, fluorescent polymers with high photostability could be used here. Typically, the Alexa Fluor-labeled dextran (AF488-Dextran) was used here, because it was reported that the sulfonic acid substituents of Alexa Fluor could increase water solubility and inhibit dye-dye interactions, which made the Alexa Fluor dyes much brighter and more stable than common dyes (e.g., Fluorescein and rhodamine), reducing quenching and bleaching[260]. As also it has been used in other research works for fluorescent visualization and encapsulation study [16, 108].

After first 10 min of UV irradiation, the complex capsules were sealed, and the AF488-Dextran was therefore retained inside, visualizing as bright fluorescent image in capsule cavities; very strong fluorescent signal intensity (more than 250 units) was detected (Figure 7.8 a). Further UV irradiation caused a gradually capsule swelling progress, which resulted in the release of encapsulated AF488-Dextran. After 7 hours of UV irradiation, only hollow capsules with limited amount of fluorescent signal can be observed (Figure 7.8 b). In the mean time, some of the swollen capsules were found collapsed in water (pointed out by the symbol ↖). Contrarily, the capsules without the PDADMAC/PAZO layers, $(DAR/Nafion)_4$ to be specifically, demonstrated a constant fluorescent signal intensity before and after 7 hours of UV irradiation (Figure 7.8 c, d). This result was attributed to the UV-induced sealing effect of the DAR/Nafion layers, which can predominantly seal the multilayer shells and not break complex capsules at relevant time-point.

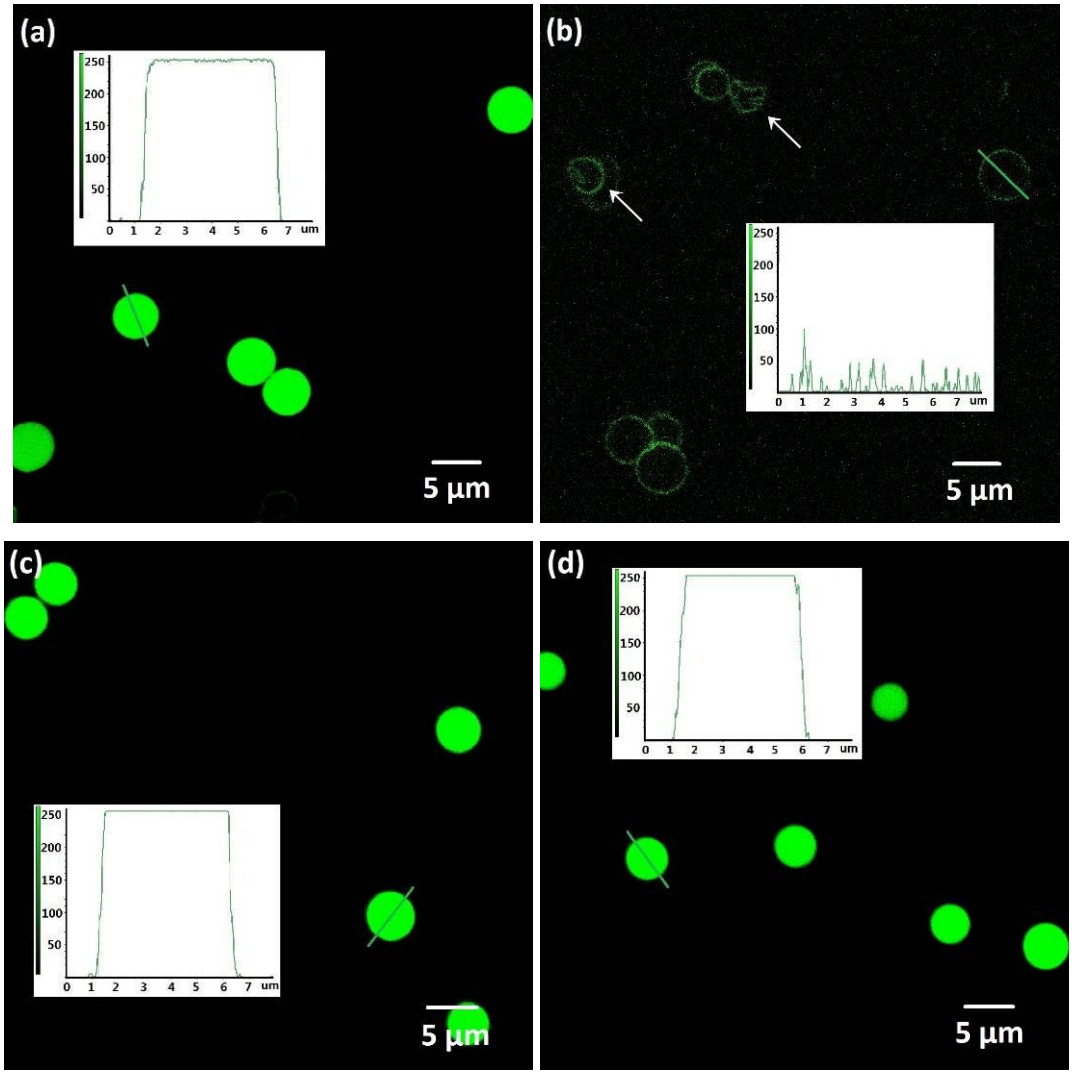

Figure 7.8 CLSM images of AF488-Dextran encapsulation in complex (top row) and $(DAR/Nafion)_4$ (bottom row) capsules right after shell sealing (a, c) and after 7 hours of additional UV irradiation (b, d). * The line scan insets showed relative fluorescent intensity in capsules; the symbol ↗ represented collapsed capsules in water.

The UV triggered release was then quantified. Briefly, capsules were re-dispersed in excess amount of fluorescent polymer AF488-Dextran solution (300 µg/ml, 2ml). After shell sealing triggered by the first 10 min of UV irradiation, capsules were sedimented, and washed several times with water to remove free fluorescent polymers. The resulting suspension was then split into two portions, one was treated with additional UV irradiation up to 7 hours, and the other part was kept in dark. The released mass of AF488-Dextran was then investigated, either released by UV irradiation or by diffusion (for experimental section see Section 3.3.8). In the meantime, an AF488-Dextran solution was also irradiated as the control group in this work, in order to monitor possible UV induced photobleaching effect. Its concentration was adjusted to be 20 µg/ml, or 8000

ng of AF488-Dextran in 400 μl to be specifically. This amount roughly matched the mass of encapsulated AF488-Dextran inside the complex capsules, determining from the results of preliminary experiments.

After set UV irradiation time, 400 μl of capsule-dye mixture was taken out, centrifuged, the supernatant was carefully collected for further measurements. The first portion of the sample containing 6.7×10^6 capsules without further UV irradiation was taken out, for quantification of the encapsulated fluorescent polymer amount. The mass of the encapsulated AF488-Dextran was found to be 7164 ng encapsulated inside 6.7×10^6 capsules, which meant that 1.07 pg of AF488-Dextran was encapsulated in one capsule. In the 7 hours of UV treatment duration, the control group (pure AF488-Dextran solution) showed very good stability against UV light, the detected amount was 7845 ng after 7 hours of UV treatment, demonstrating a roughly constant mass of AF488-Dextran at each set point (Figure 7.9, inset). Therefore, it could be believed that the influence of UV irradiation on photostability of AF488-Dextran solution with a concentration of 20 μg/ml was negligible, and the data of UV triggered AF488-Dextran release could be reliable in this duration.

With the increase of UV irradiation duration, the detected AF488-Dextran amount was found an increase tendency, as shown in Figure 7.9. For each sample containing 6.7×10^6 capsules, after 10 min of UV irradiation, 874 ng of released fluorescent polymers was found. Then extending UV irradiation to 30 min, 1243 ng was detected. When the UV irradiation duration reached 4 hours, more than 50 % of polymers (3908 ng) were released from capsules. After 7 hours, 5049 ng of the fluorescent polymers was found, which demonstrated a UV triggered release efficiency of 70.5%. On the other hand, for the capsules kept in dark, the fluorescent polymer release was found quite slow when compared with that of the irradiated ones. At the beginning, 667 ng of AF488-Dextran escaped from the porous shells. With increase the incubation duration, this natural release by diffusion showed a continuously increase tendency. However, there was only 2237 ng of AF488-Dextran detected after 7 hours of incubation, only 31% of the initial encapsulated amount.

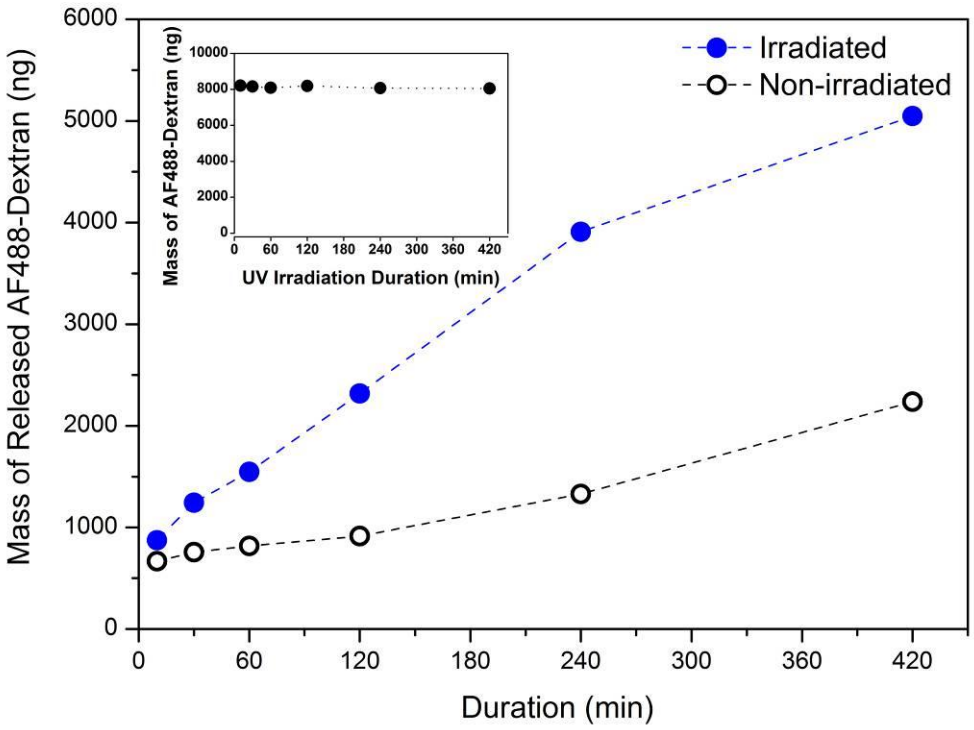

Figure 7.9 Mass of UV triggered AF 488-Dextran release from complex capsules.

* The inset showed the detected mass of AF488-Dextran of the control group after UV irradiation.

7.4 Small Molecule Encapsulation and Release Triggered By Continuous UV Light

As found in above section, the complex capsules showed the feasibility of encapsulation of macromolecules, and then the UV light triggered their release. In this section, the UV triggered small molecule release was also studied.

Typically, small fluorescent molecule Fluorescein with a molecular weight of 332 was used as an example here, as shown in Figure 7.10. Generally, after incubation with Fluorescein solution for 2 hours, the capsule-dye mixture was irradiated for 10 min to achieve molecule encapsulation through shell sealing, and then capsules were collected and washed for several times with water. Under confocal laser scanning microscopic observation, almost all the irradiated capsules were intact with an average size of 5 μm; and these capsules were filled with green dye molecules (average signal intensity of 100 units, Figure 7.10, 1st row). Exposure these dye-filled microcapsules to additional UV irradiation exhibited a gradual capsule swelling process, which was coincident with the SEM results. With the improved capsule swelling effect, the small molecules gradually

penetrated through the porous multilayers, showing as fluorescent signal intensity decrease inside these capsules. As one can see clearly, after 30 min of UV irradiation (Figure 7.10, 2nd row), part of the capsules became bigger with a diameter larger than 5.88 μm, and the encapsulated dye molecules were released, leaving an average dye intensity of ~ 50 units. When the UV irradiation time reached 1 hour (Figure 7.10, 3rd row), most of the dye molecules penetrated out, only very small amount attached on the shells, demonstrating as the same dye intensity inside and outside capsules (~ 10 units). Further extending the UV irradiation time only led to partial collapsed capsules in water (pointed out by the arrows) (Figure 7.10, 4th and 5th rows).

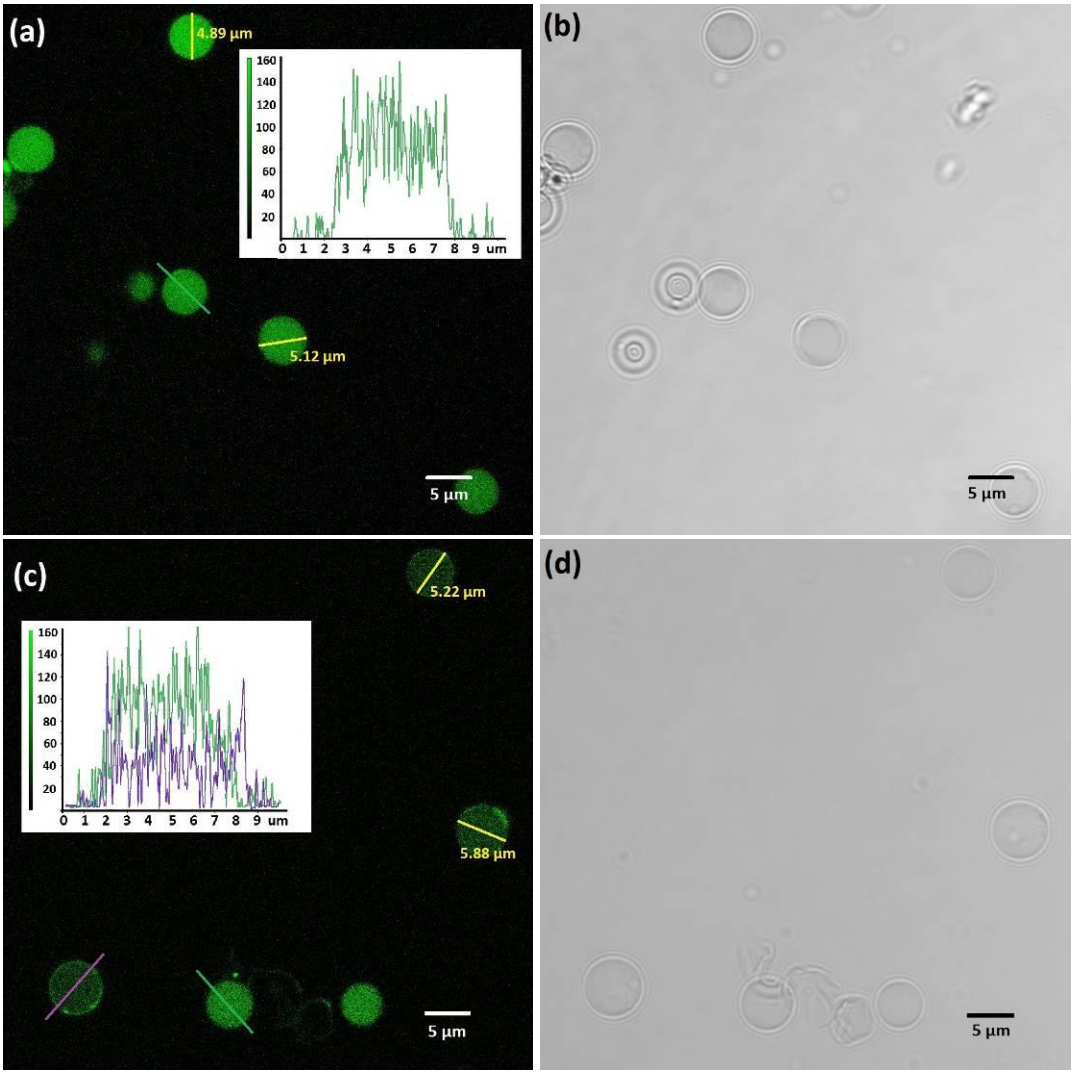

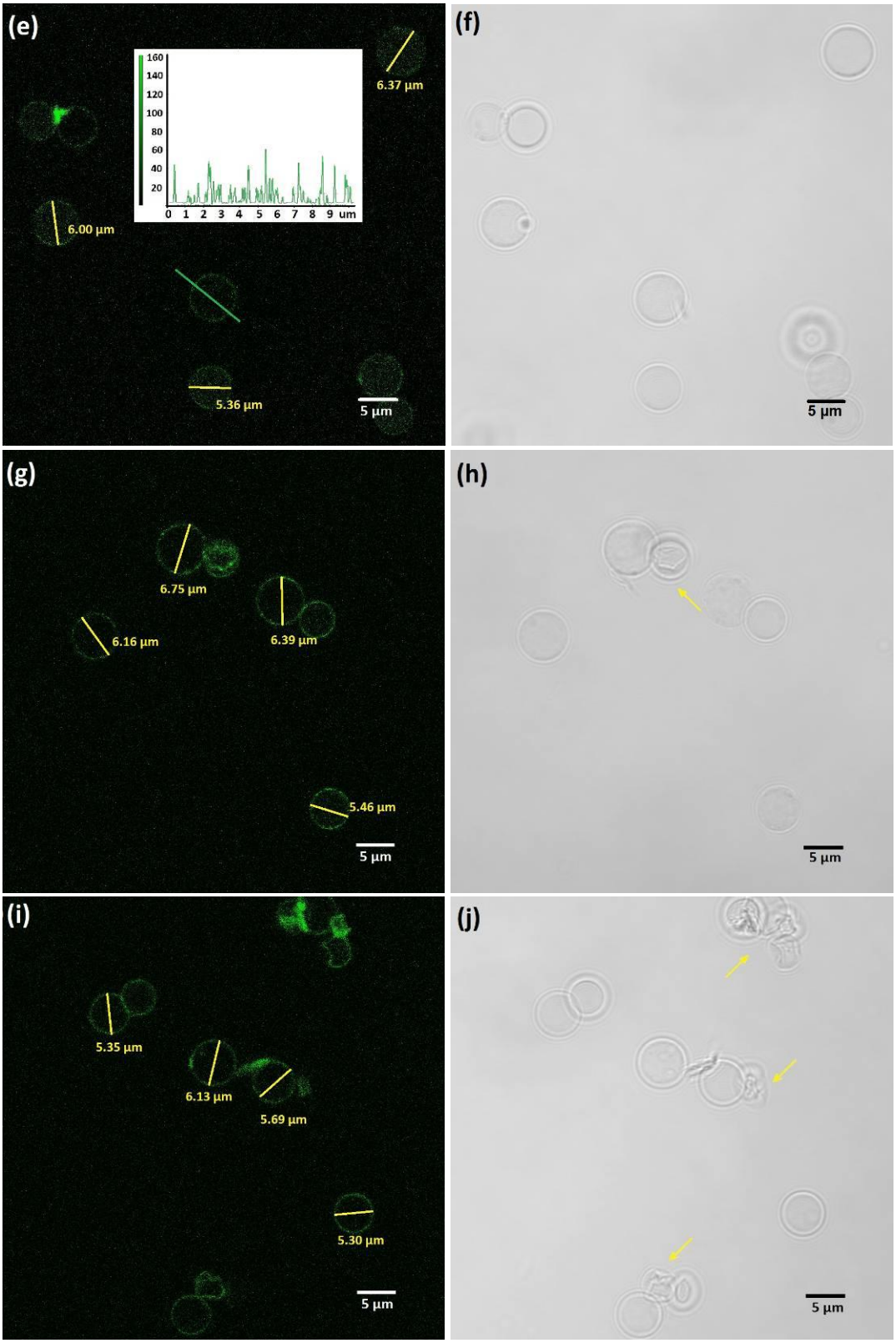

Figure 7.10 CLSM images of Flurescein encapsulated complex capsules (1st row), and triggered release under further UV irradiation of 30 min (2nd row), 1h (3rd row), 2 h (4th row) and 3h (5th row) in total. The right panel presented corresponding capsule images in bright field.

One should notice that the swollen capsules in water were found an average diameter less than 7 μm (Figure 7.10, 5th row), whereas some of the capsules observed under SEM became larger than 8 μm after 3 hours of UV irradiation (Figure 7.2). This difference could be interpreted as effect of surface tension caused by bonded water in/around multilayers. When the capsules became too large to keep their spherical structures, they were preferred to collapse in water.

Generally speaking, the encapsulated Fluorescein amount inside capsules was very small, as one can tell from the weak fluorescent images. On the other hand, upon exposure to such strong UV light for several hours, these fluorescent molecules would undergo a photobleaching progress, where a 20 % signal loss was found in similar UV irradiation experiment, though it was reported more stable than other fluorescent dyes[176]. In this work, the Fluorescein was used as a model molecule to judge the small molecule encapsulation ability of the complex capsules and possibility of UV triggered release. However, it might not be accurate to quantify the mass of released Fluorescein triggered by UV in this work, due to possible UV induced bleaching effect.

7.5 Conclusions

UV triggered dual-function complex microcapsules were fabricated in this chapter, for the purpose of integrating both encapsulation and release in one capsule system. Two different multilayer systems were introduced to build up these complex capsules, they were $(PDADMAC/PAZO)_4$ and $(DAR/Nafion)_2$. Exposure of these capsules to 10 min of UV irradiation (at 380 nm) led to sealing effect within DAR and adjacent Nafion or PAZO layers based *via* diazonium related photolysis, which facilitated cargo substance encapsulation. In this work, Fluorescein, and fluorescent polymers (AF488-Dextran and TRITC-Dextran) were used and small and macro- molecules for the encapsulation study, respectively. Later, exposure of these capsules to longer UV treatment duration (at 365 nm) caused an irreversible shell swelling-disruption progress, which was activated by the preferred J aggregations of azobenzene molecules in PDADMAC/PAZO multilayers, providing a way to release the encapsulated substances. Generally, this UV triggered release was investigated by the release of AF 488-Dextran and Fluorescein molecules. Promisingly, this complex capsule system containing two different functional multilayers would be very useful micro-container for various applications, for which

their encapsulation and controlled release could easily be trigged by continuous near-UV light. As shown in Scheme 7.2, schematic illustration of this UV triggered dual-functionalities of the complex capsule was given.

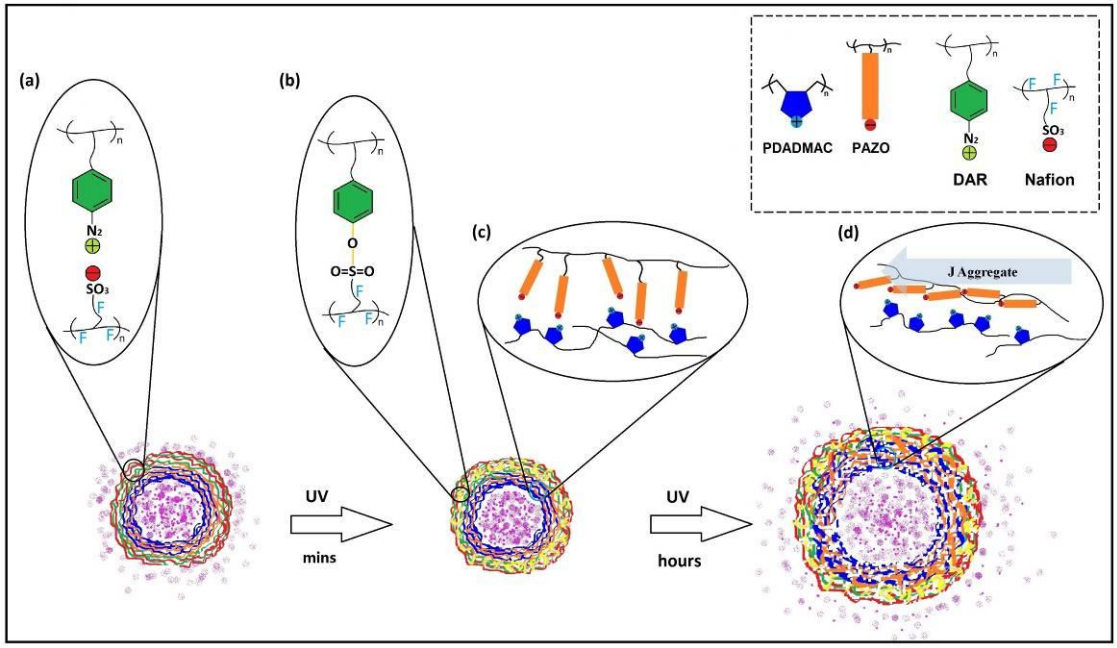

Scheme 7.2 Schematic illustration of UV induced complex capsule shell sealing and further swelling.

8. Conclusions and Future Work

8.1 General Conclusions

In this thesis, four different types of UV responsive polyelectrolyte microcapsule systems were proposed. These capsules containing different functional chemical groups were fabricated by using layer-by-layer assembly technique. Their potential applications for encapsulation and release were investigated, which were achieved by applying of externally activation from UV light with different wavelengths. Generally, all the UV exposure experiments of these microcapsules were performed in water with cooling bath directly. The corresponding changes in capsule morphology, shell stability and permeability, which were originated from underlying chemical changes of related functional groups, were investigated. The aim of these research works mainly devoted to the potential applications in special areas where the abundant UV light would be available.

In chapter 4, benzophenone groups with highly efficient and remarkable site specified molecule covalent modification ability were introduced to build up the UV responsive microcapsules $(PAH/PMA\text{-}BP)_4$. Upon exposure to UV light at 275 nm, the generation of new C–C bonds originated from initial bezophenone groups and adjacent un-reacted C–H bonds led to crosslinking within the PAH/PMA-BP multilayers, shrinking the capsule size up to 30% in diameter. The shrinkage adjusted the capsule permeability, providing a novel way to encapsulate fluorescence-labeled dextran molecules without heating. Meanwhile, crosslinking within the multilayer shells based on hydrogen abstraction *via* excited benzophenone units showed a reliable and swift approach to tighten and stabilize the capsule shell without losing the pH-responsive properties of these weak polyelectrolyte capsules.

In chapter 5, azobenzene groups which can undergo a UV induced photoisomerization were used to build up microcapsules with PDADMAC. With the combination of rigid PDADMAC polymer bearing negative charges along its molecular chain, the most commonly azobenzene molecular conformation change in plane was somewhat restricted; whereas the UV triggered self-organization of azobenzene molecules in the form of J aggregate was preferred. This re-orientation of azobenzene within capsule

multilayer formations led to great damage of capsule integrity, which caused capsules swelling and further shell disruption. Upon 2 hours of UV irradiation at 365 nm, almost all the capsules were torn into pieces, leaving capsule debris and needle-like formations. Moreover, this UV induced microcapsule disruption process based on molecule re-alignment was proved to be irreversible, even when the capsules were exposed to the visible light. Strategically, this UV induced capsule disruption offered a novel way to controlled release encapsulated cargo substances. The UV-dosage dependent release behaviours of model substances (protein and limonene) were investigated.

In chapter 6, a good active leaving group diazonium was substituted in diazo-resin (DAR), and used to build up microcapsules with perfluorosulfonic Nafion and charge reversed DAR, $(Nafion/DAR)_4$ and DAR_8 to be specifically. Upon exposure to a 380 nm UV light, the diazonium group was activated to form phenyl cation and then be substituted by sulfonate groups of paired Nafion or charge reversed DAR, converting ionic interactions in to covalent bonding in situ. This photolysis reaction offered an externally controlled method to seal the multilayer capsules. The encapsulation of macro- and small molecules (AF488-Dextran and RhB) were investigated, illustrating good retention of these molecules inside capsules for long time. DAR-related capsules were found great potential as unique micro-containers, benefiting from generation of covalent bonds and remained hydrophobic backbones. Specifically, the $(Nafion/DAR)_4$ microcapsules showed a better small molecule encapsulation ability than the DAR_8, benefiting from the existence of Nafion layers.

In chapter 7, a complex microcapsule $(PDADMAC/PAZO)_4$-$(DAR/Nafion)_2$ system containing both of the two chemical groups were fabricated, which was inspired from research works of microcapsules containing azobenzene and diazonium groups,. Dual-function of these capsules was demonstrated as a shell sealing and further swelling progress simply triggered by the same UV source. Theoretically, the shell sealing was attributed to crosslinking within DAR and adjacent Nafion or PAZO layers *via* DAR-related photolysis; the irreversible shell swelling was due to the preferred aggregations of azobenzene molecules in PDADMAC/PAZO multilayers. Such dual-functionalization of the complex capsules integrated cargo substance encapsulation and controlled release in one system, triggering by externally UV light. Fluorescein and

fluorescent labeled dextran (AF488-Dextran) were studied as the small and macro-molecules for the encapsulation and release investigations.

In summary, four UV responsive multilayer microcapsule systems with unique functional groups and architectures were prepared, in order to explore new UV light responsive vehicles for the purpose of cargo encapsulation and release. Apart from capsule fabrication process and UV induced corresponding functionalities such as small/macro- molecule encapsulation and/or triggered release, the underlying principles that attributed to the observed phenomena were also investigated. Promisingly, these strategies developed in this thesis could be applied as typical approaches for fabrication of light addressable multilayer systems for intelligent encapsulation and release based solely on optical stimuli. Hopefully, these UV-responsive capsules could offer a series of micro- vesicles or containers for the development of new optically active systems, especially the UV light active systems, to which abundant light (e.g. sunlight) could be introduced. Predicted applications could potentially be found use in various fields ranging from drug delivery, micro-reactor and photocatalysis to environmental science, material surface science, agricultural and cosmetic areas, benefiting from one or more light induced functionalities of such optically active systems. This thesis contributes to existing knowledge of photo-active LbL capsules by providing the findings:

1) Weak polyelectrolyte $(PAH/PMA\text{-}BP)_4$ microcapsules were crosslinked by 275 nm UV light through benzophenone-related hydrogen-abstraction and recombination, resulting in stabilized shells and decreased shell permeability without consumption of ionic charges.

2) $(PDADMAC/PAZO)_4$ microcapsules were gradually ruptured by ~366 nm UV light via J-styled aggregation of azobenzene molecules in multilayers.

3) $(Nafion/DAR)_4$ and DAR_8 microcapsules were sealed by ~380 nm UV light though diazonium-related photolysis, leading to good preservation ability of small molecules.

4) $(PDADMAC/PAZO)_4$-$(DAR/Nafion)_2$ complex microcapsules demonstrated rapid shell sealing and further gradually shell disruption upon exposure to UV light with different wavelengths.

8.2 Future Work

This thesis has initiated new UV responsive capsule systems for cargo substance encapsulation and/or release. However, there are still some challenges left to be overcome for improvement of these systems. Moreover, hurdles remain in the smooth transition of these experimental works into practical uses.

1) pH stimuli-responsive capsules. One possible application of these pH sensitive capsules $(PAH/PMA\text{-}BP)_4$ could be carriers for *in vivo* delivery. In order to truly evaluate the use of pH sensitive capsules proposed in this thesis (chapter 4), careful study on the capsule stability influenced by normal pH conditions (e.g. pH= 4 ~ 9) that close to biological media (body fluid, tissue and organ) should be made. Moreover, cargo substance release controlled by varied pH conditions should be investigated, in order to understand the pH-dependent drug release kinetics from these polyelectrolyte capsules.

2) Capsules for small molecule encapsulation. The $(Nafion/DAR)_4$, DAR_8 capsule systems (chapter 6) and complex capsules $(PDADMAC/PAZO)_4\text{-}(DAR/Nafion)_2$ (chapter 7) demonstrated good capability to encapsulate and release small molecules upon UV irradiation. However, due to the possible quenching and photo-bleaching effect of RhB and Flurescein molecules, long-term study on small molecule encapsulation/release in these capsules was restricted. Employment of other photo-stable substances (e.g. quantum dots) for long-term UV triggered encapsulation/release should be performed in future work. In addition, long-term storage of these capsules containing small molecule cargos would benefit their practical use. Strategies such as freeze-drying or filtration might be used to separate these cargo-loaded capsules from water, and hence to avoid cargo diffusion.

3) Successive encapsulation and release by multilayer capsules. In chapter 7, complex capsules $(PDADMAC/PAZO)_4\text{-}(DAR/Nafion)_2$ were able to achieve UV triggered sealing and further disruption. Thus more details of the influencing factors (e.g. UV-dosage, capsule architecture) on the underlying UV triggered capsule mechanical change as well as cargo encapsulation and release need to be investigated. Proper

balance control over the ratio of azobenzene/diazonium groups in capsule shells should be carefully studied.

4) UV triggered release from capsules. Considering the cargo release from PDADMAC/PAZO and complex capsule systems was triggered by UV light, thus possible application of these capsules might be stressed on sunlight controlled release. Future research emphasis should be focused on industrial areas (e.g. sunscreen and surface protecting), where the release and activation of encapsulated cargo substances could be adjusted by sunlight.

5) Capsules for *in vivo* use. One of the possible contributions of these capsules is their use as carriers for small molecular drugs. The release might be performed by diffusion from sealed capsules (e.g. Nafion/DAR cpasule) or internal stimuli-triggered capsule opening in biological media (e.g. pH). For possible *in vivo* use, carful considerations should be given to the design of the capsule carriers. Corresponding parameters such as capsule hydrodynamic size, constituents, outmost layers (coatings) which would have effect on their *in vivo* transportation, biostability and biocompatibility should be addressed. Furthermore, other functional groups or components could be integrated on capsule shells, in order to realize multi-functionalities, which might benefit potential *in vivo* applications such as targeted delivery, sensing, imaging and therapy.

References

1. Boisselier E, Astruc D: **Gold nanoparticles in nanomedicine: preparations, imaging, diagnostics, therapies and toxicity**. *Chemical Society Reviews* 2009, **38**(6):1759-1782.
2. Kataoka K, Harada A, Nagasaki Y: **Block copolymer micelles for drug delivery: design, characterization and biological significance**. *Advanced drug delivery reviews* 2001, **47**(1):113-131.
3. Samad A, Sultana Y, Aqil M: **Liposomal drug delivery systems: an update review**. *Current drug delivery* 2007, **4**(4):297-305.
4. Crampton HL, Simanek EE: **Dendrimers as drug delivery vehicles: non-covalent interactions of bioactive compounds with dendrimers**. *Polymer international* 2007, **56**(4):489-496.
5. Loretta L, Rivera-Gil P, Abbasi AZ, Ochs M, Ganas C, Zins I, Sönnichsen C, Parak WJ: **LbL multilayer capsules: recent progress and future outlook for their use in life sciences**. *Nanoscale* 2010, **2**(4):458-467.
6. Decher G: **Fuzzy nanoassemblies: toward layered polymeric multicomposites**. *Science* 1997, **277**(5330):1232-1237.
7. Sukhishvili SA: **Responsive polymer films and capsules via layer-by-layer assembly**. *Current opinion in colloid & interface science* 2005, **10**(1):37-44.
8. Lensen D, Vriezema DM, van Hest J: **Polymeric microcapsules for synthetic applications**. *Macromolecular bioscience* 2008, **8**(11):991-1005.
9. Sukhorukov GB, Donath E, Davis S, Lichtenfeld H, Caruso F, Popov VI, Möhwald H: **Stepwise polyelectrolyte assembly on particle surfaces: a novel approach to colloid design**. *Polymers for Advanced Technologies* 1998, **9**(10-11):759-767.
10. Peyratout CS, Dähne L: **Tailor-Made Polyelectrolyte Microcapsules: From Multilayers to Smart Containers**. *Angewandte Chemie International Edition* 2004, **43**(29):3762-3783.
11. Johnston APR, Cortez C, Angelatos AS, Caruso F: **Layer-by-layer engineered capsules and their applications**. *Current opinion in colloid & interface science* 2006, **11**(4):203-209.
12. Kotov NA: **Layer-by-layer self-assembly: The contribution of hydrophobic interactions**. *Nanostructured Materials* 1999, **12**(5-8):789-796.
13. Ariga K, Hill JP, Ji Q: **Layer-by-layer assembly as a versatile bottom-up nanofabrication technique for exploratory research and realistic application**. *Phys Chem Chem Phys* 2007, **9**(19):2319-2340.
14. Delcea M, Möhwald H, Skirtach AG: **Stimuli-responsive LbL capsules and nanoshells for drug delivery**. *Advanced Drug Delivery Reviews* 2011.
15. Li MH, Keller P: **Stimuli-responsive polymer vesicles**. *Soft Matter* 2009, **5**(5):927-937.
16. Bédard M, Skirtach AG, Sukhorukov GB: **Optically driven encapsulation using novel polymeric hollow shells containing an azobenzene polymer**. *Macromolecular rapid communications* 2007, **28**(15):1517-1521.
17. Yuan X, Fischer K, Schärtl W: **Photocleavable microcapsules built from photoreactive nanospheres**. *Langmuir* 2005, **21**(20):9374-9380.
18. Skirtach AG, Antipov AA, Shchukin DG, Sukhorukov GB: **Remote activation of capsules containing Ag nanoparticles and IR dye by laser light**. *Langmuir* 2004, **20**(17):6988-6992.
19. Bédard MF, Braun D, Sukhorukov GB, Skirtach AG: **Toward self-assembly of nanoparticles on polymeric microshells: near-IR release and permeability**. *ACS nano* 2008, **2**(9):1807-1816.
20. Volodkin DV, Larionova NI, Sukhorukov GB: **Protein encapsulation via porous CaCO3 microparticles templating**. *Biomacromolecules* 2004, **5**(5):1962-1972.

21. Shchukin DG, Sukhorukov GB: **Selective YF3 nanoparticle formation in polyelectrolyte capsules as microcontainers for yttrium recovery from aqueous solutions**. *Langmuir* 2003, **19**(10):4427-4431.
22. Zelikin AN, Becker AL, Johnston AP, Wark KL, Turatti F, Caruso F: **A general approach for DNA encapsulation in degradable polymer microcapsules**. *ACS nano* 2007, **1**(1):63-69.
23. Shchukin DG, Sukhorukov GB: **Nanoparticle synthesis in engineered organic nanoscale reactors**. *Advanced Materials* 2004, **16**(8):671-682.
24. Caruso F, Trau D, Möhwald H, Renneberg R: **Enzyme encapsulation in layer-by-layer engineered polymer multilayer capsules**. *Langmuir* 2000, **16**(4):1485-1488.
25. Sukhorukov GB, Brumen M, Donath E, Möhwald H: **Hollow polyelectrolyte shells: exclusion of polymers and donnan equilibrium**. *The Journal of Physical Chemistry B* 1999, **103**(31):6434-6440.
26. Köhler K, Sukhorukov GB: **Heat treatment of polyelectrolyte multilayer capsules: a versatile method for encapsulation**. *Advanced Functional Materials* 2007, **17**(13):2053-2061.
27. Kozlovskaya V, Kharlampieva E, Mansfield ML, Sukhishvili SA: **Poly (methacrylic acid) hydrogel films and capsules: Response to pH and ionic strength, and encapsulation of macromolecules**. *Chemistry of Materials* 2006, **18**(2):328-336.
28. Skirtach AG, Yashchenok AM, Möhwald H: **Encapsulation, release and applications of LbL polyelectrolyte multilayer capsules**. *Chem Commun* 2011, **47**(48):12736-12746.
29. Delcea M, Möhwald H, Skirtach AG: **Stimuli-responsive LbL capsules and nanoshells for drug delivery**. *Advanced Drug Delivery Reviews* 2011, **63**(9):730-747.
30. De Geest BG, Sanders NN, Sukhorukov GB, Demeester J, De Smedt SC: **Release mechanisms for polyelectrolyte capsules**. *Chemical Society Reviews* 2007, **36**(4):636-649.
31. Burke SE, Barrett CJ: **Controlling the physicochemical properties of weak polyelectrolyte multilayer films through acid/base equilibria**. *Pure and applied chemistry* 2004, **76**(7):1387-1398.
32. Mauser T, Déjugnat C, Sukhorukov GB: **Reversible pH-Dependent Properties of Multilayer Microcapsules Made of Weak Polyelectrolytes**. *Macromolecular rapid communications* 2004, **25**(20):1781-1785.
33. Mauser T, Déjugnat C, Möhwald H, Sukhorukov GB: **Microcapsules made of weak polyelectrolytes: templating and stimuli-responsive properties**. *Langmuir* 2006, **22**(13):5888-5893.
34. Klitzing R: **Internal structure of polyelectrolyte multilayer assemblies**. *Physical Chemistry Chemical Physics* 2006, **8**(43):5012-5033.
35. Muller AHE, Yan D, Wulkow M: **Molecular parameters of hyperbranched polymers made by self-condensing vinyl polymerization. 1. Molecular weight distribution**. *Macromolecules* 1997, **30**(23):7015-7023.
36. Tsuchida E, Osada Y, Sanada K: **Interaction of poly (styrene sulfonate) with polycations carrying charges in the chain backbone**. *Journal of Polymer Science Part A-1: Polymer Chemistry* 1972, **10**(11):3397-3404.
37. Tsuchida E, Osada Y, Ohno H: **Formation of interpolymer complexes**. *Journal of Macromolecular Science, Part B: Physics* 1980, **17**(4):683-714.
38. Kabanov VA: **Interpolymer complexes as new materials for biomedical applications**. In*: 1991*: Wiley Online Library; 1991: 425-426.
39. Dautzenberg H: **Polyelectrolyte complex formation in highly aggregating systems. 1. Effect of salt: polyelectrolyte complex formation in the presence of NaCl**. *Macromolecules* 1997, **30**(25):7810-7815.
40. Dautzenberg H, Karibyants N: **Polyelectrolyte complex formation in highly aggregating systems. Effect of salt: response to subsequent addition of NaCl**. *Macromolecular Chemistry and Physics* 1999, **200**(1):118-125.

41. Zhai L, Cebeci FC, Cohen RE, Rubner MF: **Stable superhydrophobic coatings from polyelectrolyte multilayers**. *Nano letters* 2004, **4**(7):1349-1353.
42. Shi X, Shen M, Möhwald H: **Polyelectrolyte multilayer nanoreactors toward the synthesis of diverse nanostructured materials**. *Progress in polymer science* 2004, **29**(10):987-1019.
43. Rojas OJ, Ernstsson M, Neuman RD, Claesson PM: **Effect of polyelectrolyte charge density on the adsorption and desorption behavior on mica**. *Langmuir* 2002, **18**(5):1604-1612.
44. Schoeler B, Kumaraswamy G, Caruso F: **Investigation of the influence of polyelectrolyte charge density on the growth of multilayer thin films prepared by the layer-by-layer technique**. *Macromolecules* 2002, **35**(3):889-897.
45. Salomäki M, Tervasmäki P, Areva S, Kankare J: **The Hofmeister anion effect and the growth of polyelectrolyte multilayers**. *Langmuir* 2004, **20**(9):3679-3683.
46. Poptoshev E, Schoeler B, Caruso F: **Influence of solvent quality on the growth of polyelectrolyte multilayers**. *Langmuir* 2004, **20**(3):829-834.
47. McAloney RA, Sinyor M, Dudnik V, Goh MC: **Atomic force microscopy studies of salt effects on polyelectrolyte multilayer film morphology**. *Langmuir* 2001, **17**(21):6655-6663.
48. Picart C, Mutterer J, Richert L, Luo Y, Prestwich G, Schaaf P, Voegel JC, Lavalle P: **Molecular basis for the explanation of the exponential growth of polyelectrolyte multilayers**. *Proceedings of the National Academy of Sciences* 2002, **99**(20):12531.
49. Lavalle P, Gergely C, Cuisinier F, Decher G, Schaaf P, Voegel J, Picart C: **Comparison of the structure of polyelectrolyte multilayer films exhibiting a linear and an exponential growth regime: An in situ atomic force microscopy study**. *Macromolecules* 2002, **35**(11):4458-4465.
50. Lavalle P, Vivet V, Jessel N, Decher G, Voegel JC, Mesini PJ, Schaaf P: **Direct evidence for vertical diffusion and exchange processes of polyanions and polycations in polyelectrolyte multilayer films**. *Macromolecules* 2004, **37**(3):1159-1162.
51. Porcel C, Lavalle P, Decher G, Senger B, Voegel J-C, Schaaf P: **Influence of the polyelectrolyte molecular weight on exponentially growing multilayer films in the linear regime**. *Langmuir* 2007, **23**(4):1898-1904.
52. Porcel C, Lavalle P, Ball V, Decher G, Senger B, Voegel J-C, Schaaf P: **From exponential to linear growth in polyelectrolyte multilayers**. *Langmuir* 2006, **22**(9):4376-4383.
53. Laschewsky A, Mayer B, Wischerhoff E, Arys X, Bertrand P, Delcorte A, Jonas A: **A new route to thin polymeric, non-centrosymmetric coatings**. *Thin Solid Films* 1996, **284**:334-337.
54. Koetse M, Laschewsky A, Mayer B, Rolland O, Wischerhoff E: **Ultrathin coatings by multiple polyelectrolyte adsorption/surface activation (CoMPAS)**. *Macromolecules* 1998, **31**(26):9316-9327.
55. Laschewsky A, Mayer B, Wischerhoff E, Arys X, Jonas A, Kauranen M, Persoons A: **A new technique for assembling thin, defined multilayers**. *Angewandte Chemie International Edition in English* 1997, **36**(24):2788-2791.
56. Zhang Y, Cao W: **Fabrication of an ESA multilayer film from a diazo resin by direct surface charge reversal**. *Macromolecular rapid communications* 2001, **22**(11):842-845.
57. Donath E, Sukhorukov GB, Caruso F, Davis SA, Möhwald H: **Novel hollow polymer shells by colloid-templated assembly of polyelectrolytes**. *Angewandte Chemie International Edition* 1998, **37**(16):2201-2205.
58. Antipov AA, Sukhorukov GB: **Polyelectrolyte multilayer capsules as vehicles with tunable permeability**. *Advances in colloid and interface science* 2004, **111**(1-2):49-61.
59. Gil PR, del Mercato LL, del_Pino P, Muñoz_Javier A, Parak WJ: **Nanoparticle-modified polyelectrolyte capsules**. *Nano Today* 2008, **3**(3-4):12-21.
60. Vinogradova OI: **Mechanical properties of polyelectrolyte multilayer microcapsules**. *Journal of Physics: Condensed Matter* 2004, **16**(32):R1105.

61. Gao C, Moya S, Lichtenfeld H, Casoli A, Fiedler H, Donath E, Möhwald H: **The decomposition process of melamine formaldehyde cores: the key step in the fabrication of ultrathin polyelectrolyte multilayer capsules**. *Macromolecular Materials and Engineering* 2001, **286**(6):355-361.
62. Sukhorukov GB, Antipov AA, Voigt A, Donath E, Möhwald H: **pH-Controlled Macromolecule Encapsulation in and Release from Polyelectrolyte Multilayer Nanocapsules**. *Macromolecular rapid communications* 2001, **22**(1):44-46.
63. Gao C, Donath E, Möhwald H, Shen J: **Spontaneous Deposition of Water-Soluble Substances into Microcapsules: Phenomenon, Mechanism, and Application**. *Angewandte Chemie* 2002, **114**(20):3943-3947.
64. Park MK, Xia C, Advincula RC, Schütz P, Caruso F: **Cross-linked, luminescent spherical colloidal and hollow-shell particles**. *Langmuir* 2001, **17**(24):7670-7674.
65. Shenoy DB, Antipov AA, Sukhorukov GB, Möhwald H: **Layer-by-layer engineering of biocompatible, decomposable core-shell structures**. *Biomacromolecules* 2003, **4**(2):265-272.
66. Volodkin DV, Petrov AI, Prevot M, Sukhorukov GB: **Matrix polyelectrolyte microcapsules: new system for macromolecule encapsulation**. *Langmuir* 2004, **20**(8):3398-3406.
67. Antipov AA, Sukhorukov GB, Leporatti S, Radtchenko IL, Donath E, Möhwald H: **Polyelectrolyte multilayer capsule permeability control**. *Colloids and Surfaces A: Physicochemical and Engineering Aspects* 2002, **198**:535-541.
68. Wei Q, Ai H, Gu Z: **Matrix Polyelectrolyte Capsules Based on Polysaccharide/MnCO3 Hybrid Microparticle Templates**. *Colloids and Surfaces B: Biointerfaces* 2010.
69. De Temmerman ML, Demeester J, De Vos F, De Smedt SC: **Encapsulation Performance of Layer-by-Layer Microcapsules for Proteins**. *Biomacromolecules* 2011.
70. Shchukin DG, Patel AA, Sukhorukov GB, Lvov YM: **Nanoassembly of biodegradable microcapsules for DNA encasing**. *Journal of the American Chemical Society* 2004, **126**(11):3374-3375.
71. Schneider G, Decher G: **From functional core/shell nanoparticles prepared via layer-by-layer deposition to empty nanospheres**. *Nano letters* 2004, **4**(10):1833-1839.
72. Diaspro A, Silvano D, Krol S, Cavalleri O, Gliozzi A: **Single living cell encapsulation in nano-organized polyelectrolyte shells**. *Langmuir* 2002, **18**(13):5047-5050.
73. Moya S, Georgieva R, Bäumler H, Richter W, Donath E: **Composite lipid polyelectrolyte capsules templated on red blood cells: fabrication and structural characterisation**. *Medical and Biological Engineering and Computing* 2003, **41**(4):504-508.
74. Krol S, Del Guerra S, Grupillo M, Diaspro A, Gliozzi A, Marchetti P: **Multilayer nanoencapsulation. New approach for immune protection of human pancreatic islets**. *Nano letters* 2006, **6**(9):1933-1939.
75. Lomova MV, Sukhorukov GB, Antipina MN: **Antioxidant coating of micronsize droplets for prevention of lipid peroxidation in oil-in-water emulsion**. *ACS applied materials & interfaces* 2010, **2**(12):3669-3676.
76. Shchukin DG, Köhler K, Möhwald H, Sukhorukov GB: **Gas-Filled Polyelectrolyte Capsules**. *Angewandte Chemie International Edition* 2005, **44**(21):3310-3314.
77. Leporatti S, Gao C, Voigt A, Donath E, Möhwald H: **Shrinking of ultrathin polyelectrolyte multilayer capsules upon annealing: a confocal laser scanning microscopy and scanning force microscopy study**. *The European Physical Journal E: Soft Matter and Biological Physics* 2001, **5**(1):13-20.
78. McGrath TE, Beveridge AC, Diebold GJ: **Laser-Induced "Regeneration" of Colloidal Particles: The Effects of Thermal Inertia on the Chemical Reactivity of Laser-Heated Particles**. *Angewandte Chemie International Edition* 1999, **38**(22):3353-3356.
79. Estrela-Lopis I, Leporatti S, Moya S, Brandt A, Donath E, Möhwald H: **SANS studies of polyelectrolyte multilayers on colloidal templates**. *Langmuir* 2002, **18**(21):7861-7866.

80. Köhler K, Shchukin DG, Sukhorukov GB, Möhwald H: **Drastic morphological modification of polyelectrolyte microcapsules induced by high temperature**. *Macromolecules* 2004, **37**(25):9546-9550.
81. Kreft O, Javier AM, Sukhorukov GB, Parak WJ: **Polymer microcapsules as mobile local pH-sensors**. *J Mater Chem* 2007, **17**(42):4471-4476.
82. Itoh Y, Matsusaki M, Kida T, Akashi M: **Locally controlled release of basic fibroblast growth factor from multilayered capsules**. *Biomacromolecules* 2008, **9**(8):2202-2206.
83. De Geest BG, Vandenbroucke RE, Guenther AM, Sukhorukov GB, Hennink WE, Sanders NN, Demeester J, De Smedt SC: **Intracellularly degradable polyelectrolyte microcapsules**. *Advanced Materials* 2006, **18**(8):1005-1009.
84. Caruso F, Caruso RA, Möhwald H: **Production of hollow microspheres from nanostructured composite particles**. *Chemistry of Materials* 1999, **11**(11):3309-3314.
85. Caruso RA, Susha A, Caruso F: **Multilayered titania, silica, and laponite nanoparticle coatings on polystyrene colloidal templates and resulting inorganic hollow spheres**. *Chemistry of Materials* 2001, **13**(2):400-409.
86. Shchukin DG, Sukhorukov GB, Möhwald H: **Smart inorganic/organic nanocomposite hollow microcapsules**. *Angewandte Chemie International Edition* 2003, **42**(37):4472-4475.
87. Caruso F, Susha AS, Giersig M, Möhwald H: **Magnetic core–shell particles: Preparation of magnetite multilayers on polymer latex microspheres**. *Advanced Materials* 1999, **11**(11):950-953.
88. Angelatos AS, Radt B, Caruso F: **Light-responsive polyelectrolyte/gold nanoparticle microcapsules**. *The Journal of Physical Chemistry B* 2005, **109**(7):3071-3076.
89. Lu Z, Prouty MD, Guo Z, Golub VO, Kumar CSSR, Lvov YM: **Magnetic switch of permeability for polyelectrolyte microcapsules embedded with Co@ Au nanoparticles**. *Langmuir* 2005, **21**(5):2042-2050.
90. Sukhorukov GB, Volodkin DV, Günther AM, Petrov AI, Shenoy DB, Möhwald H: **Porous calcium carbonate microparticles as templates for encapsulation of bioactive compounds**. *J Mater Chem* 2004, **14**(14):2073-2081.
91. Pavlov AM, Saez V, Cobley A, Graves J, Sukhorukov GB, Mason TJ: **Controlled protein release from microcapsules with composite shells using high frequency ultrasound—potential for in vivo medical use**. *Soft Matter* 2011, **7**(9):4341-4347.
92. Anandhakumar S, Nagaraja V, Raichur AM: **Reversible polyelectrolyte capsules as carriers for protein delivery**. *Colloids and Surfaces B: Biointerfaces* 2010, **78**(2):266-274.
93. Lvov Y, Antipov AA, Mamedov A, Möhwald H, Sukhorukov GB: **Urease encapsulation in nanoorganized microshells**. *Nano letters* 2001, **1**(3):125-128.
94. Kreft O, Georgieva R, Bäumler H, Steup M, Müller-Röber B, Sukhorukov GB, Möhwald H: **Red blood cell templated polyelectrolyte capsules: a novel vehicle for the stable encapsulation of DNA and proteins**. *Macromolecular rapid communications* 2006, **27**(6):435-440.
95. De Cock LJ, De Koker S, De Geest BG, Grooten J, Vervaet C, Remon JP, Sukhorukov GB, Antipina MN: **Polymeric multilayer capsules in drug delivery**. *Angewandte Chemie International Edition* 2010, **49**(39):6954-6973.
96. Dähne L, Leporatti S, Donath E, Möhwald H: **Fabrication of micro reaction cages with tailored properties**. *Journal of the American Chemical Society* 2001, **123**(23):5431-5436.
97. Sukhorukov G, Dähne L, Hartmann J, Donath E, Möhwald H: **Controlled precipitation of dyes into hollow polyelectrolyte capsules based on colloids and biocolloids**. *Advanced Materials* 1999, **12**(2):112-115.
98. Köhler K, Shchukin DG, Möhwald H, Sukhorukov GB: **Thermal behavior of polyelectrolyte multilayer microcapsules. 1. The effect of odd and even layer number**. *The Journal of Physical Chemistry B* 2005, **109**(39):18250-18259.

99. Köhler K, Möhwald H, Sukhorukov GB: **Thermal behavior of polyelectrolyte multilayer microcapsules: 2. Insight into molecular mechanisms for the PDADMAC/PSS system**. *The Journal of Physical Chemistry B* 2006, **110**(47):24002-24010.
100. Schwarz B, Schönhoff M: **Surface potential driven swelling of polyelectrolyte multilayers**. *Langmuir* 2002, **18**(8):2964-2966.
101. Wong JE, Rehfeldt F, Hänni P, Tanaka M, § RvK: **Swelling behavior of polyelectrolyte multilayers in saturated water vapor**. *Macromolecules* 2004, **37**(19):7285-7289.
102. Schuetz P, Caruso F: **Copper-Assisted Weak Polyelectrolyte Multilayer Formation on Microspheres and Subsequent Film Crosslinking**. *Advanced Functional Materials* 2003, **13**(12):929-937.
103. Kozlovskaya V, Sukhishvili SA: **Amphoteric hydrogel capsules: multiple encapsulation and release routes**. *Macromolecules* 2006, **39**(18):6191-6199.
104. Zhu H, McShane MJ: **Macromolecule encapsulation in diazoresin-based hollow polyelectrolyte microcapsules**. *Langmuir* 2005, **21**(1):424-430.
105. Kreft O, Skirtach AG, Sukhorukov GB, Möhwald H: **Remote control of bioreactions in multicompartment capsules**. *Advanced Materials* 2007, **19**(20):3142-3145.
106. Radt B, Smith TA, Caruso F: **Optically addressable nanostructured capsules**. *Advanced Materials* 2004, **16**(23-24):2184-2189.
107. Munoz Javier A, Del Pino P, Bedard M, Ho D, Skirtach A, Sukhorukov G, Plank C, Parak W: **Photoactivated release of cargo from the cavity of polyelectrolyte capsules to the cytosol of cells**. *Langmuir* 2008, **24**(21):12517-12520.
108. Skirtach AG, Muñoz Javier A, Kreft O, Köhler K, Piera Alberola A, Möhwald H, Parak WJ, Sukhorukov GB: **Laser-Induced Release of Encapsulated Materials inside Living Cells**. *Angewandte Chemie International Edition* 2006, **45**(28):4612-4617.
109. Skirtach AG, De Geest BG, Mamedov A, Antipov AA, Kotov NA, Sukhorukov GB: **Ultrasound stimulated release and catalysis using polyelectrolyte multilayer capsules**. *Journal of Materials Chemistry* 2007, **17**(11):1050-1054.
110. Shchukin DG, Gorin DA, Möhwald H: **Ultrasonically induced opening of polyelectrolyte microcontainers**. *Langmuir* 2006, **22**(17):7400-7404.
111. Kolesnikova TA, Gorin DA, Fernandes P, Kessel S, Khomutov GB, Fery A, Shchukin DG, Möhwald H: **Nanocomposite microcontainers with high ultrasound sensitivity**. *Advanced Functional Materials* 2010, **20**(7):1189-1195.
112. Lu Z, Prouty MD, Guo Z, Golub VO, Kumar CS, Lvov YM: **Magnetic switch of permeability for polyelectrolyte microcapsules embedded with Co@ Au nanoparticles**. *Langmuir* 2005, **21**(5):2042-2050.
113. Hu S-H, Tsai C-H, Liao C-F, Liu D-M, Chen S-Y: **Controlled rupture of magnetic polyelectrolyte microcapsules for drug delivery**. *Langmuir* 2008, **24**(20):11811-11818.
114. Katagiri K, Nakamura M, Koumoto K: **Magnetoresponsive smart capsules formed with polyelectrolytes, lipid bilayers and magnetic nanoparticles**. *ACS applied materials & interfaces* 2010, **2**(3):768-773.
115. Lu J, Ma S, Sun J, Xia C, Liu C, Wang Z, Zhao X, Gao F, Gong Q, Song B: **Manganese ferrite nanoparticle micellar nanocomposites as MRI contrast agent for liver imaging**. *Biomaterials* 2009, **30**(15):2919-2928.
116. Barnett BP, Arepally A, Karmarkar PV, Qian D, Gilson WD, Walczak P, Howland V, Lawler L, Lauzon C, Stuber M: **Magnetic resonance–guided, real-time targeted delivery and imaging of magnetocapsules immunoprotecting pancreatic islet cells**. *Nature medicine* 2007, **13**(8):986-991.
117. Petrov AI, Antipov AA, Sukhorukov GB: **Base-acid equilibria in polyelectrolyte systems: From weak polyelectrolytes to interpolyelectrolyte complexes and multilayered polyelectrolyte shells**. *Macromolecules* 2003, **36**(26):10079-10086.

118. Mauser T, Déjugnat C, Sukhorukov GB: **Reversible pH-Dependent Properties of Multilayer Microcapsules Made of Weak Polyelectrolytes**. *Macromolecular rapid communications* 2004, **25**(20):1781-1785.
119. Kato N, Schuetz P, Fery A, Caruso F: **Thin multilayer films of weak polyelectrolytes on colloid particles**. *Macromolecules* 2002, **35**(26):9780-9787.
120. Shiratori SS, Rubner MF: **pH-dependent thickness behavior of sequentially adsorbed layers of weak polyelectrolytes**. *Macromolecules* 2000, **33**(11):4213-4219.
121. Fery A, Schöler B, Cassagneau T, Caruso F: **Nanoporous thin films formed by salt-induced structural changes in multilayers of poly (acrylic acid) and poly (allylamine)**. *Langmuir* 2001, **17**(13):3779-3783.
122. Gao C, Möhwald H, Shen JC: **Enhanced biomacromolecule encapsulation by swelling and shrinking procedures**. *ChemPhysChem* 2004, **5**(1):116-120.
123. Büscher K, Graf K, Ahrens H, Helm CA: **Influence of adsorption conditions on the structure of polyelectrolyte multilayers**. *Langmuir* 2002, **18**(9):3585-3591.
124. Antipov AA, Sukhorukov GB, Möhwald H: **Influence of the ionic strength on the polyelectrolyte multilayers' permeability**. *Langmuir* 2003, **19**(6):2444-2448.
125. Ge L, Möhwald H, Li J: **Phospholipase A2 hydrolysis of mixed phospholipid vesicles formed on polyelectrolyte hollow capsules**. *Chemistry-A European Journal* 2003, **9**(11):2589-2594.
126. Johnston AP, Read ES, Caruso F: **DNA multilayer films on planar and colloidal supports: sequential assembly of like-charged polyelectrolytes**. *Nano letters* 2005, **5**(5):953-956.
127. Haynie DT: **Physics of polypeptide multilayer films**. *Journal of Biomedical Materials Research Part B: Applied Biomaterials* 2006, **78**(2):243-252.
128. Berth G, Voigt A, Dautzenberg H, Donath E, Möhwald H: **Polyelectrolyte complexes and layer-by-layer capsules from chitosan/chitosan sulfate**. *Biomacromolecules* 2002, **3**(3):579-590.
129. Shu S, Zhang X, Wu Z, Wang Z, Li C: **Gradient cross-linked biodegradable polyelectrolyte nanocapsules for intracellular protein drug delivery**. *Biomaterials* 2010, **31**(23):6039-6049.
130. Szarpak A, Cui D, Dubreuil Fdr, De Geest BG, De Cock LJ, Picart C, Auzély-Velty R: **Designing hyaluronic acid-based layer-by-layer capsules as a carrier for intracellular drug delivery**. *Biomacromolecules* 2010, **11**(3):713-720.
131. Brown J, Srivastava R, McShane MJ: **Encapsulation of glucose oxidase and an oxygen-quenched fluorophore in polyelectrolyte-coated calcium alginate microspheres as optical glucose sensor systems**. *Biosensors and Bioelectronics* 2005, **21**(1):212-216.
132. De Geest BG, Jonas AM, Demeester J, De Smedt SC: **Glucose-responsive polyelectrolyte capsules**. *Langmuir* 2006, **22**(11):5070-5074.
133. Bowden ME, Benfey OT: **Robert Burns Woodward and the art of organic synthesis**: Chemical Heritage Foundation; 1992.
134. Katagiri K, Matsuda A, Caruso F: **Effect of UV-irradiation on polyelectrolyte multilayered films and hollow capsules prepared by layer-by-layer assembly**. *Macromolecules* 2006, **39**(23):8067-8074.
135. Bayrakceken F, Demir OJ, Tuncyurek L, Karaaslan IS: **Triplet-triplet energy transfer from naphthalene to biacetyl in the vapor phase**. *Spectrochimica Acta Part A: Molecular and Biomolecular Spectroscopy* 2006, **65**(1):27-31.
136. Bayrakçeken F: **Singlet–singlet intermolecular optical energy transfer from naphthalene to benzophenone in the vapor phase**. *Spectrochimica Acta Part A: Molecular and Biomolecular Spectroscopy* 2008, **71**(2):572-577.
137. Dorman G, Prestwich GD: **Benzophenone photophores in biochemistry**. *Biochemistry* 1994, **33**(19):5661-5673.

138. Prucker O, Naumann CA, Rühe J, Knoll W, Frank CW: **Photochemical attachment of polymer films to solid surfaces via monolayers of benzophenone derivatives**. *Journal of the American Chemical Society* 1999, **121**(38):8766-8770.
139. Knowland J, McKenzie EA, McHugh PJ, Cridland NA: **Sunlight-induced mutagenicity of a common sunscreen ingredient**. *FEBS letters* 1993, **324**(3):309-313.
140. Stokes R, Diffey B: **How well are sunscreen users protected?** *Photodermatology, photoimmunology & photomedicine* 1997, **13**(5-6):186-188.
141. Breslow R: **Biomimetic control of chemical selectivity**. *Accounts of Chemical Research* 1980, **13**(6):170-177.
142. Breslow R: **Artificial enzymes and enzyme models**. *Advances in Enzymology and Related Areas of Molecular Biology* 1986:1-60.
143. Lee HS, Dimla RD, Schultz PG: **Protein-DNA photo-crosslinking with a genetically encoded benzophenone-containing amino acid**. *Bioorganic & medicinal chemistry letters* 2009, **19**(17):5222-5224.
144. Hino N, Okazaki Y, Kobayashi T, Hayashi A, Sakamoto K, Yokoyama S: **Protein photo-cross-linking in mammalian cells by site-specific incorporation of a photoreactive amino acid**. *Nature Methods* 2005, **2**(3):201-206.
145. Park MK, Deng S, Advincula RC: **pH-sensitive bipolar ion-permselective ultrathin films**. *Journal of the American Chemical Society* 2004, **126**(42):13723-13731.
146. Park MK, Deng S, Advincula RC: **Sustained release control via photo-cross-linking of polyelectrolyte layer-by-layer hollow capsules**. *Langmuir* 2005, **21**(12):5272-5277.
147. Bédard MF, De Geest BG, Skirtach AG, Möhwald H, Sukhorukov GB: **Polymeric microcapsules with light responsive properties for encapsulation and release**. *Advances in Colloid and Interface Science* 2010, **158**(1):2-14.
148. Brown EV, Granneman GR: **Cis-trans isomerism in the pyridyl analogs of azobenzene. Kinetic and molecular orbital analysis**. *Journal of the American Chemical Society* 1975, **97**(3):621-627.
149. Haberfield P, Block PM, Lux MS: **Enthalpies of solvent transfer of the transition states in the cis-trans isomerization of azo compounds. Rotation vs. the nitrogen inversion mechanism**. *Journal of the American Chemical Society* 1975, **97**(20):5804-5806.
150. Diau EW-G: **A new trans-to-cis photoisomerization mechanism of azobenzene on the S1 (n, π*) surface**. *The Journal of Physical Chemistry A* 2004, **108**(6):950-956.
151. Knoll H: **Chapter 89. Photoisomerism of azobenzenes**. *CRC Handbookof Organic Photochemistry and Photobiology* 2004, **2**(17):89-85.
152. Rau H: **Photoisomerization of azobenzenes**. *Photochemistry and Photophysics* 1990, **2**:119-141.
153. Priimagi A, Cattaneo S, Robin H, Valkama S, Ikkala O, Kauranen M: **Polymer-dye complexes: a facile method for high doping level and aggregation control of dye molecules**. *Chemistry of Materials* 2005, **17**(23):5798-5802.
154. Advincula RC, Fells E, Park M: **Molecularly ordered low molecular weight azobenzene dyes and polycation alternate multilayer films: aggregation, layer order, and photoalignment**. *Chemistry of Materials* 2001, **13**(9):2870-2878.
155. Balasubramanian S, Wang X, Wang HC, Yang K, Kumar J, Tripathy SK, Li L: **Azo chromophore-functionalized polyelectrolytes. 2. Acentric self-assembly through a layer-by-layer deposition process**. *Chemistry of Materials* 1998, **10**(6):1554-1560.
156. Wang X, Balasubramanian S, Kumar J, Tripathy SK, Li L: **Azo chromophore-functionalized polyelectrolytes. 1. Synthesis, characterization, and photoprocessing**. *Chemistry of Materials* 1998, **10**(6):1546-1553.
157. Ma N, Wang Y, Wang Z, Zhang X: **Polymer micelles as building blocks for the incorporation of azobenzene: enhancing the photochromic properties in layer-by-layer films**. *Langmuir* 2006, **22**(8):3906-3909.

158. Matsumoto M, Terrettaz S, Tachibana H: **Photo-induced structural changes of azobenzene Langmuir–Blodgett films**. *Advances in Colloid and Interface Science* 2000, **87**(2):147-164.
159. Yu Y, Ikeda T: **Alignment modulation of azobenzene-containing liquid crystal systems by photochemical reactions**. *Journal of Photochemistry and Photobiology C: Photochemistry Reviews* 2004, **5**(3):247-265.
160. Matharu AS, Jeeva S, Ramanujam P: **Liquid crystals for holographic optical data storage**. *Chem Soc Rev* 2007, **36**(12):1868-1880.
161. Cao T, Chen J, Yang C, Cao W: **Fabrication of photoactive self-assembled ultra-thin films from diazoresin and poly (4-vinylphenol) via H-bonding**. *New J Chem* 2001, **25**(2):305-307.
162. Chen J, Cao W: **Fabrication of a covalently attached self-assembly multilayer film via H-bonding attraction and subsequent UV-irradiation**. *Chem Commun* 1999(17):1711-1712.
163. Cao W, Ye S, Cao S, Zhao C: **Novel polyelectrolyte complexes based on diazo-resins**. *Macromolecular rapid communications* 1997, **18**(11):983-989.
164. Sun J, Wu T, Sun Y, Wang Z, Zhang X, Shen J, Cao W: **Fabrication of a covalently attached multilayer via photolysis of layer-by-layer self-assembled films containing diazo-resins**. *Chem Commun* 1998(17):1853-1854.
165. Sun J, Wu T, Liu F, Wang Z, Zhang X, Shen J: **Covalently attached multilayer assemblies by sequential adsorption of polycationic diazo-resins and polyanionic poly (acrylic acid)**. *Langmuir* 2000, **16**(10):4620-4624.
166. Lu C, Luo C, Cao W: **Self-assembly of a covalently attached magnetic film from diazoresin and Fe3O4 nanoparticles**. *J Mater Chem* 2002, **13**(2):382-384.
167. Li B, Cao T, Cao W, Shi Z, Gu Z: **Self-assembly of single-walled carbon nanotube based on diazoresin**. *Synthetic metals* 2002, **132**(1):5-8.
168. Hou X, Wu L, Sun L, Zhang H, Yang B, Shen J: **Covalent attachment of deoxyribonucleic acid (DNA) to diazo-resin (DAR) in self-assembled multilayer films**. *Polymer Bulletin* 2002, **47**(5):445-450.
169. Plewa A, Niemiec W, Filipowska J, Osyczka AM, Lach R, Szczubiałka K, Nowakowska M: **Photocrosslinkable diazoresin/pectin films–Synthesis and application as cell culture supports**. *European Polymer Journal* 2011, **47**(8):1503-1513.
170. Gokmen MT, De Geest BG, Hennink WE, Du Prez FE: **"Giant" Hollow Multilayer Capsules by Microfluidic Templating**. *ACS applied materials & interfaces* 2009, **1**(6):1196-1202.
171. Cabane E, Malinova V, Meier W: **Synthesis of Photocleavable Amphiphilic Block Copolymers: Toward the Design of Photosensitive Nanocarriers**. *Macromolecular Chemistry and Physics* 2010, **211**(17):1847-1856.
172. Thompson S, Spoors JA, Fawcett MC, Self CH: **Photocleavable nitrobenzyl-protein conjugates**. *Biochemical and biophysical research communications* 1994, **201**(3):1213-1219.
173. Fomina N, McFearin C, Sermsakdi M, Edigin O, Almutairi A: **UV and near-IR triggered release from polymeric nanoparticles**. *Journal of the American Chemical Society* 2010.
174. Zhao Y, Bertrand J, Tong X: **Photo-cross-linkable polymer micelles in hydrogen-bonding-built layer-by-layer films**. *Langmuir* 2009, **25**(22):13151-13157.
175. Chandra B, Subramaniam R, Mallik S, Srivastava D: **Formulation of photocleavable liposomes and the mechanism of their content release**. *Org Biomol Chem* 2006, **4**(9):1730-1740.
176. Cabane E, Malinova V, Menon S, Palivan CG, Meier W: **Photoresponsive polymersomes as smart, triggerable nanocarriers**. *Soft Matter* 2011, **7**(19):9167-9176.
177. Goodwin AP, Mynar JL, Ma Y, Fleming GR, Fréchet JMJ: **Synthetic micelle sensitive to IR light via a two-photon process**. *Journal of the American Chemical Society* 2005, **127**(28):9952-9953.

178. Boisselier E, Astruc D: **Gold nanoparticles in nanomedicine: preparations, imaging, diagnostics, therapies and toxicity**. *Chem Soc Rev* 2009, **38**(6):1759-1782.
179. Jain PK, Huang X, El-Sayed IH, El-Sayed MA: **Noble metals on the nanoscale: optical and photothermal properties and some applications in imaging, sensing, biology, and medicine**. *Accounts of Chemical Research* 2008, **41**(12):1578-1586.
180. Esser-Kahn AP, Odom SA, Sottos NR, White SR, Moore JS: **Triggered Release from Polymer Capsules**. *Macromolecules* 2011.
181. Weissleder R: **A clearer vision for in vivo imaging**. *Nature Biotechnology* 2001, **19**(4):316.
182. Eustis S, El-Sayed MA: **Why gold nanoparticles are more precious than pretty gold: noble metal surface plasmon resonance and its enhancement of the radiative and nonradiative properties of nanocrystals of different shapes**. *Chemical Society Reviews* 2006, **35**(3):209-217.
183. Link S, Mohamed M, El-Sayed M: **Simulation of the optical absorption spectra of gold nanorods as a function of their aspect ratio and the effect of the medium dielectric constant**. *The Journal of Physical Chemistry B* 1999, **103**(16):3073-3077.
184. Jana NR, Gearheart L, Murphy C: **Seed-mediated growth approach for shape-controlled synthesis of spheroidal and rod-like gold nanoparticles using a surfactant template**. *Advanced Materials* 2001, **13**(18):1389-1393.
185. Nikoobakht B, El-Sayed MA: **Preparation and growth mechanism of gold nanorods (NRs) using seed-mediated growth method**. *Chemistry of Materials* 2003, **15**(10):1957-1962.
186. Oldenburg S, Averitt R, Westcott S, Halas N: **Nanoengineering of optical resonances**. *Chemical Physics Letters* 1998, **288**(2-4):243-247.
187. Hirsch LR, Stafford R, Bankson J, Sershen S, Rivera B, Price R, Hazle J, Halas N, West J: **Nanoshell-mediated near-infrared thermal therapy of tumors under magnetic resonance guidance**. *Proceedings of the National Academy of Sciences* 2003, **100**(23):13549.
188. Kreibig U, Genzel L: **Optical absorption of small metallic particles**. *Surface Science* 1985, **156**:678-700.
189. Kelly KL, Coronado E, Zhao LL, Schatz GC: **The optical properties of metal nanoparticles: the influence of size, shape, and dielectric environment**. *The Journal of Physical Chemistry B* 2003, **107**(3):668-677.
190. McFarland AD, Van Duyne RP: **Single silver nanoparticles as real-time optical sensors with zeptomole sensitivity**. *Nano letters* 2003, **3**(8):1057-1062.
191. Lee KS, El-Sayed MA: **Gold and silver nanoparticles in sensing and imaging: sensitivity of plasmon response to size, shape, and metal composition**. *The Journal of Physical Chemistry B* 2006, **110**(39):19220-19225.
192. Jain PK, El-Sayed MA: **Surface plasmon resonance sensitivity of metal nanostructures: physical basis and universal scaling in metal nanoshells**. *The Journal of Physical Chemistry C* 2007, **111**(47):17451-17454.
193. Malinsky MD, Kelly KL, Schatz GC, Van Duyne RP: **Chain length dependence and sensing capabilities of the localized surface plasmon resonance of silver nanoparticles chemically modified with alkanethiol self-assembled monolayers**. *Journal of the American Chemical Society* 2001, **123**(7):1471-1482.
194. Haes AJ, Hall WP, Chang L, Klein WL, Van Duyne RP: **A localized surface plasmon resonance biosensor: First steps toward an assay for Alzheimer's disease**. *Nano letters* 2004, **4**(6):1029-1034.
195. Ho W, Yu JC, Lee S: **Low-temperature hydrothermal synthesis of S-doped TiO2 with visible light photocatalytic activity**. *Journal of Solid State Chemistry* 2006, **179**(4):1171-1176.

196. Liao D, Badour C, Liao B: **Preparation of nanosized TiO2/ZnO composite catalyst and its photocatalytic activity for degradation of methyl orange**. *Journal of Photochemistry and Photobiology A: Chemistry* 2008, **194**(1):11-19.
197. Ren W, Ai Z, Jia F, Zhang L, Fan X, Zou Z: **Low temperature preparation and visible light photocatalytic activity of mesoporous carbon-doped crystalline TiO2**. *Applied Catalysis B: Environmental* 2007, **69**(3-4):138-144.
198. Wu L, Yu JC, Fu X: **Characterization and photocatalytic mechanism of nanosized CdS coupled TiO2 nanocrystals under visible light irradiation**. *Journal of Molecular Catalysis A: Chemical* 2006, **244**(1-2):25-32.
199. Wang Z-S, Sasaki T, Muramatsu M, Ebina Y, Tanaka T, Wang L, Watanabe M: **Self-assembled multilayers of titania nanoparticles and nanosheets with polyelectrolytes**. *Chemistry of Materials* 2003, **15**(3):807-812.
200. Katagiri K, Koumoto K, Iseya S, Sakai M, Matsuda A, Caruso F: **Tunable UV-Responsive Organic– Inorganic Hybrid Capsules**. *Chemistry of Materials* 2008, **21**(2):195-197.
201. Mauritz KA, Moore RB: **State of understanding of Nafion**. *Chemical Reviews* 2004, **104**(10):4535-4585.
202. Ashwood-Smith M, Morris G, Fowler R, Appleton T, Ashorn R: **Physical factors are involved in the destruction of embryos and oocytes during freezing and thawing procedures**. *Human Reproduction* 1988, **3**(6):795-802.
203. Smith P, Krohn RI, Hermanson G, Mallia A, Gartner F, Provenzano MD, Fujimoto E, Goeke N, Olson B, Klenk D: **Measurement of protein using bicinchoninic acid**. *Analytical biochemistry* 1985, **150**(1):76-85.
204. Pavlov AM, Sapelkin AV, Huang X, P'ng KMY, Bushby AJ, Sukhorukov GB, Skirtach AG: **Neuron cells uptake of polymeric microcapsules and subsequent intracellular release**. *Macromolecular bioscience* 2011, **11**(6):848-854.
205. Cappella B, Dietler G: **Force-distance curves by atomic force microscopy**. *Surface science reports* 1999, **34**(1):1-104.
206. Carpick RW, Salmeron M: **Scratching the surface: fundamental investigations of tribology with atomic force microscopy**. *Chemical Reviews* 1997, **97**(4):1163-1194.
207. Drazba J: **Introduction to Confocal Microscopy**. *Microscopy and Microanalysis* 2006, **12**(S02):1756-1757.
208. Gottlieb HE, Kotlyar V, Nudelman A: **NMR chemical shifts of common laboratory solvents as trace impurities**. *Journal of Organic Chemistry* 1997, **62**(21):7512-7515.
209. Sabot A, Krause S: **Simultaneous quartz crystal microbalance impedance and electrochemical impedance measurements. Investigation into the degradation of thin polymer films**. *Analytical chemistry* 2002, **74**(14):3304-3311.
210. Sauerbrey G: **Use of vibrating quartz for thin film weighing and microweighing**. *Z Phys* 1959, **155**(2):206-222.
211. Kim BS, Vinogradova OI: **pH-controlled swelling of polyelectrolyte multilayer microcapsules**. *The Journal of Physical Chemistry B* 2004, **108**(24):8161-8165.
212. Lulevich VV, Vinogradova OI: **Effect of pH and salt on the stiffness of polyelectrolyte multilayer microcapsules**. *Langmuir* 2004, **20**(7):2874-2878.
213. Tong W, Gao C, Möhwald H: **Stable weak polyelectrolyte microcapsules with pH-responsive permeability**. *Macromolecules* 2006, **39**(1):335-340.
214. Elsner N, Kozlovskaya V, Sukhishvili SA, Fery A: **pH-Triggered softening of crosslinked hydrogen-bonded capsules**. *Soft Matter* 2006, **2**(11):966-972.
215. Balamuralidhara V, Pramodkumar T, Srujana N, Venkatesh M, Gupta NV, Krishna K, Gangadharappa H: **pH sensitive drug delivery systems: A review**. *Am J Drug Discovery Dev* 2011, **1**:24-48.
216. Chaturbedy P, Jagadeesan D, Eswaramoorthy M: **pH-sensitive breathing of clay within the polyelectrolyte matrix**. *ACS nano* 2010, **4**(10):5921-5929.

217. Kolli S, Wong SP, Harbottle R, Johnston B, Thanou M, Miller AD: **pH-Triggered nanoparticle mediated delivery of siRNA to liver cells in vitro and in vivo**. *Bioconjugate chemistry* 2013.
218. Pastoriza-Santos I, Schöler B, Caruso F: **Core–shell colloids and hollow polyelectrolyte capsules based on diazoresins**. *Advanced Functional Materials* 2001, **11**(2):122-128.
219. Yi Q, Wen D, Sukhorukov GB: **UV-crosslinkable Multilayer Microcapsules Made of Weak Polyelectrolytes**. *Langmuir* 2012, **28**:10822-10829.
220. Petros RA, DeSimone JM: **Strategies in the design of nanoparticles for therapeutic applications**. *Nature Reviews Drug Discovery* 2010, **9**(8):615-627.
221. DeLongchamp DM, Hammond PT: **Fast ion conduction in layer-by-layer polymer films**. *Chemistry of Materials* 2003, **15**(5):1165-1173.
222. Birabassov R, Landraud N, Galstyan TV, Ritcey A, Bazuin CG, Rahem T: **Thick dye-doped poly (methyl methacrylate) films for real-time holography**. *Applied optics* 1998, **37**(35):8264-8269.
223. Dante S, Advincula R, Frank CW, Stroeve P: **Photoisomerization of polyionic layer-by-layer films containing azobenzene**. *Langmuir* 1999, **15**(1):193-201.
224. Skirtach AG, Dejugnat C, Braun D, Susha AS, Rogach AL, Parak WJ, Möhwald H, Sukhorukov GB: **The role of metal nanoparticles in remote release of encapsulated materials**. *Nano letters* 2005, **5**(7):1371-1377.
225. Daiko Y, Katagiri K, Yazawa T, Matsuda A: **Thickness dependences of proton conductivity for ultrathin Nafion multilayers prepared via layer-by-layer assembly**. *Solid State Ionics* 2010, **181**(3):197-200.
226. Jiang S, Liu Z, Tian Z: **Layer-by-Layer Self-Assembly of Composite Polyelectrolyte–Nafion Membranes for Direct Methanol Fuel Cells**. *Advanced Materials* 2006, **18**(8):1068-1072.
227. Hemmerlé J, Roucoules V, Fleith G, Nardin M, Ball V, Lavalle P, Marie P, Voegel JC, Schaaf P: **Mechanically responsive films of variable hydrophobicity made of polyelectrolyte multilayers**. *Langmuir* 2005, **21**(23):10328-10331.
228. Kreuer K: **On the development of proton conducting polymer membranes for hydrogen and methanol fuel cells**. *Journal of membrane science* 2001, **185**(1):29-39.
229. Daiko Y, Katagiri K, Matsuda A: **Proton Conduction in Thickness-Controlled Ultrathin Polycation/Nafion Multilayers Prepared via Layer-by-Layer Assembly**. *Chemistry of Materials* 2008, **20**(20):6405-6409.
230. Liang Z, Chen W, Liu J, Wang S, Zhou Z, Li W, Sun G, Xin Q: **FT-IR study of the microstructure of Nafion® membrane**. *Journal of membrane science* 2004, **233**(1):39-44.
231. Buffeteau T, Labarthet FL, Pézolet M, Sourisseau C: **Photoinduced orientation of azobenzene chromophores in amorphous polymers as studied by real-time visible and FTIR spectroscopies**. *Macromolecules* 1998, **31**(21):7312-7320.
232. Hamm P, Ohline S, Zinth W: **Vibrational cooling after ultrafast photoisomerization of azobenzene measured by femtosecond infrared spectroscopy**. *The Journal of chemical physics* 1997, **106**:519.
233. Armstrong D, Clarkson J, Smith W: **Vibrational analysis of trans-azobenzene**. *The Journal of Physical Chemistry* 1995, **99**(51):17825-17831.
234. Okamoto H, Tasumi M: **Picosecond transient infrared spectroscopy of electronically excited 4-dimethylamino-4'-nitrostilbene in the fingerprint region (1640-940 cm^{-1})**. *Chemical physics letters* 1996, **256**(4):502-508.
235. Hafiz H, Nakanishi F: **Photoresponsive liquid crystal display driven by new photochromic azobenzene-based Langmuir–Blodgett films**. *Nanotechnology* 2003, **14**(6):649.
236. Seki T, Tamaki T, Suzuki Y, Kawanishi Y, Ichimura K, Aoki K: **Photochemical alignment regulation of a nematic liquid crystal by Langmuir-Blodgett layers of azobenzene polymers as" command surfaces"**. *Macromolecules* 1989, **22**(8):3505-3506.

237. Plewa A, Niemiec W, Filipowska J, Osyczka AM, Lach R, Szczubialka K, Nowakowska M: **Photocrosslinkable diazoresin/pectin films-Synthesis and application as cell culture supports**. *European Polymer Journal* 2011.
238. Song X, Geiger C, Leinhos U, Perlstein J, Whitten DG: **trans-Stilbene Aggregates in Microheterogeneous Media: Evidence for a Chiral Cyclic Supramolecular Unit**. *Journal of the American Chemical Society* 1994, **116**(22):10340-10341.
239. Lutkenhaus JL, Hammond PT: **Electrochemically enabled polyelectrolyte multilayer devices: from fuel cells to sensors**. *Soft Matter* 2007, **3**(7):804-816.
240. Liu X, Gao C, Shen J, Möhwald H: **Multilayer Microcapsules as Anti-Cancer Drug Delivery Vehicle: Deposition, Sustained Release, and in vitro Bioactivity**. *Macromolecular bioscience* 2005, **5**(12):1209-1219.
241. Antipov AA, Sukhorukov GB, Donath E, Möhwald H: **Sustained release properties of polyelectrolyte multilayer capsules**. *The Journal of Physical Chemistry B* 2001, **105**(12):2281-2284.
242. Song W, He Q, Möhwald H, Yang Y, Li J: **Smart polyelectrolyte microcapsules as carriers for water-soluble small molecular drug**. *Journal of Controlled Release* 2009, **139**(2):160-166.
243. Dai Z, Möhwald H: **Highly Stable and Biocompatible Nafion-Based Capsules with Controlled Permeability for Low-Molecular-Weight Species**. *Chemistry-A European Journal* 2002, **8**(20):4751-4755.
244. Köhler K: **Unpublished data in Temperature-Induced Rearrangements of polyelectrolyte Multilayer Capsules: Mechanisms and Applications (Doctroal thesis). Max Planck Institute of Colloids and Interfaces, Potsdam, Germany 2006, Ch. 5.**
245. Nuyken O, Voit B: **The photoactive diazosulfonate group and its role in polymer chemistry**. *Macromolecular Chemistry and Physics* 2003, **198**(8):2337-2372.
246. Lvov Y, Ariga K, Ichinose I, Kunitake T: **Assembly of multicomponent protein films by means of electrostatic layer-by-layer adsorption**. *Journal of the American Chemical Society* 1995, **117**(22):6117-6123.
247. Vogel A, Venugopalan V: **Mechanisms of pulsed laser ablation of biological tissues**. *Chemical Reviews* 2003, **103**(2):577-644.
248. Nuyken O, Voit B: **The photoactive diazosulfonate group and its role in polymer chemistry**. *Macromolecular Chemistry and Physics* 1997, **198**(8):2337-2372.
249. Zhao S, Li X, Yang M, Sun C: **Fabrication and characterization of covalently attached multilayer films containing iron phthalocyanine and diazo-resins**. *J Mater Chem* 2004, **14**(5):840-844.
250. Yang Z, Cao T, Chen J, Cao W: **Self-assembly of homopolymer and copolymers of *N*-4-hydroxyphenyl-acrylamide with diazoresin via H-bonding attraction**. *European Polymer Journal* 2002, **38**(10):2077-2082.
251. Shi F, Wang Z, Zhao N, Zhang X: **Patterned polyelectrolyte multilayer: Surface modification for enhancing selective adsorption**. *Langmuir* 2005, **21**(4):1599-1602.
252. Jianhao B, Sebastian B, Yein TS, Dieter T: **Self-Assembly of Polyamines as a Facile Approach to Fabricate Permeability Tunable Polymeric Shells for Biomolecular Encapsulation**. *ACS applied materials & interfaces* 2011, **3**(5):1665-1674.
253. Smith RC, Riollano M, Leung A, Hammond PT: **Layer-by-Layer Platform Technology for Small-Molecule Delivery**. *Angewandte Chemie* 2009, **121**(47):9136-9139.
254. Chen ZG: **Small-molecule delivery by nanoparticles for anticancer therapy**. *Trends in molecular medicine* 2010, **16**(12):594-602.
255. Kim I, Rabolt JF, Stroeve P: **Dynamic monolayer behavior of a photo-responsive azobenzene surfactant**. *Colloids and Surfaces A: physicochemical and engineering aspects* 2000, **171**(1):167-174.

256. Kawai T, Umemura J, Takenaka T: **UV absorption spectra of azobenzene-containing long-chain fatty acids and their barium salts in spread monolayers and Langmuir-Blodgett films**. *Langmuir* 1989, **5**(6):1378-1383.
257. Sun J, Wang Z, Wu L, Zhang X, Shen J, Gao S, Chi L, Fuchs H: **Investigation of the Covalently Attached Multilayer Architecture Based on Diazo-Resins and Poly (4-styrene sulfonate)**. *Macromolecular Chemistry and Physics* 2001, **202**(7):967-973.
258. Song X, Perlstein J, Whitten DG: **Supramolecular Aggregates of Azobenzene Phospholipids and Related Compounds in Bilayer Assemblies and Other Microheterogeneous Media: Structure, Properties, and Photoreactivity1**. *Journal of the American Chemical Society* 1997, **119**(39):9144-9159.
259. Lin YL, Chang HY, Sheng YJ, Tsao HK: **Photoresponsive Polymersomes Formed by Amphiphilic Linear–Dendritic Block Copolymers: Generation-Dependent Aggregation Behavior**. *Macromolecules* 2012.
260. Panchuk-Voloshina N, Haugland RP, Bishop-Stewart J, Bhalgat MK, Millard PJ, Mao F, Leung W-Y, Haugland RP: **Alexa dyes, a series of new fluorescent dyes that yield exceptionally bright, photostable conjugates**. *Journal of Histochemistry & Cytochemistry* 1999, **47**(9):1179-1188.

Publications

1. Yi Q, Wen D, Sukhorukov GB: **UV-crosslinkable Multilayer Microcapsules Made of Weak Polyelectrolytes**. *Langmuir* 2012, **28**:10822-10829.

2. Yi Q, Sukhorukov GB: **Externally Triggered Sealing of Microcapsules to Entrap Small Molecules.** Accepted by ACS Applied Materials and Interfaces.

3. Yi Q, Sukhorukov GB: **UV-induced Disruption of Microcapsules with Azobenzene Groups**. Submitted to Soft Matter.

4. Yi Q, Sukhorukov GB: **UV Triggered Dual-Function of Complex Microcapsules Composing of Different Functional Multilayers**. Submitted to ACS nano.

5. Yi Q, Sukhorukov GB: **Novel Molecule Encapsulation in Polyelectrolyte Microcapsules *via* Diazo-resin Related Photolysis.** In preparation.

6. Yi Q, Sukhorukov GB: **A New Route to Fabricate Single Component Polyelectrolyte Microcapsules from Diazoresin.** In preparation.

7. Yi Q, Li D, Luo D, Pavlov AM, Ai H, Sukhorukov GB: **MRI for Monitoring of Magnetic Polyelectrolyte Capsules *in vivo* Delivery.** In preparation.